6.2. Posters

P01 ABRASIVE STREEPING VOLTAMMETRY OF PYRITE

IVA BARTÁKOVÁ[a, b] and MARIE STUDNIČKOVÁ[b]
[a]*Department of Biochemistry, Faculty of Science, Masaryk University, Kotlářská 2, 611 37 Brno, Czech Republic; 15124@mail.muni.cz,* [b]*Department of Theoretical and Physical Chemistry, Faculty of Science, Masaryk University, Kotlářská 2, 611 37 Brno, Czech Republic*

Introduction

The aim of our study was to prove existence of goethite coating on the pyrite surface, which was exposed to ferric sulphate solution for several months. Stripping analysis appears as usable method for the determination of weathering processes. The chemical reaction of dissolution of FeOOH giving rise to Fe^{2+} ions is generally described by the Eq. 1:

$$FeOOH + 3\ H^+ + e^- \rightarrow Fe^{2+} + 2\ H_2O \qquad (1)$$

The Eq. 2 expresses the relationship between the current and charge passed during the reaction, the constant *g* has been interpreted as the geometric factor[1]:

$$I = k\ .\ Q_0\ .\ (Q_t/Q_0)^g \qquad (2)$$

where Q_0 is the total charge passed during the reaction.

Experimental

Pyrite was leached in sulphuric acid (12.5 mM) for 146 days (pulp density of 2%). The solid material was washed in distilled water (three times). Pyrite was dried and used for electrochemical experiments. Electrochemical measurements were performed in a three-electrode compartment with a saturated calomel electrode, reference electrode and auxiliary Pt-electrode (polarograph Tacussel). The working electrode contained the pyrite particles immobilised on carbon electrode. The electrolyte was purged with nitrogen and a nitrogen atmosphere was maintained above the electrolyte during experiments. The current passing through the working electrode was measured under the constant potential (the virtual pulse 42.5 ms was inserted after 0.1 s). The potential of –0.2 V was inserted on the pyrite electrode, and the potential of +0.2 V was inserted on the auxiliary electrode. The cyclic voltammetric curves were obtained in the potential range –0.6 V–0.8 V (SCE) by scan rate 2 mV s^{-1}.

Results and discussion

Fig. 1. shows the voltammetric curves of pyrite after leaching experiment. The changes on the pyrite surface are shown in Fig. 2. The current values in the first scan are higher in comparison with the second, third and forth scan because of the higher concentration of the leaching products on the surface. In the case of potential values lower than –0.4 V, the arise of H_2S was observed similarly to the behaviour of other sulphides[2,3]. The rice of H_2S under the potential lower than –0.4 V can be described by the equation:

$$FeS_2 + 4\ H^+ + 2\ e^- \rightarrow Fe^{2+} + 2\ H_2S \qquad (3)$$

Current peak under the potential –0.1 to –0.4 V (Fig. 1., scan 1) was assigned to the reduction of elemental sulphur formed on the previous positive potentials:

$$S + 2\ H^+ + 2\ e^- \rightarrow H_2S \qquad (4)$$

Elemental sulfur arises probably during the passivation at 0.1–0.2 V by reaction:

$$FeS_2 \rightarrow Fe^{2+} + 2\ S + 2\ e^- \qquad (5)$$

The ferric iron hydrooxide formation occures at 0.6 V– –0.7 V or higher:

$$Fe^{2+} + 2\ H_2O \rightarrow Fe^{III}OOH(s) + 3\ H^+ + e^- \qquad (6)$$

The abrasive streeping voltammetry was realized at 0.6 V. The charge of 0.457 C passed during 90 minutes. This result is equivalent to the amount of 4.74 μmol e^-. The total iron concentration in solution increased during this time. 0.59 μmol of iron left the pyrite surface. Thus, the amount of 1.18 μmol S^- from the pyrite was subjected to oxidation. Each S^- transmitted around 4 electrons. Therefore, the tetrathionate appears to be the first product during this oxidation. This result explains the detection of tetrathinates during the pyrite biooxidation[4].

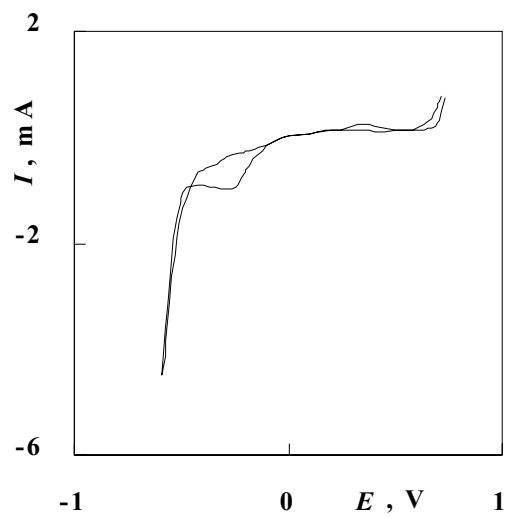

Fig. 1. **Voltammetric curve of pyrite after leaching experiments. Scan rate 2 mV s^{-1}, 4.5 mg of pyrite, 25 ml of 37.3 mM sulphuric acid, the 1st scan (—)**

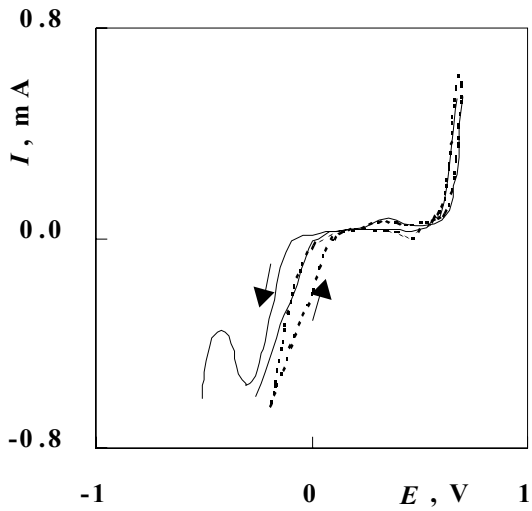

Fig. 2. **Voltammetric curves of pyrite after leaching experiments. Scan rate 2 mV s^{-1}, 4.5 mg of pyrite, 25 ml of 37.3 mM sulphuric acid, the 3st scan (—), the 4nd scan (---) to the determination of the changes of pyrite surface**

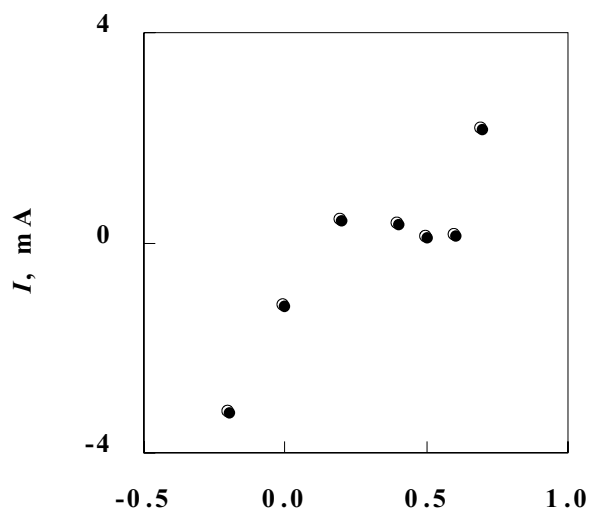

Fig. 3. **The initial values of current during abrasive streeping voltammetry of pyrite electrode. Plot of current against potential. 4.5 mg of pyrite, 25 ml of 37.3 mM sulphuric acid, [Fe^{3+}] = 2.56 mM**

The decrease of current during the abrasive streeping voltammetry under the potential of –0.2 V during 279 s was observed. The values of k and g obtained in our experiment were $6.3 . 10^{-3}$ s^{-1} and 1.32, respectively. These results suggest the presence of α-FeOOH on the pyrite surface. Signal of Fe^{3+}(aq) on the pyrite electrode under different potential values is shown in Fig. 3. The imaginary current peak between the potentials +0.2 V and +0.4 V is the result of presence Fe^{3+}. This peak is evident in Figs. 1. and 2.

Conclusion

The results of voltammetry of immobilised pyrite showed that H_2S arises under low redox potential. The coating of pyrite surface with Fe^{3+}-minerals was proved by abrasive streeping voltammetry under the potential value of –0.2 V. The fresh pyrite layer shows the highest initial current value during abrasive streeping voltammetry under the potential value –0.2 V due to the presence of the highest ratio of oxidised products on the surface. The first product of pyrite oxidation at the potential +0.6 V (SCE) is tetrathionate.

REFERENCES

1. Grygar T.: Collect. Czech. Chem. Commun. *60*, 1261 (1995).
2. Ásbjörnsson J., Kelsall G. H., Vaughan D. J., Pattrick R. A. D., Wincott P. L., Hope G. A.: J. Electroanal. Chem. *570*, 145 (2004).
3. Ásbjörnsson J., Kelsall G. H., Pattrick R. A. D., Vaughan D. J., Wincott P. L., Hope G. A.: J. Electrochem. Soc. *151* E250 (2004).
4. Schippers A., Jozsa P., Sand W.: Appl. Environ. Microbiol. *62*, 3424 (1996).

P02 LYOPHILISATION OF PHOTOGRAPHIC PAPERS

HANA BUREŠOVÁ and FRANTIŠEK KRČMA
Brno University of Technology, Faculty of Chemistry, Purkyňova 118, 612 00 Brno, Czech Republic
krcma@fch.vutbr.cz

Introduction

Many archive documents were inundated during the catastrophic flood in 2002 in the Bohemia, dominantly in many Prague central institutions and archives. The documents were frozen in huge packets just after the water receded and at present they are saved in freezing storages at the temperature under –30 °C. The frozen materials usually contain various kinds of documents, dominantly on paper with written of printed information. A significant part of the material is photographic materials, both negatives and positives. Drying of the stored frozen materials (their total volume is more than 10 000 m^3) is an urgent task[1]. The frozen material drying techniques are of two main kinds. The first group of the processes uses the de-freezing with consequent drying by dry or ambient air flow, in some cases coupled with microwave heating. These processes do not protect the dried material from additional microbiological damage and their application is not recommended for valuable archive documents[2]. The second possible technique uses a direct sublimation of water fixed in the frozen material. The vacuum sublimation called lyophilisation is the most effective process[3,4]. This work presents the first results obtained during the study of positive photographic materials lyophilisation.

Experimental setup

Lyophilisation is one of the vacuum drying techniques that are widely used in industry, especially in food and pharmaceutical applications. The water contained in the frozen material in the crystalline and residual liquid forms is sublimated at the pressure in the range of hundred Pascals. The material temperature during this process decreases down to –56 °C. The water vapor tension at this temperature is very low, and thus the drying process is very long – it takes several weeks (approximately 4 weeks for frozen blocks of 2000 A4 office paper sheets).

Two sets of samples were prepared for the experiment. The first set of them contains the black and white fiber based photographic papers (Fomabrom N 111) with exposed standard gray scales. Modern papers on RC substrate (Konica Digital Long Life 100) with standard RGB profiling color scale formed the second set. The solutions of humic acids in three concentrations (1.9, 6.9 and 31.9 mg l^{-1}) at two pH values (about 5.5 and 7.8) were prepared to simulate the filtered flood water. Free sheets from both sets were dipped in these solutions for the period of 0–10 days at the temperature of 24 °C and then they were stored with a separating tracing paper to eliminate the gluing of sensitive layers to another sample. Under the sample we added filtering paper to enhance the water vapor removal from the center of sheets. The final packet (A4 format, 8 cm thick) was stored in freezer at–18 °C for 1 month. The lyophilisation itself taking 4 weeks was done at the commercial apparatus located at Technical Museum in Brno where simultaneously the samples from the Czech Museum of Music were dried.

Results

The experiment gave the first result just after the samples dipping in humic acids solutions. The sensitive layers were stable for a few days only (fiber based paper for 2 days, RC paper for 4 days) and the stability depends on the solution properties. The yellow layer was stable for all the time. The sample dipped in the demineralised water was stable for all the studied period. The humic acids also diffused into the photographic paper material, and thus changed its colour to brown. The fiber based paper was also attacked by the mould at the dipping time longer than 7 days. The other results were obtained after the lyophilisation.

The maps of salts crystallised from the dipping solution were observed only on the surface of colour samples (i. e. on the RC paper). These small crystals had to remove easily from the surface mechanically, without a visible damage.

The main part of the study focuses on the mechanical properties of photographic papers. The changes in the photographic paper thickness were the first studied parameter. The fiber based paper thickness was independent of all the experimental parameters within the experimental error. Its value was determined as (0.290 ± 0.005) mm. Thickness of the RC paper shows a clear dependence on the dipping time, more or less independently of the humic acid concentration (see Fig. 1.) at the slightly basic pH. The acid dipping solutions

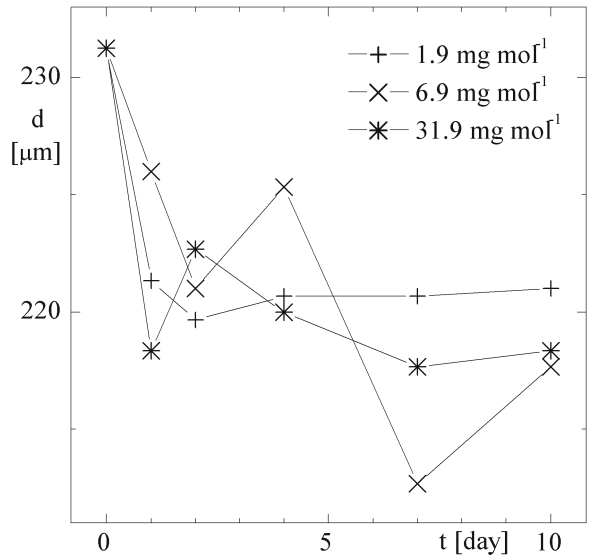

Fig. 1. **Thickness of an RC colour paper after lyophilisation as a function of the dipping time in humic acid solutions with the pH 7.5**

gives non-clear dependencies, but as a result the thickness slightly decreases with the increasing dipping time.

The tensile strength and Young's modulus in tension were measured for the fiber based papers as a function of the dipping time using the Universal Testing Machine ZWICK Z010/TH2A after sample dimensions measurement. The tensile test to failure were carried out by a Universal tensile test[5] at a constant crosshead speed of 0.1 mm min^{-1} at a laboratory temperature. Fig. 2. shows the results of the Young's modulus in tension. It can be seen that its value after an initial slight increase decreases more or less linearly with the increasing dipping time and it is not significantly dependent on the humic acid concentration. The pH of the solution is an important parameter because the modulus value is about 30% lower at the higher pH. Similar results were obtained also for the tensile strength.

The relative stretch of the samples increases with the increase of the dipping time up to about 4 days (see Fig. 3.). Its value slightly decreases at a longer dipping time. The relative stretch dependencies on the humic acid concentration and on pH are in the same order as the experimental error, and thus they could not be estimated.

Conclusion

The presented results show that lyophilisation of photographic positive materials can induce some changes in the material. Changes in the fiber based paper thickness are not significant; the thickness of the RC paper slowly decreases with the increase of the dipping time. The influence on the tensile strength and Young's modulus in tension of the fiber based paper are more significant. The results show after a small initial increase a slight decrease of these quantities

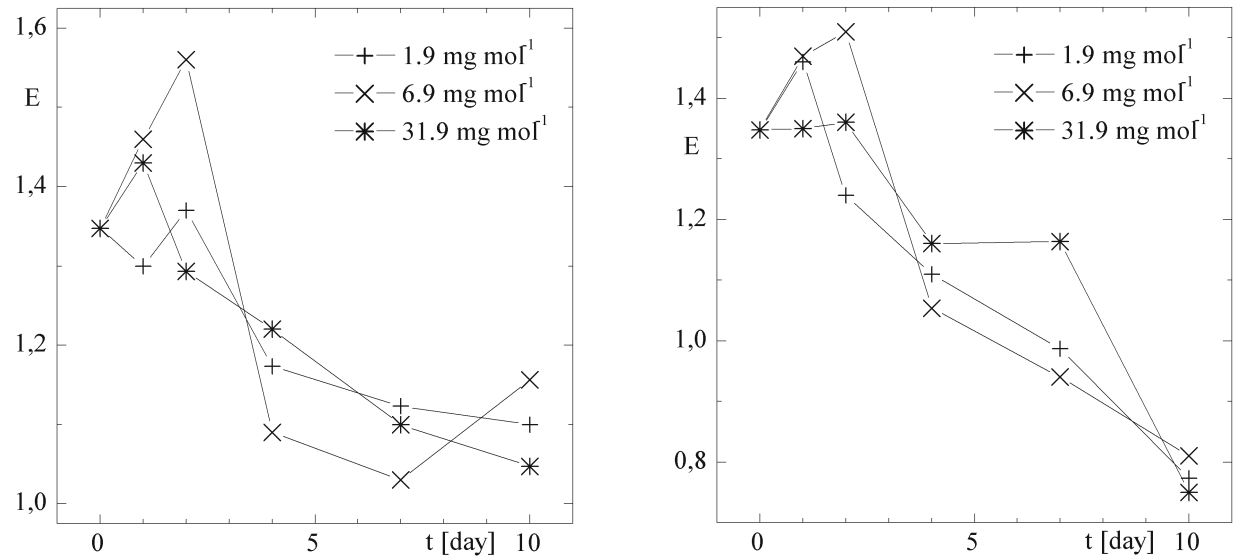

Fig. 2. **Young's modulus in tension in kN mm^{-2} of a fiber based paper after lyophilisation as a function of the dipping time in humic acid solutions; at the pH 6.5 on the left, at the pH 7.5 on the right**

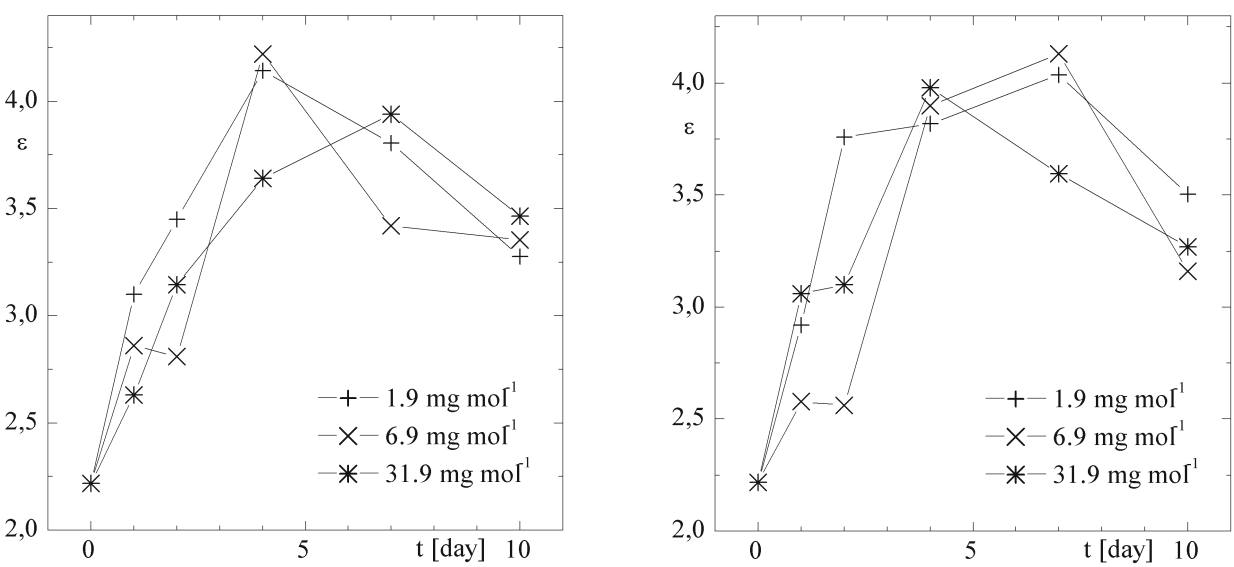

Fig. 3. **Relative extinction of a fiber based paper after lyophilisation as a function of the dipping time in humic acid solutions; at the pH 6.5 on the left, at the pH 7.5 on the right**

with the increasing dipping time. The effect can be more remarkable at a higher pH value and it is not dependent on the humic acid concentration in the dipping solution. The relative stretch of samples depends only on the dipping time, no dependence on pH and concentration were observed. The comparison with other drying processes will be given in the near future. The changes in the colour by the used dipping solution will be a subject of the next study.

REFERENCES

1. http://www.mkcr.cz, link to Povodne 2002.
2. http://www.nkp.cz/povodne/suseni.htm.
3. McCleary J. P.: General Information Programme and UNISIST, UNESCO, Paris, *63* (1987).
4. Soren C.: Proc. 9th Int. Congress of IADA, Copenhagen (1999).
5. US standard ASTM D-3379.

P03 IMPACT OF ELEVATED CARBON DIOXIDE CONCENTRATION ON CARBOHYDRATE CONTENT IN NORWAY SPRUCE NEEDLES

JANA CABÁLKOVÁ[a, b] and JOSEF CHMELÍK[b]
[a]*Brno University of Technology, Faculty of Chemistry, Purkyňova 118, Brno 612 00, Czech Republic, cabalkova@fch.vutbr.cz,* [b]*Institute of Analytical Chemistry Academy of Science of the Czech Republic, Veveří 97, Brno 611 42, Czech Republic*

Introduction

Carbohydrates are known to serve as carbon energy sources, osmotic agents, stress protectants regulatory and signaling molecules and may also serve as immediate carbohydrate supply in stress defense reactions in plants[1]. Being formed during the light-independent reactions of photosynthesis (known as the Calvin-Benson cycle) when carbon dioxide (CO_2) is fixed to produce P-trioses as the main precursors for carbohydrate synthesis[1], their content responds to the changes in atmospheric CO_2 concentration. Therefore, analysis of carbohydrates extracted from various plant tissues has become an important tool for prediction of plant behavior growing under elevated CO_2 conditions in recent time.

This study is focused on determination of the carbohydrate (up to tetrasacharidres) content, (using high performance liquid chromatography (HPLC) equipped with refractive index (RI) detection), in Norway spruce needles and grown under different CO_2 concentration with regard to the needle seasonal course.

Experimental

Materials and samples

All chemicals used were of the analytical-reagent grade. Investigations were carried out with Norway spruce needles (*Picea abies* [L.] Karst) grown under different CO_2 concentrations: i) control (C-variant), ii) ambient (AC-variant) and iii) elevated (EC-variant) (i.e. ambient +350 ppm CO_2 (v/v)); collected during one year needle course (from May to September) in Ecological site Bílý Kříž in the Czech Republic[2].

Sample treatment

100 mg of spruce needles were frozen in liquid nitrogen, grounded, dissolved by adding 1.0 ml of a mixture (methanol: chloroform: water (12/5/3 v/v %)[3]), immediately shaken, heated, sonificated and centrifuged. 500 µl of deionized water was added to the supernatant, mixed, shaken and centrifuged to break the emulsion into a i) colorless part (water-methanol phase) and ii) colored part (chloroform phase). Colorless part was filtered using 0.22 µm PVDF Millipore filter and concentrated using vacuum evaporator. Samples for HPLC analysis were dissolved in a mixture (acetonitrile (ACN)) and water (W) (50/50 v/v %)).

Analytical instrumentation

Analyses were performed with Hewlet Packard 1100 Series system equipped with refractive index detector (RID – HP 1100 Series, Palo Alto, CA, USA) using a 100 µl sample injection loop. Carbohydrate determination was achieved on a Carbohydrate analysis column (4.6 × 250 mm, 5-micron, Agilent Technologies, USA) using a mobile phase of ACN/W (70/30 v/v %) at a flow rate of 1,2 ml $min.^{-1}$ Standards were dissolved in ACN/W (50/50 v/v %) solution.

Results and discussion

Since the light is one of the most stressful environmental conditions that can affect needle structure, function and so the carbohydrate and other assimilate content, our study was primarily focused on the behavior of non-structural carbohydrates (NSC) in needles collected in sunny-exposed sites.

Firstly, carbohydrate composition in spruce needles during the annual cycle was investigated and significant fluctuations depending on the needle development stage were observed. Fig. 1. shows an example of NSC content in needles grown under elevated CO_2 conditions, presented here by the two different stages of needle development. The first stage presents the late dormant state in May (in relation to the climatic conditions in the Beskydy mountain site), when new (i. e. current (*C*)) needles broke through the buds. During this time one-year-old needles (*C + 1*) play the most important role for development support of (*C*) needles which resulted in an increased content of NSC, namely due to accumulation of major carbohydrates (fructose, glucose and sucrose).

The second stage was chosen to stand for the autumn (September) needle development, when the needle growth was retarded. This stage was accompanied by slow increase of the hexose needle content, namely accumulation of galactose and pinitol was observed. In general, these carbohydrates serve as main precursors for accumulation of raffinose family oligosaccharides (RFOs)[4] and their impact to frost tolerance in needles of coniferous has been discussed by many authors[5].

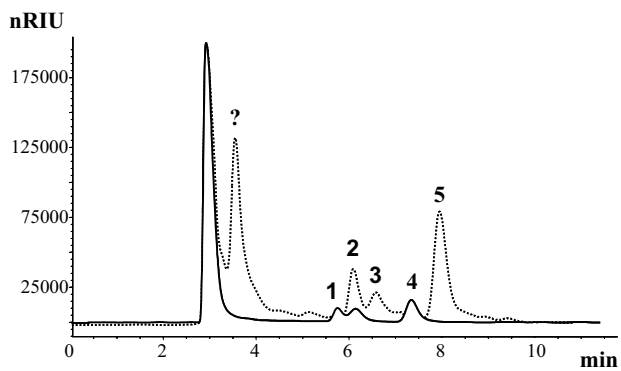

Fig. 1. **Seasonal changes in carbohydrate composition for C+1 needles grown in EC-variant both from sunny-exposed site collected in: I) May – dotted line and II) September – full line. Peaks: ? – unknown, 1 – pinitol, 2 – fructose, 3 – glucose, 4 – galactose, 5 – sucrose**

To illustrate the effect of CO_2 concentration on carbohydrate composition independently from seasonal patterns, the differences in NSC grown in AC-, EC- and C-variant are shown in Fig. 2.

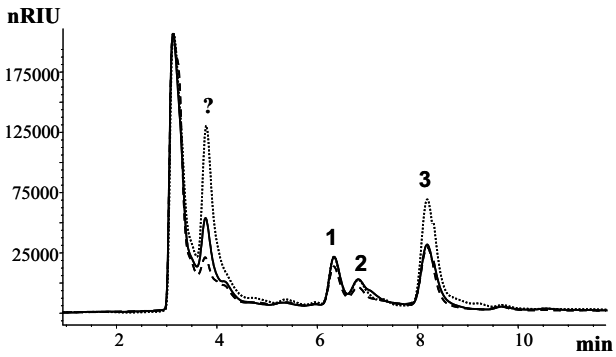

Fig. 2. **Effect of carbon dioxide concentration on carbohydrate concentration of one-year-old (C+1) needles from sunny exposed site collected in May and grown in: I) ambient (AC-variant) – dashed line, II) elevated (EC-varinat) – dotted line and III) control (C-variant) – full line. Peaks: ? – unknown, 1 – fructose, 2 – glucose, 3 – sucrose.**

There were no differences in carbohydrate composition between AC- and EC-variant althought some fluctuations in concentration levels occurred. The needles grown in EC-variant showed an increase in NSC, namely a higher concentration of sucrose was observed. A larger accumulation of NSC has been reported in many papers as a consequence of the long-term exposure to elevated CO_2 (ref.[6]) and in addition increased levels of sucrose can eventually lead to decrease in photosynthetic activity.

Conclusion

Analysis of carbohydrate composition using HPLC-RI during season showed some fluctuations, which were in accordance with the seasonal development of needles. Glucose, fructose and sucrose were highest in late dormant stage (May), while galactose occurred in late summer (September) at the beginning of winter needle dormancy stage to serve as precursor for RFOs synthesis. Independently of seasonal course a small increase of NSC, namely sucrose content, was observed for needles grown under elevated CO_2 concentration.

This work is supported by the grant No. 526/03/1182, Grant Agency of the Czech Republic and Institutional research plan AVO Z40310501.

REFERENCES

1. Voet D., Voet J. G.: *Biochemistry*. John Wiley & Sons, Inc., New York 1990.
2. Urban O., Janouš D., Pokorný R., Marková I., Pavelka M., Fojtík Z., Šprtová M., Kalina J., Marek M. V.: Photosynthetica *39*, 395 (2001).
3. Haissig B. E., Dickson R. E.: Physiol. Plant. *47*, 151 (1979).
4. Minorsky P. V.: Plant Physiol. *131*, 1159 (2003).
5. Lipavská H., Svobodová H., Albrechtová J.: J. Plant. Physiol. *157*, 365 (2000).
6. Wiemken V., Ineichen K.: J. Plant. Physiol. *156*, 746 (2000).

P04 THE STUDY OF THE THERMOOXIDATIVE STABILITY OF POLYISOPRENE WITH ADDITION OF P-PHENYLENEDIAMINES USING DSC

ZUZANA CIBULKOVÁ, ERIK KLEIN
and PETER ŠIMON
Department of Physical Chemistry, Faculty of Chemical and Food Technology, Radlinského 9, 812 37 Bratislava, Slovak Republic, zuzanacibulkova@centrum.sk

Introduction

Oxidation belongs to the main reasons of deterioration of rubber products properties. The rate of this process can be significantly reduced using antioxidants. Aromatic secondary amines, particularly *p*-phenylenediamines (PPDs) represent the most important group of antidegradants used in rubber industry[1,2].

Since the oxidation is an exothermic process, differential scanning calorimetry (DSC) can be used for its study. In this work, the antioxidant activity of several *p*-phenylenediamines in polyisoprene rubber (PIR) is studied under non-isothermal conditions. At the end of induction period (which corresponds to the beggining of the oxidation), antioxidants lose their protective effect and the material properties suddenly deteriorate. Dependence of the induction period on temperature can be expressed by an Arrhenius-like relationship[3]:

$$t_i = A \cdot \exp\left[B/T\right] \tag{1}$$

where A and B are constants and T is the absolute temperature. In the case of linear increase of temperature, the parameters A and B in Eq. 1 can be obtained from Eq. 2[3]:

$$\beta = \int_0^{T_i} \frac{\mathrm{d}T}{A \cdot \exp\left[B/T\right]} \tag{2}$$

Materials and Methods

The calorimeter Perkin Elmer DSC-7 was employed to study the thermooxidation stability of the samples. The samples of 2–4 mg were placed in crimped standard aluminium pans, where the lid of each pan was perforated by ten pinholes. Heating rates were 1, 3, 5, 7, 10 and 15 K min^{-1}. The purge gas forming the reaction atmosphere was oxygen. The starting temperature of oxidation was determined as the onset

temperature of the oxidation peak. Mixtures of polyisoprene rubber with antioxidants were prepared in the Research Institute of Chemical Technology, Bratislava, Slovak Republic. Characteristics of the antioxidants under study are given in Table I and the composition of the samples in Table II.

Table I
Characteristics of the antioxidants under study

Antioxidant	Name	Summary formula
Durazone 37	2,4,6-tris-(*N*-1,4-dimethyl-pentyl-*p*-phenylenediamino) -1,3,5-triazine	$C_{42}H_{63}N_9$
Flexzone 11	mixture of *N*-alkyl-*N′*-phenyl--*p*-phenylenediamines	–
BOPA	bis-(4-octylphenyl)amine	$C_{28}H_{43}N$
TMBPDT	2,4,6-tris-(*N*-1,1,4,4-tetramethyl-butyl-*p*-phenylenediamino)- -1,3,5-triazine	$C_{45}H_{69}N_9$

Table II
Values of the kinetic parameters *A* and *B* and their standard deviations

Antioxidant/phr	*A* [min]	$B \cdot 10^{-3}$ [K]
none	$(9.9 \pm 5.6) \cdot 10^{-13}$	12.90 ± 0.56
Durazone 37/0.2	$(2.0 \pm 2.0) \cdot 10^{-13}$	14.6 ± 1.1
Flexzone 11/0.2	$(6.0 \pm 3.2) \cdot 10^{-13}$	14.87 ± 0.59
BOPA/0.2	$(9.0 \pm 8.2) \cdot 10^{-16}$	17.10 ± 0.96
TMBPDT/0.2	$(1.2 \pm 1.0) \cdot 10^{-16}$	17.41 ± 0.83

Results and discussion

From the nonisothermal measurements, the kinetic parameters *A* and *B* in Eq. 2 have been obtained by minimizing the sum of squares between experimental and theoretical values of heating rates by the simplex method[4]. The integration indicated in Eq. 2 was carried out by the Simpson method. The values of *A* and *B* for all samples are listed in Table II.

Protection factor has been defined as the ratio of the lengths of the induction periods of stabilized and unstabilized polymer[5]:

$$PF = \frac{t_i(\mathrm{PIR+AOx})}{t_i(\mathrm{PIR})} \qquad (3)$$

From Eq. 3 it is obvious that if the value of *PF* is greater than one, the additive has a stabilizing effect on the polymer. Temperature dependences of *PF*s for antioxidants under study are depicted in Fig. 1. These dependences exhibit increasing tendency with decreasing temperature. It can be seen that the values of *PF*s are greater than one in the temperature range of PIR practical use.

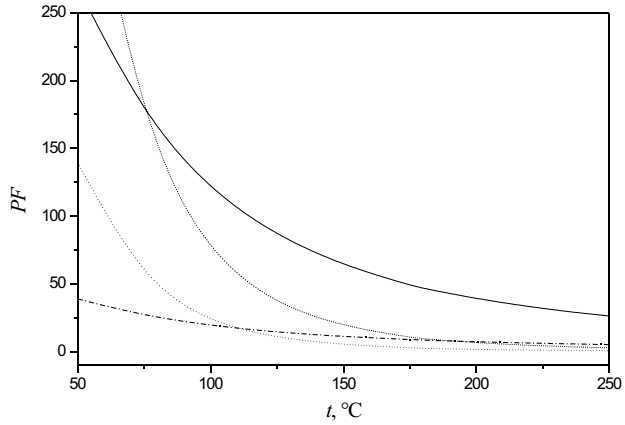

Fig. 1. **Temperature dependences of the protection factors for Durazone 37 (dash-dotted line), Flexzone 11 (solid line), BOPA (dashed line) and TMBPDT (dotted line)**

Since the dependences of the protection factors of PPDs on their relative mass ratios are almost linear, antioxidant effectiveness (*AEX*) has been defined as a slope of this dependence in our previous work[5]:

$$AEX = \frac{PF - 1}{X} \qquad (4)$$

where *X* is expressed in phr. *AEX* brings about a normalization of the protection factor so that the values of PF for various stabilizer content can be compared. Since *PF* depends on temperature, also *AEX* is a function of temperature. The antioxidant effectiveness of individual stabilizers for the temperature 180 °C are listed in Table III. This temperature was chosen since it is a standard temperature for isothermal stability tests[6]. The order of antioxidant effectiveness decreases in the following order: Flexzone 11 > BOPA > Durazone 37 > TMBPDT. The highest ranking of Flexzone 11 indicates that a synergism exists between the components of this antioxidant. The lowest antixidant effectiveness of the last additive can be explained by the sterical effect of the bulky tetramethylbutyl groups.

Table III
Antioxidants effectiveness for the temperature of 180 °C.

Antioxidant	*AEX*
Durazone 37	38
Flexzone 11	229
BOPA	43
TMBPDT	8

Conclusions

The antioxidant effect of *p*-phenylenediamines in thermal oxidation of polyisoprene rubber has been studied by non-isothermal DSC measurements. For the treatment of experimental data, our method for the description of the lengths

of induction periods[3] was employed. DSC appeared powerful and fast technique for studying the oxidation of elastomers and to evaluate the efficiency of various antioxidants in retarding the thermooxidative degradation.

The values of the protection factors and antioxidant effectiveness have been calculated. Using both criteria, the synergistic effect of the components in Flexzone 11 is indicated. The results obtained in this study show that the new additives tested have a promising potential as antioxidant agents.

T*his work has been supported by Science and Technology Assistance Agency under the contract No APVT-20-005004. The work has been also supported by Slovak Grant Agency (Project No. 1/0054/03).*

REFERENCES

1. Cataldo F.: Eur. Polym. J. *38*, 885 (2002).
2. Cataldo F.: Polym. Deg. Stab. *72*, 787 (2001).
3. Šimon P., Kolman Ľ.: J. Therm. Anal. Cal. *64*, 813 (2001).
4. Nelder J. A., Mead R.: Computer J. *7*, 308 (1965).
5. Cibulková Z., Šimon P., Lehocký P., Balko J.: Polym. Deg. Stab. *87*, 479 (2005).
6. Abdel-Aziz M. M., Basfar A. A.: Polym. Testing *19*, 591 (2000).

P05 IRON-GALL INK CORROSION: ESTIMATION OF THE PROGRESS OF PAPER DEGRADATION USING INFRARED SPECTROSCOPY AND STANDARD MECHANICAL TEST

LINDA CSEFALVAYOVÁ[a], BOHUSLAVA HAVLÍNOVÁ[a], HANA PAULUSOVÁ[b], ALENA MAKOVÁ[c] and MIROSLAVA PETROVIČOVÁ[a]

[a]*Department of Graphic Arts and Applied Photochemistry, Faculty of Chemical and Food Technology, Slovak University of Technology in Bratislava, Radlinského 9, SK-812 37, Slovak Republic, bohuslava.havlinova@stuba.sk* [b]*National Archive in Prague, Czech Republic,* [c]*Slovak National Library, Martin, Slovak Republic*

Introduction

Ink corrosion is considered to be the results of two major degradation processes: acid-catalysed hydrolysis and iron(II)-catalysed oxidation of cellulose, contributing to a loss in the mechanical properties of paper[1].

In this work, we present some measurements carried out on laboratory samples consisting of paper initially immersed in solutions of iron sulphate and iron-gall ink respectively. We try to simulate a historical paper production by producing sized paper with gelatine and aluminium sulphate as additive. The purpose of this paper sizing was to make paper hydrophobic to such extent that aqueous inks can be applied. Moreover, the machanical properties were enhanced[2].

The loss of paper's mechanical properties versus artificial ageing was evaluated with bursting strength measurements, as this method most closely resembles real-life situations, where papers burst along the corroded ink lines[3]. The cellulose oxidation was detected via FTIR spectroscopy. FTIR has become a valuable tool which is capable of rapid, non-destructive, qualitative analysis of microscopic samples[4].

Experimental

The experiments on paper substrate were performed using Whatman No. 1 (Cat. No. 10001917) filter paper. The set of the paper squares (10 × 10 cm) was immersed in a 1% gelatine solution and 5% solution of aluminium sulphate for 5 minutes.

The paper supports (10 × 10 cm) were soaked in a freshly prepared ink and 5.10^{-3}M aqueous solution of $FeSO_4$ respectively for approximately 10 seconds. The samples were then dried in an ambient atmosphere.

The iron-gall ink was composed of $FeSO_4.7H_2O$, gallic acid (Aldrich No. 39822–5) and gum arabic, the molar ratio of iron and gallic acid was 5.5 : 1[3].

The samples were artificially aged in a OMT OVEN for 1 day to 10 days at 60 °C and 65 % RH.

The bursting strength of paper was determined using a normalized bursting tester (Lorentzen & Wettre) according to standard STN EN ISO 2758 for the bursting strength of paper.

The oxidation rate of the paper materials was estimated by Attenuated Total Reflectance FTIR spectroscopy. At the room temperature FTIR spectra of paper samples in the spectral range of 600–4000 cm^{-1} were recorded on a FTIR Nexus (ThermoNicolet) spectrometer using Smart MIRacle ATR for ThermoNicolet with a spectral resolution 4 cm^{-1} and scan number 256. The absorption spectra were converted into Kubelka-Munk function.

Results and discussion

Mechanical test

Fig. 1.–3. present the changes of bursting strength during accelerated ageing. As shown, the bursting strength values measured on non-aged samples are similar to that of original, virgin paper. We suppose that the influence of iron sulphate alone on the degradation of paper is too small to be measured by this mechanical test. On the contrary, the radical influence of ink on the paper degradation appears clearly from the third day on. The real bursting strength of the highly damaged samples is presumed to go below the obtained values.

As it can be seen from the starting values on Fig. 2. and 3., the gelatine treatment increases the initial bursting strength. As shown on Fig. 3., this mechanical stabilization effect vanishes during accelerated ageing and after 1 day no differences can be measured.

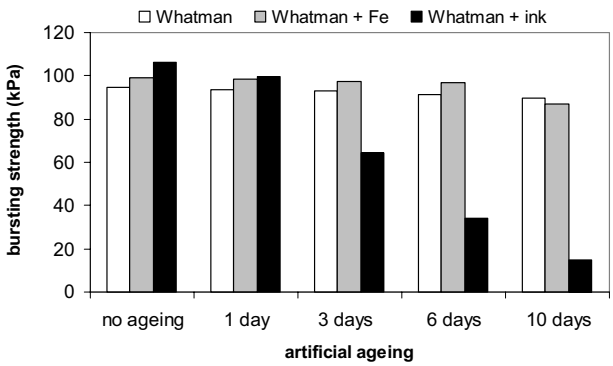

Fig. 1. **Evolution of bursting strength versus artificial ageing (at 60 °C and 65 % RH) for Whatman cellulose paper (Whatman) impregnated with two different solutions: iron sulphate (Whatman + Fe) and iron-gall ink (Whatman + ink)**

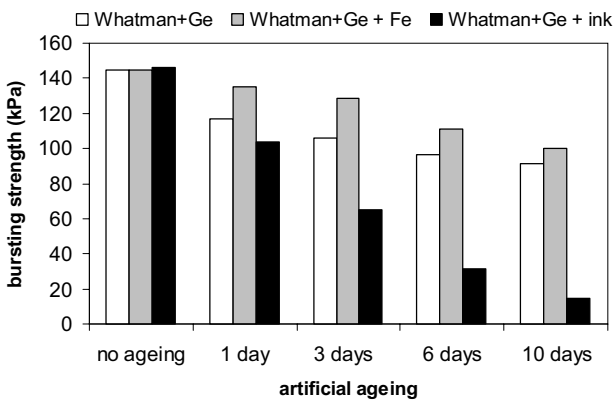

Fig. 2. **Evolution of bursting strength versus artificial ageing (at 60 °C and 65 % RH) for Whatman paper sized with gelatine in combination with aluminium sulphate (Whatman + Ge) and impregnated with two different solutions: iron sulphate (Whatman + Ge + Fe) and iron-gall ink (Whatman + Ge + ink)**

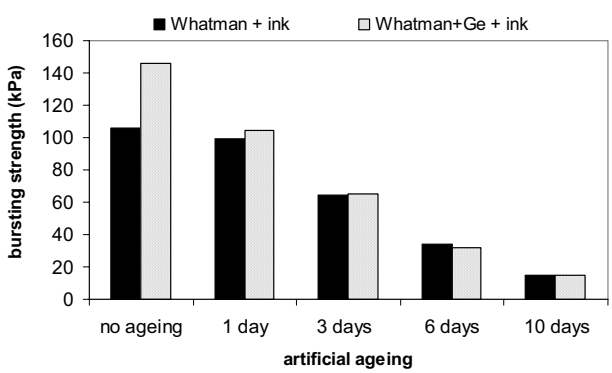

Fig. 3. **Effect of gelatine sizing of Whatman paper on bursting strength of inked paper aged at 60 °C and 65 % RH. Whatman paper impregnated with iron-gall ink (Whatman + ink), Whatman paper sized with gelatine and aluminium sulphate and then impregnated with iron-gall ink (Whatman + Ge + ink)**

F T I R m e a s u r e m e n t s

From the FTIR measurements we can summarize following facts:

No clear distinction can be formulated between the spectra of pure cellulose Whatman paper, paper impregnated with iron sulphate and inked paper. The concentration of sulphates and gelatine is low to modify the cellulose structure. Indeed, these constituents are too diluted in the paper to give a proper signal.

After artificial ageing, small variations in absorption appear in the region between 1600 and 1750 cm^{-1}, which is characteristic for alkenes and carbonyl groups stretching vibration and the changes of absorption bands are attributed to cellulose oxidation products.

The changes of band in spectral region at 3330 cm^{-1} are evidenced for samples with different pH (Fig. 4.). This band corresponds to the OH stretching vibrations and its decrease can reflect the changes of OH environment.

We first notice that the gelatine-treated paper profile is very close to the pure cellulose profile; furthermore it is noticeable that gelatine-treated paper absorption is much less. We propose that gelatine forms film on the surface of the cellulose fibre web. This film is considerably hydrophobic and works as an effective barrier against humidity fluctuations[2].

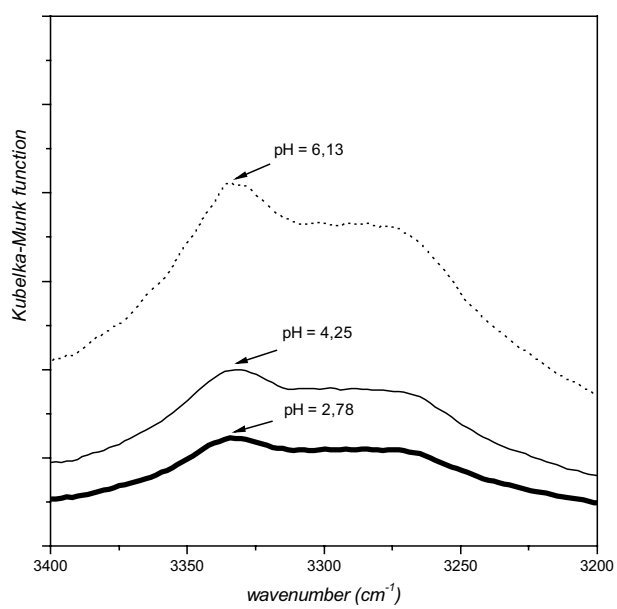

Fig. 4. **FTIR absorption spectra of Whatman cellulose paper impregnated with two different solutions containing iron sulphate and iron-gall ink, and artificially aged for 10 days at 60 °C and 65 % RH. Dotted line:pure unaged cellulose, thin line: Whatman paper impregnated with iron sulphate, thick line: inked Whatman paper**

Conclusion

Typically, paper degradation progress is traced by mechanical properties that provide only macroscopic information. From the results obtained by mechanical tests, gelatine

sizing has no clear long term effect on ageing stability of iron-gall ink containing paper.

By contrast, infrared spectroscopy is sensitive to structural changes in materials. The interpretation of spectra is rather difficult because the ink degradation and the paper degradation may have combined influences and different structures can coexist in the same part of paper, unmodified or differently oxidized cellulose, hydrocellulose, etc. Since discrepancies between inked or even strongly damaged paper, when paper lost its mechanical properties, and pure cellulose FTIR spectra and absorption bands are rather small, we suggest to explore other FTIR techniques to confirm these assumptions.

This work was supported by Science and Technology Assistance Agency (Slovakia) under the contract No. APVT-20-034202.

REFERENCES

1. Banik G.: Phänomene und Ursachen von Tntenfrass auf Papier – eine Einführung. *Tintenfraßschäden und ihre Behandlung*. Verlag W. Kohlhammer Stuttgart 1999, 13–24.
2. Kolbe G.: Restaurator 2004, *16*, 26–39.
3. Neevel J.: Restaurator 1995, *16*, 143–160.
4. Sistach M., Ferrer, N.: *Iron-gall ink corrosion in manuscripts*. The Postprints of the Iron Gall Ink Meeting, Newcastle upon Tyne, University of Northumbria 2000.

P06 PHOTODEGRADATION OF ANTHRACENE AND ITS DERIVATIVES IN ISOOCTANE AND DICHLOROMETHANE SOLUTIONS

OLGA CVRČKOVÁ[a] and MIROSLAV CIGANEK[a,b]
[a]Brno University of Technology, Faculty of Chemistry, Purkyňova 118, 612 00 Brno, Czech Republic, cvrckova@fch.vutbr.cz, [b]Veterinary Research Institute, Hudcova 70, 621 32 Brno, Czech Republic, ciganek@vri.cz

Introduction

Anthracene belongs to the group of Polycyclic aromatic hydrocarbons (PAHs). These pollutants have high chemical and physical stability and they are resistant to the biological degradation.

Several studies have demonstrated that anthracene undergoes relatively rapid decomposition[1–7].

This study occupies with photostability of anthracene as an example of basic PAHs and its derivatives, which were investigated for better understanding to an influence of functional groups to photostability.

Experimental part

Samples of PAHs dissolved in dichloromethane and isooctane were exposed to simulated near UV light in Light simulator Sanyo Gallenkamp (25 °C/60% RH – relative humidity; lamp with continuous spectrum 320–400 nm; 200 Wh m^{-2} exposition – 7 W m^{-2} per hour). Samples were stored in closed glass vials (with 60% light permeability in the range of 320–400 nm) At intervals of approximately 30 Wh m^{-2}, 1 μl of each tested sample was analysed by GC-MS. Concentration of each PAH under study was calculated from peaks area. Identification of degradation products was deduced from their retention times and were realised by comparison their mass spectrums with MS databases (NIST and Wiley), by using rules for mass spectrum interpretation and by technique multiple mass spectrometry (ion trap-MS/MS).

Results and discussion

Molecule of anthracene in dichloromethane was decomposed faster then in isooctane, because degradation was accelerated by chlorine radicals originated from dichloromethane. From this fact we assumed that dichloromethane is not photostable solvent and that is why it is not very suitable solvent for PAHs analysis. Degradation of 9,10-anthraquinone followed pseudo-zero and other PAHs followed first-order kinetic. Half times are quoted in Table I.

Table I
Half lives of Anthracene and its derivatives in isooctane (ISO) and dichloromehane (DCM)

PAH	$\tau_{1/2}$ – ISO [W h m^{-2}]$^{-1}$	$\tau_{1/2}$ – DCM [W h m^{-2}]$^{-1}$
Anthracene	73.74	44.15
9-nitroanthracene	7.12	7.00
1-methylanthracene	68.46	–
2-methylanthracene	80.12	–
9-methylanthracene	60.64	22.8
Anthrone	70.01	59.88
9,10-anthraquinone	990.21	2631.58

Identificated photoproducts are quoted in Table II. Decay curves of anthracene in both solvents are shown in Figs. 1. and 2.

Anthracane was at first oxidized to 9,10-anthraquinone, which was degraded in following ways (see Scheme 1): photoreduction, multiple α-fragmentation, photoxidation, chlorination (fragmentation of dichloromethane to $CH_2Cl\bullet$ and $Cl\bullet$, furhter radical attack of anthracene and/or chlorine molecule recombination with consequent adition-elimination substitution to aromatic ring – see Scheme 2 and 3).

9-nitroanthracene underwent rearrangement to nitrite, which was dissociated to radicals RO-NO → $RO^\bullet$ + $^\bullet NO$. Possible further reactions in the state 3(n, π*) were hydrogen cleavage from an acceptable donor (solvent), oxidation or reduction.

Methylanthracenes degraded in similar way as anthracene. Methyl-group does not influence photostability of anthracene to an excessive degree.

Table II
Degradation photoproducts of anthracene and its derivatives

PAH	Photoproducts – isooctane
Anthracene	9,10-anthraquinone, anthrone, phthalic anhydride, 9*H*-fluorenone, 4-hydoxy-9H-fluornenone, hydroxyanthrone
9-nitroanthracene	9,10-anthraquinone
1-methylanthracene	9,10-anthraquinone, 1-methylanthracenediol, anthrone, anthraldehyde, anthracene
2-methylanthracene	9,10-anthraquinone, 1-methylanthracenediol, 9,10-dihydro-1-methyalnthracene, anthrone, anthraldehyde, anthracene
9-methylanthracene	9,10-anthraquinone, 1-methylanthracenediol, anthrone, anthraldehyde, anthracene, 10-hydroxy-9-anthrone
Anthrone	9,10-anthraquinone, anthracene, phthalic anhydride, 9*H*-fluorenone, 9,10-anthracenediol, 4-hydroxy-9H-fluorenone, hydroxyanthrone
9,10-anthraquinone	anthrone, hydroxyanthrone, phthalic anhydride, 9*H*-fluorenone, 4-hydroxy-9H-fluorenone
PAH	**Photoproducts dichloromethane**
Anthracene	9,10-anthraquinone, anthrone, 2,2'-diethyl-1,1'-biphenyl, 2-hydroxybenzoic acid, benzofurane, 2-hydroxyphenacetic acid, hydroxy-9,10-anthraquinone, phthalic anhydride, benzoic acid, 9,10-anthracenediol, 9*H*-fluorenone, 4,4'-dichlorobenzophenone
9-nitroanthracene	9,10-anthraquinone, anthrone, anthracene, phthalic anhydride, chloro-9,10-anthraquinone, dichloro-9,10-anthraquinone, chloro-benzendicarboxylic acid
1-methylanthracene	9,10-anthraquinone, 1-methylanthracenediol, anthrone, anthraldehyde, anthracene
2-methylanthracene	9,10-anthraquinone, 1-methylanthracenediol, 9,10-dihydro-1-methyalnthracene, anthrone, anthracenecarbaldehyde, anthracene
9-methylanthracene	9,10-anthraquinone, 1-methylanthracenediol, anthrone, anthraldehyde, anthracene, 10-hydroxy-9-anthrone
Anthrone	9,10-anthraquinone, anthracene, phthalic anhydride, 9*H*-fluorenone, 9,10-anthracenediol, 4-hydroxy-9*H*-fluorenone, hydroxyanthrone, 10-chloroanthraldehyde
9,10-anthraquinone	anthrone, hydroxyanthrone, phthalic anhydride, 9*H*-fluorenone, 9,10-anthracenediol

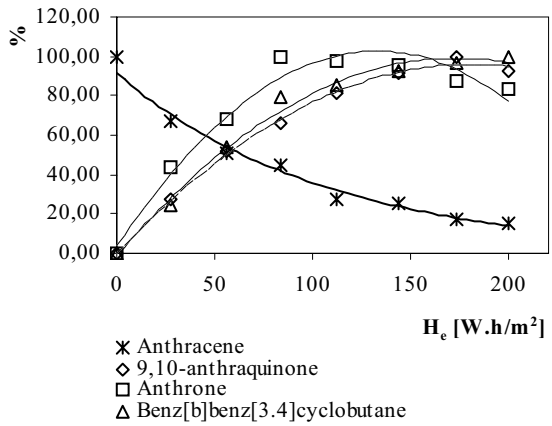

Fig. 1. **Photodegradation of Anthracene in isooctane (ISO)**

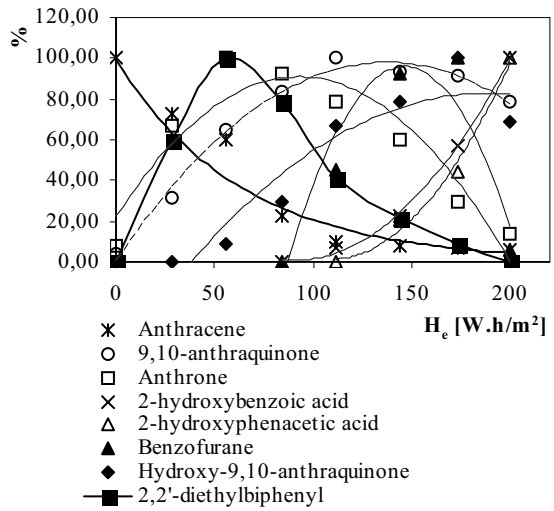

Fig. 2. **Photodegradation of Anthracene in dichloromethane (DCM)**

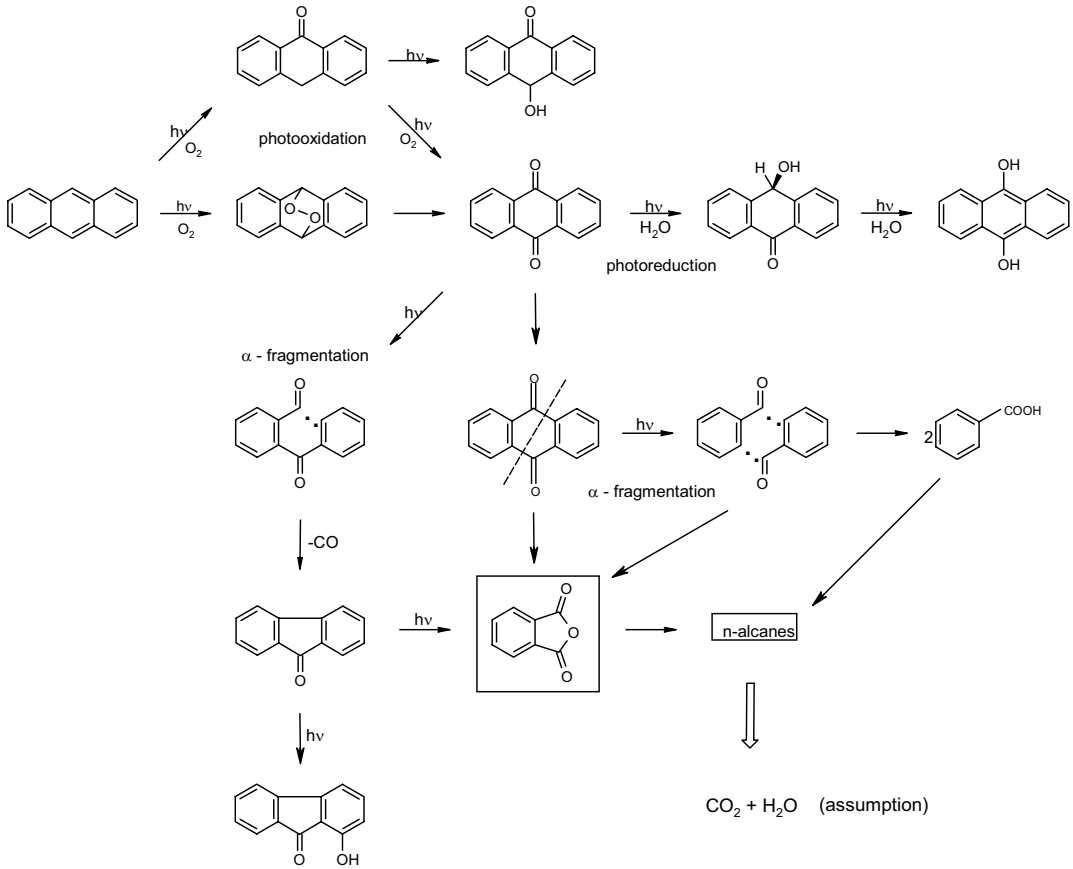

Scheme 1 **Photodegradation of anthracene in isooctane**

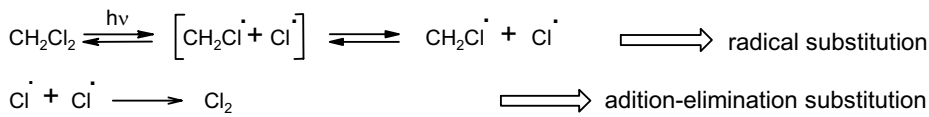

Scheme 2 **Fragmentation of dichloromethane**

Scheme 3 **Photodegradation of anthracene in dichloromethane**

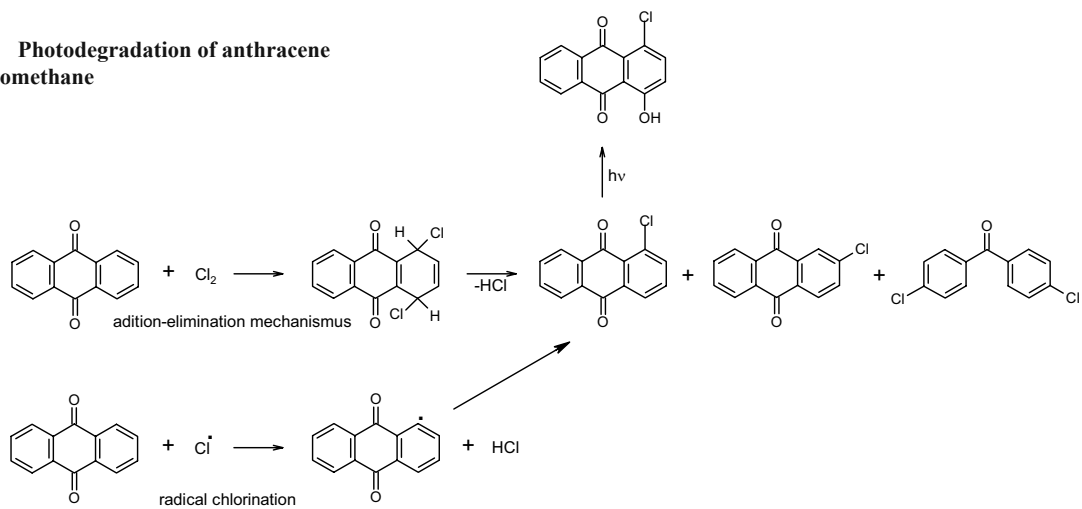

Conclusion

Photostability of anthracene, its methyl- derivatives and anthrone is similar. Reactivity of methyl- derivatives decreased in sequence: 9-methylanthracene > 1-methylanthracene > 2-methylanthracene. 9,10-anthraquinone as one of the most significant indentificated degradation products (vide infra) was very stable but on the other hand 9-nitroanthracene completely decomposed in one hour. It was due to photolabile chromophoric group $–NO_2$, which contributed to a more rapid oxidation and substitution of aromatic ring.

Photooxidation was the most significant reaction of PAHs and NPAHs in UV-VIS interval of spectrum. Main photoproducts of this reaction in both solvents were carbonyl and carboxyl compounds. Chlorinated derivates of PAHs and NPAHs were formed in dichloromethane owing to its photolytic instability.

This work was partly supported by the Czech Ministry of Agriculture, grant No. MZE 0002716201.

REFERENCES

1. Letho K. M., Vuorimaa E., Lemmetyinen J. H.: Journal of Photochemistry and Photobiology, A: Chemistry. *136*, 53 (2000).
2. Barbas J. T, Dabestani R., Sigman M. E.: Journal of Photochemistry and Photobiology, A: Chemistry. *80*, 103 (1994).
3. Dabestani R., Ellis K. J., Sigman M. E.: Journal of Photochemistry and Photobiology, A: Chemistry. *86*, 231 (1995).
4. Dabestani R., Nelson M., Sigman M. E.: Journal of Photochemistry and Photobiology, A: Chemistry. *64*, 80 (1996).
5. Barbas J. T, et al.: Journal of Photochemistry and Photobiology, A: Chemistry. *109*, 229 (1997).
6. Reyes C. et al.: Journal of Photochemistry and Photobiology, A: Chemistry. *112*, 277 (1998).

P07 DEACIDIFICATION AND STABILIZATION OF PAPER

KATARÍNA ČEPCOVÁ[a], ALENA MAKOVÁ[b] and BOHUSLAVA HAVLÍNOVÁ[a]

[a]*Faculty of Chemical and Food Technology STU, Department of Graphic Arts Technology and Applied Photochemistry, Radlinského 9, Bratislava, Slovak Republic, bohuslava.havlinova@stuba.sk,* [b]*SNK, J. C. Hronského 1, Martin, Slovak Republic,*

Introduction

Paper as a record medium, documenting the history of each nation, is determined by its durability. The paper ages and changes its characteristics during the time, which results in gradual degradation and disintegration as a final consequence. For stability evaluation of the paper material characteristics a permanence, indicating the preservation of the original paper properties accenting the chemical stability, is defined. The permanence changes are described by chemical parameters[1].

Taking the effect of warm and wet during the time, the change in paper characteristics comes up. One of the most important mechanism is the acid hydrolysis. Acid hydrolysis is a hydrolytic decomposition of glycosidic bonds of cellulose and hemicellulose macromolecules, catalyzed by present acids, H^+ ions. The decomposition of the paper as a consequence of acid hydrolysis could be ceased (or significant delayed) by inactivation of free acids present in the paper, with neutralization. The alkali reserve in the form of calcium carbonate, or magnesium carbonate, loaded simultaneously into the paper creates the reserve for progressive neutralization of incipient acids formed as a consequence of natural ageing and absorption of airy oxides of S and N. This reserve prevents the fibers for ageing until depletion of this reserve. Such a paper becomes suitable for archiving and long-time storage.

In our work, we choose the modification of water neutralization, for purpose of paper neutralization and creating adequate alkali reserve, following the utilization of antioxidant (reducer, deoxidizer)[2] for delaying of degradation and additionally straining of the paper with sizing to improve the mechanical properties and general stability of the paper samples[3].

In present work we are monitoring the changes of chemical properties (pH of cold aqueous extract and alkali reserve) and optical properties (b-parameter) of acid paper support, during accelerated ageing by using the dry hot air and wet hot air, to define the suitability of the paper samples for archive purposes as a consequence. Accelerated ageing was realized according to norm STN ISO 5630 dry hot air (105 °C) and wet hot air (85 °C, 65 % RH) during the time period of 0, 1, 3, 7, 14 and 28 days. We suppose that 3 days under such a conditions (dry hot air) correspond to 25 years of natural ageing[4].

Experimental procedure

Used materials: Within the accelerated ageing method we applied hot dry air (105 °C) and hot wet air (85 °C, 65% RH) methods to writing partly groundwood acid paper (80 g m^{-2}, pH = 4.4 made in Slavošovské papierne, Slavošovce, Slovak Republic). For modification of paper samples we used deionized water, magnesia hydrogen carbonate, calcium hydrogen carbonate, potassium iodide and Empresol N.

Apparatus and experimental methods: Paper samples were conditioned according to norm STN ISO 187 by temperature of 23 °C and 50% RH for 24 hours before particular measurements.

By measuring of chemical properties of paper samples we observed the STN and STN ISO norms, experiments were realized on following apparatus:

JENWAY 3510 pH Meter

ELREPHO DATACOLOR 2000

Sample preparation (method, procedure):

eluting unmodified paper (N) in deionized water for purpose of soluble acid products (K)

deacidification with the aim of neutralization of paper and creating alkali reserve (Mg)

second neutralization for the purpose of increasing of the generated alkali reserve (Ca)

using an antioxidant for the retardation of paper degradation during the ageing (S)

glue sizing for modification of mechanical properties of paper (E).

Results and discussion

One of the most important decrease of pH values during application of accelerated ageing (with dry and wet air) occurs by Empresol modified samples (KMgSE, KMgCaE), applied for improvement of mechanical properties. Minimal changes were obtained by samples treated by neutralization (dry air accelerated ageing, KMg) and by samples conditioned with antioxidant (the deceleration of decreasing pH values in spite of following use of Empresol is evident).

The Fig. 1a, 1b shows the pH values in the given time of ageing depending on influence of particular modifications. As the figure illustrates, the partial modification of the paper

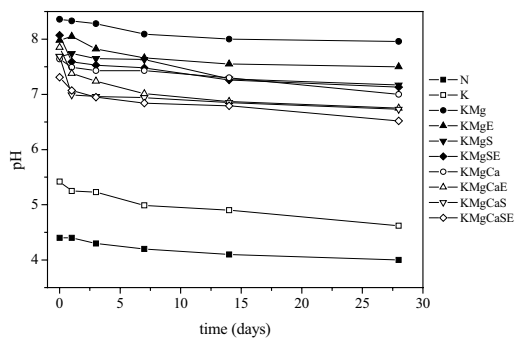

Fig. 1a **pH values in the given time of dry hot air accelerated ageing in the dependence of the influence of particular modifications**

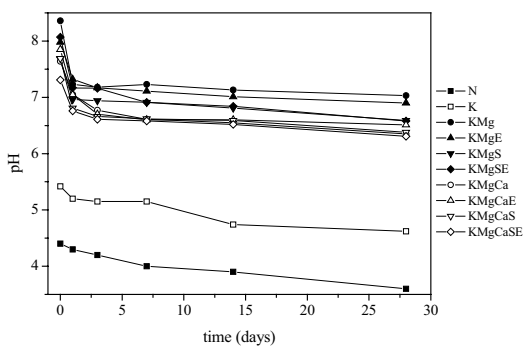

Fig. 1b **pH values in the given time of wet hot air accelerated ageing in the dependence of the influence of particular modifications**

samples with eluting by deionized water results in a low increase of pH values. The using of Empresol has a positive effect on stabilization of pH values in opposite to the low negative effect of using the antioxidant (however it is offset by the stabilization of samples during ageing, in the opposite to samples with applied Empresol).

The minimal change of alkali reserve values after accelerated ageing with dry air (Fig. 2a) occurs by samples treated by second neutralization and using antioxidant, decreasing the negative effects of Empresol, which causes the greatest decrease of alkali reserve values (KMgE). In the case of wet air accelerated ageing (Fig. 2b), the positive influence of antioxidant application (KMgCaS, KMgCaSE) is verified.

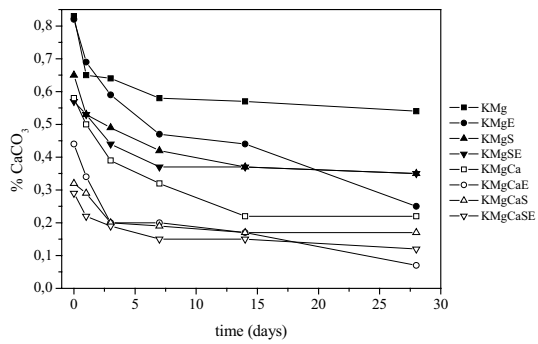

Fig. 2a **Alkali reserve values in the given time of dry hot air accelerated ageing in the dependence of the influence of particular modifications**

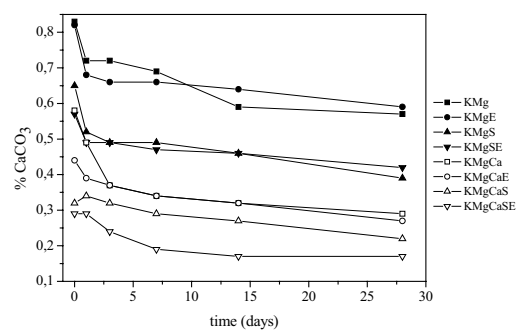

Fig. 2b **Alkali reserve values in the given time of wet hot air accelerated ageing in the dependence of the influence of particular modifications**

The minimal change of chromaticity coordinate b* values until accelerated ageing (Fig. 3a, 3b) occurs by samples treated by second neutralization and using an antioxidant (KMgCa and KMgS). The most important increase of chromaticity coordinate b* values were obtained by unmodified samples, eluted by deionized water and by Empresol modified samples (KMgSE, KMgCaSE).

Conclusion

We studied the changes of chemical properties (pH of cold aqueous extract and alkali reserve) of acid paper sam-

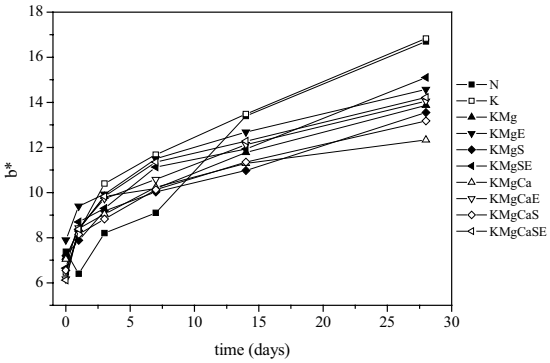

Fig. 3a **Chromaticity coordinates b* values in the given time of dry hot air accelerated ageing in the dependence of the influence of particular modifications**

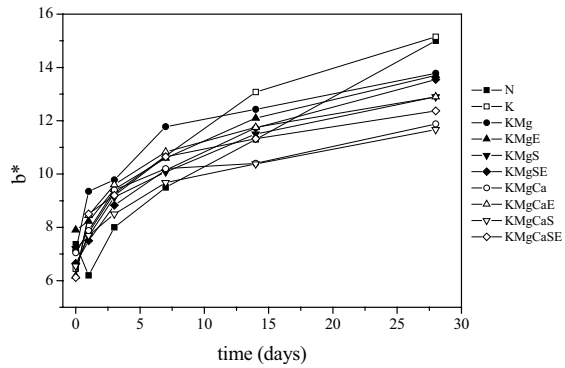

Fig. 3b **Chromaticity coordinates b* values in the given time of wet hot air accelerated ageing in the dependence of the influence of particular modifications**

ples before and after applied accelerated ageing. We used series of modifications for deceleration of paper degradation (eluting with deionized water, neutralization, stabilization with antioxidant and straining by sizing). Considering the obtained experimental results we can predicate that the studied properties are considerably improved and the ageing after modification of paper samples (especially after neutralization and using antioxidant) is decelerated.

This work was supported by Science an Technology Assistance Agency (Slovakia) under the concract No. APVT-20-03 4202.

Ministry of education of the Slovak Republic for the financial support of projects KNIHA SK.

REFERENCES

1. Havlínová B., Brezová V., Belányi F., Szeiffová G.: Papier a celulóza *57*, 338 (2002).
2. Kolar J., Strlič M.: *Stabilization of alkaline cellulose with halides and pseudo-halides*, WPP 2003: 422–423
3. Maková A.: *Natívne a modifikované škroby v reštaurátorsko-konzervátorskej praxi*, Buničina a papier, Zbor. z medzin. konf., pp.189-197, 2001.
4. Bukovský V.: Restaurator 77 (1999).

P08 ORGANIC MATERIALS FOR PHOTOVOLTAIC SOLAR CELLS

KAROLÍNA ČERNÁ and MARTIN WEITER
Institute of Physical and Applied Chemistry, Faculty of Chemistry, Brno University of Technology, Purkyňova 118, 612 00, Brno, cerna@fch.vutbr.cz

Introdution

An interesting alternative for inorganic solar cells is given by the semiconducting polymers, which combine the optoelectronic properties of conventional semiconductors exhibit the excellent mechanical and processing properties of polymeric. These can be processed from the solution at the room temperature onto flexible substrates using simple and therefore cheaper deposition method like spin coating. Organic electronic materials are particularly conjugated solids where both optical absorption and charge transport are dominated by partly delocalized π and $\pi*$ orbitals. In these materials photo-generated excitons are strongly bound and do not dissociate into separate charges. Charge transport proceeds by hopping between localized states, rather than transport within a band, which results in low mobility. The spectral range of optical absorption is relatively narrow compared to the solar spectrum and absorption coefficients are high ($\sim 10^5$ cm^{-1}) so that high optical densities can be achieved.

The device consisted of a layer of organic material sandwiched between two different conducting contacts, indium tin oxide (ITO) and low work function metal aluminium (Al). The difference in work function provides an electric field that drives separated charge carriers towards the respective contacts. This electric field is seldom sufficient to break up the generated exciton. Instead the exciton diffuses within the organic layer until it reaches a contact, where it may be broken up to supply separate charges, or recombine. Since exciton diffusion lengths are short, typically 1–10 nm, exciton diffusion limits charge carrier generation in such a device. Photo-carrier generation is, therefore, a function of not only bulk optical absorption, but also of available mechanisms of exciton dissociation. Other loss factors are non-radiative recombination at the interfaces and non-geminate recombination at impurities or trapped charges.

Experiment

In our experiments we characterize materials including phenyl-substituted poly(phenylene vinylene) type copolymer (PhPPV), poly[2-methoxy-5-(2'-ethylhexyloxy)-1,4-phenylene vinylene] (MEH-PPV), poly[2-methoxy-5-(3', 7'-dimethyloxy)-1,4-phenylene vinylene] (MDMO-PPV), poly[2-methoxy-5-(2-ethyloxy)-1,4-phenylene vinylene-alt-1,4-phenylene vinylene] (poly(MEHPV-alt-PV)), poly(N-

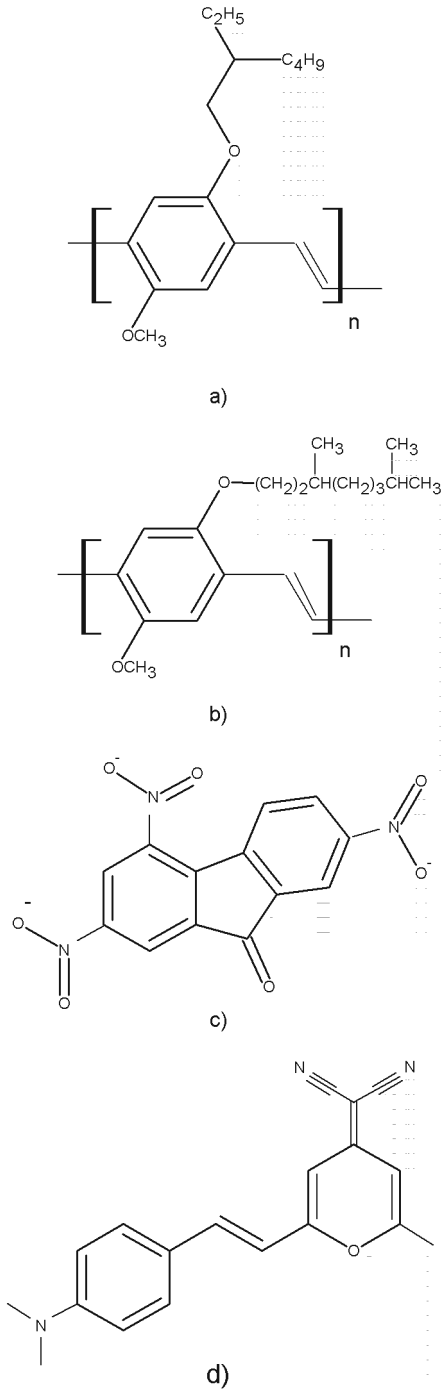

Fig. 1. **The chemical structure of a) MEH-PPV, b) MDMO--PPV, c) TNF and d) DCM**

-vinylcarbazole) (PVK). These materials were doped by 2,4,7-trinitro-9-fluorenone (TNF), 6-nitro-1',3',3',-trimethylspiro(2H-1-benzopyran-2,2'-indoline) (SP), 4-(Dicyanomethylene)-2-methyl-6-(p-dimethylaminostyryl)-4H-pyran (DCM), 9-(2-carboxyphenyl)-3,6-bis(diethylamino)xanthylium chloride (Rhodamine), perylene diimide (Per). Examples of their chemical structure are given in Fig. 1.

In order to describe the power conversion efficiency η of solar cell the maximum output power P_{max} has to be related to the power of the incident light P_{light}

$$\eta(\lambda) \equiv \frac{I_{SC}(\lambda) \cdot V_{OC}(\lambda) \cdot FF(\lambda)}{P_{light}},$$

where λ is proper wavelength, I_{sc} is shortcut current i. e. current at zero voltage, V_{oc} is open circuit voltage i. e. voltage at zero current and *FF* is the fill factor comprising the series resistance from the ohmic loss in the two electrodes and the shunt resistance from leakage currents. The current-voltage characteristics were measured by Keithley 6517A electrometer. For particular device characterization an impedance spectroscopy was used. It allows one to investigate intrinsic material parameters, such as frequency dependence of the conductivity, device structure and interfacial stability of the polymer layer. This would provide better insight into the mechanism of carrier transport and thus would make way to improve device performance. The impedance measurements were performed using HP 4192A LF impedance analyzer.

Results

The aim of this work was the study of the processes connected with exciton dissociation in a bulk of doped semiconducting polymers. Power conversion efficiency measurements on PPV derivatives without and with controlled doping show that intentional doping by 1% can therefore increase the photogeneration of charge carriers by about a factor of 2 only. The higher concentrations of dopants increase the power conversion efficiency η till dopant concentration of about 25 %. However the power conversion efficiency does not exceed 0.1 %. On the contrary, the dopant concentrations increase the recombination of the charge carriers and thus decrease η. The efficiency of charge generation is strongly dependent on the applied electric field. These results are in good agreement with results published in[1–3].

The measured data (complex impedance *Z* obtained by impedance spectroscopy) were analyzed in the form of Cole--Cole diagram (Real part of (*Z*) vs. imaginary part of (*Z*)) wherein the frequency increases from right to left. This figure shows the pronounced voltage dependence of the device impedance in the low frequency range. At high frequency region the impedance is independent of bias voltage and shows a small semicircle close to origin. With increasing bias voltage, two distinct semicircles are detectable and simultaneously at higher voltage the right semicircle disappears. These two semicircles observed in the Re(*Z*) and Im(*Z*) plot may be represented by a parallel combination of bulk resistance (*Rb*) and capacitance (*Cb*) in series with a parallel arrangement of the junction resistance (*Rj*) and capacitance (*Cj*). The low frequency semicircle corresponds to junction region, whereas the high frequency semicircle corresponds to bulk region.

This work was supported by the grant 203/03/133 from the Czech Science Foundation and by 0021630501 the pro-

ject No. 0021630501 from the Ministry of Education, Youth and Sports.

REFERENCES

1. Havlínová B., Brezová V., Belányi F., Szeiffová G.: Papier a celulóza *57*, 338 (2002).
2. Kolar J., Strlič M.: *Stabilization of alkaline cellulose with halides and pseudo-halides*, WPP 2003: 422–423
3. Maková A.: *Natívne a modifikované škroby v reštaurátorsko-konzervátorskej praxi*, Buničina a papier, Zbor. z medzin. konf., pp.189–197, 2001.
4. Bukovský V.: Restaurator 77 (1999).

P09 DYNAMIC CONTACT ANGLE MEASUREMENTS ON HYDROPHILIC SURFACES

PETR DZIK and MICHAL VESELÝ
Faculty of chemistry, Brno University of Technology, Purkyňova 118, 612 00 Brno, Czech Republic, petr@dzik.cz

Introduction

Contact angle (CA) measurement is probably the most common method of solid surface tension measurement. It can provide us with important information about the studied surface properties, while the instrumentation is quite straightforward using relatively inexpensive equipment. However, the interpretation of measured data is not always unambiguous and the correct use of CA measurement requires understanding of the thermodynamic status of the observed angles.

In 1805 formulated T. Young the relation expressing the equilibrium between the forces on liquid droplet on solid surface (Fig. 1.).

$$\gamma_{sg} - \gamma_{sl} = \gamma_{lv} \cos \theta,$$

where γ_{ij} represent the equilibrium interfacial tension between solid, liquid a vapor phases and θ is the so called wetting angle (the contact angle between the liquid and solid phase). From the thermodynamic background of this phenomenon, it follows that the surface tension is the parameter that controls the surface composition of a material. It will control all the physical interfacial events, such as the surface composition of an isolated material, wetting phenomena and adhesion behavior. Therefore the solid surface tension value is a very important variable characterizing the surface properties.

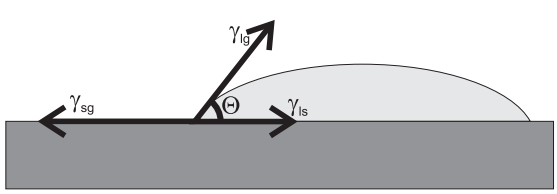

Fig. 1. **Forces acting on a liquid – solid – vapor interface**

If we want to determine the solid surface tension value from the contact angle measurements, we have to face to problems:

1. The problem coming from the Young's relation is that only two of the four variables of the Young's equation can be readily measured, that is the *liquid interfacial tension* and the *contact angle*. If we want to obtain the solid surface tension, a further relation must be found (if it exists at all): $\gamma_{sl} = f(\gamma_{sg}, \gamma_{lv})$. The search for this relation has been continuing since the presentation of Young's theory. Since then, several theories describing this relation have been proposed and much controversy has arisen between them. At present, no general theory applicable to any surface type exists. The existing theories are usually designed to describe a certain type of surfaces.

2. Other problems arise from the non-ideal behavior of the drop deposited on the analyzed surface. Instead of the single equilibrium contact angle value predicted by Young's equation, the drop usually is able to *occupy a range* of contact angles. Moreover, the CA on some surfaces has tendency to be *dependent on time*.

In this paper, the authors would like to point out some aspects of measuring contact angle on real, non-ideal hydrophilic surfaces, where the problems described in point 2 are significantly pronounced.

CA measurement challenges

As mentioned above, a drop of liquid deposited on a real surface suffers from two major deviations from the behavior predicted by Young's equation. The most obvious one, which takes place on most real surfaces, is the existence of a range of allowed contact angles. This phenomenon is often referred as thermodynamic CA hysterezis and can be most clearly illustrated by depositing a drop on a real surface and increasing and decreasing its volume (Fig. 2.) If the drop behavior was ideal, it would continuously increase/decrease its contact area with the support without changing the CA value. Instead,

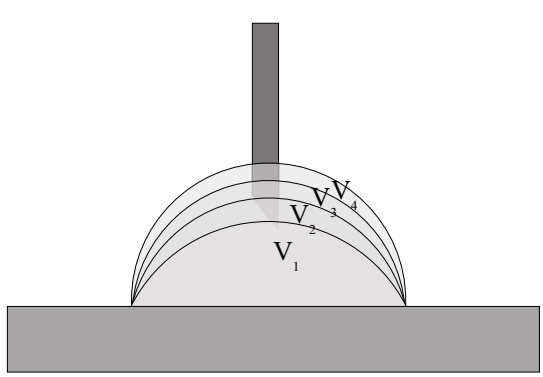

Fig. 2. **A the drop volume increases, drop can occupy a range of allowed contact angles**

different values of CA can be observed and the contact area changes step-wise when the drop volume exceeds a limiting values. Consequently, different CA values can be measured for advancing and receding drop.

This problem was addressed by Wenzel and Cassie who modified the Young's equation in order to include the influence of surface roughness and heterogeneous domain structures, that are believed to be the cause for this behavior. Wenzel proposed the relation

$$r\,(\gamma_{sg} - \gamma_{sl}) = \gamma_{lv} \cos\theta,$$

where r is so called roughness factor (Fig. 3.). Cassie included the effect of domain patchy structure of real surface. For a two component heterogeneous surface structure,

$$\cos\theta_c = Q_1 \cos\theta_1 + Q_2 \cos\theta_2,$$

where Q is the fractional coverage and θ is its Young contact angle.

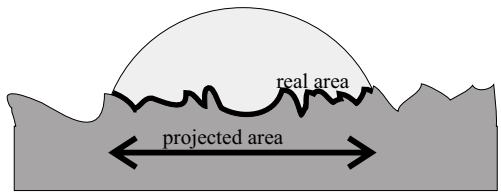

r = real area / projected area

Fig. 3. **The influence of real surface roughness**

The observed hysteresis of contact angle can be explained using these two phenomena in the following way: The presence of surface roughness and heterogeneities give rise to a large number of meta-stable states of the drop shape. These local energetic minima then hinder the free motion of drop, creating energy barriers that result into a range of allowed CA values.

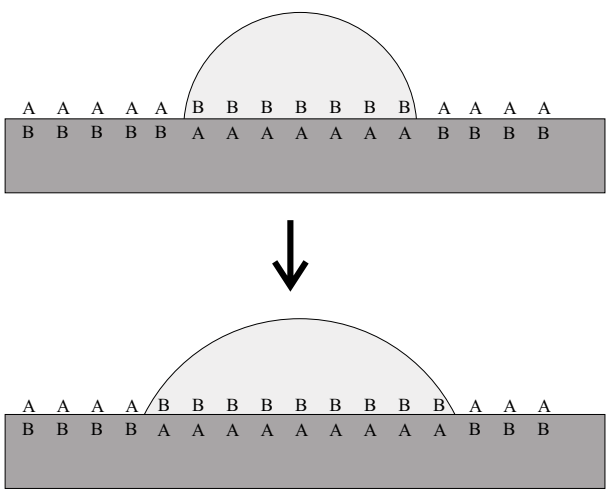

Fig. 4. **CA change due to network segment reorientation**

Apart from the decribed time-independent thermodynamic hysterezis, some surfaces exhibit a kinetic hysterezis, caused by time dependent solid-liquid interactions. These interactions result into the modification of the solid or liquid phase or both. If the measurement time scale is comparable to the interaction time scale, a time-dependance of observed CA will be present.

Such behavior is often present in materials of amphiphilic nature that contain two components of different hydrophility. Typical examples include swollen gels whose network segments keep a certain level of mobility. In such a system, the network segments have tendency to reorient on contact with a liquid phase to occupy an energetically more favourable position. Such reorientation will then result into a change in the surface energy and the contact angle value be chancing with time.

Experimental Example

The authors have adopted the CA kinetic hysteresis measurement for the study of swelling behaviour of crosslinked PVAl films and their interaction with aqueous phase. The studied materials were synthetized by our team and are intended as ink-jet printing substrates. Obviously, during ink-jet printing, quite the same processes take place as during the CA measurement, therefore this analysis can give us important information about the behavior of ink drops on the prited substrate.

So the aim of this measurement was to obtain the data for the dependence of the water droplet contact angle value on time. The measurements were done on the Contact Angle System OCA machine equipped with a TV camera transferring the image into a PC. The images from the camera were transferred to a PC, digitalized and the contact angle was calculated by the controlling software. The contact angle was measured in 2-second intervals as long as the drop kept shape enabling the software to calculate the contact angle. The droplet spreading rate obtained by this method of measurement is expressed as the slope of the graph of contact angle versus time. Naturally, the obtained data have no absolute scale, but this method can be used for the comparison of relative properties of individual samples.

The data for 3 samples of modified PVAl before and after crosslinking are presented. PVAl was modified with varying amount of maleic anhydride and then crosslinked by photoinitiated polymerization. The measured data is summarized in Table I. The first trend to be observed it the CA increase with the conversion degree; the polymer becomes more hydrophobic. One interesting aspect should be noted: As the amount of modifying agent increases, so does the drop spreading rate. This can be assigned to the decrease of crystalline fraction in modified polymer and/or reduced hydrogen bonding between PVA chains. As more maleic groups are introduced, these prevent the polymer chains from acquiring long-range order and the concentration of crystalline domains is lower, therefore the chain segments are are more mobile upon swelling. Naturally, the extend of crosslinking increases with the

amount of modifying agents as determined by another study. After crosslinking, a decrease in drop spreading rate is observed in all cases, indicating that macromolecular segment movement was hindered by created crosslinks. However, the *relative change* in water droplet spreading rate is the biggest in the case of sample A (the least modified sample). It seems that the influence of crosslinking is the most prominent in the case of least modified sample, resulting into the greatest change.

Table I
CA measurement data

Sample No	Crosslinkable groups conten [molar %]	Initial water CA [°]	Drop spreading rate [°. s^{-1}] raw	crosslinked	Relative change
A	2.5	70±2	0.0644	0.0212	3.0297
B	5.1	76±2	0.1020	0.0379	2.6889
C	8.3	79±2	0.1337	0.0710	1.8813

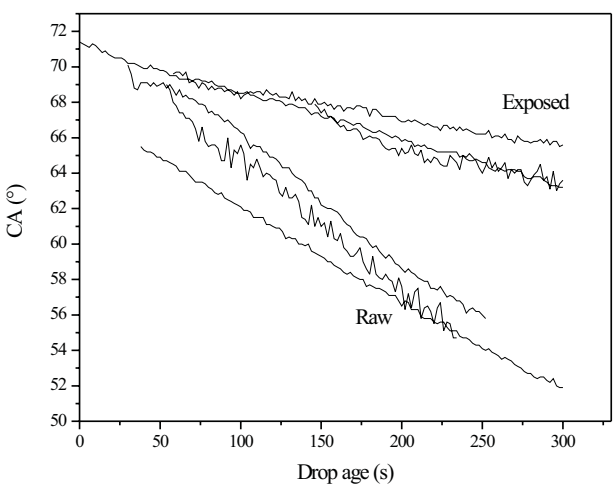

Fig. 5. **Sample A – the difference in drop spreading rates before and after crosslinking**

Conclusion

Contact angle measurement is a straightforward and powerful method for surface analysis. However, the interpretation of measured data is not always unambiguous and the correct use of CA measurement data requires understanding of the thermodynamic status of the observed angles. Advanced CA measuring techniques taking into account the thermodynamic and kinetic hysteresis can provide us with even more specific information on the surface nature. This is illustrated by an example of crosslinked PVAl study.

P10 STUDY OF HUMIC ACIDS BY SYNCHRONOUS FLUORESCENCE SPECTROSCOPY

NADĚŽDA FASUROVÁ and HANA ČECHOVSKÁ
Brno University of Technology, Faculty of Chemistry, Institute of Physical and Applied Chemistry, Purkyňova 18, 612 00 Brno, Czech Republic, fasurova@fch.vutbr.cz

Introduction

Humic substances (HS) like humic acids (HA), fulvic acids (FA) and humins play the major role in natural process, for example in soils. The quality of soils depends on physical and chemical properties of this compounds. The natural origin of HS can be separated in to soils, peats, lignitic, lakes, seas and rivers humic substances. The composition of humic acids depends on many factors. This fact is mainly dependent on locality with different degree of decay died organisms and residues of plants and therefore with different content of C, N, O and S. The structure of HA is complex because it includes more aromatic polycyclic compounds with substituents such as carboxyles, amino groups, hydroxyles. Humic acids include both low molecular and high molecular chains.

Samples of HA or FA can be characterised by different spectral methods as UV-VIS, IR, EEM, SFS etc.

It is generally known that after excitation of humic acid molecules, emission is observed. Fluorescence measurements can be used for multicomponental analysis. The Excitation- emission matrix (EEM) is frequently used[1]. The SFS method (Synchronous fluorescence spectroscopy, or Synchronous fluorescence scan spectroscopy) is another common fluorescence method for humic substance analysis[2,3]. The term „synchronous“ means measurement under a constant difference of both monochromators, marked as Δλ. The resulting SFS spectra are of higher resolution of spectral peaks than for example EEM.

Methods

Humic acids were isolated from South Moravian lignite (Mikulčice, Czech Republic) using alkaline extraction with NaOH and $Na_4P_2O_7$ (standard procedure of International Humic Substances Society = IHSS). The extract was purified with precipitation of HCl and HF solution, and then the preparate was washed, centrifugated and dried. The sample of isolated HA was dissolved in 0.5 M-NaOH solution and pH has been adjusted by 0.5 M-HCl to 7. This solution was dialysed in water with Spectrapor dialyses membranes, 3500 MWCO (Spectrum Labs.). This way, two preparates of sodium humates NaHAN and NaHAHJK were prepared. After dialysis, the NaHAN sample was dried and NaHAHJK was lyophilized. For fluorescence measurement these preparates of sodium humates were dissolved in distilled water and pH value was adjusted with HCl or NaOH solution in range from 3 to 9. One sample of humic acid (LHA) was dissolved in NaOH. Concentration of samples was 0.01 g dm^{-3}.

A sample of humic acid LHA (Leonardite humic acids standard) was ordered from IHSS, a sample of humate tech-

nical quality NaHAR was ordered from Humintech Corp. (Catalogue name: Humin S-775).

Synchronous fluorescence spectra were measured with Aminco Bowman spectrofluorimeter, Series 2. The synchronous scan spectra were measured in the range of the wavelength from 300 to 600 nm, at the constant monochromators distance of $\Delta\lambda = 20$ nm. The samples were measured in to Suprasil cuvette (1 cm) at room temperature.

Results

In this work were compared results of SFS measurements of sodium humates and one sample of humic acid (LHA). Preparation of sodium humate salt is needed for a better solubility in water, because humic acids are soluble in alkaline solutions, only. Synchronous fluorescence spectra from 300 to 600 nm, at pH value 7 and concentration 0.01 g dm^{-3} are showed on the Fig. 1. From this figure can be seen that all samples have seven peaks at the same wavelengths. Synchronous fluorescence spectra were observed at $\Delta\lambda$ 20 nm at $\lambda_{ex.}/\lambda_{em.}$: 468/488, 340/360, 360/380, 400/420, 450/470, 480/500, 492/512 nm. The main peak was marked at 488 nm. The most intensive SFS spectra at 488 nm has NaHAR sample with highest intensity 6.12. The lowest intensity of fluorescence 3.46 had NaHAHJK sample. Humate NaHAHJK had the lower content of carbon and on the contrary LHA sample had the highest content of carbon. It is well known, that lignitic HA contain more aromatic rings than for example soil HA. Therefore they show emissions above 450 nm. It is assumed that the emissions at 488, 500 and 512 nm give fluorophores with different substituents on the same aromatic ring. A fluorophores which emite under 480 nm are derivates of coumarine or quinone[3,4].

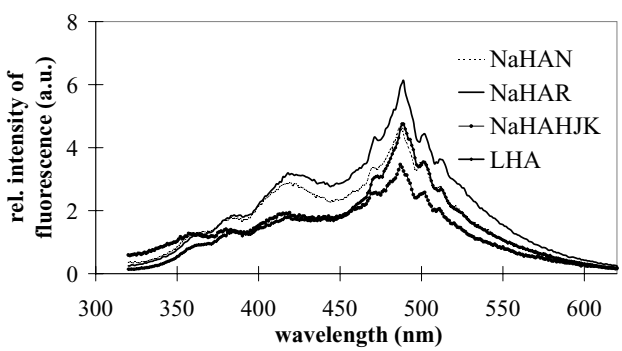

Fig. 1. **SFS spectra humates and LHA standard at Δλ 20 nm a pH 7**

The dependence of relative intensity of fluorescence on pH value was also studied for four following samples (two humic acids and two humate salts). The samples exhibited different spectral behaviour. As an example the spectrum of NaHAN are shown (Fig. 2.). Big changes in SFS spectra of sodium humate in pH from 3 to 9 were observed. It was supposed that significant influence of pH value on the structure of humate is at lower values. The most intensive spectrum had sample at pH 5.5. It corresponds to the changes in zeta potential measurements, too. At lower pH value on the particle surface hydrogen bridges are formed. The structure can be splitted into shorter and longer parts like the polymer chains. The lowest relative intensity of fluorescence had sample at pH 9.

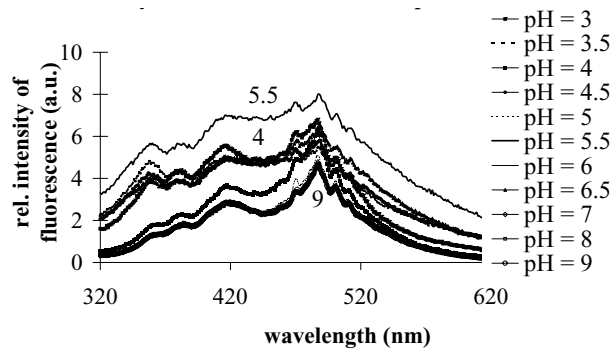

Fig. 2. **The dependence of relative intensity fluorescence on pH. SFS spectra of NaHAN sample at Δλ 20 nm**

This work was supported by Grant Agency of Czech Republic, "Study of colloidal properties of humic substances isolated from lignite" Project No. 104/03/D135.

REFERENCES

1. Sierra M. M. D., Giovanela M., Parlanti E., Soriano-Sierra E. J.: Chemosphere *58*, 715 (2005).
2. Pullin M. J., Cabaniss S. E.: The Environmental Science of Technology *29*, 1460 (1995).
3. Miano T. M., Senesi N.: The Science of the Total Environment, *117/118*, 41 (1992).
4. Valeur B.: *Molecular fluorescence. Principles and Applications,* Wiley-VCH Verlag, Weinheim-New York 2002.

P11 PREPARATION AND CHARACTERIZATION OF TRANSPARENT TiO_2 COATED GLASS

JANA CHOVANCOVÁ, MICHAL VESELÝ and JANA CHOMOUCKÁ
Brno University of Technology, Faculty of Chemistry, Institute of Physical and Applied Chemistry, Purkyňova 118, 612 00 Brno, Czech Republic, chovancova@fch.vutbr.cz

Introduction

Titanium dioxide (TiO_2) thin films find extensive application in several fields such as photocatalysts, photoelectrodes, electrochromic displays and gas sensors. A great deal of research has been directed at TiO_2 use in applications involving the photoreactions of organic materials, in particular the photodestruction of organic pollutants in the solid, liquid and gas phases. In the field of pollutant removal much work has been done with phenol, chlorophenols and related compounds[1].

Photooxidative transparent TiO_2 films on glass could form the basis for self-cleaning indoor windows, lamps or automotive windshields[2]. It has been known that TiO_2 thin films on glass have also anti-bacterial and anti-virus activities under ultraviolet irradiation.

This paper reports the preparation and physical characterization of TiO_2 transparent nanocrystalline thin film, together with results from kinetic studies of the photodegradation of 2,6-dichloroindophenol using this material.

Experimental

Materials

Ethanol p. a. (absolute, Penta), n-propanol pure (Lachema), titanium isopropoxide (97%, Aldrich), titanium butoxide (99%, Aldrich), acetylacetone p.a. (99.5%, Lachema), ethyl acetoacetate (99%, Aldrich), sulphuric acid (93%, Lachema), nitric acid (65%, Lachema).

Preparation of sol

Two types of sols were prepared: the first of titanium isopropoxide (TIP), the second of titanium tetrabutoxide (TTB). The former, according to Paz and Heller[3], was made of a precursor solution prepared by mixing 4.5 ml of TIP with 10 ml of propanol and 1.6 ml of acetylacetone. After aging for a week at room temperature (about 20 °C–25 °C), a casting solution was prepared by mixing 1.0 ml of the precursor solution with 1.8 ml of water/propanol (1 : 9 v/v). A clear yellow casting solution stable for at least two months was obtained.

The later sol was prepared as follows. We weight 7.1 g of TTB, put it into the beaker and slowly added 11.6 ml of ethanol from the burette. Then we prepared another solution into the different beaker by mixing 2.7 g of ethylacetoacetate, 11.6 g of ethanol and 0.2 g of nitric acid. We mixed these two solutions by adding the solution of ethylacetoacetate drop by drop into the constantly stirred alcoxide solution. A clear orange casting solution was obtained and stored in fridge.

Film preparation

The substrates used as film supports were soda-lime glass (50 × 50 × 1.2 mm). Substrates were cleaned just before performing the deposition process. It has been suggested by Heller and Paz[3] that migration of Na_2O from a soda-lime glass substrate into TiO_2 films causes a reduction in photocatalytic activity. Therefore the glass slides were successively immersed in boiling 50% H_2SO_4 for 45 min to avoid sodium ions effect. Finally, the substrates were washed with deionized water and dried.

Spin coating process: 400 µl of the casting solution was then spread on the glass substrate which was spun after the application for 1 or 2 minutes at different speed (1000, 1400, 1800 and 2200 rpm) to dryness using diaphragmal vacuum pump. In the next stage, the substrates coated by films of TIP were directly calcinated whereas when TTB was used, the films firstly hydrolyzed for 48 hours before being calcinated. The calcination transformed the product of the hydrolytic reaction into a microcrystalline oxide, removed all organic residues, and bound the TiO_2 film to the substrate. Multiple TiO_2 layers were produced by applying another layer after calcination process and by new calcining.

The deposited films were slowly heated at a rate of 10 °C min^{-1} to temperature of 450 °C and then holding at that temperature for 3 hours. Because of lack of soda-lime glass heat-resistance, the calcination temperature did not exceed 500 °C.

Photodegradation of 2,6-dichloroindophenol

The photocatalytic property of the TiO_2 films was evaluated by oxidation of 2,6-dichloroindophenol (2,6-DCIP) under UV irradiation. Photodecomposition reactions were performed in a beaker with stirring during the reaction to maintain uniform concentration and temperature. The spin-coated TiO_2 plate carrying either one, two or three coats of TiO_2 was immersed into a 100 ml reaction solution. The initial concentration of 2,6-DCIP was 1.10^{-5} M and the reaction temperature was around 25 °C. Air was continuously bubbled through the solution. Illumination was provided with medium pressure mercury lamp (125 W, Phillips) with intensity of 970 µW cm^{-2}. The lamp was placed in upper side of the reactor. The concentration of 2,6-DCIP was determined by measuring the absorbances at a wavelength of 596 nm in quartz cuvette using UV/VIS spectrometer Helios α (Spectronic Unicam).

Film characterization

TiO_2 film thickness measurements were performed using scanning electron microscopy (Quanta 200, Phillips). The samples were cut into pieces under nitrogen atmosphere. Film thickness was studied in the edges as well as in the middle. The films homogeneity was observed using optical microscope.

To determine the hydrophilic properties, the contact angle was measured by Contact Angle System, model OCA 10 (Dataphysics). It was observed a great decrease of

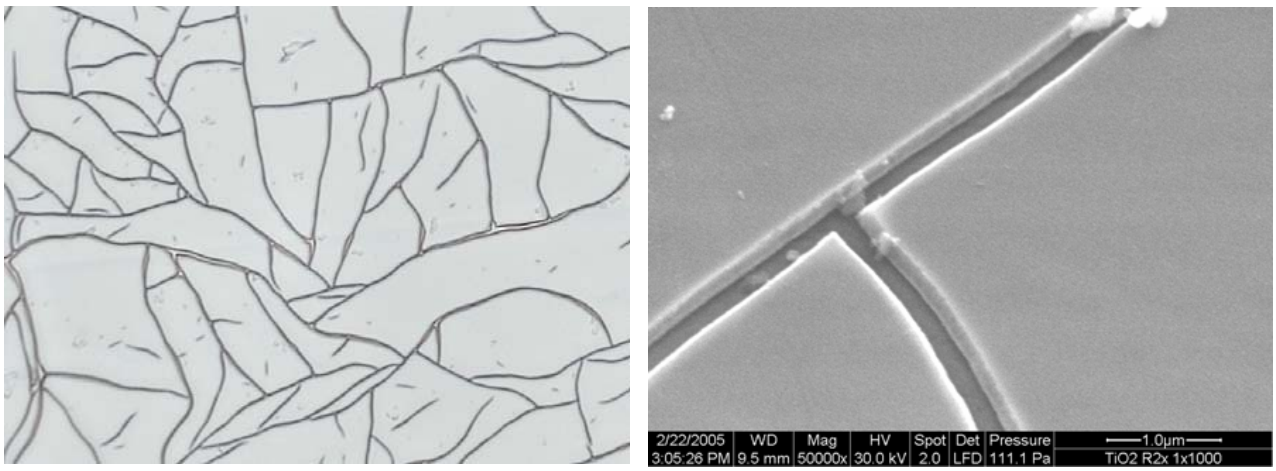

Fig. 1. **The TiO_2 layer in optical microscope with magnitude of 640 (left) and in SEM with magnitude of 50 000 (right)**

contact angle after exposing the coated slides to UV light of variable intensity.

Results and discussion

The obtained TiO_2 films showed reflection-interference colors (yellow, orange, pink and green) in dependence on the thickness and speed of spin coating process. The higher was speed of spin coating process, the thinner was TiO_2 film.

The film thickness was between 0.12–0.19 µm in dependence on the distance from the centre of glass substrate. The films are resistant to scratching, but they show a rough structure.

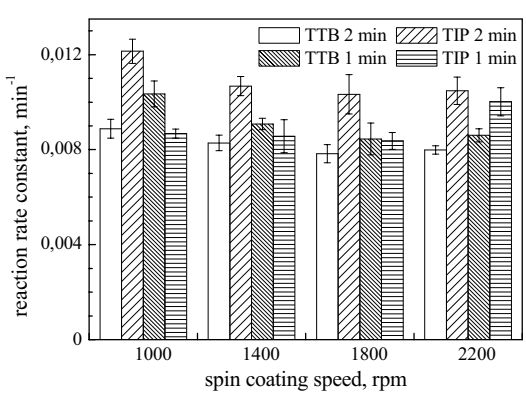

Fig. 2. **Dependence of 1. order formal reaction rate constants of 2,6-DCIP photooxidation on spin coating speed at coating time of 1 and 2 min for TTB and TIP once coated slide**

Conclusion

From the previous experiments we observed that sodium ions effect was significantly eliminated by treated the glass substrates in sulphuric acid prior to coating. We found that using of multiple TiO_2 layers did not improve the photocatalytic efficiency of TiO_2 films significantly and moreover, the layers did not adhere good to the glass substrates. Therefore we use only one TiO_2 layer for all next reactions.

In the case of 2 minutes coating time, the photocatalytic activity of TIP was 25 % higher compared with TTB. While for the spin coating time of 1 minute, the kinetic results of 2,6-DCIP photodegradation were almost the same for TTB and TIP. We observed that TIP layers possessed better optical and mechanical properties.

The follow up reactions did not induce the significant changes in photocatalytic efficiency, so we could use the same substrate repeatedly.

REFERENCES

1. Fretwell R., Douglas P.: J. Photochem. Photobiol. A: Chem. *143*, 229 (2001).
2. Oh S. H., Kim D. J., Hahn S. H., Kim E. J.: Mater. Lett. *57*, 4151 (2003).
3. Heller A., Paz Y.: PCT Int. Appl. WO 97 07069.

P12 SURFACE AND SOLUBILIZATION PROPERTIES OF HYALURONIC DERIVATIVES

MARTIN CHYTIL[a, b], VIEROSLAV KRÁTKÝ[b] and MILOSLAV PEKAŘ[a]
[a]*Institute of Physical and Applied Chemistry, Faculty of Chemistry, Brno University of Technology, Purkyňova 118, 612 00 Brno, Czech Republic; pekar@fch.vutbr.cz*
[b]*CPN Ltd., 561 02 Dolní Dobrouč 401, Czech Republic; mchytil@email.cz*

Introduction

Hyaluronic acid (HA) is a well-known and widely naturally occurring polysaccharide. It occurs in namely higher organisms, particularly in their connective tissues such as synovial fluid of joints, cartilage, vertebrate disks; it is a structural component of vitreous body of the eye[1] etc. HA can be produced by a fermentation of bacteria strains as well[2].

HA extraordinary properties, like a strong hydrophilic character, unique rheological properties, biocompatibility, etc., are used particularly in medicine – drug delivery, surgery, etc.[3] – pharmacy, cosmetics and elsewhere. To broaden its practical applications HA can be modified through its numerous functional groups. For instance, alkyl hydrophobic chains can be attached to the main backbone to change and control hydrophilic-hydrophobic behavior of the macromolecule[3]. Due to a presence of alkyl chains on the polysaccharide backbone, such modified HA could obtain a solubilization capability for drugs insoluble in water, and could be used as a drug carrier.

Solubilization requires existence of micelle-like aggregates with hydrophobic domains in a system. Classic methods investigating a micelle or aggregates formation are, for instance, surface tension measurement[4] and measurement of absorbance of a dye solubilized in hydrophobic domains, or another dye polarity probe of the dye's microenvironment[5].

Aim of the Research

The aim of this research was to carry out surface tension measurements of hyaluronic buffered aqueous solutions with regard to the length of an alkyl chain attached to the macromolecular backbone and to the *substitution degree (SD)* of single HA derivatives. Furthermore, to compare the surface tension measurement results with the results of method of a dye solubilization by the derivatives studied, and lastly, make an estimation of potential utilization of HA derivatives particularly in pharmacy.

Experimental

HA derivatives or **hydrophobically modified HA (hHA)** synthesized from a bacterially produced HA were investigated. Two types of hHA were provided: the derivatives with epoxy bound alkyl chains and the derivatives with carbamate bound alkyl chains to the polysaccharide backbone. The derivatives differed in molecular weights (30 000–850 000), in SD (3.3–100%), which represents number of alkyl chains per disaccharide unit of HA, and in the length of an alkyl chain (C4-C12).

Preparation of samples for surface tension measurement: samples were dissolved in a buffer into a set of solutions with appropriate concentrations. The buffer solution consisted of $H_2PO_4^-$, HPO_4^- ions, NaCl or KCl with pH 7. These solutions were let shaken for 24–48 hours at 25 °C. The measurements were performed at (23 ± 1) °C using K-10 KRÜSS tensiometer.

Preparation of samples for evidence of hydrophobic micro domain formation: samples were prepared in the same way as the samples for surface tension measurement. Furthermore, certain amount of Sudan Black dye (CAS [4197-25-5]) was added into the diluted solutions, and samples with the dye were stirred for 24–72 hours at 25–30 °C. Absorbance spectrum of the dye in centrifugated solutions was measured. Besides the Sudan Black dye, the Coomassie Brilliant Blue (CBB) dye, which reacts on the difference of its micropolarity by shifting its absorbance maximum[5], was tried for detection of an aggregation process too.

Results and Discussions

The surface tension measurements results showed that HA, by its hydrophobic modification, obtains surface active properties. That means that such hHA reduces surface tension of an aqueous environment, while pure unmodified HA is not surface active (Fig.1.).

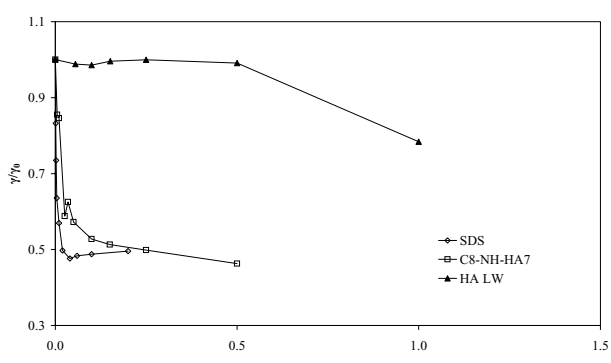

Fig. 1. **Comparison of surface activity of unmodified HA (LW – lower molecular weight 5.6 . 10[5]), a carbamate HA derivative with C8 alkyl and the classic surfactant sodium dodecyl sulfate (SDS); γ represents a sample surface tension, γ_0 represents the buffer surface tension**

The hHA surface activity greatly depends on an alkyl chain length (Fig. 2.) and substitution degree (SD). However, the hHA studied displayed slightly different surface active behavior in comparison to SDS. Nevertheless, some critical points, on the breakages of surface tension dependence on concentration, could be noticed. Those points probably indicate an aggregates formation[4,5], or correspond to CMC-like concentration[4].

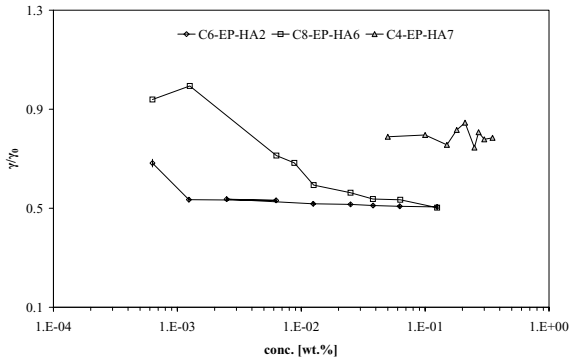

Fig. 2. **An alkyl chain length influence on surface activity of HA epoxy derivatives. Molecular weight of the samples was approximately 1.10^5. SD (C4-EP-HA7) = 6.7 %, SD (C6-EP-HA2) = = 31 %, SD (C8-EP-HA6) = 32 %**

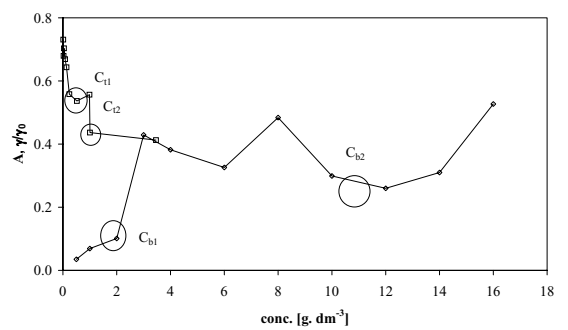

Fig. 3. **Comparison of results from a surface tension measurement and a measurement of the Sudan Black dye absorbance in C10-NH-HA9 (Mw = 29 290, SD = 5.28 %) solutions. C_{ti} or C_{bi} represent critical points on the dependences**

From the Fig. 3. is obvious an increase of absorbance of the dye with the concentration of the HA derivative. That means increasing of an extent of hydrophobic domains presented in the solutions. On the absorbance concentration dependences, some critical points were also distinguished. While the critical points determined from the surface tension measurements, signed as C_t, represent a state of saturation of a solution surface by the surfactant[5], the critical points C_b on the absorbance concentration curve correspond to the onset of formation of hydrophobic clusters in a bulk solution[5]. These two different critical concentrations underline the complex behavior of amphiphilic polymers in aqueous solutions[5].

Conclusions

Surface activity and therefore a solubilization ability of HA derivatives are greatly dependent on the length of an alkyl chain attached to the polysaccharide backbone and substitution degree. Some of the HA derivatives are able to solubilize a hydrophobic agent, and therefore might be used as a drug carrier or for drug delivery purposes. This ability is perhaps conditioned by the convenient length of an alkyl chain and by the biocompatibility of an employed substitution degree of such amphiphilic polysaccharide.

REFERENCES

1. Lapčík L. jr., Lapčík L., De Smedt S., Demesteer J., Chrabreček P.: Chemical Reviews *98*, 2663 (1998).
2. http://www.cheque.uq.edu.au/research/bioengineering/research/Metabolic_Engineering/HA.html.
3. Vercruysse K. P., Prestwich G. D.: Critical Reviews in Therapeutic Drug Carrier Systems *15*, 513 (1998).
4. Zhang T., Marchant R. E.: Journal of Colloid and Interface Science *177*, 419 (1996).
5. Duval-Terrié C., Huguet J., Miller G.: Colloids and Surfaces A: Physicochem. Eng. Aspects *220*, 105 (2003).
6. Barreiro-Iglesias R., Alvarez-Lorenzo C., Concheiro A.: International Journal of Pharmaceutics *258*, 179 (2003).
7. Chytil M.: *Colloidal Properties of Polysaccharides Derivates*. Diploma Thesis. Faculty of Chemistry, BUT, Brno 2004.

P13 INFLUENCE OF NEW CELLULOSE PROTECTORS IN OZONE BLEACHING

MICHAL JABLONSKÝ, MILAN VRŠKA, GABRIELA SZEIFFOVÁ and ŠTEFAN ŠUTÝ
Department of Chemical Technology of Wood, Pulp and Paper, Slovak University of Technology, Radlinského 9, 812 37 Bratislava, Slovak Republic,
michal.jablonsky@stuba.sk

Introduction

Considerable efforts has been devoted to find an additive or pretreatment procedure that would protect the cellulose and make the ozone react preferentially with the lignin in the fiber[1–4]. The substances are expected to decrease or completely eliminate the degradative reactions that destruct polysaccharides chains. This paper describes the influence of the new additives as methylhydroxyethyl cellulose, zirconium(IV) propoxide, cationic potato starch derivative, 2-*tert*-butyl-5-aminopyrimidine, D-mannitol and magnesium ethoxide on ozone bleaching.

Experimental

The following additives were used: methylhydroxyethyl cellulose (Tylose MH 300 P2, viscosity 300 mPa s^{-1} (20 °C), SE Tylose GmbH & Co.KG), zirconium(IV) propoxide solution (70 wt. % in 1-propanol, Lambda Life), 2-*tert*-butyl-5-aminopyrimidine (p. a.), ammonium molybdate ($(NH_4)_6Mo_7O_{24}.4H_2O$, 81–83 % as MoO_3, Sigma), urea (Merck), salicylic acid (Merck), cationic potato starch derivative (Empresol NE 2 SE, degree of substitution ≤ 0.035,

Emsland – Stärke GmbH.), D-mannitol (Sigma), magnesium ethoxide (purum ≥ 95.0% (T), Lambda Life).

The kraft pulp after oxygen stage was used with the following characteristics: kappa number 9.92, viscosity of 876 ml g^{-1} and brightness of 46.93 % ISO. The ozonization of the 50 g o. d. pulp in a rotating vessel with 250 ml volume was carried out at the following conditions: the pulp consistency was 35%, pH 3, temperature 40 °C, oxygen flow rate was 4.45 l O_2 min^{-1}, ozone production was 7.563 mg $O_3.l^{-1}O_2$ as determined by iodometric titration, ozone charge (0.3 % o. d. pulp). The ozonization 1 % additives on o.d. pulp as a cellulose protector were used. The pulp was characterized: kappa number (TAPPI T236), viscosity (TAPPI T230) and brightness (TAPPI T452).

The selectivity of ozone bleaching was evaluated using both the decrease in kappa number (Slc_K) and increase in brightness (Slc_B) both related to the unit change of the intrinsic viscosity. The efficiency of the lignin removal was evaluated through the decrease of the kappa number (Efc_K) and the pulp brightness gain (Efc_B) related to the ozone consumption[5]. The reactivity of ozone bleaching was calculated according to Lidholm[6].

Results and Discussion

The influence of the 1 % o. d. pulp additon additives on the characteristic parameters: ozone consumption, kappa number, viscosity, brightness of the pulp after ozonization are shown in Table I. The effect of additives on the reactivity of the pulp with ozone, can be seen in Fig. 1. The effect of additives on the efficiency of ozone bleaching in brightness (Efc_B), the efficiency in kappa number (Efc_K), selectivity in brightness (Slc_B) and selectivity in kappa number (Slc_K) are presented in Fig. 2.

As can be seen from Table I and Fig.1., the presence of the methylhydroxyethyl cellulose and 2-*tert*-butyl-5-aminopyrimidine increases both the ozone consumption and reactivity.

The presence of all additives enhanced brightness (Table I) and improved the selectivity of ozone bleaching in brightness Slc_B (Fig. 2.). The highest increase above 5% was achieved by salicylic acid, ammonium molybdate, D-mannitol and urea.

The selectivity of ozone bleaching in kappa number Slc_K was increased in the presence of D-mannitol (Fig. 2.). D-mannitol protects carbohydrates in ozone bleaching, increases the intristic viscosity (Table I) and promotes the lignin removal during ozonization evidenced by a decrease in kappa number from 6.39 to 6.03 (Table I) at constant 0.3 % o. d. pulp ozone charge.

The experimental results showed that the efficiency of ozone bleaching expressed as brightness gain on the ozone consumption increased by all additives (Fig. 2.). Ammonium molybdate, salicylic acid, magnesium ethoxide and urea increased the efficiency in brightness 9.36–10.39 times.

2-*tert*-butyl-5-aminopyrimidine has a fairly negative effect on the efficiency of the lignin removal (Fig. 2.). Enhanced positive effect was spotted at substances such as magnesium ethoxide, D-mannitol, urea and minor effect was observed with additives such as cationic potato starch, salicylic acid and ammonium molybdates.

Conclusion

All additives examined in this investigation cause improvement of the selectivity of ozone bleaching (Slc_B) and also efficiency of ozone bleaching (Efc_B).

Presence of substances improved the efficiency of the removal of lignin in respectivetly: magnesium ethoxide > D-mannitol > urea > amonium molybdate > cationic potato starch > salicylic acid.

D-mannitol is the sole agent invoking favourable effect on the selectivity of ozone bleaching in kappa number. The best overall bleaching result with additive was attained by addition of D-mannitol as cellulose protector.

Table I
The influence of (1 % o. d. pulp) additives on the characteristic parameters of the ozonized pulp

Type of additive	Ozone consumption [% o. d. pulp]*	Kappa no. –	Viscosity [ml g^{-1}]	Brightness [% ISO]
Without additive	0.1852	6.39	763	47.92
Methylhydroxyethyl cellulose	0.2393	7.34	647	54.36
Zirconium(IV)propoxide	0.1535	8.41	723	49.43
2-tert-butyl-5-aminopyrimidine	0.1964	10.17	808	50.25
Ammonium molybdate	0.1311	6.99	745	54.21
Urea	0.1330	6.36	745	53.58
Salicylic acid	0.1664	6.45	728	56.14
Cationic potato starch	0.1397	6.93	740	51.13
D-mannitol	0.1444	6.03	814	50.17
Magnesium ethoxide	0.1432	5.90	693	54.25

*ozone charge is 0.3 % ozone on o. d. pulp

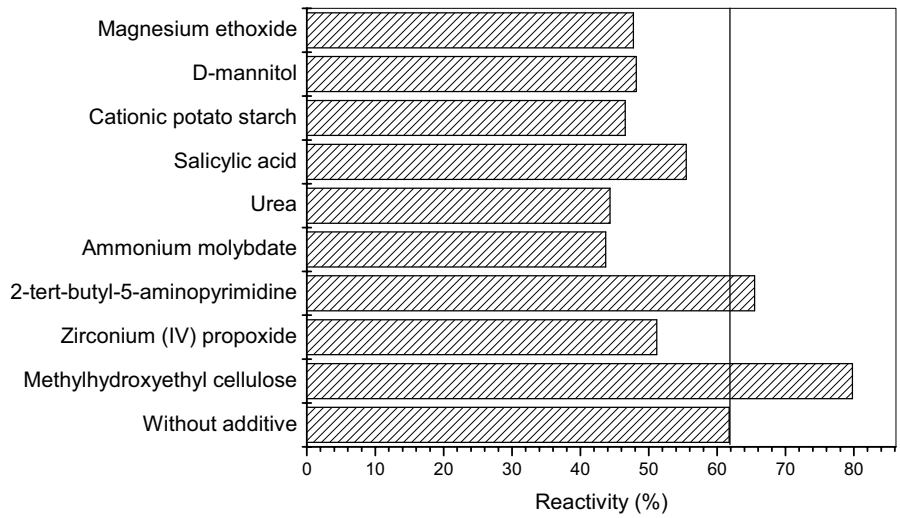

Fig. 1. **The effect of additives (1 % o. d. pulp) on reactivity of ozone stage. Oxygen-predeligniefied hardwood kraft pulp at 35 % consistency, pH = 3, T = 40 °C and ozone charge 0.3 % o. d. pulp**

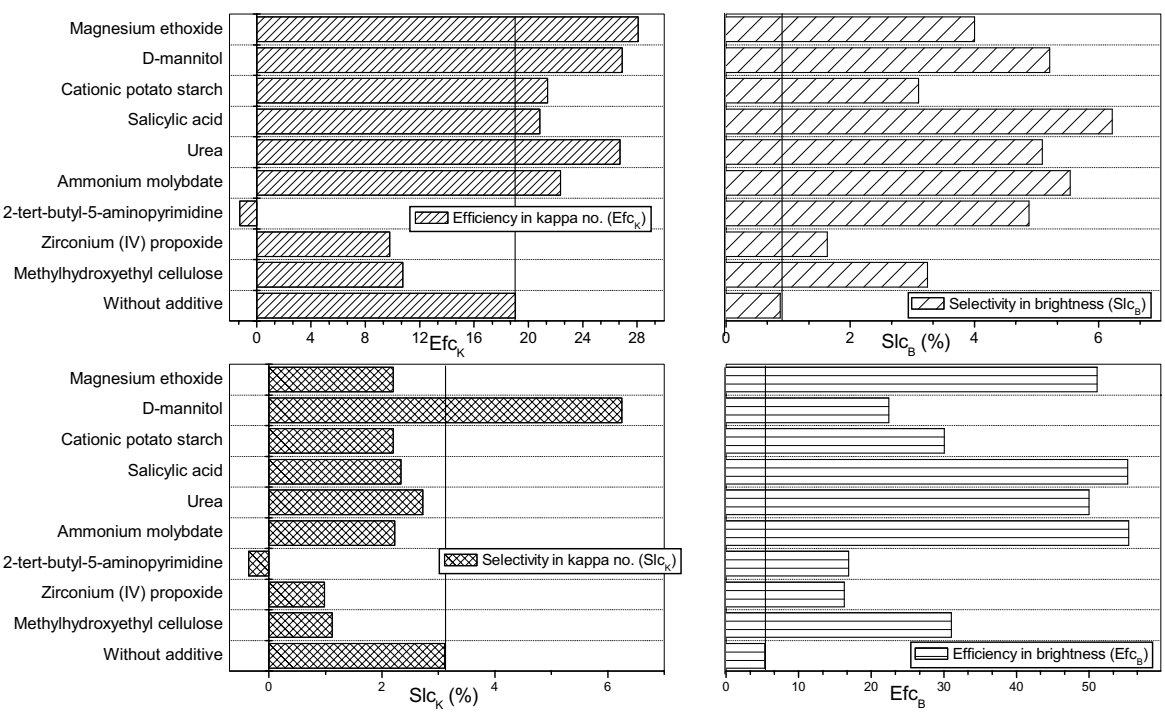

Fig. 2. **The effect of additives (1 % o. d. pulp) on efficiency in brightness, selectivity in brightness, selectivity in kappa and efficiency in kappa. Oxygen-predeligniefied hardwood kraft pulp at 35 % consistency, pH = 3, T = 40 °C and ozone charge 0.3 % o. d. pulp**

The autors express their thanks to the VEGA agency for financial support of the projekt No. 1/0061/03.

REFERENCES

1. Liebergot N., Van Lierop B., Skothos A.: Tappi J. *75*, 145 (1992).
2. Liebergot N., Van Lierop B., Skothos A.: Tappi J. *76*, 117 (1992).
3. Medwick V. B. Jr., Gratzl J. S., Singh R. P.: Tappi J. *77*, 207 (1992).
4. Jablonský M., Vrška M., Katuščák S.: Wood Res. *49*, 71 (2004).
5. Roncero M. B., Colom J. F., Vidal T.: Carbohydr. Polym. *51*, 243 (2002).
6. Lindholm C.-A.: Paperi ja Puu *3*, 211 (1987).

P14 STUDY OF *P*-PHENYLENEDIAMINES ANTIOXIDANT ACTION

ERIK KLEIN[a], VLADIMÍR LUKEŠ[b] and ZUZANA CIBULKOVÁ[a]

[a]*Department of Physical Chemistry, Slovak University of Technology, Radlinského 9, 812 37 Bratislava, Slovak Republic, erik.klein@stuba.sk,* [b]*Department of Chemical Physics, Slovak University of Technology, Radlinského 9, 812 37 Bratislava, Slovak Republic*

Technical and economic problems arising from negative influence of the environment on polymer durability have been studied since the commercial introduction of the polymers. Oxidation is enhanced especially at elevated temperatures during the processing of the polymer[1,2]. The loss of mechanical properties represents the main consequence.

Rubber products undergo degradation caused mainly by oxygen, ozone, heat and dynamic stress. The thermal oxidation of rubber is an autocatalytic, free radical chain reaction. Its rate can be reduced using antioxidants. Chain-breaking antioxidants, i. e., arylamines and hindered phenols, donate labile hydrogen to a peroxy radical so interrupting the propagation step[2]. The most widely used antioxidants in rubber industry are *N,N*'-substituted *p*-phenylenediamines (PPDs). The antioxidant activity of *N,N*'-substituted *p*-phenylenediamines in polyisoprene rubber has been studied by Differential scanning calorimetry[3,4] and antioxidant effectiveness values, *AEM*, have been determined for the temperature 180 °C.

The aim of this study is an insight into the energetics of the antioxidant action of seven *N,N*'-substituted *p*-phenylenediamines: *N*-phenyl-*N*'-dimethyl-butyl-*p*-phenylenediamine (6PPD), *N*-*o*-cumyl-phenyl-*N*'-dimethyl-butyl-*p*-phenylenediamine (oC-6PPD), *N*-*p*-cumyl-phenyl-*N*'-dimethyl-butyl-*p*-phenylenediamine (pC-6PPD), *N*-phenyl-*N*'-isopropyl-*p*-phenylenediamine (IPPD), *N*-phenyl-*N*'-(α-methylbenzyl)-*p*-phenylenediamine (SPPD), *N*-(2-methoxybenzyl)-*N*'-phenyl-*p*-phenylenediamine (MBPPD), *N*-(1-methyl-1-phenylethyl)-*N*'-phenyl-*p*-phenylenediamine (CPPD), Fig. 1. Molecules and their radical structures were studied using the PM3 semi-empirical quantum chemical method[5–7] in order to calculate the bond dissociation energies of hydrogen atom abstraction from three possible reaction centers – N(1), N(2) or C(3) atoms. Besides, we would like to correlate *AEM* values with the calculated reaction enthalpies of homolytic hydrogen atom splitting-off.

In this study we have restricted our attention to the most stable conformations of studied molecules – the energy difference between the most stable conformation of the antioxidant molecule and the other conformations does not exceed 1.5 kcal mol^{-1}. Table I shows the Boltzmann's weighted mean reaction enthalpies of radical formation calculated for 180 °C and *AEM* values[3,4].

We have focused on the correlation of the reaction enthalpies of hydrogen atom splitting-off from N(1), N(2)

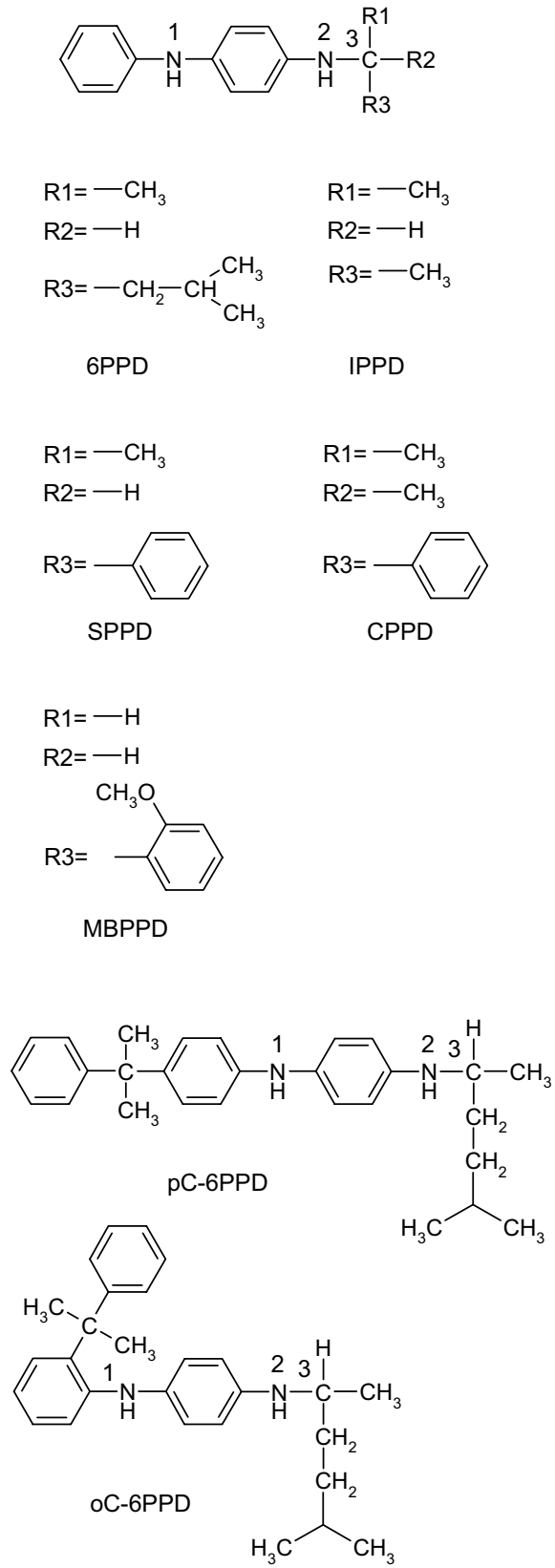

Fig. 1. **Structures and notations of the studied antioxidants**

Table I
AEM values and weighted mean reaction enthalpies at 180 °C

Antioxidant	*AEM* (kg mol^{-1})	$\Delta_r H_{1w}$ (kcal mol^{-1})	$\Delta_r H_{2w}$ (kcal mol^{-1})	$\Delta_r H_{3w}$ (kcal mol^{-1})
SPPD	351[a]	85.858	88.574	77.379
6PPD	277[a]	85.797	87.887	78.650
pK-6PPD	375[b]	85.696	87.588	78.171
oK-6PPD	263[b]	88.177	88.419	77.519
IPPD	177[a]	85.916	87.783	79.417
MBPPD	152[a]	85.612	87.899	80.689
CPPD	0[a]	86.232	88.651	—

[a]) Data taken from Table V in ref.[3]
[b]) Data taken from Table III in ref.[4]

and C(3) atoms with antioxidant effectiveness of the studied compounds. Roughly linear dependence was found between $\Delta_r H_{1w}$ and *AEM* values for all antioxidants, except oC-6PPD and MBPPD. The higher the $\Delta_r H_{1w}$ value, the lower the effectiveness of the antioxidant. Difference between pC-6PPD and oC-6PPD proves the effect of the cumyl group position on N(1)–H bond and *AEM* value. Although the $\Delta_r H_{1w}$ value in case of oC-6PPD is the highest, its *AEM* value is comparable with that of 6PPD. For IPPD, 6PPD, pC-6PPD, and SPPD the relationship between *AEM* and $\Delta_r H_{3w}$ is almost linear, too. No clear trend between *AEM* and $\Delta_r H_{2w}$ can be found. Moreover, if we compare the values for IPPD, 6PPD, oC-6PPD, and SPPD, we obtain unreasonable trend: the higher $\Delta_r H_{2w}$ value, the higher *AEM* value.

We suppose that overall antioxidant action expressed in terms of *AEM* can be ascribed to all three reaction centers in the molecules. Hydrogen splitting-off runs simultaneously from N(1), N(2), and C(3) atoms, though the energy requirement is lowest for C(3)–H bond cleavage. Since the motion of antioxidant molecules and polymer chains is restricted, antioxidant cannot react exclusively through C(3)–H bond cleavage.

The aim of this work is also to find relation between AEM and reaction enthalpies $\Delta_r H_{1w}$, $\Delta_r H_{2w}$, and $\Delta_r H_{3w}$, which can be useful for the other PPDs *AEM* prediction. We have searched for the linear $AEM = f(\Delta_r H_{1w}, \Delta_r H_{2w}, \Delta_r H_{3w})$ dependence. In the calculation we included these antioxidants: SPPD, 6PPD, pC-6PPD, IPPD, and MBPPD. We excluded oC-6PPD due to partial charge on N(1) significantly different from the other antioxidants, and CPPD which has no hydrogen on C(3). In the case of MBPPD we used in calculation $\Delta_r H_{3w}$ value for sterically non-hindered hydrogen on C(3). The found dependence is

$$AEM = 39876.0 - 330.1 \,.\, (\Delta_r H_{1w}/\text{kcal mol}^{-1}) - 44.5 \,.\, (\Delta_r H_{2w}/\text{kcal mol}^{-1}) - 93.6 \,.\, (\Delta_r H_{3w}/\text{kcal mol}^{-1})$$

Differences between calculated and experimental *AEM* values are in 0.3–1.7 % range. This equation is valid for the antioxidants in polyisoprene rubber with partial charge on N(1) atom in 0.102–0.117 range, on N(2) atom in 0.012–0.038 range, and on C(3) atom in range from –0.081 to 0.080. It would be appropriate to use larger number of the antioxidants in the regression, but more antioxidants have not been synthesized yet. Our results show, that quantum chemical methods may complement experimental study – the energetics of radical formation (the first step in antioxidant action) is in good agreement with experimentally determined antioxidant effectiveness values.

This work has been supported by Science and Technology Assistance Agency under the contract No APVT-20-005004.

REFERENCES

1. Gugumus F.: *Oxidation inhibition in organic materials*, Vol. 1. CRC Press, Boca Raton 1990.
2. Pospíšil J., Horák J., Pilař J., Billingham N. C., Zweifel H., Nešpůrek S.: Polym. Degrad. Stab. *82*, 145 (2003).
3. Cibulková Z., Šimon P., Lehocký P., Balko J.: Polym. Degrad. Stab. *87*, 479 (2005).
4. Cibulková Z., Šimon P., Lehocký P., Balko J.: J. Therm. Anal. Cal., in press.
5. Stewart J. J. P.: J. Comp. Chem. *10*, 221 (1989).
6. Stewart J. J. P.: J. Comp-Aided Mol. Design *4*, 1 (1990).
7. HYPERCHEM, rel. 7.5 for Windows, Hypercube, Inc., 2003.

P15 FLOW BEHAVIOUR OF LIGNITE-CARBOXY METHYLCELLULOSE-WATER DISPERSION SYSTEM

MICHAL KLIMOVIČ and MILOSLAV PEKAŘ
Brno University of Technology, Faculty of Chemistry, Institute of Physical and Applied Chemistry, Purkyňova 118, 612 00 Brno, Czech Republic, klimovic@fch.vutbr.cz

Introduction

Recently we have reported on rheological problems in processing lignite pastes to form elements for lignite alternative applications outside the power generation industry[1,2]. We have also shown how these problems can be overcome using cellulosic derivative as a rheological aid[3]. Further, our work delt with the study of much more diluted suspensions of liquid-like appearance. We have found that small amount of lignite surprisingly lowered apparent viscosity of the solution comparing with the pure solvent. This work reports on flow behaviour of inorganic particle dispersions in the same medium. The aim was to find whether this thinning effect is specific to lignite or not.

Experimental

Carboxymethylcellulose (in the form of sodium salt; CMC) was supplied by Aldrich. Two preparations were used with following producer's specifications: high molecular weight, M_w = 700 000 g mol^{-1}, degree of substitution 0.9; low molecular weight, M_w = 90 000 g mol^{-1}, degree of substitution 0.7. Moisture content was determined as 8.2 and 9.4 %.

Two types of filler were used for preparation of dispersions, the foundry sand from laboratory of FSI VUT Brno and microsil from Silchem. The fraction of foundry sand captured between 0.15 and 0.30 mm sieves was used for subsequent experiments. Microsil is Silchem trademark of glass microspheres; type G080 was used.

The preparation of suspensions consisted in suspending weighted amounts of filler and CMC in corresponding amount of warm (70 °C) deionized water. Mixture was stirred for one hour, temperature was maintained for the first 30 min only.

Measurements of flow properties were carried out at 25 °C on Haake RS100 rheometer equipped with the double cylinder sensor Z20 DIN both in constant rate and in constant stress mode. All reported data points are averages from three replicates.

Results and discussion

Fig 1. shows flow curves for increasing sand contents measured immediately after preparation with suspensions based on the high molecular weight cellulose derivative. Higher sand loadings (7 % and more) shift flow curves up, to higher shear stress values, on increasing sand contents and also apparent viscosity rises. On contrary, flow curves for low sand loadings (5 %) lie bellow the curve of blank CMC solution giving also lower apparent viscosities. Thus, adding sand to the carboxymethylcellulose solution does not increase its (apparent) viscosity as expected, unless the sand concentration is sufficiently high. The same effect was observed for lignite as a filler.

Suspensions prepared from the low molecular weight cellulose derivative did not show this untypical behaviour.

The same behaviour of suspensions was observed at carboxymethylcellulose-microsil-water dispersions (Fig. 2.).

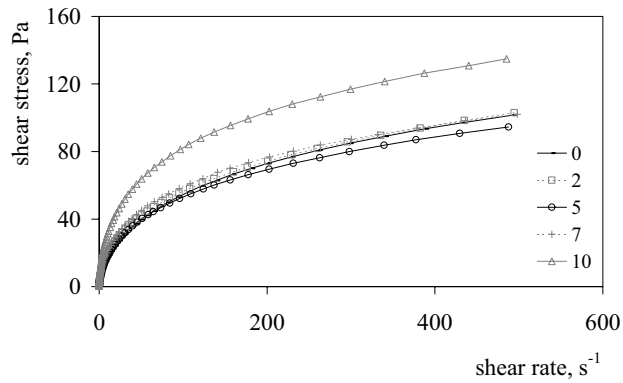

Fig. 1. **The dependence of shear stress on shear rate for dispersions of pure CMC solution and different concentrations of sand in CMC solution (2 %, 5 %, 7 %, 10 %)**

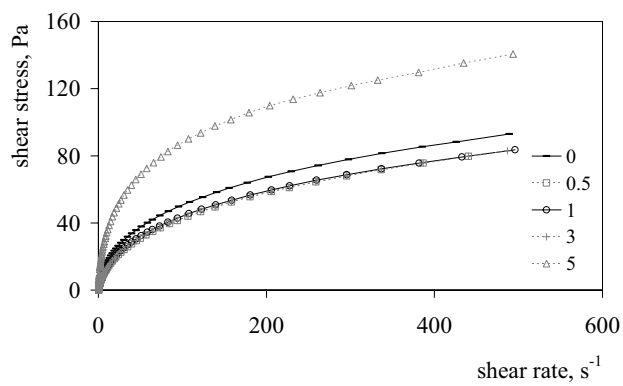

Fig. 2. **The dependence of shear stress on shear rate for dispersions of pure CMC solution and different concentrations of microsil in CMC solution (0.5 %, 1 %, 3 %, 5 %)**

Measured flow curves can be adequately fitted by the Ostwald-de Waele model

$$\tau = K\dot{\gamma}^n$$

Model parameters reflected the influence of lignite on suspension flow behaviour.

Results of this study indicate that lowering apparent viscosity of suspensions prepared from water solution of high molecular weight carboxymethylcellulose may be quite common phenomenon when concentration of dispersed

particles is low (approximately in orders of tenths up to ten weight percent). The cause is probably in easier movement of particles entrapped within long biopolymer chains like balls in ball-bearing.

Conclusion

Flow curves determined in this study showed that lowering suspension apparent viscosity at moderate amount of particles suspended in high molecular weight carboxymethylcellulose solution is not specific effect of lignite particles. The same effect was observed also for sand and even for glass microspheres, which are usually used as thickener. Results thus confirm our hypothesis on some "ball-bearing" effect, which enables easier flow of long macromolecular chains then when they are in closer contact in pure solution.

REFERENCES

1. Lapčík Ľ., Lapčíková B., Filgasová G.: Colloid Polym. Sci. *278*, 65 (2000).
2. Pekař M. *Flow behaviour of concentrated lignite dispersions*. In Proceedings of the XIIIth International Congress on Rheology, Cambridge, vol. 4. British Society of Rheology, Glasgow, 4 (2000).
3. Pekař M., Divišová P., Klimovič M.: submitted to Colloid. Polym. Sci. (2005).

P16 SEPARATION OF HUMIC ACIDS ON MICRO-MEMBRANE

MARTINA KLUČÁKOVÁ
and MIROSLAVA MALENOVSKÁ
Institute of Physical and Applied Chemistry, Faculty of Chemistry, Brno University of Technology, Purkyňova 118, 612 00 Brno, Czech Republic, klucakova@fch.vutbr.cz

Introduction

Humic acids (HA) belong to wide group of organic compounds formed during decomposition of organic matter of vegetable origin. As a result of the large number of different organic compounds in living organisms their degradation and recombination processes lead to nearly infinite number of molecules[1–4]. In general, HA are the fraction of humic substances which is soluble in alkaline solutions. They are the mixture of many various organic substances therefore their structure cannot be precisely defined. To study structure and properties of HA comprehensively it is suitable to divide HA into several fractions. Many various methods as ultrafiltration[5–6], gel chromatography[7–8], organic solvents[9–10] or buffer fractionation[11–12] etc. are utilized for HA fractionation.

Separation of HA on micro-membrane GR 61 PP is studied in this contribution. The aim of the work is to find optimal separation conditions. Humic acid has a big structure full of conjugate bounds and ion's groups. It is rightful suppose, that such a big structure could mean problem for permeation. Concentration polarization phenomena could influence permeation. Concentration polarization is an additional complication that arises when hydrocolloids, macromolecules (such proteins) and other relatively large solutes or particles are filtered. These compounds are largely rejected by membrane. Thus they form the layer on the surface of the membrane. This layer could be viscous or gelatinous, depend on the type of solid. This additional layer is called by various terms such as the gel layer, CP layer, cake or polarization layer. This layer is not to be confused with the fouling layer that occurs because of membrane-solute interactions[13].

Experimental part

To find optimal separation conditions a set of HA solutions in NaOH was prepared. Initial concentration of HA was 0.01–0.05 g dm^{-3}. Three various NaOH solutions (0,001 M; 0,01 M and 0,1 M) were used as solvents for HA separation. These solutions were filtrated through membrane under various pressures (1–5 kPa). Obtained fractions were measured on UV/VIS spectrometer Perkin Elmer 320. Humic acid concentration in individual fractions was computed by means of calibration curve determined in advance. All experiments were carried out in Denmark Techniske Universitet.

Results and discussion

The comparison of results obtained for various initial HA concentrations in 0.01 M NaOH is shown in Fig. 1. We can see that optimal initial HA concentration is 30 mg dm^{-3}, because concentration of filtrate is sufficiently high and it is not dependent on pressure. If highly concentrated initial HA solution is used, filtrate concentration depends on pressure. The layer of humic particles is formed on the membrane surface. This layer makes separation more difficult, therefore effective filtration is possible only under high pressure.

The influence of concentration of used solvent is represented in Fig. 2. We can see that filtrate concentration is strongly influenced by concentration of used NaOH.

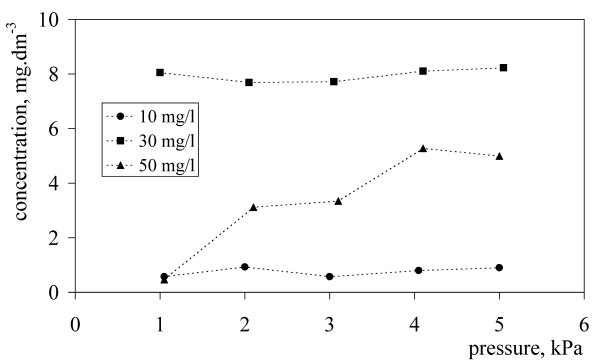

Fig. 1. **Dependence of filtrate concentration on pressure for various initial HA concentration in 0.01 M NaOH**

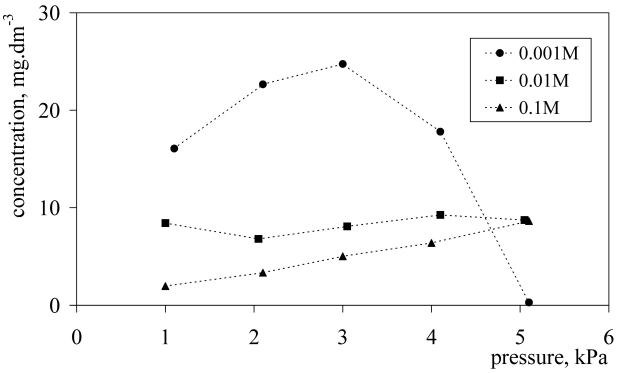

Fig. 2. **Dependence of filtrate concentration on pressure for initial HA concentration 30 mg dm^{-3} in various NaOH solutions**

The decrease of filtrate concentration and its dependence on pressure were observed for highly concentrated solvent. Probably high ionic strength causes stronger polarization on membrane surface, which negatively influences separation process. On the other hand, clogging membrane complicates filtration in the case of 0.001M NaOH mainly under high pressure. Optimal NaOH concentration is thus 0.01 M.

Conclusions

On the basis of experimental results the optimal separation conditions were chosen to achieve high separation efficiency and humic acid fractions of reproducible properties.

REFERENCES

1. Schnitzer M., Kahn S. U.: *Humic Substances in the Environment.* Dekker, New York 1972.
2. Aiken G. A., McKnight M. D., Wershaw R. L., MacCarthy P.: *Humic Substances in Soil, Sediment and Water.* Wiley, New York 1985.
3. Frimmel F. H., Christmann R. F.: *Humic Substances and Their Role in Environment.* Wiley, Chichester 1988.
4. Frimmel F. H., Abbt-Braun G., Heumann K. G., Hock B., Lüdemann H. D., Spiteller M.: *Refractory Organic Substances in the Environment.* Wiley, Weinheim 2002.
5. Li L., Zhao Z., Huang W., Peng P., Sheng G., Fu J.: Org. Geochem. *35*, 1025 (2004).
6. Kučerík J., Pekař M., Klučáková M.: Petrol. Coal *45*, 58 (2003).
7. Wershaw R. L., Pinckney D. J.: J. Res. U. S. Geolog. Surv. *1*, 361 (1973).
8. Gonet S. S., Wegner K.: Chem. Anal. – Warsaw *36*, 275 (1991).
9. Senesi N., Sipos S.: Org. Geochem. *8*, 157 (1985).
10. Klučáková M., Zemanová A.: Chem. listy *96*, S77 (2002).
11. Klučáková M.: *Proceedings of International Scientific Conference Humic Substances in Ecosystems 5* (Gonet S. S., Zaujec A., Debska B., eds.), p. 39. Duszniki Zdroj 2003.
12. Kučerík J., Conte P., Pekař M., Piccolo A.: Fresen. Environ. Bull. *12*, 683 (2003).
13. Cheryan M.: *Ultra Filtration and Micro Filtration Handbook.* Technomic Publishing Co., Lancaster, PA. 1998.

P17 INFLUENCE OF PH VALUES AND ACCELERATED AGEING ON LIGHT STABILITY OF PAPER

ZDENKA KLUČIAROVÁ, BOHUSLAVA HAVLÍNOVÁ, MIRIAM TURANOVÁ and MICHAL ČEPPAN
Department of Graphic Arts Technology and Applied Photochemistry, Radlinského 9, 812 37 Bratislava, Slovak Republic, zdenka.kluciarova@stuba.sk

Introduction

Cultural property includes many archival and library materials like pictures, graphics etc. which belongs to cultural heritage of every state. Most of these materials written in past 150 years have bean destroyed by ageing, which leads to total lost of printed and written documents in libraries and archives[1]. The best method to ensure long durability of texts and pictures stays prevention, therefore using materials, which are up to standard for holdback quality and utility of articles[2–4]. Influence of ageing on paper caused permanent deterioration of optical properties and yellowing of paper occurs. This phenomenon is attributed to the presence of chromophores found in some of the products formed from the degradation of paper components. Actually, the ageing process of paper is very slow. For this reason, simulation of accelerated ageing conditions is necessary[5]. For archiving, papers which are up to standard STN ISO 7906 and ANSI/NISO Z 39.48-1992 are used. Laboratory search of accelerated ageing affords sufficient information about selection of suitable paper for archiving[6–8].

This study is oriented on monitoring of optical (brightness, color difference) and chemical (pH of cold aqueous extract) properties of different papers. We choose ageing method using hot air and moist heat ageing on all paper samples. These methods were realized according to standards STN ISO 5630 during required time period (0, 8, 24, 72, 168, 336 and 672 hours). 3 days of accelerated ageing respond to 25 years of native ageing[9].

Consequently, the results obtained accelerated ageing can help to predict the changes in paper for the period of hundredths of years.

Experimental procedures

M a t e r i a l s

Four types of papers were used:

A – classic woodfree offset alkali paper, supplied by Bratislavská papierenská spoločnosť, Bratislava, Slovak Republic

B – printing voluminous paper classic, polished unsized paper, with contend of 65% mechanical wood pulp and 35% unbleached sulphite pulp, made in Jihočeské papírny, Větrní, Czech Republic

C – writing partly groundwood acid paper Slavošovské papierne, Slovak Republic

D – fine printing groundwood sized paper, with contend of 54 % mechanical wood pulp, 18 % unbleached sulphite pulp and sulphate pulp, 15 % clay, made in Jihočeské papírny, Větrní, Czech Republic

A p p a r a t u s

All paper samples were submitted accelerated ageing in accord with standard ISO 5630–1 at 105 ± 2 °C in the hot-air drying unit WSU 100 (VEB MLW Labortechnik, Illmenau, Germany) during the required time period (0, 8, 24,72, 168, 336 and 672 hours).

Moist heat ageing was performed in climatize unit Feutron GmbH Greis, Germany, at 80 °C and 65% RH.

Brightness was measured by filter photometer ELREPHOMAT DFC-5 SNR.

The pH values of the cold aqueous extracts were measured at 25 °C by pH-meter Jenway model 3510 (England) complies with Europe standards: EN 50081-1, EN 50082-1, EN 61010-1.

Results and discussion

Table I summarizes the mean values of characteristic parameters of papers A–D. Paper A is characterized with high values of brightness (102, 4) and sufficient pH values of cold aqueous extract (9, 6) for alkali reserve. Paper B and groundwood sized paper D have the lowest values of brightness (64, 2 and 68, 5), moreover the pH values are similar (5, 9 and 6, 2).

Table I
The mean values of properties for the original Paper samples

Paramter	Paper samples A	B	C	D	
Basic weight g/m^2	80	50	80	60	STN ISO 536
pH of cold aqueous extract	9.6	5.9	4.4	6.2	STN ISO 6588
Brightness (%)	102.4	64.2	76.4	68.5	STN ISO 2470

Original paper C shows lower values of brightness (76.4) and significant acid value of cold aqueous extract (pH 4, 4).

Table II summarizes the mean values of characteristic parameters of paper samples submitted hot-air and moist heat accelerated ageing after 672 hours.

Fig. 1a, b shows relative decrease of brightness upon accelerated ageing for papers A–D. The most significant decrease was recorded in case of voluminous paper B.

Exponential decay of brightness during hot-air and moist heat ageing was observed (Fig. 2.). These values show good resistance to yellowing during ageing for paper A whereas final decrease of brightness was approximately 17.8 %. Final loss of brightness was compared for all used papers.

Fig. 3. shows color difference after accelerated ageing for papers A–D. The largest color difference was obtained for paper B.

Influence of ageing on chemical properties of given papers was studied on pH values of cold aqueous extract. Experimental results obtained by measuring of pH were displayed in Table III and plot in Fig. 4a, b. These results show the eventual ability of paper A to neutralize acid products created in process of accelerated ageing and so high resistance in ageing process. Resistance of pH on optical properties are shown in Fig. 5a, b.

Table II
The mean values of paper properties corresponding 672 hours of accelerated ageing

Accelerated ageing	Parameter	Paper samples A	B	C	D
Hot air (105 °C)	pH of cold aqueous extract	8.6	4.9	4	4.7
	Brightness %	84.4	40.1	50.4	46.6
moist heat 80 °C, 65 % RH	pH of cold aqueous extract	9.2	5	3.6	4.4
	Brightness %	83.4	37.2	51.7	44.6

Table III
The pH values for different papers under conditions of accelerated ageing

		pH of cold aqueous extract			
		A	B	C	D
Original sample		9.6	5.9	4.4	6.2
105 °C	8 h	9.2	5.9	4.4	5.9
	24 h	9.1	5.8	4.4	5.7
	72 h	9	5.6	4.3	5.5
	168 h	8.9	5.4	4.2	5.3
	336 h	8.7	5.1	4.1	4.9
	672 h	8.6	4.9	4	4.7
80 °C, 65 % RH	8 h	9.4	6.2	4.3	6
	24 h	9.4	6.1	4.2	5.8
	72 h	9.3	5.8	4.3	5.6
	168 h	9.3	5.5	4	5.2
	336 h	9.2	5.2	3.9	4.8
	672 h	9.2	5	3.6	4.4

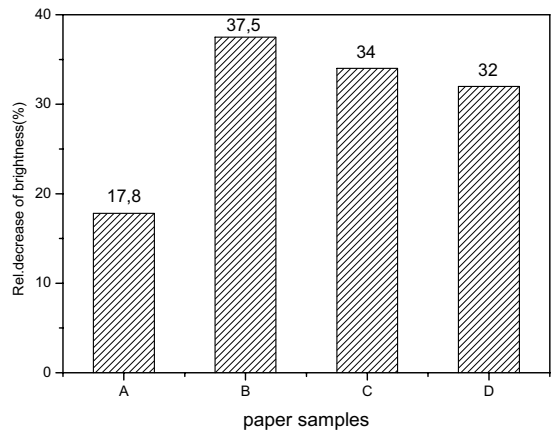

Fig. 1a

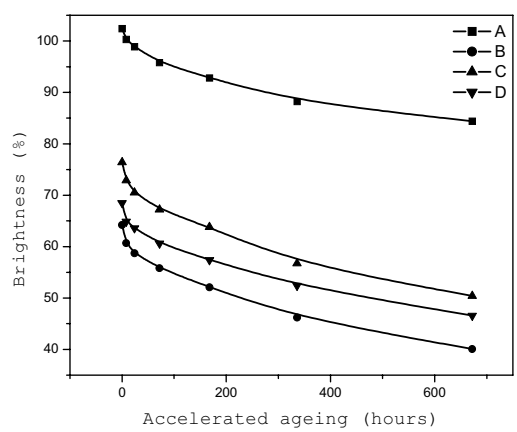

Fig. 2a

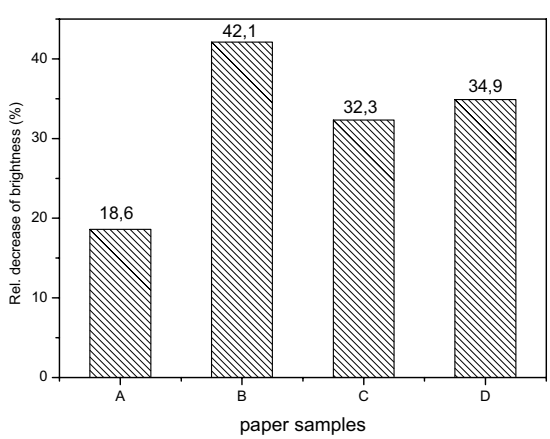

Fig. 1b

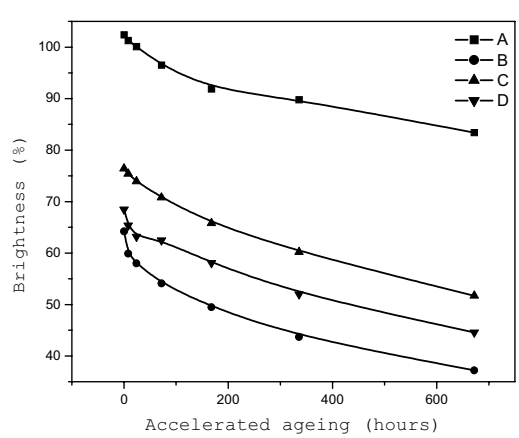

Fig. 2b

Fig. 1a, b **Relative decrease of brightness for papers A–D after hot-air (1a) and moist heat (1b) ageing**

Fig. 2a, b **Exponential decay of brightness during hot-air (2a) and moist heat (2b) ageing for paper samples A–D**

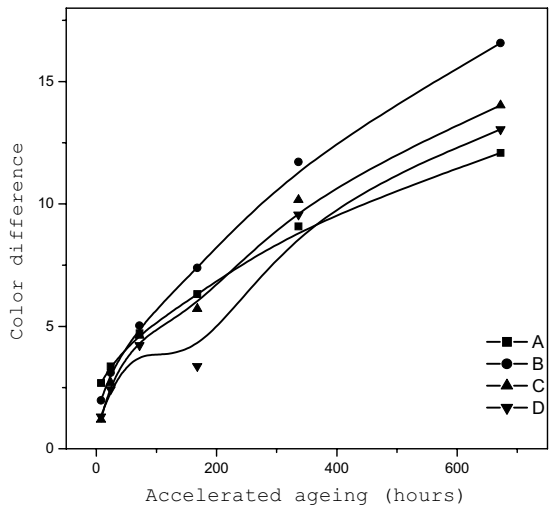

Fig. 3a

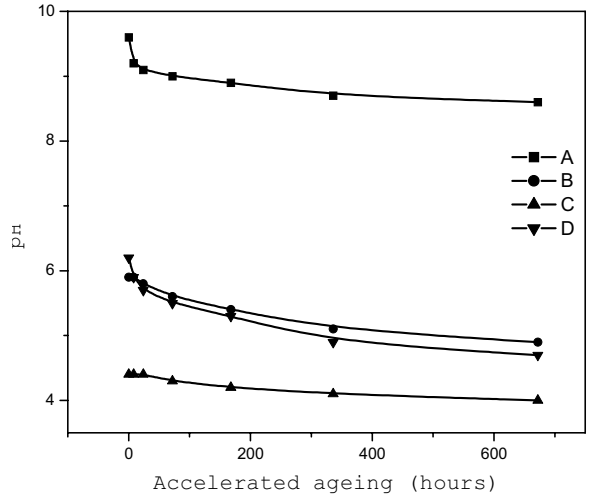

Fig. 4a

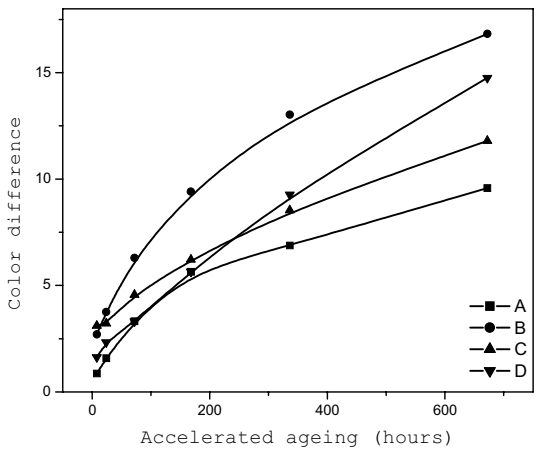

Fig. 3b

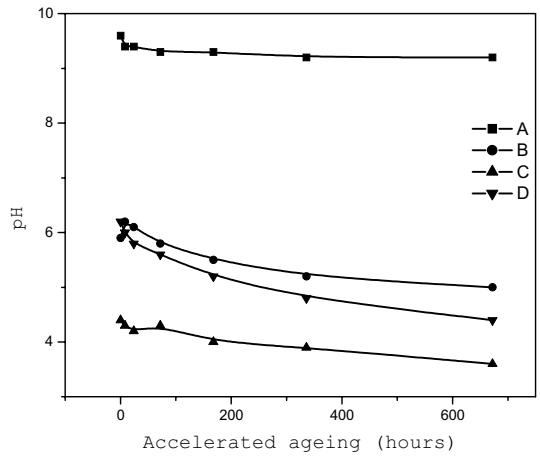

Fig. 4b

Fig. 3a, b **Color difference after hot-air (3a) and moist heat (3b) accelerated ageing for papers A–D**

Fig. 4a, b **The changes of pH values monitored during accelerated ageing of paper samples A–D**

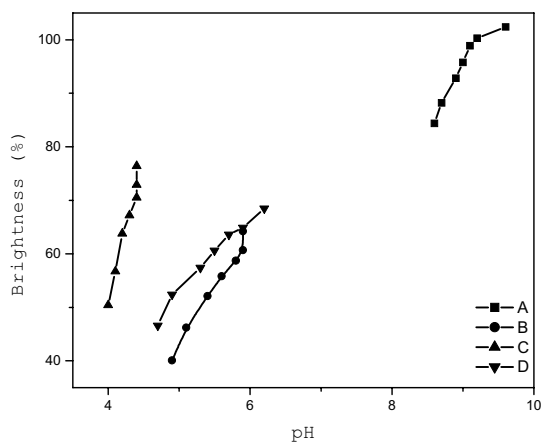

Fig. 5a

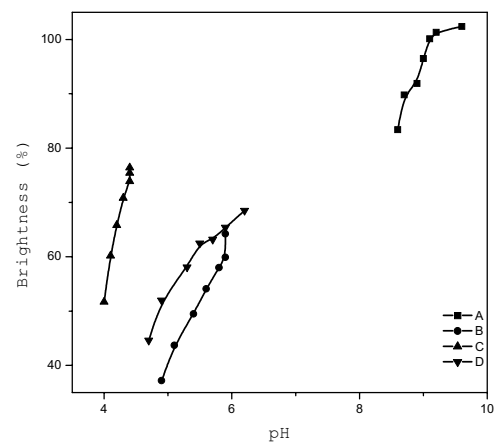

Fig. 5a

Fig. 5a, b **Resistance of pH on optical properties during hot-air (5a) and moist heat (5b) accelerated ageing for papers A–D**

Conclusions

Optical and chemical properties were observed on four types of papers. All paper samples were treated by accelerated ageing and studied under the given conditions. The best stability after ageing was obtained for paper A. We can consider that this kind of paper is the most suitable for storage and printing documents. The most significant changes of properties were obtained in case of voluminous paper B. The acid paper C showed small decrease of pH after ageing. This kind of paper could be suitable for storage after deacidification process. Papers B and D are not suitable for long-time storage on the gound of their initial properties which caused deterioration of optical and mechanical parameters.

This work was supported by Science and Technology Assistance Agency (Slovakia) under the contract No. APVT-20-034202 and Slovak Grant Agency (Project VEGA 1/2455/05).

REFERENCES

1. Bredecker K, Siller-Grabenstein A.: Restaurator *9*, 113 (1988).
2. Havermans J. B. G. A.: Restaurator *16*, 209 (1995).
3. Wedinger R., Abbey Newslett. *13*, 126 (1989).
4. Middleton R. S. Scalan M. A., Zou X., Page D. H.: Tappi *79*, 187 (1996).
5. ISO Standard 5630–1 (50 0375): *Papier a lepenka, Urýchlené starnutie; part 1.: Pôsobenie tepla za sucha pri teplote 105 °C* (1999).
6. Bukovský V.: Restaurator *20*, 77 (1999).
7. Bégin P., Deschantelets S., Grattan D., Gurnagul N.: Restaurator *19*, 135 (1998).
8. Shahani C. J., Hengemihle F. H., Lee S. B.: Abst. Papers Am. Chem. Soc. *216*, 38 (1998).
9. Carter H. A., J. Chem. Educ. *73*, 1068 (1996).

P18 THE COMPARISON OF PROPERTIES OF PHOTOREACTIVE MODIFIED PVAL USED IN INKJET PRINTING

IVA KRÁLOVÁ[a], MICHAL VESELÝ[a] and PETR DZIK[a]
[a]*Brno University of Technology, Faculty of Chemistry, Institute of Physical and Applied chemistry, Purkyňova 118, 612 00 Brno, kralova@fch.vutbr.cz*

Introduction

With expansion of inkjet printers to the array branches, requirements on inkjet media are increased too and must be improved. Once of frequent material which is used for preparation of special layers, is PVAl, which takes advantage of solubility of PVAl in water. Modification of PVAl therefore further widens the field of PVAl application[1].

Our basic aim is based on the idea of introduction of photoreactive lateral groups to the backbone macromolecule of receiving layer-forming polymer. We seek highly hydrophilic thin polymer layer with effective conversion. We performed numerous experiments with PVAl modified by maleic anhydride, but this product has serious disadvantages as low aqueous solubility at higher conversion degrees and very low photographic sensitivity[2]. So we have modified PVAl with other compounds which contain double bond, as glycidylmethacrylate (GMA), methacrylic acids (MAA), methacryloyl-aminoacetadehyde dimethyl acetal (MA-MAA-DA) and its derivatives. These compounds are essentially hydrophobic, leading to lower surface energy and hydrophobization. On the other hand they are highly susceptible to photoinitiated cross-polymerization, and the effective crosslinking speed of these compounds is much higher than maleinized PVAl.

Experimental

Poly(vinyl alcohol) modified by maleinanhydride (Mowiol 8/88, as solvent dimethylformamid, temperation on 70 °C, as catalyzer DMAP, maleinanhydride in the amount of 5, 10, 20 w. %, reaction time 2 hours at 70 °C) is used[2].

Other modification is in progress with methacrylic acid (80 ml of water, different ratios of acetic acid and methacrylic acid), mixture is stirred in a beaker in water bath at 40 °C, then PVAl (20 g) is added and mixture is then stirred for another 36 hours)[3].

Glycidylmethacrylated PVAl is prepared by dissolving of PVAl (20 g) in a mixed solvent consisting of 100 ml DMFA and 50 DMSO at 70 °C. After complete dissolution, GMA in the amount of 1, 2, 4 and 8 w. % is slowly added and then 5 ml of methanolic solution of KOH (5 w. %) is added in the same manner. The reaction mixture is stirred at 70 °C for 2hours.[4]

The last modification process: Mowiol 10/98 (10 g) is completely dissolved in water, then dimethylacetal in the amount of 2.5, 5, 10 and 20 w. % is slowly added. After complete dissolution, acetic acid (15 ml) is added and hydrochloric acid (4 ml). The reaction mixture is stirred at 70 °C for 2 hours.

Prepared modified polymers were used for further study to evaluate their suitability for the projected purpose, i.e. ink receiving layers. To do so, they were characterized by analytical methods including infrared and UV spectroscopy, surface characterization by dynamic contact angle measurement, photoresist speed determination, thermal analysis, swelling kinetics study and image analysis. With respect to the limited space for this paper, this article is dealing with infrared and UV spectroscopy in detail, mainly with degree of conversion and synthesis effectivness.

Results

Degree of conversion

According to the amount of modifying agent used, various products were obtained. In order to be able to relate the prepared product properties to their chemical composition, it is essential to determine their conversion degree, ie. the extend of modification expressed as a molar fraction of modified monomeric units. The degree of conversion of malenized

PVAl was determined by titration of excess of KOH and such is determined as molar amount of groups containing ester group and non-esterificate OH groups as publish in previous works, but we created the new and easier method for this determination. This method utilizing UV spectroscopy is based on the oxidation of organic compounds by potassium permanganate. In aqueous solutions, potassium permanganate acts as a powerful oxidizing agent, completely destroying most organic compounds. Our method is based on spectrophotometric detection of the oxidation products at 280 nm. At 20 °C, the reaction with double bonds proceeds very fast and significant changes in the oxidation products concentration can be detected after 10 minutes of reaction time. On the other hand, blank samples containing unmodified PVA show no changes for up to 1 hour, thus enabling spectophotometric measurements with good accuracy.

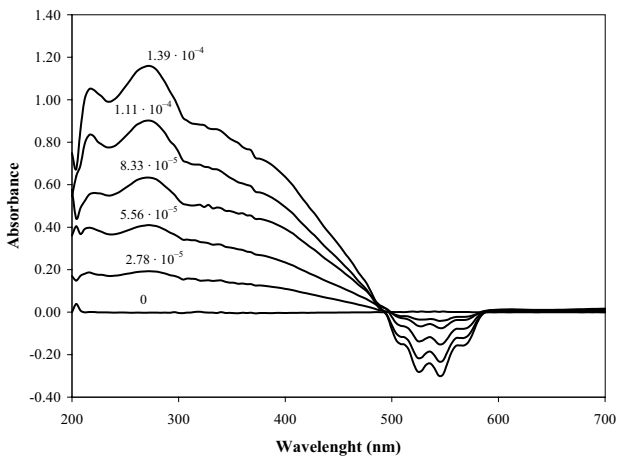

Fig. 1. **UV-VIS spectra of different acrylate concentration**

We prepared 4 grades of malenized PVAl and methacrylated PVAl. The samples differed in their conversion degree. The conversion degree was determined by UV spectroscopy for malenized PVAl in the amount of maleinanhydride 5, 10 and 20 % mol and 2, 5, 10 and 20 molar % of methacrylated units in table below:

Modification agent [w. %]	Degree of conversion of modified PVAl	
	maleinanhydride	glycidylmethacrylate
2	X	3.2
5	4.35	6.1
10	9.52	9.5
20	14.99	insoluble

Infrared spectroscopy

Thin films were prepared from the grades of modified PVAl. These films were analysed by FTIR and transmission IR spectra were recorded. It was shown positive change in comparison with unmodified, so absorbefacient maximum in the area 1640 cm^{-1}. The absorption peak at 1640 cm^{-1} corresponds with incorporation of double bond C = C into the macromolecule. The C = O bond in modified macromolecule corresponds with absorption maximum in the area 1740 cm^{-1}.

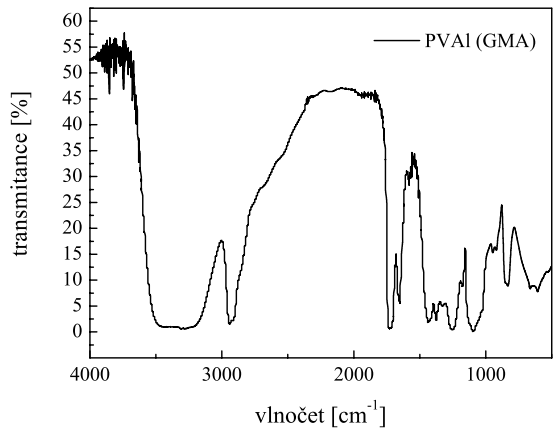

Fig. 2**. The comparison of IR spectra: PVAl 8-88 with PVAl modified by glycidylmethacrylate**

REFERENCES

1. Finch C. A.: *Polyvinyl Alcohol – Properties and Applications*. 1st edition, New York: John Wiley & Sons, Inc., 1992, 598 p.
2. Králová I., Veselý M., Dzik P.: Chem. Listy, *98*, 717 (2004).
3. Mühlebach A., Müller B., Pharisa C., Hofmann M., Guerry D.: Journal of Polymer Science: Part A: Polymer Chemistry, *35*, 3603 (1997).
4. Solomons, T. W. G: *Organic Chemistry*. 6th edition, New York: John Wiley & Sons, Inc., 1996, pp. 450–451.
5. Abd El-Kader K.M., Orabi A.S.: Polymer Testing 21, 591 (2002).

P19 DIAGNOSTIC OF PLASMACHEMICAL REMOVAL OF COPPER BASED CORROSION LAYERS

FRANTIŠEK KRČMA[a] , MAREK CIHLÁŘ[a] and MILOŠ KLÍMA[b]

[a]Brno University of Technology, Faculty of Chemistry, Purkyňova 118, 612 00 Brno, Czech Republic, krcma@fch.vutbr.cz

[b]Masaryk University Brno, Faculty of Science, Kotlářská 2, 611 37 Brno, Czech Republic

Introduction

Plasmachemical treatment of archaeological artifacts is a relatively new technique developed during the 1980s[1,2]. The process is based on using low-pressure hydrogen plasma in which the artifacts are treated for several hours, usually in more steps[3–5]. The problem is how long period of the

plasmatic treatment is optimal and how to characterize its efficiency. The studies focused on the composition of the layers show that various oxide and chloride complexes, usually containing also crystalline water, are the dominant compounds of the layer[5]. Recently the technique monitoring the plasmachemical oxide corrosion removal process was developed and successfully tested on silver ancient coins[6]. The monitoring of the ·OH spectrum was chosen as a finger point for the process control. The situation when the corrosion layers are more complex has not been studied up to now.

Experimental setup

The simplified scheme of our experimental device is presented in Fig. 1. The experiment usually takes place at the total gas pressure of 100–110 Pa and at the hydrogen flow rate of 100 Sccm. The capacitively coupled RF power supply gives the total power of 400–450 W. The sample temperature during the first 15 minutes of discharge increases up to about 280 °C and then it is more or less constant. Details concerning the experimental device as well as the complete list of the operating conditions can be found in bibliographical sources[7]. The optical spectrum emitted from the discharge in the part just behind the treated sample was measured by a spectrometer Jobin Yvon TRIAX 550 coupled with a multichannel UV CCD detector. To minimize the disturbing effects and to eliminate the discharge instabilities, we used a relatively long integration time of 10 s.

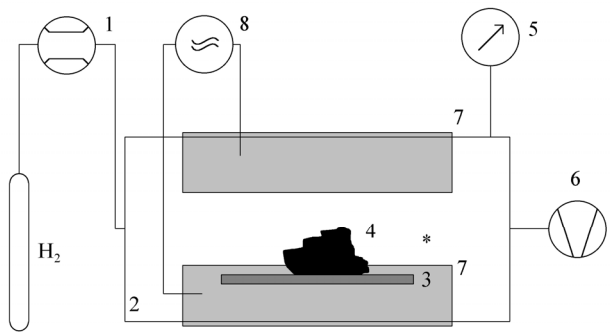

Fig. 1. **Experimental setup: 1 – mass flow controller; 2 – Pyrex glass reactor (length 88 cm, inner diameter 10 cm); 3 – sample glass holder; 4 – treated sample; 5 – baratron gauge; 6 – rotary oil pump; 7 – outer cylindrical copper electrodes (length 50 cm); 8 – RF power supply; * – point of spectroscopic measurements**

Corroded samples preparation

Two sets of copper corroded samples were prepared for the study. The first one was in acid atmosphere; in the other case the basic atmosphere was applied. The acid atmosphere was prepared as a saturated vapor mixture of three water solutions (HCl (18.5 %), HNO_3 (32.5 %) and $HCl + Na_2CO_3 + Na_2SO_3$ mixture). The last compound was added to obtain the chloride, sulfate and carbon corrosion layers. The composition of the basic atmosphere was similar, only the NH_3(aq.) was applied instead of the HNO_3. The technical copper samples (70 × 100 × 0.6 mm) were initially cleaned by an alkaline galvanic solution and then they were placed on a glass grating in the dessiccator where they were stored at the temperature of 20 °C. The samples were removed after six days and dried at ambient air.

Various corrosion compounds were detected at the surface, depending on the corrosion atmosphere. The $CuCO_3$, $CuCO_3.2Cu(OH)_2$, $CuSO_4$, and $CuSO_4.Cu(OH)_2$ compounds were the main in the case of acid corrosion atmosphere. In the other case, the NH_3 complexes were dominant. The CuO, CuO_2, and CuS compounds represented only a minority in both cases (about 10% of the surface).

Results

Spectra emitted from the discharge during the plasmachemical treatment were measured as a function of the treatment time. Identification of the atomic lines and the molecular band was the first step. An example of the spectrum with the main identified bands is presented in Fig. 2. Besides the hydrogen Lyman's lines and the lines of molecular hydrogen (not presented in Fig. 2.), many other bands were observed.

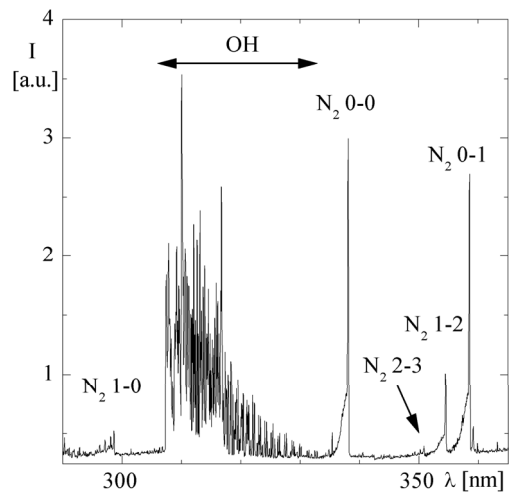

Fig. 2. **Selected part of the identified spectrum during the treatment (10 min.) of the sample prepared in the acid corrosion atmosphere**

The most intense are the nitrogen second positive system and the OH spectra, and also the nitrogen first negative system when the basic corroded sample was used. The CN violet bands and the NO^{β} system give spectra of a relatively low intensity. Intensities of all measured spectral lines and bands are strongly dependent on the plasma treatment duration and on the kind of corrosion. The band head intensities of nitrogen containing species were used as an intensity marker, the integral intensity in the range of 305–325 nm was chosen for the OH spectrum. The time evolution of the intensities of the selected bands is presented in Fig. 3. for the sample prepared in the acid atmosphere, Fig. 4. shows the same dependencies for the sample corroded in basic atmosphere.

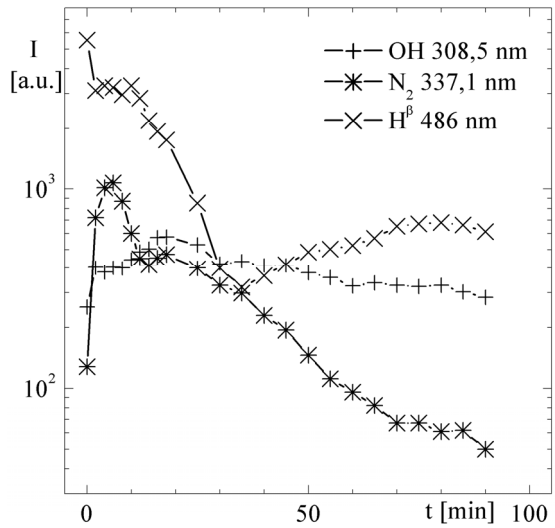

Fig. 3. **Intensities of the selected bands as a function of the plasma treatment duration (sample corroded in the acid atmosphere)**

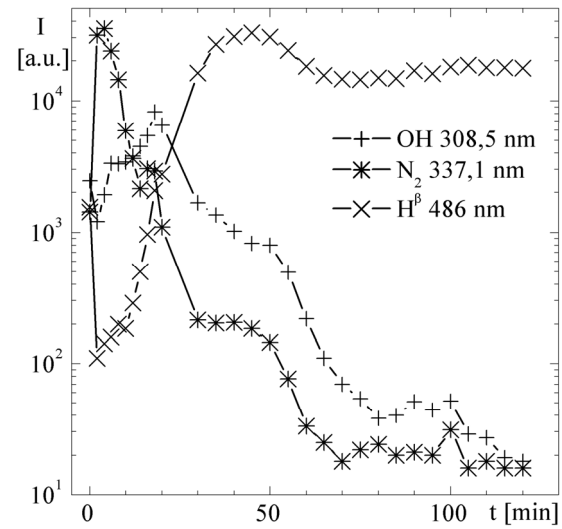

Fig. 4. **Intensities of the selected bands as a function of the plasma treatment duration (sample corroded in the basic atmosphere)**

The time dependencies show two completely different shapes. The intensities of the nitrogen bands (both neutral and ionized) decrease during the discharge treatment more or less exponentially. These bands can be negligible after about one hour of the discharge with the acid atmosphere corroded sample, in the other case the shape is similar, but the process takes a longer time due to a higher nitrogen concentration in the corrosion layer. The intensity of ·OH radicals decreases with the increasing treatment time more slowly than the intensity of nitrogen bands. This decrease is more or less linear, and thus the emission from ·OH radicals becomes dominant after a longer treatment time. These results are in a good agreement with our previous experiments with the removal of a dominantly oxide corrosion layers[6].

The intensities of the NO and CN bands can be studied in the time evolution only with difficulties, because their intensities are relatively low and their main vibrational bands are overlapped by the molecular hydrogen radiation within a short time.

Intensities of the hydrogen lines show an opposite dependence with respect to the OH radical intensity. An interpretation of this observation is clear – with the decrease of the oxygen concentration in the corrosion layer the ·OH production decreases, and thus the concentration of atomic hydrogen proportionally increases.

Conclusion

The corrosion layers removal by the low pressure hydrogen plasma was studied by the optical emission spectroscopy. The copper samples were corroded in acidic and basic atmosphere to obtain different kinds of corrosion layers. The results show that the oxygen removal from the sample takes a longer time than removal of the other elements, dominantly nitrogen containing compounds, contained in the corrosion compounds. Due to this fact, monitoring of the OH radical spectrum could be sufficient during the plasma treatment of more complex corrosion layers than oxide layers and the simple monitoring device presented in[6] can be applied independently of the corrosion kind.

This work was completed in co-operation with Methodic Centre of Conservation at Technical Museum in Brno and it was supported by Czech Ministry of Education, project No. 0894/2003.

REFERENCES

1. Veprek S., Patscheider J., Elmer J.: Plasma Chem. Plasma Process. *5*, 201 (1985).
2. Veprek S., Elmer J., Eckmann Ch., Jurcik-Rajman M.: J. Electrochem. Soc. *134*, 2398 (1987).
3. Klíma M.: Archeologické Rozhledy *50*, 255 (1998).
4. Klíma M., Zajíčková L., Janča J. et al.: Zeitschrift für Schweizerische Archäologie und Kunstgeschichte *54*, 2398 (1997).
5. Klíma M., Zajíčková L., Janča J.: Zeitschrift für Schweizerische Archäologie und Kunst-geschichte *54*, 29 (1997).
6. Rašková Z., Krčma F., Klíma M., Kousal J.: Czech. J. Phys. *52*, D927 (2002).
7. Klíma M.: *Plasmachemical Regeneration of Degraded Ancient Artifacts*, PhD Thesis, Masaryk University Brno, 2000.

P20 KINETICS OF THE NITROGEN PINK AFTERGLOW

FRANTIŠEK KRČMA and VĚRA MAZÁNKOVÁ
Institute of Physical and Applied Chemistry, Faculty of Chemistry, Brno University of Technology, Purkyňova 118, 612 00 Brno, Czech Republic, krcma@fch.vutbr.cz

Introduction

The nitrogen afterglow kinetics is a really complicated problem that is a subject of many studies during more then last 50 years[1–5]. The pink afterglow is a special part of the pure nitrogen post-discharge. It is characterised by the strong enhancement of the pink light radiation. The emission of the nitrogen first and second positive and first negative spectral systems is dominant during this period. The mechanisms populating the upper states of these spectral systems must be discussed separately for the neutral molecule (N_2 ($B\ ^3\Pi_g$) and N_2 ($C\ ^3\Pi_u$) states) and for the molecular ion (N_2^+ ($B\ ^2\Sigma_u^+$) state).

Results

Neutral nitrogen

The N_2 ($B\ ^3\Pi_g$) and N_2 ($C\ ^3\Pi_u$) states are dominantly created by pooling reactions of lower metastable states, especially by vibrational excited ground state and lowest 8 levels of N_2 ($A\ ^3\Sigma_u^+$) state[2,6]. These reactions show the creation of both these states but they cannot explain the strong population enhancement during the pink afterglow. Therefore another process must be considered. It is known that in nitrogen post-discharge kinetics of the ground state the initial Boltzmann distribution changes by v-v process into the Treanor-Gordiets distribution that can be characterized by the enhancement of populations at higher vibrational levels. In the creation of N_2 ($B\ ^3\Pi_g$) and N_2 ($C\ ^3\Pi_u$) states by pooling, the ground state must be excited at least to the levels v = 4, resp. v = 19 when pooling is with N_2 ($A\ ^3\Sigma_u^+$) state or v = 14, resp. v = 24 when two ground states are involved. It is clear that at the end of an active discharge all these species are present in the gas but their concentrations are much lower than concentrations of lowly excited molecules. The creation of higher vibrational levels takes some time, of course, and thus the dark space between end of the active discharge and pink afterglow is observed. The pooling reactions can also lead to creation of the ($A\ ^3\Sigma_u^+$) state and thus the pink afterglow effect is further enhanced. The reaction scheme can be written as follows (for references and rate constants see in[7]:

$$N_2\left(X\,^1\Sigma_g^+,v\right)+N_2\left(X\,^1\Sigma_g^+,w\right)\rightarrow N_2\left(X\,^1\Sigma_g^+,v+1\right)+N_2\left(X\,^1\Sigma_g^+,w-1\right) \quad (1)$$

$$2\,N_2\left(X\,^1\Sigma_g^+,v\geq 12\right)\rightarrow N_2\left(A\,^3\Sigma_u^+\right)+N_2 \quad (2)$$

$$2\,N_2\left(X\,^1\Sigma_g^+,v\geq 14\right)\rightarrow N_2\left(B\,^3\Pi_g\right)+N_2 \quad (3)$$

$$N_2\left(X\,^1\Sigma_g^+,v\geq 4\right)+N_2\left(A\,^3\Sigma_u^+,v\right)\rightarrow N_2\left(B\,^3\Pi_g\right)+N_2 \quad (4)$$

$$N_2\left(A\,^3\Sigma_u^+\right)+N_2\left(A\,^3\Sigma_u^+\right)\rightarrow N_2\left(B\,^3\Pi_g\right)+N_2 \quad (5)$$

$$2\,N_2\left(X\,^1\Sigma_g^+,v\geq 24\right)\rightarrow N_2\left(X\,^1\Sigma_g^+\right)+N_2\left(C\,^3\Pi_u\right) \quad (6)$$

$$N_2\left(X\,^1\Sigma_g^+,v\geq 19\right)+N_2\left(A\,^3\Sigma_u^+\right)\rightarrow N_2+N_2\left(C\,^3\Pi_u\right) \quad (7)$$

$$N_2\left(A\,^3\Sigma_u^+\right)+N_2\left(A\,^3\Sigma_u^+\right)\rightarrow N_2\left(X\,^1\Sigma_g^+\right)+N_2\left(C\,^3\Pi_u\right) \quad (8)$$

$$N_2\left(A\,^3\Sigma_u^+\right)+N_2\left(B\,^3\Pi_g\right)\rightarrow N_2\left(X\,^1\Sigma_g^+\right)+N_2\left(C\,^3\Pi_u\right) \quad (9)$$

The first two reactions form the precursors, the other lead to formation of both radiative states. The other metastable states, especially singlet states, must be included in the scheme when a numeric modeling will be used but this simplified form clearly demonstrates the principle of the pink afterglow creation.

Molecular ion

The kinetics of the molecular ion radiative state is more complicated and it can be explained in a two-step scheme. Before the pink afterglow the charged particles concentration is very low[8] but during the pink afterglow it significantly increases. So, the first step must lead to the molecular ion creation.

Due to the fact that the post-discharge is without any external energy source some of the kinetic processes must be enough efficient for the ionization. The whole process is known as a step-wise ionization[4,5]. In its principle, the highly excited neutral metastable molecules (both electronically and vibrationally) during their collisions can have energy sufficient for the ionization. Precursors for the ionizing collisions are created by the process (1) and by processes similar to (2).

When the molecular ion is created the excitation to the radiative state must be completed. Recent studies have shown that the main process populating the radiative N_2^+ ($B\ ^2\Sigma_u^+$) state is the collisionally induced energy transfer from the vibrationally excited neutral ground state[6].

The reactions describing the kinetics of molecular ion are, besides the reaction (1), as follows:

$$N_2\left(X\,^1\Sigma_g^+,v\right)+N_2\left(X\,^1\Sigma_g^+,w\right)\rightarrow N_2^*+N_2 \quad (10)$$

$$2\,N_2\left(X\,^1\Sigma_g^+,v\geq 32\right)\rightarrow N_2^+\left(B\,^2\Sigma_u^+\right)+N_2+e \quad (11)$$

$$N_2\left(X\,^1\Sigma_g^+,v\right)+N_2^*\rightarrow N_2^+ + N_2+e \quad (12)$$

$$N_2\left(X\,^1\Sigma_g^+, v \geq 12\right) + N_2^+\left(X\,^2\Sigma_g^+\right) \rightarrow N_2\left(X\,^1\Sigma_g^+\right) + N_2^+\left(B\,^2\Sigma_u^+\right) \quad (13)$$

The N_2^* in the reactions above means an electronically excited neutral molecule.

The same molecular states (N_2 ($X\,^1\Sigma_g^+$, $v \geq 12$)) are the reactants in the reactions (2) and (13). Because the experimental results show more or less the same dependencies for all observed spectral systems, it can be concluded that the highly vibrationally excited neutral nitrogen ground state molecules are the dominant species in the nitrogen post-discharge kinetics. The presented kinetic model could not explain the decrease of the vibrational populations of molecular ion by decreasing the temperature and this effect thus must be further studied.

This work was supported by the Czech Science Foundation under project No. 202/05/0111.

REFERENCES

1. Beale G. E., Broida H. P.: J. Chem. Phys. *31*, 1030 (1959).
2. Piper L. G.: J. Chem. Phys. 88, 231 and 6911 (1988); *91*, 864 (1989).
3. Guerra V., Sa P. A., Loureiro J.: J. Phys. D, Appl. Phys. *34*, 1745 (2001).
4. Polak L. S., Sloveckii D. I., Sokolov A. S.: Opt. Spectrosc. *32*, 247 (1972).
5. Paniccia F., Gorse C., Cacciatore M., Capitelli M.: J. Appl. Phys. *61*, 3123 (1987).
6. Krčma F., Protasevich E. T.: *Post-discharges in Pure Nitrogen and in Nitrogen Containing Halogenated Hydrocarbon Traces*, Tomsk Polytechnic University Publishing, Tomsk, Russia, 2003.
7. Krčma F.: http://www.fch.vutbr.cz/home/krcma/publications/95-thesis-appendix1.pdf.
8. Janča J., Tálský A., El Kattan N.: Folia Physica *27*, 23 (1978).

P21 PHOTOMETRIC STUDY OF THE APPARENT UV-LIGHT ABSORPTION BY SOME BIOLOGICAL BUFFERS

MIROSLAVA KRČMOVÁ[a] and RADIM VESPALEC[b]
[a]*Brno University of Technology, Faculty of Chemistry, Institute of Physical and Applied Chemistry, Purkyňova 118, 612 00 Brno, Czech Republic, xckrcmova@fch.vutbr.cz,* [b]*Institute of Analytical Chemistry, Czech Academy of Science, Veveří 97, 611 42 Brno, Czech Republic, vespalec@iach.cz*

Introduction

Synthetic compounds called biological buffers are widely used for the pH control in the pH range of 5.5–11.4 (ref.[1]). Zwitterionic Good buffers, one of subgroups biological buffers, frequently serve as protein solubilization agents in aqueous solutions[2], too. Popularity of biological buffers in biochemistry and in analytical chemistry follows from two facts. Photometric detection dominates in modern instrumental analytical methods and biological buffers are free of chromophores absorbing UV-light above 200 nm. Despite this, it was reported recently that aqueous solutions of three biological buffers pronouncedly affect the intensity of the passing UV-light beam in the short-wavelength range[3]. The aim of our study is the verification of this finding for three most frequently utilized zwitterionic Good buffers.

Experimental part

The UV-Vis spectrophotometer VARIAN – CARY 50 Probe (Varian BV, Netherlands) equipped with the quartz cell of 1 cm optical path length served for photometric measurements in the range of 190–300 nm. Investigated buffers (Table I) are from Sigma-Aldrich (Prague, Czech Republic). The pH of their 4–200 mmol l^{-1} solutions in redistilled water was adjusted with sodium hydroxide (Lachema, Brno, Czech Republic).

Table I
Investigated GOOD buffers[1]

Buffer	Formula	MW [g mol^{-1}]	pK_a [25 °C]	pH range
MOPS	$C_7H_{15}NO_4S$	209.26	7.2	6.5–7.9
MES	$C_6H_{13}NO_4S$	195.24	6.1	5.5–6.7
CAPSO	$C_9H_{19}NO_4S$	237.32	9.6	8.9–10.3

Results

Investigated Good buffers, 2-morpholinoethanesulfonic acid (MES), 3-morpholinopropanesulfonic acid (MOPS) and 3-(cyclohexylamino)-2-hydroxy-1-propanesulfonic acid (CAPSO) cover almost completely pH range of the Good buffers applicability. The investigated buffers are free of chromophores absorbing light above 190 nm disregarding their chemical identity and pH. Weakening of a light beam passing through their aqueous solutions cannot be therefore classified the light absorption even if it is displayed in absorbance units by the used instrument. Three pH units below their pK_a values, the buffers are only in the zwitterionic form considering the measurement precision. At $pH = pK_a$, the concentration of the zwitterionic form and of the anionic form is identical. At $pH = pK_a + 3$, practically only anions exist in solution.

Experiments with purely zwitterionic solutions of MES, MOPS (Fig. 1.) and CAPSO revealed that their formal absorbance increases with both increasing concentration and with the decreasing wavelength of the passing light. The maximum measured absorbance depended on the dissolved compound. In the range of usually utilized concentrations of Good buffers, ranging from 20 to 60 mmol l^{-1}, the light

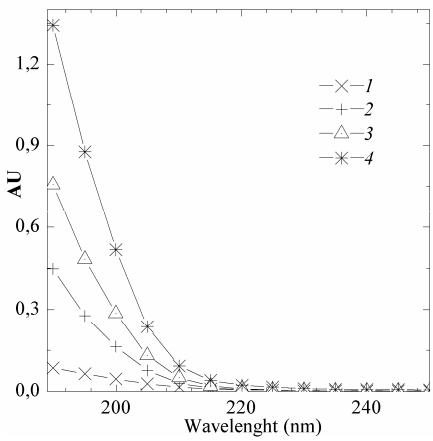

Fig. 1. **Typical course of the dependence of the formal absorbance of dissolved zwitterionic buffers on the passing light wavelength documented on the example of MOPS. The MOPS concentration is given as a parameter: 1) 4.1 mmoll^{-1}, 2) 50 mmol l^{-1}, 3) 100 mmol l^{-1}, 4) 200 mmol l^{-1}**

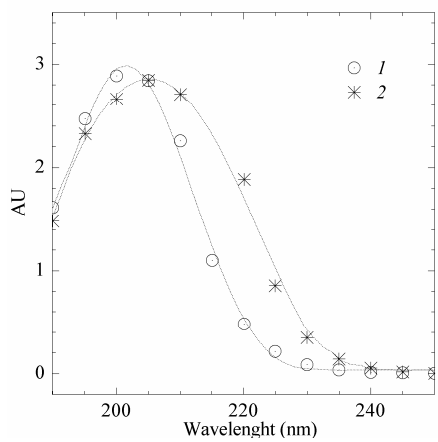

Fig. 3. **Typical course of the dependence of the formal absorbance of dissolved zwitterionic buffers on the buffer pH at 1) pH = pK_a and 2) pH = pK_a + 3 documented on the example of MOPS**

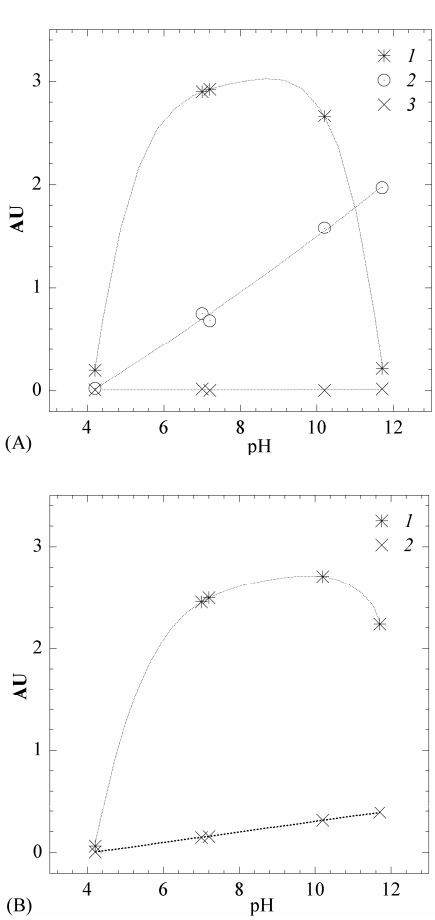

Fig. 2. **Typical course of the dependence of the formal absorbance of dissolved zwitterionic buffers on the buffer pH documented on the example of MOPS. The wavelength of the passing light is given as a parameter: (A) 1) 200 nm, 2) 220 nm and 3) 250 nm, (B) 1) 210 nm and 2) 230 nm**

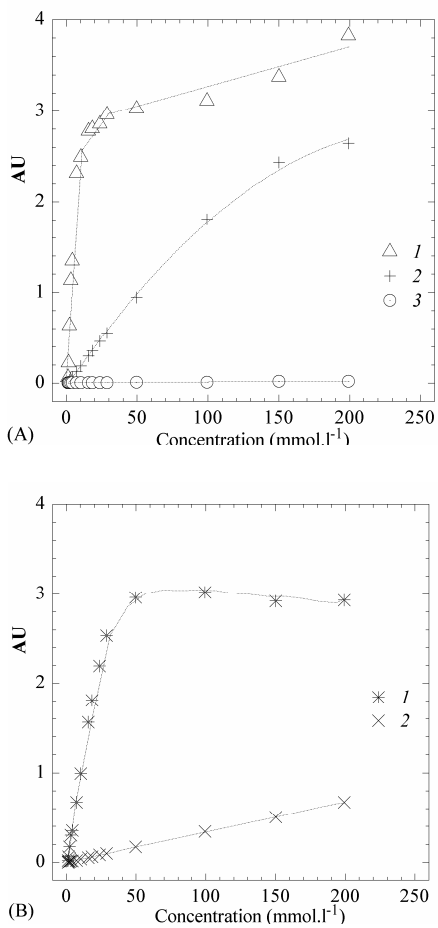

Fig. 4. **Typical course of the dependence of the formal absorbance of dissolved zwitterionic buffers on their concentration documented on the example of MOPS. The wavelength of the passing light is given as a parameter: (A) 1) 200 nm, 2) 220 nm and 3) 250 nm, (B) 1) 210 nm and 2) 230 nm**

absorption was acceptably low above 200 nm. Zero absorbance was obtained at the wavelength of 250 nm and higher disregarding the compound and its concentration.

The (pH–pK_a) difference affects the light beam weakening dramaticly at concentrations up to pH = pK_a (Fig. 2.). At pH > pK_a, the absorbance rises up much less. The dependences of formal absorbance at pH = pK_a and pH = pK_a + 3 on the light beam wavelength differ therefore only slightly (Fig. 3.). The steepness of the concentration dependence of the apparent absorbance rises up with the decreasing wavelength (Fig. 4.) as may be expected from previous experiments.

Conclusions

Photometric experiments evidenced general aggregation capability of investigated zwitterionic Good buffers MES, MOPS and CAPSO and, in agreement with the previous communication[3], dramatic increase of this capability in the pH range in which the concentration of the anionic form of the buffer approaches 50 % of its total concentration. Formation of aggregates from dissolved MES, MOPS and CAPSO, which disperse the passing UV-light beam, is a possible interpretation of presented experiments. Conductivity measurements not presented here evidence that the aggregates are not micelles. This finding controverts the explanation proposed in the article[3].

Presented results of photometric experiments evidence correctness of experiments given in Ref. 3. The results also substantiate continuation of the presented research.

REFERENCES

1. Sigma-Aldrich cataloque 2000–2001.
2. Hames B. D., Rickwood D.: *Gel Electrophoresis of Proteins.* 2-nd edition, p. 153, OIRL Press, Oxford, 1990.
3. Vespalec R, Vlčková M., Horáková H.: J. Chromatogr. A *1051*, 75 (2004).

P22 DIELECTRIC PROPERTIES OF POLYMERS PART I. SOLID FILMS OF HYDROXYETHYLCELLULOSE

ALENA MACHÁČKOVÁ and PAVEL URBAN
Institute of Physics and Material Engineering, Faculty of Technology, Tomas Bata University, Nad Stráněmi 4511, 760 05 Zlín, Czech Republic

Abstract

There were studied electrophysical properties of two types of solid films of hydroxyethylcellulose. Measurements of dielectric relaxation spectra of Natrosol 250 H4R and Natrosol 250 LR in the frequency range from 1 to 1400 MHz have been realized. The dependencies of real part ε'(f) and imaginary one ε''(f) were determined. It has been found that the results of the measurement are strongly influenced with traces of binary electrolytes and also with a thermal history of the studied samples, and small amounts of water situated in the inner part of films and on the surface, especially.

Introduction

Many papers from the recent years dealt with the polymeric dynamics of polysaccharides in the solid state[1–3]. It has been found that the main relaxation measured in the low temperature range (–120 °C to 0 °C) is associated with the local backbone or segmental motion of the chain. This process is called β-relaxation in comparison with the motion of the side groups at the repeating unit named γ-relaxation and β_{wet}-relaxation measured in all wet or swollen systems[4].

Segmental mobility of a polymer chain determines many properties of macromolecular compounds, e. g. the ability of free vacance creation, and for this reason also a transport resistibility of matter in processes of viscous flow, diffusion phenomena and many others[5–8].

One of the methods to characterize materials is based on the analysis of their dielectric spectra. Dielectric analysis provides the information about the motion of entities having an electric charge or an electric dipole moment, i.e. about dipole reorientation, rotations of the main and segmental chains and conductivity mechanism. Dielectric relaxation in hydroxyethylcellulose has been studied by K. Liedermann and L. Lapčík, Jr. and coworkers[9–11]. In this papers the origin of the relaxation in the hydroxyethylcellulose is interpreted as being due to the reorientation of the double ethylene oxide groups constrained by their large size and inter-chain bounding by hydrogen bridges. The authors[9–11] also pointed out the fact that the relaxation phenomena are often masked by the conductivity component. On the contrary, the relaxation due to secondary hydroxyl groups is assumed to take place at higher frequencies (in the MHz to GHz range).

Marianiová D., Lapčík L., Jr. and M. Pisárčík[12] have studied the temperature and frequency dependences of electric conductivity of hydroxyethylcellulose, carboxymethylcellulose, 2.5 cellulose acetate, and cellulose triacetate in the temperature range from 20 °C to 150 °C and in frequency range from 0.5 to 100 kHz. This study was completed by DTA measurements. The glass transition temperature and the values of the activation energies have been determined and discussed with respect of the structure of the cellulose derivatives. The authors[12] measurements have proved semicrystalline structure of the mentioned derivatives connected with the ionization and polarization processes in the samples in the external electric field. The reciprocal penetration of corresponding segments has a complex character and can be explained by two different groups of powers. Electrostatic and repulsion powers between electrical charges of ions, i. e. coulombic powers modifying especially the corresponding distribution of solvated ions and change of quasi-crystalline structure of the electrolyte, and polymorphic and conformation changes of the solid films dominate in the first group, too. The second group interactions, the solvation, i. e. interactions between ions and molecules of solvents (water), cause the decomposition of water structure and bound water

molecules and ions to a more or less configurated system (but usually not by covalent bonds).

In this study, the behavior and dielectric properties of hydroxyethylcellulose in the frequency range from 1 MHz to 1500 MHz are studied.

Experimental

The study was realized on two types of commercial samples of hydroxyethylcellulose (HEC) from Hercules Inc. (Natrosol 250 LR and Natrosol 250 H4R) in the thin layer film form of thickness from 0.05 to 0.25 mm. These films were prepared from water solutions of HEC (40 g of HEC in 750 ml of redistilled water) by casting on Petri dishes and following slow water evaporation in dissiccator (over NaOH solid pellets) at constant temperature 25 °C. Frequency dependence of dielectric constant – real part ε' and imaginary one ε'' – was measured with LCR meters (Hewlett-Packard 4291A) equipped with a parallel plate type of cell) to which the specially prepared Pt-Pt electrodes were attached. The measurements were performed at constant temperature 25 °C.

Results and Discussion

The principal property of solid polar polymer film seems to be a possibility of a certain electrostatic field existence inside it. Such electric field can exhibit a strong influence on charge particular entities localized inside the sample and this phenomenon prevents them from free movement on longer distance. This is in principle the difference from conductors of metallic type. When such a dielectricum is inserted into an external electric field the certain shifts of charged entities can be identified and permanent and induced dipolar structure reorientation in electric field direction is usually observed. In the structural formula of HEC can be distinguished a few such dipolar structures in fundamental monomeric unit (Fig. 1.).

On the other hand, the vectorial additivity of the polar structural elements (–O–H, R–O–R, R'vO-R, …) leads to a certain spectrum of harmonic resonators with characteristic dielectric properties responses. These effects are to be observable on frequency dependences of real ε'(f) and ε''(f) parts of dielectric constants (mentioned above).

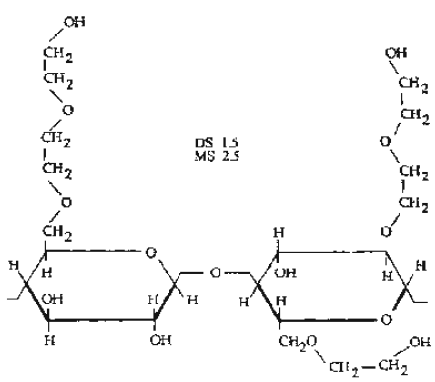

Fig. 1. **The structural formula of HEC**

From the point of view of the studied HEC films, characteristic by a certain thermal history, implemented in the systems during their preparation, it should be taken into regard also a fact, that the films prepared by casting cannot exhibit isotropic properties, especially in perpendicular direction to the free outer surface plane. It may be different a self-organization of the HEC chain molecules in the outer phase boundary of that inside the thin layer and then the ε'(f) and ε''(f) curves might differ of each other with sample thickness. It was found that for the most studied samples of HEC the following empiric formula can be utilized (Fig. 2.):

$$\frac{1}{\ln \varepsilon'} = kf \,, \tag{1}$$

where ε' is real part of complex permittivity. On the base of the result presented in Fig. 3. and the others, there is possible to receive the value of static permittivity ε_s.

$$\varepsilon_s = \lim_{f \to 0} \frac{1}{\ln \varepsilon'} \,, \tag{2}$$

Table I
HEC samples thickness and their numeric notation

HEC	Sample No.	Thickness [mm]	Root mean square deviation of thickness ± σ
Natrosol	1.07	0.052	0.002
250 H4R	1.15	0.062	0.002
Natrosol	2.25	0.232	0.002
250 LR	2.27	0.304	0.002
	2.30	0.316	0.002

The symmetric structural aggregates on the surface of polymer films after solvent evaporation were identified by S. Sakurai, Ch. Furukawa, A. Okutsu, A. Miyoshi and S. Nomura[13]. The same effects we have found in thin films of water soluble derivatives of cellulose and these results will be published later[14]. Especially in the case of polyelectrolytes this complexes can be very easy iden- tified[15].

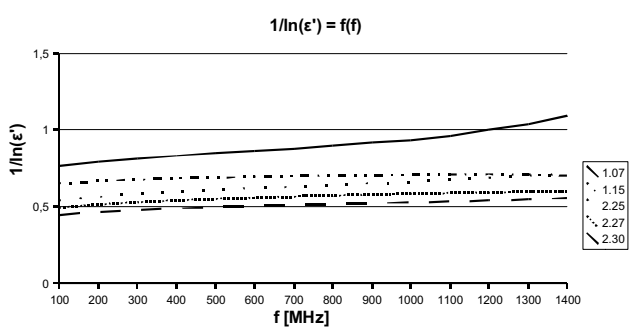

Fig. 2. **The frequency dependence of 1/ln(ε') for several random chosen samples of HEC**

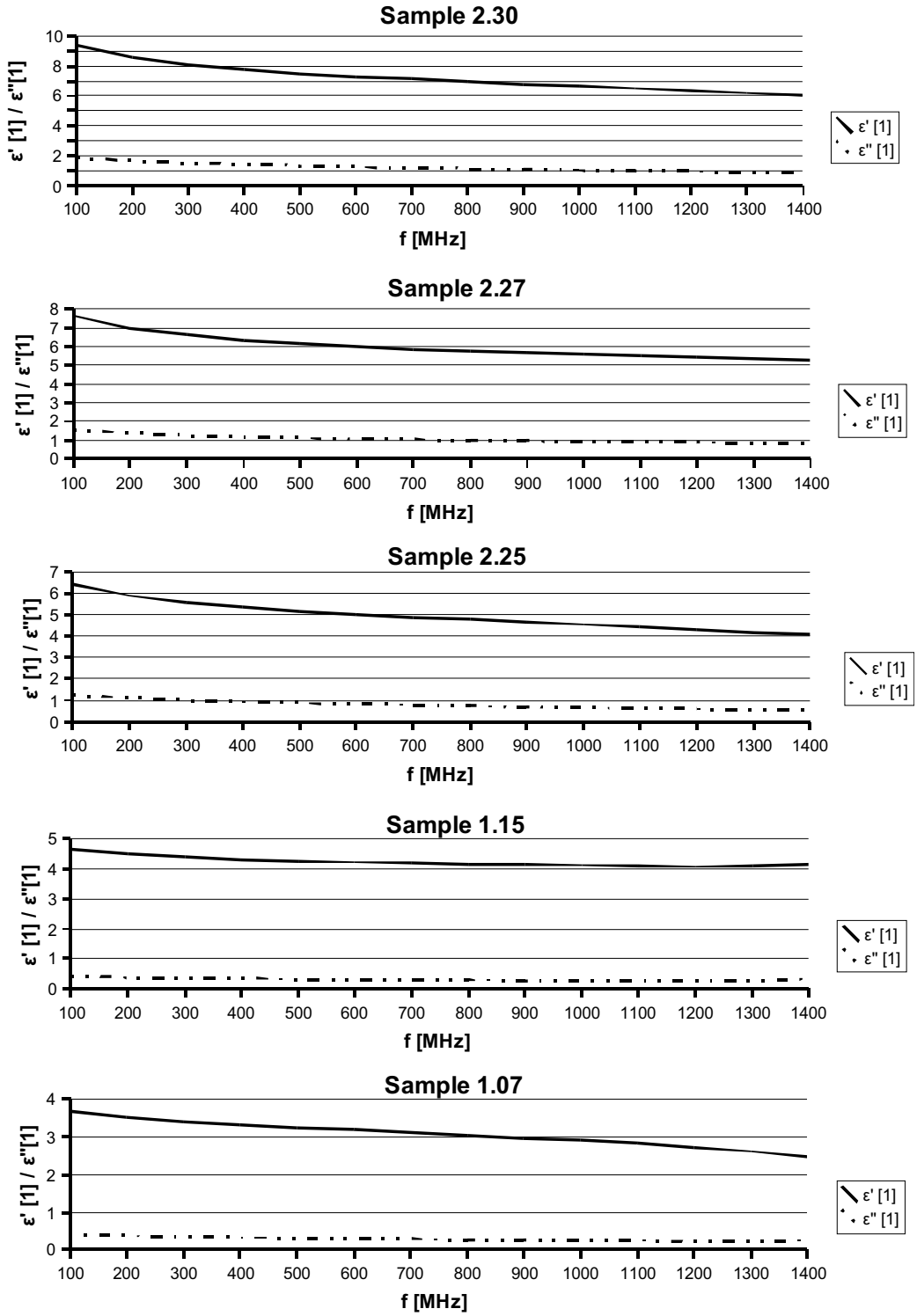

Fig. 3. **The frequency dependence of ε'= ε'(f) and ε"= ε"(f) for samples given in Fig. 2.**

REFERENCES

1. Liedermann K., Lapčík L. Jr.: Chem. Papers *50*, 218 (1996).
2. Saad G. R., Ken-ichi Furuhata, Polym. Int. *42*, 356 (1997).
3. Einfeldt J., Meissner D., Kwasniewski A., Einfeldt L.: Polymer *42*, 7049 (2001).
4. Einfeldt J., Meissner D., Kwasniewski A.: Macromol. Chem. Phys. *201*, 1669 (2000).
5. Flory P. J.: *Principles of Polymer Chemistry*, Cornell Univ. Press, Ithaca 1953, Chapter 14.
6. Holzmüller W., Altenburg K.: *Physik der Kunststoffe*, Akademie Verlag, Berlin 1961, Czech Edition – SNTL, Prague 1966, Chapter 4 and 7.
7. Lechner M. D., Gehrke K., Nordmeier: *Makromolekulare Chemie*, Birkhäuser Verlag, Basel 1996, 2nd Edition, Chapter 5.
8. Maiti S.: *Analysis and Characterization of Polymers*, Anusandham Prakashan, Midnapore 2003, Chapter 13, 14 and 15.
9. Liedermann K., Lapčík L. Jr.: Chem. Papers *50*, 218–223 (1996).
10. Liedermann K., Lapčík L. Jr.: Carbohydrate Polymers *42*, 369 (2000).
11. Liedermann K., Lapčík L. Jr.: Demeester J.: *Dielectric Spectroscopy of Plasma Modified Polysaccharides for Medical Applications*, in Proceedings of the 5th International Conference on Properties and Applications of Dielectric Materials, Vol.1., pp 541–544, Seoul (Korea) 1997.
12. Marianiová D., Lapčík L. Jr., Pisárčík M.: Acta Polymer *43*, 303 (1992).
13. Sakurai S., Furukawa Ch., Okutsu A., Miyoshi A., Nomura S.: Polymer (London) *43*, 3359 (2002).
14. Lapčík L. and coworkers: unpublished results.
15. Philipp B., Dautzenberg H., Linow K. J., Kötz J., Dawydoff W.: Progr. Polym. Sci. *14*, 91 (1989).

P23 OPTICAL, SPECTRAL AND MECHANICAL CHANGES OF AGED PAPER

MILAN MIKULA, ALEXANDRA VALASEKOVÁ, BRANISLAV PROSNAN and ŠTEFAN ŠUTÝ
Department of Graphic Arts Technology and Applied Photochemistry, Faculty of Chemical and Food Technology, Slovak University of Technology, Radlinského 9, SK-812 37 Bratislava, milan.mikula@stuba.sk

Abstract

Stability of white offset paper, uncoated and coated was tested by artificial accelerated thermal aging according new method of Begin-Kaminska. The mechanical, optical, chemical and structural changes were characterized by optical spectrometry, brightness, whiteness, gloss, absorption Fourier transform infrared (FT-IR) spectroscopy, double-bending and breaking length. IR spectroscopy techniques, single diamond ATR (attenuated total reflection) for surface characterization and diffuse reflectance (DRIFT) techniques for deeper attack were compared. DRIFT is more suitable at low absorption regions (above 1080 cm^{-1}), however diamond ATR is better at higher absorption (below 1080 cm^{-1}). Correlations among the original and aged paper parameters were considered, while the biggest changes were found in mechanical properties and in whiteness, brightness and gloss.

Introduction

Many efforts are focused to preserve archival documents and to measure the changes of papers, inks and the whole system including interactions. Mechanical, optical and chemical properties of documents are irreversible changed upon aging[1,2]. Destructive mechanical tests methods as fold endurance, tear and breaking tests are sensitive, reliable, but expensive and time consuming. Optical and spectral methods are nondestructive, simple and quick, but less correlated and sensitive to aging effects. Besides visible measurements, FT-IR spectroscopy is now used for chemical, structural and crystallinity analysis mainly studding IR various absorption bands ratios (1280/690, 1430/900 and 2900/1370, in cm^{-1}) (ref.[3]). The aim of this work is to evaluate and to correlate the extent of mechanical, optical and spectral changes.

Experimental

Standard uncoated (100 g m^{-2}) and coated (130 g m^{-2}) offset alkaline papers were aged artificially by new accelerated method by Begin-Kaminska[4]: 9 g of treated paper was preconditioned at relative humidity RH = 50% (at 23 °C), afterwards enclosed into 300 ml glass bottle, covered by Viton® (DuPontDow) sealing and heated to 100 °C for 5 days. The aging better correlates with the natural one than a dry or wet aging. Original and aged papers were tested mechanically, optically and spectroscopically:

Mechanical tests: Fold endurance were measured by double bending technique (Schopper instrument).

Tear strength F_{max}, breaking length l_t, tensile strain δ_t and Young modulus E were measured and calculated by INSTRON 1122.

Optical tests: Lightness L* with coordinates, a*, b*, and brightness R457 (blue light reflection at 457 nm) were measured by ELREPHO Datacolor 2000. Spectral whiteness W (Y, x, y) was calculated from L*, a*, b* data: $W = Y + 800(x_n - x) + 1700(y_n - y)$, where x_n and y_n are coordinates of the white standard. Gloss was measured by red laser diode light reflection at the angle of 60 °, defined as $G = R_s/R_{stand} \cdot 100\ \%$ (R_s and R_{stand} are light reflections of the sample and a black glossy standard, respectively).

Spectroscopy: Fourier Transform IR (FTIR) spectrometer, Excalibur, DigiLab was used to measure remission spectra by DRIFT (Diffuse Reflectance Infrared FT) method and absorption spectra by Single reflection Diamond ATR technique (just ~1 μm surface layer absorption). Kubelka-

-Munk (KM) procedure for remission DRIFT spectra was used to get KM function (f_{KM}) that is proportional to absorption: $f_{KM} = (1 - R)^2/2R$, where R is measured remission.

Results and conclusions

Mechanical properties deteriorate the most with aging, as expected. Double Folds indicate less decrease with aging (to 30–80 %) than tear parameters (to 10 %), Fig. 1. Lengthwise folds (machine direction, MD) decreased more than cross folds (CD), while all tear parameters decreased perfectly to the same relative values with no respect to fiber direction, despite big differences in absolute values. This confirms isotropic aging rate of paper, equal character of inter-fiber bonds and perfect quality of tear measurements. For aging studies one tear parameter is representative enough.

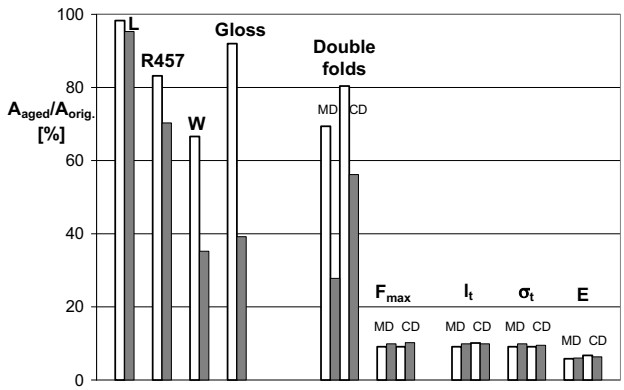

Fig. 1. **Relative decrease of optical and mechanical parameters of aged papers, uncoated – light bars, coated – dark bars, MD – machine, CD – cross direction**

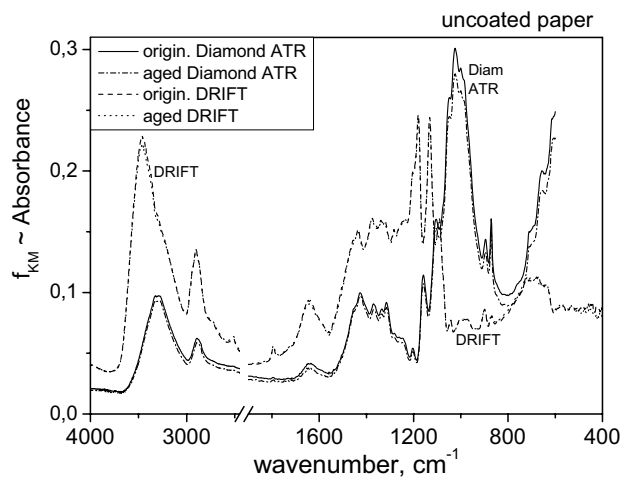

Fig. 2. **Comparison of DRIFT (Kubelka-Munk) and ATR absorption spectra. (DRIFT is divided by 100)**

Considerable optical changes were confirmed in whiteness and brightness, for coated papers also in gloss, however, the lightness L* is changing a very little.

FTIR absorption spectra of papers differ when using DRIFT or Diamond ATR techniques, Fig. 2. DRIFT gives the information about the whole semitransparent paper (due to IR light scattering inside the paper). This mixed reflection/absorption spectrum is useful outside the regions of high absorption, where the internal remission exceeds the influence of gloss. Contrary, diamond ATR is sensitive mainly at high absorption region, because of single reflection – single contact of IR wave with sample surface just to the depth of several microns. So it measures just coatings in the coated paper case.

Spectral changes cased by aging are very week comparing with mechanical or optical changes. Just very precise and detail measurements can show some trends. Global increase of DRIFT absorption with aging, Fig. 3., is not caused by chemical changes, but by the increase of physical surface (roughness) of aged papers.

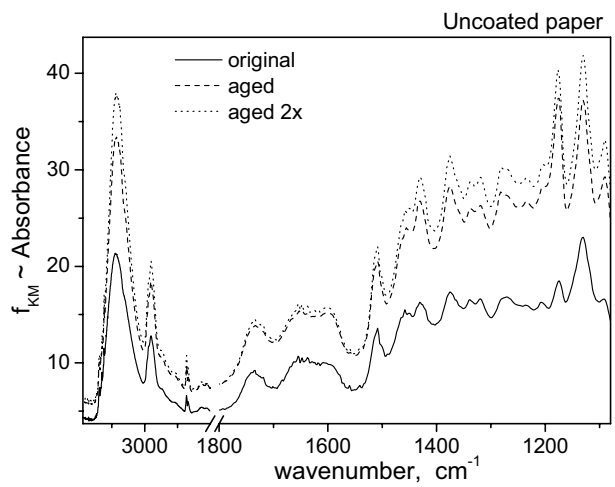

Fig. 3. **DRIFT Kubelka-Munk spectra of uncoated paper, original, aged, and two times aged**

We thank the Slovak Grant Agency VEGA (project VEGA 1/2454/05) and Science and Technology Assistance Agency (contract APVT-20-034202) for financial support.

REFERENCES

1. Browning B. L.: *Analysis of paper*, 2nd ed. New York, Marcel Dekker, 1977.
2. Havlínová B., Babiaková D., Brezová V., Ďurovič M., Novotná M., Belányi F.: Dyes and pigments *54*, 173 (2002).
3. Ali M., Emsley A. M., Herman H., Heywood R. J.: Polymer *42*, 2893 (2001).
4. Bégin P. L., Kaminska E.: Restaurator *23*, 895 (2002).

P24 STUDY OF GENOTOXICITY/ ANTIMUTAGENICITY OF HUMIC ACIDS

ANDREA MIKULCOVÁ[a], EDITA TIHLÁŘOVÁ[a], JITKA KUBEŠOVÁ[a], JIŘÍ KUČERÍK[b], MILOSLAV PEKAŘ[b] and IVANA MÁROVÁ[a]

[a]*Department of Food Chemistry and Biotechnology, Faculty of Chemistry, Brno University of Technology, Purkyňova 118, 612 00, Czech Republic, mikulcova@fch.vutbr.cz,* [b]*Department of Physical and Applied Chemistry, Brno University of Technology, Purkyňova 118, 612 00, Czech Republic, kucerik@fch.vutbr.cz*

Introduction

Mutagenesis is process in which specific changes in genome are formed. These changes comprise substitution, deletion or insertion in sequences of nucleotide which are called mutations. The induced or spontaneous mutations are formed by action of mutagens – it means chemical, physical or biological factors. The antimutagen is substance able to reduce occurrence of spontaneous or induced mutations.[1]

Humic acids belong to wide group of organic compounds formed during decomposition of organic matter of vegetable origin. Humic acids are operationally defined as fraction of humic substances, which is not soluble under acidic conditions. Isolation of humic acids from natural sources as soil, coal or peat is based on acidifying alkaline extract to pH 1–2, which results in precipitation of humic acids[2].

Structure of humic substances is composed of alkyl/aromatic formations linked by groups of oxygen and nitrogen. Carboxylic acid, hydroxyls of alcohols and phenols are the main functional groups. Humic acids are more aromatic and in the H^+ – exchange form are not soluble in water[3].

It is well known that soil organic matter has a favorable effect on the physical, chemical, and biological characteristics of soils. This effect is now realized to be caused by the active components of the inorganic and humus fraction[4].

The adsorption, dispersion or emulsification property and other attributes of humic matter attract the interest of medical science and the pharmaceutical industry. Using humic matter in the pharmaceutical industry is derived from a number of reasons. The oldest reason comes perhaps from peat, which has been known for its therapeutic properties. In the modern cosmetic industry, face muds are offered for curing and removing old skin. These healing properties have been currently ascribed to humic acid, the dominant component of peat. The potential of use of humic acids as antiviral, anti-inflammatory, estrogenic, profibrinolytic and anti-coagulatory agents has been under serious investigations[4]. Active substances from group made from tannins, catechins, humans, humic acids, gallic acids and other components or combination two or more of these components are used in the therapy of asymptotic infections of HIV and other diseases caused by retrovirus, quickly proceeding infections of clinical AIDS, hepatitis B and cancer[3].

The aim of this work was the study of the potential genotoxic/antimutagenic effects of some preparatives of humic acids using two biological test systems: (i) specific yeast *Saccharomyces cerevisiae D7* and (ii) a protozoon *Euglena gracilis*.

Methods

For testing of biological properties of water soluble sodium humate the *Saccharomyces cerevisiae D7* test and *Euglena gracilis* test were used. The humates are in essence the salts of humic or fulvic acids. As technical grade chemicals these humates are also the fertilizers[4]. In this work four different partially purified samples of sodium humate were tested.

In the *Saccharomyces cerevisiae D7* test biological effects were observed as ability to inhibit the formation of mutant colonies (tryptophane-conversions, isoleucine-reversions) caused by affect of standard mutagen 4-N-nitroquinoline-N-oxide (4-NQNO). The yeast suspension of *S. cerevisiae D7* in the logarithmic phase of growth in the liquid YPD medium was divided into test tubes. The cells were centrifugated (4500 rpm, 5 minutes, 20 °C) and cell sediment was washed twice by the Sörensen (phosphate) buffer pH 6.98. The 10 ml of the yeast suspension in the Sörensen buffer was influenced by 1% and 0.125% water solution of sodium humate and 0.1 ml of 0.06 mg ml^{-1} 4-NQNO. After 20 hours of incubating at 28 °C yeasts cells were centrifugated and washed twice by the Sörensen (phosphate) buffer pH 6.98 again.

Yeast suspension (0.1 ml of 10^6 cells ml^{-1}) was inoculated in the selective medium without tryptophane and/or isoleucine. The number of the tryptophane conversions was evaluated after 5 days while the colonies of isoleucine reversions were counted after 10 days of incubation on Petri dishes at 28 °C.

The *Euglena gracilis* test was carried out with ofloxacin as standard mutagen which caused reduction of chlorophyll absorption. Antimutagenic effect is based on reduction of number of white mutant colonies formed in the presence of ofloxacin.

The 6 ml of culture of *E. gracilis* in the logarithmic phase of growth was affected by the same concentrations of water solution of sodium humate as in the *S. cerevisiae D7* test. The concentration of ofloxacin in the 6 ml of culture was 430 μmol l^{-1}. The extent of biological effect of sodium humate in the cells of *E. gracilis* was determined by measuring of absorbance of chlorophylls *a* and *b* after 12 days of incubating cells in the presence of light (20 W). The isolation of chlorophylls was carried out by extraction using 99.5% acetone. After 1 hour extraction in the dark and at room temperature the absorbance of chlorophylls was measured spectrophotometrically at 663 nm (chlorophyll *a*) and 645 nm (chlorophyll *b*).

Results

Using two biological test systems a pilot study of genotoxicity/antimutagenicity of sodium humate was observed.

In the *S. cerevisiae D7* test the results were obtained by comparison of the number of the yeast colonies grown in the presence of mixture of sodium humate and the standard mutagen (4-NQNO) and the number of the yeast colonies in the Petri dish which were influenced with the standard mutagen (in the absence of sodium humate). In this test all used concentrations of water solutions of standard sodium humate led to suppression of growth of yeasts cells. Some slight antimutagenic effects were observed using 0.125 % concentration of purified sodium humate preparatives. For future testing lower concentrations of sodium humate solutions should be used.

In the *E. gracilis* test the biological activity of sodium humate was evaluated by comparison of content of chlorophyll *a* and *b* in the cells after influence with mutagen and/or sodium humate with the content of chlorophylls in the unaffected cells. The results of the *E. gracilis* test showed that 1% sodium humate acted as powerful promutagen while the 0.125% sodium humate perfomed as the antimutagen. The contents of both chlorophylls in the cells affected by 0.125% sodium humate itself (in the absence of mutagen) proved some effect of sodium humate on the cell growth.

This work was supported by the project MSM 0021630501 of the Czech Ministry of Education, Youth and Sports.

REFERENCES

1. Malachová K.: *Mutagenita a karcinogenita kontaminant životního prostředí,* Oftis, Ostrava 1993.
2. Klučáková M., Pekař M.: Colloids and Surfaces A: Physicochem. Eng. Aspects *252*, 157, (2005).
3. Linhartová P.: *Diploma thesis*. Brno University of Technology, Brno, 2001.
4. Kim H. Tan: *Humic Matter in Soil and the Environment, Principles and Controversies,* Marcel Dekker, Inc, New York 2003.

P25 STUDY OF PHOTOCHEMICAL OXIDATION OF HOLE-SCAVENGERS IN AQUEOUS SOLUTION

PETRA MOŽÍŠKOVÁ, MICHAL VESELÝ and JIŘÍ ZITA
Brno University of Technology, Faculty of Chemistry, Department of Physical Chemistry, Purkyňova 118, 612 00 Brno, Czech Republic, moziskova@fch.vutbr.cz

Introduction

Recently, industrial activities have been disturbing the geological equilibrium of metal ions through the release of large quantities of toxic metal ions into the environment.

Toxic metal ions are generally released into the environment through human activities such as coal burning, trash incineration and industrial emission. They are usually used in metallurgical, pharmaceutical, chemical and petrochemical industries and in paints, electronics, batteries, dental materials, pesticides, fungicides, herbicides, insecticides, bactericides etc.

A heterogeneous photocatalytic system consists of semiconductor particles (photocatalyst), which are in a close contact with a liquid or gaseous reaction medium.

Upon exposing the catalyst to light, excited states are generated and these are able to initiate subsequent processes such as redox-reactions and molecular transformations. The presence of hole scavengers in the water solutions is important. They are organic and inorganic compounds, which are easily oxidized in photocatalytic systems.

Theoretical part

The basic principles of heterogeneous photocatalysis can be summarized shortly as follows. A semiconductor (*SC*) is characterized by an electronic band structure in which the highest occupied energy band, called the valence band (*vb*), and the lowest empty band, called the conduction band (*cb*), are separated by a band gap (characterized by band gap energy, E_g), i. e. a region of forbidden energies in a perfect crystal. Semiconductors have typically the band gap energy E_g in the 1 eV – 4 eV range.

When a photon of energy higher or equal to the band gap energy is absorbed by a semiconductor particle, an electron from the *vb* is promoted to the *cb* with simultaneous generation of a hole ($h+$) in the vb. The $e_{cb}-$ and the $h_{cb}+$ can recombine on the surface or in the bulk of the particle in a few nanoseconds (and the energy dissipated as heat) or can reach particle surface where they can react with donor (*D*) or acceptor (*A*) species adsorbed or close to the surface of the particle. Thereby, subsequent anodic and cathodic redox reactions can be initiated.

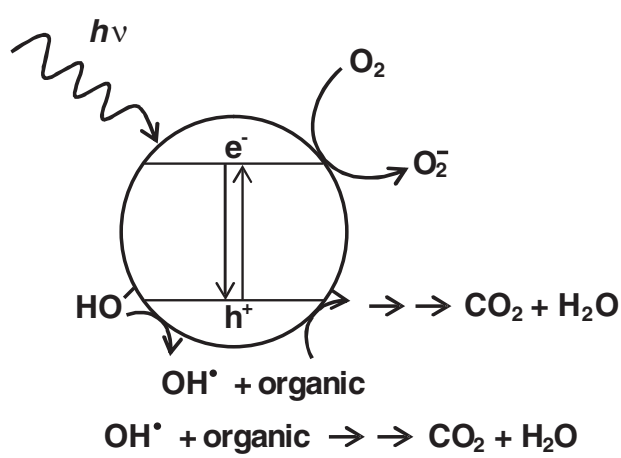

Fig. 1. **Schematic representation of the processes occurring in and on semiconductor particles during the photocatalytic mineralization of organic molecules by oxygen**

A variety of organic molecules can be photocatalytically oxidized and eventually mineralized according to the following general reaction:

$$\text{organic molecule} + O_2 \xrightarrow{h\nu \geq E_g,\ \text{semiconductor}} CO_2 + H_2O + \text{mineral acids} \quad (1)$$

Experimental part

In our work the photochemical oxidations of hole-scavengers in aqueous solutions of silver nitrate were studied. The concentration of Ag^+ ions was 200 mg dm^{-3}. Organic and inorganic compounds were used as the hole-scavengers. We used easily oxidizable compounds in our photocatalytic system, e. g. phenol and sodium thiosulphate. Next, it is important that the photocatalyst were present in the system. The most widely used one is titanium dioxide (Degussa P25), which was used in a powder form (reaction solution is in suspension with this TiO_2). Reactions were performed in an immersionwell bath reactor. Total volume of the suspension was 370 cm^{-3}.

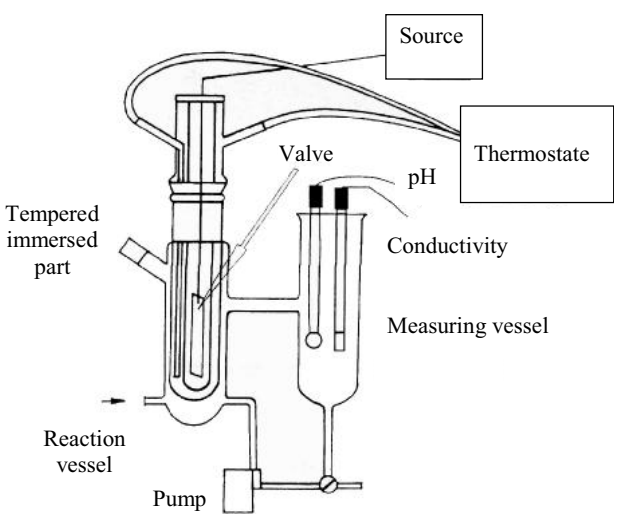

Fig. 2. **Photochemical immersion well bath reactor**

Discussion

The determination of its rate constant is the most widespread approach to the analysis of photochemical reactions. Formal first-order reaction kinetics is usually applied. In this work, we have tried to develop a kinetic model of photochemical reduction of silver ions and to describe quantitatively the changes of hole-scavengers concentrations.

REFERENCES

1. Litter M. I.: Applied Catalysis B: Environmental *23*, 89 (1999).
2. Chen D., Ray A. K.: Chemical Engineering Science *56*, 1561 (2001).

P26 PYRENE FLUORESCENCE STUDY OF HYDROPHOBIZED HYALURONATES AGGREGATION

FILIP MRAVEC[a,b] and MILOSLAV PEKAŘ[a]
[a]*Institute of Physical and Applied chemistry, Faculty of Chemistry, Brno University of Technology, Purkyňova 118, 612 00 Brno, pekar@fch.vutbr.cz,*
[b]*CPN, spol. s. r. o., 561 02 Dolní Dobrouč 401, filip.mravec@centrum.cz*

Introduction

The primordial study of aggregation behaviour of the new polysaccharides–based surfactants is presented. The alkyl modified hyaluronic acid, prepared by CPN spol. s r. o., are in the forefront of our research. The unique derivative (Fig. 1.) has, contrary to derivatives prepared by common ways like esterification, free carboxylic group. From this point we speak about amphiphilic polyelectolytes.

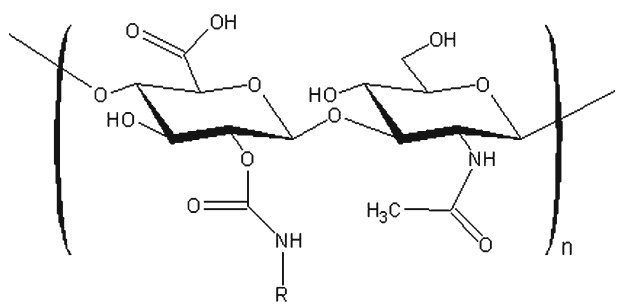

Fig. 1. **Derivatives presented in this study – carbamate (-NH-)**

Experimental

Materials. Hydrophobized hyaluronate derivatives (hHA) were purchased from CPN spol. s r. o. Fluorescence probe pyrene was purchased from Fluka and used without further purification. Acetone p. a. and n-heptane p. a. were taken from Lachema a. s. and dimethylsulfoxide SPECTRANAL®, ≥ 99.7% (GC) was purchased from Riedel-de-Haën. Sodium dodecylsulphate was purchased from Lachema a. s. Water was doubly distilled (Millipore).

Instrumentation. Fluorescence spectra of pyrene in aqueous solution of hHA were recorded on AMINCO-Bowman Series 2 Spectrofluorometer at 25 °C ± 0.1.

Results and discussion

Fluorescence measurement, pyrene 1 : 3 ratio method ($Py_{1:3}$), is widely used and well defined method[1] for determination of the critical micelle concentration (CMC). As "1" is meant band with maximum around 372 nm of pyrene emission spectra and "3" is band localized closely to 383 nm at the same spectra. Dependence of 1 : 3 ratio on logarithm of concentration is described by a decreasing Boltzman's S-type curve. This curve is four-parametric (Eq. 1)

$$y = \frac{a-b}{1+e^{\left(\frac{x-x_0}{\Delta x}\right)}} + b\,, \qquad (1)$$

where a is equal to maximum, b to minimum, Δx to gradient and from its inflex point, located at x_0, is determined the CMC directly or as a lower limit for definition of the CMC range. Upper limit can be then taken from dependence of the excimer-to-monomer ratio, E : M (maximum of excimer fluorescence is around 470 nm) or of the fluorescence intensity (F) on logarithm of concentration.

First dependence of $Py_{1:3}$ on macroscopic relative permittivity (ε_r^M) of probe environment was determined. Acetone ($\varepsilon_r^M = 20.7$) and n-heptane ($\varepsilon_r^M = 1.91$) were chosen in different volume fraction as a model system. Expected decreasing of $Py_{1:3}$ with decreasing ε_r^M were observed ($1:3 = 0.037\,\varepsilon_r^M + 0.4569$; $R^2 = 0.996$). For pure acetone $Py_{1:3}$ value was found equal to 1.22 and for n-heptane to 0.53.

Behavior of pyrene fluorescence spectra in micellar system was tested on sodium dodecylsulphate SDS in the aqueous solution. Expected jump-change in the dependence of $Py_{1:3}$ on the logarithm of concentration was observed and was resolved with S-curve. Literature value for CMC of SDS is reported[2] to be around 8.0 mM at 25 °C. From our measurement CMC value was determined around 1 mM (1.08 mM). For verifying this value CMC was evaluated also from the dependence of fluorescence intensity on the logarithm of concentration. It was found nearby 1 mM too (1.32 mM).

As model derivatives of hyaluronic acid is presented DEC–NH–HA (DEC…C_{10}; –NH–…carbamate bridge; HA…hyaluronic acid) where alkyl chain is C_{10} with substitution degree (SD), determined from ^{1}H NMR measurement, 10, 30, 50, 70 % and molecular weight, determined from light-scattering measurements, 134 000 g mol^{-1}. From lyophilized samples stock solution was prepared in concentration 2 g l^{-1}. From this stock concentration sets were diluted to flask with constant contents of pyrene evaporated from its stock solution. After 24 h standing at laboratory temperature the fluorescence spectra were recorded. The first and third vibronic bands were taken and 1 : 3 ratio plotted against the logarithm of hHA concentration. Data were fitted with the Boltzmann's S-type curve using "Resolver" function of MS-Excel and sum of squared deviations as the criterion. CMC was taken as x_0 parameter of the model.

It is predictable that CMC's of hHAs, with the same alkyl chain type and molecular weight , is depending on their SD. Four hHAs, with M = 134 000 g mol^{-1}, -NH- type and C_{10}, substituted to 10, 30, 50, and 70 % respectively are shown in Fig. 2. We can observe decreasing tendency of CMC with increasing SD. This is in agreement with prediction that hHA including more side alkyl chains is less soluble than hHA with smaller SD.

Value of the $Py_{1:3}$ at concentration above CMC gives evidence about quality of interior environment of a domain formed by hHA. The limiting concentration value of $Py_{1:3}$

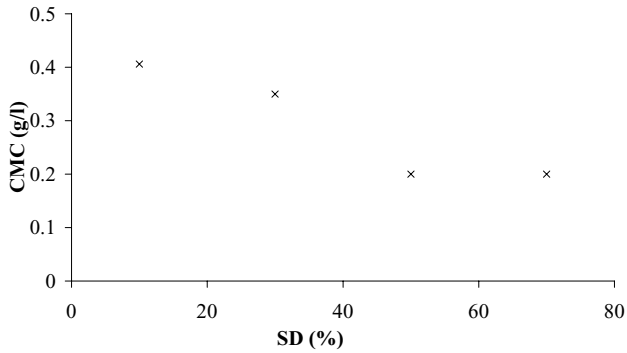

Fig. 2. **Dependence the CMC on SD for C_{10} derivatives**

(~1.2 g l^{-1}), directed by solubility of hHA, is changing with the SD value (Fig. 3.). The lowest value of $Py_{1:3}$ was obtained for the hHA with SD 50 %. These values are above the value for pure n-heptane.

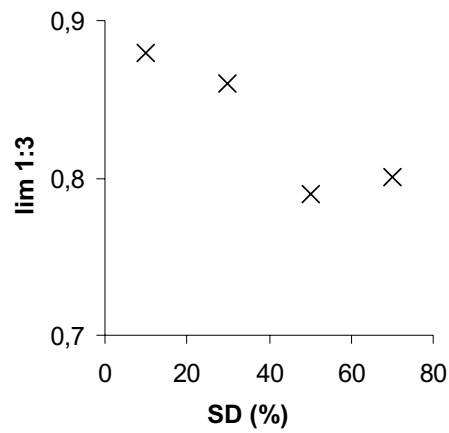

Fig. 3. **Dependence of the limiting value of $Py_{1:3}$ on SD for C_{10} derivatives**

Conclusion

The hydrophobized derivatives of hyaluronate make in water solution micelle-like hydrophobic domains. These domains have interior relative dielectric constant lower than 11. This value is higher than value in pure hydrocarbons, so it is possible that domain contains polar groups which changing microenvironment properties of domain core.

Fluorescence spectroscopy looks useable for determination of CMC in the water solution of hHA. The best way, how to determine CMC and interior properties of hydrophobic domain, seems the $Py_{1:3}$ ratio method.

REFERENCES

1. Aguiar J., Carpena P., Molina-Bolívar J. A., Ruiz C. C.: J. Colloid Interface Sci. *258*, 116 (2003).
2. Ruiz C. C.: Colloids Surf. A *147*, 349 (1999).

P27 PHOTOCHEMICALLY ACTIVE POLYMEROUS LAYERS BASED ON MODIFIED GELATINE

IVETA MRLLÁKOVÁ, VIERA JANČOVIČOVÁ and MILAN MIKULA
Faculty of Chemical and Food Technology, Slovak Technical University, Radlinského 9, 812 37, Bratislava, Slovak Republic, iveta.mrllakova@stuba.sk

Introduction

Gelatin layers have very low oxygen permeability. Therefore they can be used as barrier layers in food packing industry. However, they are soluble in warm water, what is considerable deficiency for using such surfaces. Gelatin has the same structure as collagen, they are both α-amino acids bonded in peptide chain[1].

Side groups of molecules allow coating the chemical cross-linking. So gelatin can be kept at higher temperatures than its melting point. Beside those advantages, gelatin has some disadvantages which include brittleness by low moisture and the layer has tendency to wave by wrong application[1].

The modification of gelatin is a way how to overcome this problem. Electron beam curing or UV exposure are possible ways how to cross-link the modified gelatin[2]. By the function modification of gelatin with glycidyl acrylate and glycidyl methacrylate Koepff, Brauner and Babel prepared biological degradable, water resistant polymeric material with defined composition and properties suitable to packing materials production such as foils and films. Acrylic and methacrylic groups are able to cross-link and curing of coating takes place. The properties of treated materials is possible to adapt to their usage according to reaction conditions.

In this study, gelatin derivates[3] have been prepared by the chemical reaction of gelatin and glycidyl methacrylate (GMA), which posses functional groups able to UV cure by short expositions.

Experiment

M a t e r i a l s

Gelatin, glycidyl methacrylate (Merck, Germany), sodium hydroxide (Lachema, Brno), sulphuric acid (Lachema, Brno), initiator Irgacure 2959 (Ciba, Switzerland) and KBr were used as received.

M e t h o d s

Preparation of gelatin derivates

100 g of gelatin was solved in 900 ml of distilled water by strirring at 50 °C. pH of dissolved gelatin was changed to 8.5 by 1M NaOH. 4.45 ml of glycidyl methacrylate (GMA) was added after changing pH. The solution was allowed to proceed for 1 h at 50 °C and neutralized to pH 7 by 1M H_2SO_4 finally. Gelatin without changing its pH was also prepared.

I n s t r u m e n t a t i o n

The gelatine systems were studied by FTIR spectrometer, EXCALIBUR, FTS 3000 MX (*DIGILAB, USA*), set in transmission mode. Spectrum of GMA was obtained using KBr pellet technique. Gelatinous systems were measured on aluminium plates by single reflection technique. The influences of exposure on modification of film barrier properties were investigated. Observation of curing process was carried out by discontinuous UV exposition and taking the spectrum in the cut-off time. Coated samples were cured by medium pressure mercury UV lamp at exposure intensity of 12 mW cm^{-2} and power of 250 W.

To study the surface hydrophility contact angle measurements and the swelling method by Dogatkin were used. Dogatkin method includes measuring the volume of absorbed distilled water Q in ml g^{-1} (at 20 °C) by a dry sample in the time range from 1 to 45 minutes. Systems with 1 % of initiator Irgacure 2959 were exposed for 1 hour and their barrier properties were investigated also.

Reflex goniometer Contact Angle Meter, Kernco Instruments (USA) was used for acquisition the contact angle. The angle was taken 15–20 seconds after the drop of water was applied to the coated support.

The printability properties of coated foil by black-ink were determined and the humidity resistance of such samples was also evaluated. To study thin polymerous layers used as receiving medium in ink-jet printing the ink affinity to the layer is needed to quantify[4]. The concrete fractal analysis is talked about here. The most important are the parameters *fractal measure* K and *fractal dimension* D, from which percent dot area after printing are easy to calculate[5]. Box Counting method was chosen for the fractal analysis. In spite of densitometry this method doesn't need the calibration and references values for the percent dot area calculations[4]. The disadvantage is masking the picture before analysis[5]. Squares were printed with the percent dot area in the range from 0 to 100 % on the coated plastic foils. Printer HEWLETT PACKARD 970CX1 with the 400 dpi resolution was used. Consequently the foils were scanned on the CANON FS 4000. Obtained pictures were cut into individual squares in Photoshop, expanded to format 800 × 800 pixels and saved as tiff files without compression. Level of masking for 50 % dot area was assigned and associated to the value of 148 in program HarFA[4] to separate the tones to white and black and. The real percent dot area was calculated in Excell. Finally density of all squares was verified on densitometer MEO-DENZI TDR 04. Thicker foils in the format A6 were used for this purpose.

The influence of moist environment on printed material was simulated. Printed foils in the size 3.5 × 8.0 cm were wrapped with wet filtration paper and weighted with 1 kg to 17 hours. Resistance printed exposed (0.5 h) foils were tested also. The samples were scanned, the percent dot area was obtained as mentioned above and the density for all squares was measured.

Results and discussion

The FTIR spectra of GMA, modified gelatins and raw gelatin are shown in Fig. 1. GMA peak at 908 cm^{-1} respon-

ded to asymmetric valence vibration of epoxy group. Two absorption peaks at 1640 cm^{-1} (stretching vibrations) and 810 cm^{-1} (twist vibrations) are used for identification double bonds. It is impossible to observe the peak at 1640 cm^{-1} because of strong band of raw gelatin in this region. If the peaks at 810 cm^{-1} in the spectra of modified gelatins belonged to the rest of GMA, the peak at 908 cm^{-1} would occur also, which is stronger than first mentioned. This fact shows successful modification. It is assumed that the very small peak at 810 cm^{-1} is due to low content of double bonds inbuilt during the reaction.

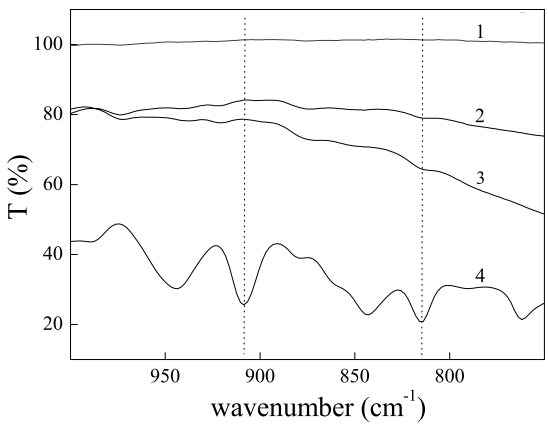

Fig. 1. **FTIR spectra of raw gelatin (1), MZ1 (2), MZ2 (3) and GMA (4) (Table I)**

Table I
Used shortcuts

Shortcut	Description
Z	raw gelatin
MZ1	modified gelatin with adjusting pH
MZ2	modified gelatin without adjusting pH
I	initiator Irgacure 2959

The penetration results were characterized by exponential relation in form $Q = Q_{max} (1 - e^{-k.\,t})$. It is evident that within the modification of gelatin the swelling degree decreases (Fig. 2.). Considerable decrease was found when the modified gelatin prepared according Koepff, Brauner and Babel (MZ1) was used, and Q_{max} declined through 18 %. Swelling degree Q of both modified gelatins was stabilized at Q_{max} 9 ml g^{-1} for the sample MZ1 (Fig. 3.) and at 7 ml g^{-1} for the sample MZ2 (Fig. 3.) after UV exposure. Decrease of the swelling degree confirms curing termination and the modification of gelatin.

Curing of foils should be established with contact angle measurements accordingly. Changing of hydrophility was significant. Hence the water as measuring liquid was sufficient for this purpose. Expected decrease of contact angle was not performed after exposure. Surprisingly, all three systems appeared to be hydrophilic (Table II). The UV exposure caused decrease of contact angle. Some portion of water could be evaporated from the layer during the exposure. Water-evaporation changed the measurement conditions, what sometimes caused troubles by spectra identification. We have decided not to measure C = C bonds, because of false absorption bonds.

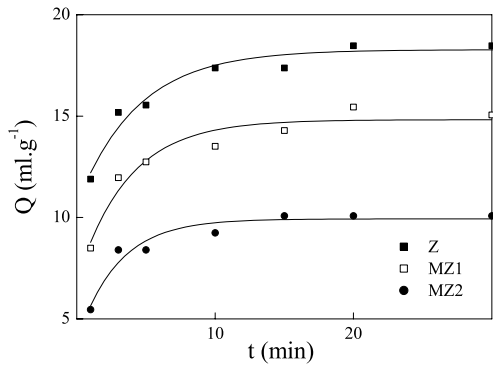

Fig. 2. **Swelling degree of three different saples as a function of time**

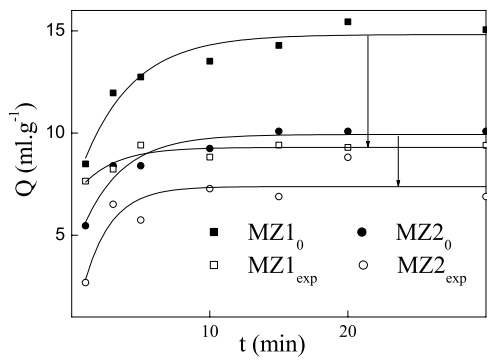

Fig. 3. **Swelling degree of two different compositions as a function of time after 1 hour exposition, (Table I, unexposed sample – 0, exposed sample – exp)**

Table II
Results of contact angle before the exposition (θ_o) and after 1 hour the exposition (θ_e)

Composition	Contact angle θ_o [°]	θ_e [°]
Z + I	86	21
MZ1 + I	73	34
MZ2 + I	79	41

Printability properties of the samples have been evaluated using fractal analysis method and density measurements. In general, gelatin is relatively good printable (Fig. 4., 5.),

the squares had sharp edges and uniform percent dot area. The best agreement between theoretic and real percent dot area was found for modified gelatins, without the influence of pH during preparation of modified gelatin. Average deviation moves in the range from 0.1 to 4 %. Ink-jet ink fixes well on the prepared layers (Fig. 6.). There is no remarkable leakage of ink after the 17 hour resistance test. UV exposure didn't influence a lot the resistance of substrates toward water. The greatest decrease in density, from 2.02 to 1.51, is observed for the sample MZ2 at 100 % square (Fig. 7.).

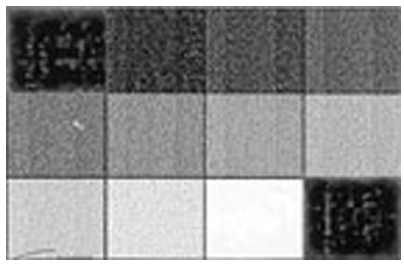

Fig. 4. **Printed foil coated with composition Z + I**

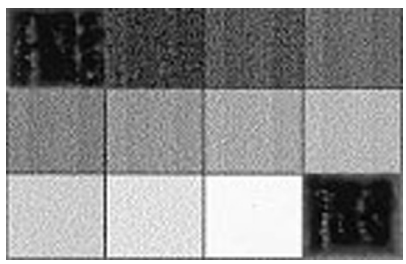

6 a)

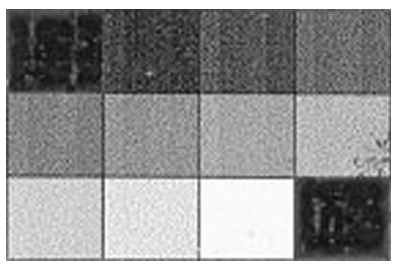

6 b)

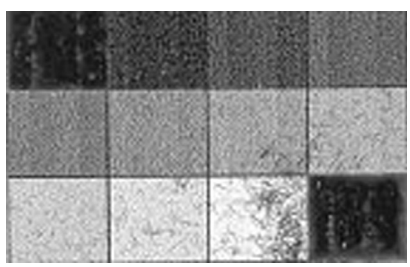

6 c)

Fig. 6. **Printed foil coated with composition MZ2 + 2, a) immediately after printing, b) after resistance test, c) after exposure and resistance test**

Conclusion

Gelatin has been modified by GMA and characterized by FTIR spectroscopy. Sensitized compositions have been prepared containing modified gelatin and initiator Irgacure 2959. Effect of medium pressure mercury UV lamp has been investigated by the properties of thin layer. UV exposition leads to considerable lower swelling degree of compositions and doesn't affect the resistance of printed substrates to water.

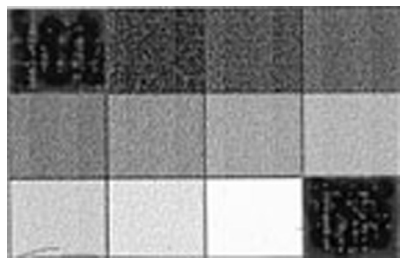

Fig. 5. **Printed foil coated with composition MZ1 + I**

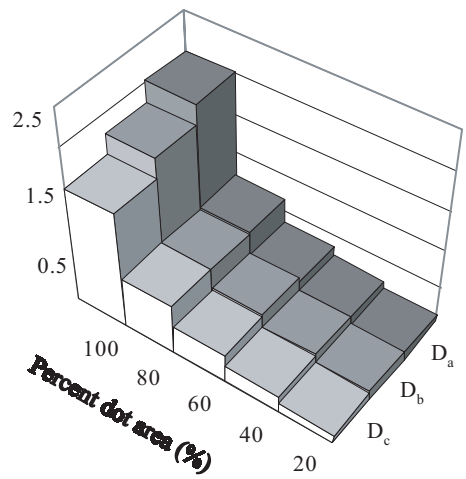

Fig. 7. **Densities of printed foil coated by composition MZ2 + I, D_a – immediately after printing, D_b – after resistance test, D_c – after exposure and resistance test**

We thank the Slovak Grant Agency VEGA (project VEGA 1/2454/05) and Science and Technology Assistance Agency (contract APVT-20-034202) for financial support.

REFERENCES

1. Curme H. G.: *Gelatine, General Properties, The Theory of Photographic Process,* Third edition, p. 45, 1996.
2. Scherzer T., Beckert A.: *Electron Beam Curing of Methacrylated Gelatin Studied by EPR and FT–Raman Spectroscopy,* Macromol. Symp. 119, p. 299–307, 1997.
3. Koepff P., Braeumer K., Babel W.: Patent DE4210334, esp@cenet – Bibliographic data and abstract.

4. Veselý M., Zmeškal O., Dzik P., Zita J.: VI. *Polygrafický seminář,* 2003, Pardubice, Book of Abstracts, p. 114–116, Univerzita Pardubice 2003.
5. Králová I., Dzik P., Veselý M.: *Symposium Polygrafia Academica,* Bratislava, 2004, Book of Abstracts, p. 161, FChPT STU, Bratislava 2004.

P28 PREPARATION AND PROPERTIES OF PHOTOCATALYTICALY ACTIVE HYBRID TIO_2-SIO_2-POLYDIMETHYLSILOXANE LAYERS

PETRA NOVOTNÁ and JOSEF KRÝSA
Institute of Chemical Technology, Department of Inorganic Technology, Technická 5, CZ-166 28 Prague 6, Czech Republic

Introduction

Sol-gel method was used for the preparation of photocatalytic hybrid layers consistig of two inorganic components (TiO_2 and SiO_2) and one organic component (polydimethylsiloxane). TiO_2 causes photocatalytic activity, SiO_2 increases the resistance against corrosive environment, and polydimethylsiloxane (PDMS) guarantees good adhesion of the films on the substrate and facilitates the formation of crack-free coatings. The present paper describes the influence of the amount of inorganic components, namely TiO_2 and SiO_2, on the properties of the resulting hybrid layers.

Experimental

M a t e r i a l s

Polydimethylsiloxane (PDMS, mol. wt. = 550, Sigma--Aldrich Chemie), tetraethoxysilan (TEOS, 98%, Fluka Chemie) and titaniumisopropoxide (TiP, Sigma-Aldrich Chemie) were used as the starting inorganic and organic compounds; tetrahydrofuran (THF, p. a.), isopropanol (IPA, p. a) and acetylacetone (AcAc, p. a.) served as solvents; hydrochloric acid (HCl, 36%) was used as a catalyst.

P r e p a r a t i o n

The sols with various molar ratio of TiO_2/PDMS and SiO_2/PDMS were prepared. The molar ratio PDMS/H_2O/HCl was fixed at 0.5/0.9/0.15. The simple principle of the preparation of hybrid materials consisting TiO_2/SiO_2/PDMS was following: one third of the total amount of solvents was mixed with the PDMS, TEOS and TiP. Then, the solution was homogenized for about 2 hours. After that, the rest of solvents, demineralised water and hydrochloric acid were added. The solution was coated on the glass substrate (microscope slides; 25.4 mm × 76.2 mm, thickness: 1–1.2 mm) after 24 hours of stirring by dip coating method. Finally, the coated substrate was dried (30 min. at the room temperature) and burned out (250–400 °C).

C h a r a c t e r i z a t i o n

The following measurements were chosen to demonstrate that the given expectations were fulfiled: measurement of photocatalytic activity (static tests in water solution of methylene blue), measurement of chemical resistance (corrosion of the layers in water – optical microscopy), and measurement of thickness of the layers (SEM analysis, Talystep, spectrometer Avaspec-2048-2).

Results and discussion

The thickness of the layers ranged from 0.2 to 1.2 μm, depending on the burning temperature (Table I) and on the composition of the layers (Table II).

Table I
The influence of heat treatment on the thickness of layers with molar ratio of precursors Ti/Si/PDMS=1/1/0.5

Heat treatment [°C]	Thickness [nm]
250	1250
300	1100
350	990
400	800

Table II
The influence of molar ratio of Ti/Si/PDMS on the thickness of layers

Molar ratio Ti/Si/PDMS	Thickness [nm]
1/0/0.5	200
1/0.25/0.5	550
1/0.5/0.5	800
1/1/0.5	990

The influence of amount TiO_2 on the photocatalytic activity of layers is shown in Fig. 1. The molar ratio SiO_2/PDMS was fixed at 1/0.5, the molar ratio TiO_2/PDMS was changed.

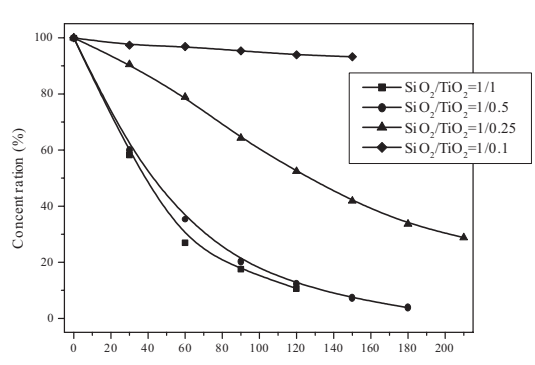

Fig. 1. **The influence of amount TiO_2 on the photocatalytic activity**

The results indicated that the decrease of concentration of methylene blue was nearly the same for the molar ratios TiO_2/PDMS = 1/0.5 and 0.5/0.5. In the case of molar ratio TiO_2/PDMS = 0.25/0.5 the degradation rate was lower and for the ratio TiO_2/PDMS=0.1/0.5 was almost negligible.

The images a), b) and c) in Fig. 2. show the layers with molar ratio TiO_2/SiO_2/PDMS=1/1/0.5 after 8 hours exposition in water at 85 °C. The heat treatment of samples was a) 250 °C, b) 350 °C and c) 450 °C. The layer burned at 250 °C was dissolved after 8 hours (Fig. 2a)) and this was visible by naked eyes. The amount of cracks on the surface was lower in the case of layer burned out at 450 °C (Fig. 2c)). It means that the higher burning temperature the better resistance of the layers against corrosive environment.

Fig. 3a), b) and c) describe surface of layers with molar ratio TiO_2/SiO_2/PDMS = 1/0.5/0.5 burned at 350 °C a, b) and 450 °C c). The image a) shows the layer which was not exposed. The other surfaces b, c) are depicted after 8 hours exposition in water at 85 °C. The layer b) was dissolved after 8 hours exposition (It was detected by naked eyes). From the comparison of Fig. 2b)–3b) and Fig. 2c) and 3c) we can conclude that the lower amount of SiO_2 in the layer results in the decrease of chemical resistance.

This research was supported by the Ministry of Education, Youth and Sports of the Czech Republic (project number 1M4531477201).

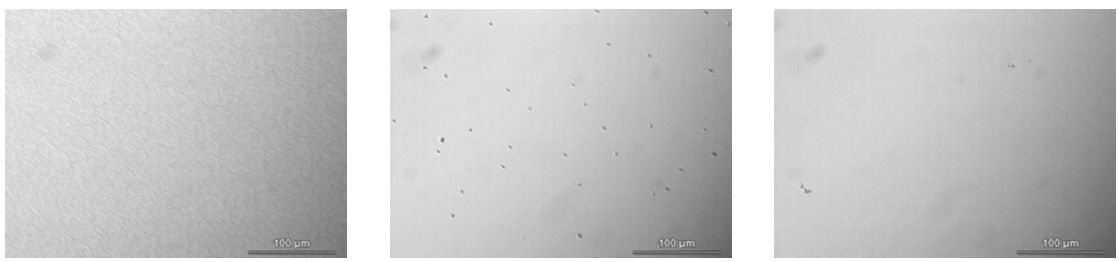

Fig. 2. **The surface of hybrid layers with molar ratio Ti/Si/PDMS = 1/1/0.5 after 8 hour exposition in water at 85°C. The heat treatment of samples was 250 °C a); 350 °C b) and 450 °C c)**

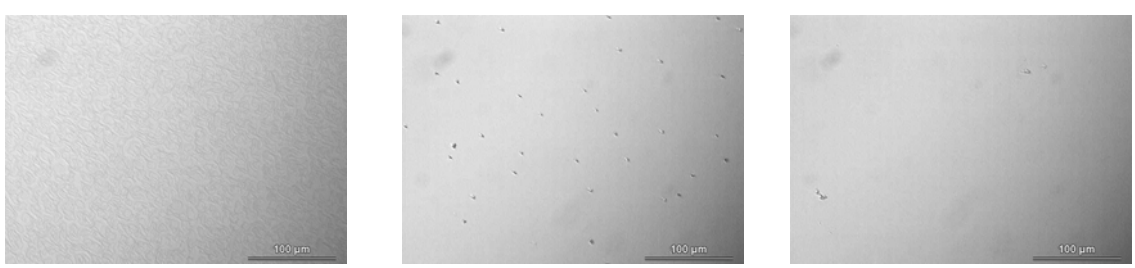

Fig. 3. **The surface of hybrid layers with molar ratio Ti/Si/PDMS = 1/0.5/0.5 burned out at 350 °C (a; b) and 450 °C (c)**

P29 CONFORMATIONAL ANALYSIS OF CYCLOPROPYL DERIVATIVES OF TWO PUSH-PULL ENAMINES

JÚLIA PIGOŠOVÁ[a], ANTON GATIAL[a], VIKTOR MILATA[b] and NAĎA PRÓNAYOVÁ[c]
[a]Department of Physical Chemistry, [b]Department of Organic Chemistry, [c]Central Laboratories, Faculty of Chemical and Food Technology, Slovak University of Technology in Bratislava, Radlinského 9, SK-812 37 Bratislava, Slovak Republic, julia.pigosova@stuba.sk

Introduction

Cyclopropyl derivatives of enamines are often used in synthesis of biologically active heterocyclic compounds[1,2]. Their reactivity and stereochemistry of reaction is strongly dependent on the nature of electron donor and acceptor substituents on double C = C bond and polarity of environment[3]. In our study we have investigated the influence of the polarity of environment on the structure and conformational behavior of two cyclopropyl enamines 3-cyclopropyl-2-acetylpropenenitrile and 3-cyclopropyl-2-methylsulfonyl-propenenitrile differing by one from the electron acceptor groups. The infrared and NMR experiments has been supported by theoretical

DFT calculations performed in gas phase and also in polar environment.

Experimental

The synthesis of both samples was performed by similar way from ethoxy derivatives of appropriate reactant by replacement of ethoxy group with secondary amino group: $CpNH_2 + H_5C_2–O–CH = C(CN)Y \rightarrow CpNH–CH = C(CN)Y + C_2H_5OH$ where Y is $–COCH_3$ or $–SO_2CH_3$ group and Cp is cyclopropyl.

The ^1H and ^{13}C NMR spectra were collected on a Varian VXR-300 spectrometer at room temperature in DMSO and $CDCl_3$. Mid IR spectra were recorded on Nicolet model NEXUS 470 FTIR spectrometer in solid phase and in solutions of acetonitrile and chloroform at ambient temperature. The IR spectra at various temperatures in acetonitrile were recorded using standard variable temperature cell Specac equipped with KBr windows. All theoretical calculations were run in GAUSSIAN03 program on DFT level with B3LYP functional and standard 6-31G** basis set. Polarizable continuum model was employed to include the solvent effects into the calculations.

Results and discussion

Although the synthesis of both compounds started from E-isomers of appropriate reactants the E-isomer of CPACS and Z-isomer of CPACA (first letter in marking) were obtained as it was confirmed by NMR spectroscopy according to $^3J_{H\text{-}CN}$ coupling constants (Fig. 1.) [4]. It implies that during the preparation lead in the polar methanol solution the C=C double bond in CPACA polarizes to such an extent that the rotation about it can occur. Consequently, the formation of the most stable ZZa conformer which contains an intramolecular hydrogen bond between the acetyl and secondary amino group is preferred. According to the theoretical calculations it is the most stable arrangement for this molecule. Although there is the possibility to form two other conformers by rotation about C-N (ZZs) and C-CO bond (ZEa) both have very high relative energies with respect to ZZa conformer (Table I). The highly polar environment evidently decreases the rotational barrier about C = C bond causing partial isomerisation as it is seen from ^1H NMR spectrum in DMSO compared with those in $CDCl_3$ at Fig. 2. In acetonitrile solution a new weak band at 1620 cm^{-1} was observed in infrared spectrum after several minutes which did not appeared in less polar chloroform. This fact confirmed that polar environs causes large polarization of C = C bond and reduces the multiple character of this bond.

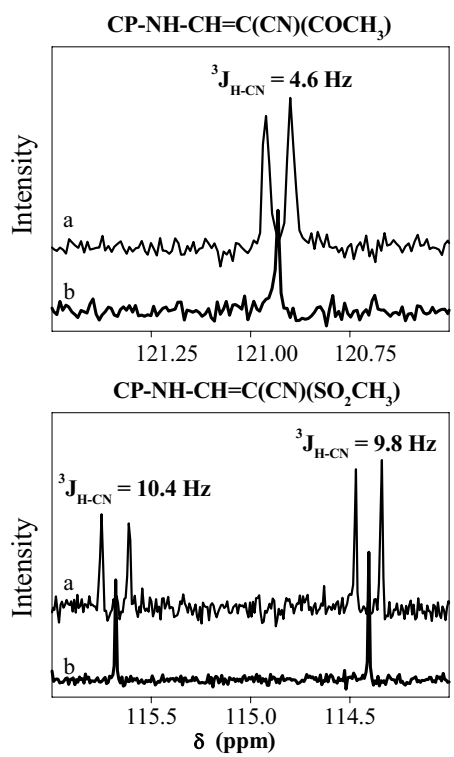

Fig. 1. **Detail of coupled a) and decoupled b) ^{13}C NMR spectra of CPACA (top) and CPACS in DMSO solution at room temperature**

Table I
Calculated DFT relative energies and dipole moments of possible conformers and isomers of CPACA and CPACS

Conformer	E [kJ mol^{-1}]	μ D
CPACA		
ZZa	0.00	5.11
ZZs	49.35	5.24
ZEa	57.78	9.59
EZa	16.01	4.54
EZs	26.68	4.75
EEa	35.23	8.37
EEs	49.65	8.52
CPACS		
Zaa	0.00	6.34
Zas	0.45	6.53
Zs	36.07	4.54
Eaa	3.87	6.55
Eas	4.14	6.65
Esa	12.30	6.42
Ess	12.84	6.63

As we have calculated the more stable structure for CPACS is Zaa conformer with dipole moment 6.34 D similarly as in the case of CPACA. But maybe due to starting compound as well as synthetic conditions the E-isomer was obtained. E-CPACS can exist in two different conformations syn or anti according to the orientation of cyclopropyl towards or out from C = C bond (marked by second letter). The more stable is anti conformer with calculated dipole moment 6.55 D which should crystallize in solid phase. In acetonitrile solution we have observed in infrared spectrum new strong

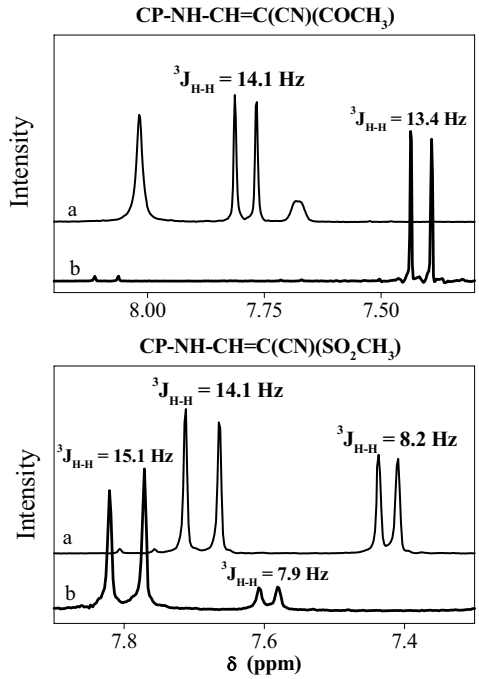

Fig. 2. **Detail of ^{1}H NMR spectra of CPACA (top) and CPACS in DMSO a) and in $CDCl_3$**

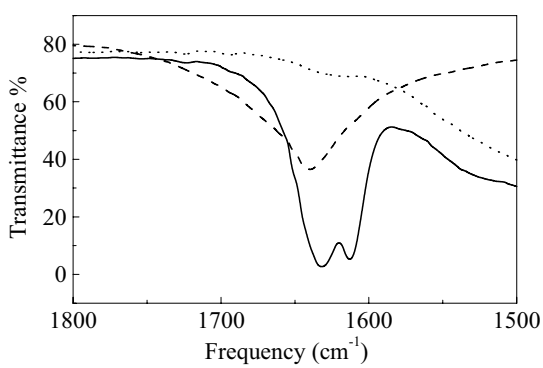

Fig. 3. **Comparison of infrared spectrum of CPACS in solid phase (dashed line) and in acetonitrile solution (solid line) at room temperature. Dotted line represents the infrared spetrum of pure acetonitrile**

band positioned at 1613 cm^{-1} which was assigned to C = C stretching frequency of syn conformer (Fig. 3.) and its intensity increased with increasing temperature. The enthalpy difference between these conformers calculated in gas phase is 8.43 kJ mol^{-1}. Taken into account preferable anticlinal arrangement of sulfonyl group[5] for all E-isomers of CPACS there is also another possibility to form the conformations arising from the mutual position of cyclopropyl and methyl group bound with sulfonyl. These can be also in anti or syn position (denoted by last s or a letter) but the calculated enthalpy difference between such structures is very small, less than 1 kJ mol^{-1}. Such small difference should not be observed by NMR spectroscopy but our measurements revealed two different E-conformers of studied compound because of similar $^3J_{H\text{-}CN}$ coupling constant (Fig. 1.). The amount of less stable syn conformer evidently increases with increasing polarity of solvent (Fig. 2.).

Conclusions

We have found that in polar solutions partial conversion around = C–N bond from anti to syn conformer of CPACS occurs. Calculated enthalpy difference between the syn and anti CPACS in acetonitrile is 1.65 kJ mol^{-1} while the experimental value obtained from IR temperature measurements is ~ 1 kJ mol^{-1}. The most stable conformer of CPACA is that with intramolecular hydrogen bond between the carbonyl and amino group and with dipole moment 6.34 D. Probably due to significant lowering of rotational barrier around polarized C = C bond, the more favorable for this molecule in polar solutions is isomeric interconversion.

We thank Slovak Grant Agency (Projects VEGA/1/0052/03 and VEGA/1/0058/03) for its financial support and the IBM Slovakia for computing facilities.

REFERENCES

1. Dyke S. F.: *The Chemistry of Enamines*. Cambridge University Press, London 1973.
2. Rajappa S.: Tetrahedron *55*, 7065 (1999).
3. Pappalardo R. R., Sanchez Marcos E., Ruiz-López M. F., Rinaldi D., Rivail J.-L.: J. Phys. Org. Chem. *4*, 141 (1991).
4. Gatial A., Sklenák Š., Milata V., Klaeboe P., Biskupič S., Scheller D., Jurašková J.: Struct. Chem. *7*, 17 (1996).
5. Oelichmann H.-J., Bougeard D., Schrader B.: J. Mol. Struct. *77*, 179 (1981).

P30 CHEMICAL PROPERTIES OF HUMIC ACIDS ISOLATED FROM ARABLE SOILS.

ĽUBICA POSPÍŠILOVÁ, EDUARD POKORNÝ and JIŘÍ JANDÁK
Mendelova zemědělská a lesnická univerzita, Agronomická fakulta Ústav agrochemie půdoznalství, mikrobiologie a výživy rostlin, Zemědělská 1, 613 00 Brno, ČR, lposp@mendelu.cz

Introduction

Humic acids, the main component of soil organic matter, reflect intensity of soil cultivation and their chemical properties are very useful for evaluation of soil quality. Agricultural and ecological role of humic acids (HAs) results not only from their presents in soils, but also affect physical and chemical soil properties and dynamic of soil organic matter. Their specific structure contained a number of functional

Table I
Elemental Composition of Humic acids isolated from Eutric cambisol

	C [%]	H [%]	N [%]	O [%]	C:H	O:C	C:N	H:C
HAs	36.2	41.6	2.4	19.54	0.9	0.54	15.1	1.15
	35.8	43.2	2.52	19	0.83	0.53	14.21	1.21
	36.2	41	2.5	18.8	0.9	0.52	14.48	1.13
AVERAGE	36.0667	41.933	2.47333	19.1133	0.87667	0.53	14.5967	1.16333
SDEV	0.18856	0.92856	0.05249	0.31255	0.033	0.00816	0.37259	0.03399

groups such as carboxyl, phenolic, amidic and others which are very active in interacting with organic and mineral component in the soil and can act as scavengers for various kind of soil contaminants[1]. One of the main criteria characterising HAs of various kind is their absorbance (465 nm–665 nm) and value of coloured quotient (E1/6). It was found out that absorbance of humate solutions in the UV-VIS ranges increases with the carbon content in the HAs molecules. Coloured quotient positively correlated with H/C ratio and negatively with ratio O/H (calculated from elemental composition). Kumada[3] determined maturity of HAs on the basic of the delta log K parameter value and classified HAs into three basic categories according to their UV-VIS range. Type A includes HAs of very high humification degree (delta log K up to 0.6). Type B includes HAs with delta log K within the range 0.6 to 0.8. Type Rp comprising of HAs with delta log K parameter ranging 0.8 to 1.1.

FTIR spectra has been widely used for characterising chemical composition of HAs, content and nature of functional group (e. g. carboxylic, phenolic) and also for spatial arrangement of functional group (Stevenson, 1982).

The objective of this study was to isolate preparation of HAs from arable soil (Eutric Cambisol). We also aimed our study at evaluation of their chemical properties (elemental composition and optical properties).

Material and methods

Our study is a part of a larger investigation on the chemical, physical and biological soil properties under different type of land use. Long-term field experiments at Vatín in the Czech–Moravian Highland have been started in autumn 1998. Soil type was classified according to the FAO system as Eutric Cambisol. Soil samples were collected from the humic horizon (0–20 cm).

Humus content was determined according to Walkley–Black method (modification Novák–Pelíšek, In: Jandák, 2003).

Isolation of HA preparation was made according to the IHSS method (Hayes, 1985). Elemental composition was determined using the elementary micro-analyser EA 1108 Carlo Erba, Italy.

Optical density (UV-VIS spectra) was measured according to the standard IHSS method using UNICAM 8625 UV/VIS spectrometer within the range 400 nm–665 nm. Ratio E1/6 was calculated according to Kumada[3]. Ratio Q 4/6 was calculated according to Orlov[4].

FTIR spectra were obtained using the diffuse reflection spectroscopic method (the powder sample is mixed with KBr and briguetted into a pellet). Also attenuated total reflection (ATR) method was used. The last is popular not only in FTIR but also in conventional dispersive IR. This is because it is not necessary to chemically treat, or machine, the samples. We used FT-IR spectrometer FTS165 Bio-Rad, laboratories GmbH (München). All data were statistically calculated using t-test, A-nova.

Results and discussion

The aim of our study was focused on to chemical characterisation HAs isolated from arable land (Eutric Cambisol). Special attention was given to the isolation of HAs preparation according to the IHSS method.

Results of elemental composition and atomic ratios are typical for this soil type (Table I). Carbon content was assed as low, oxygen and hydrogen content was high. The maturity and dominant processes in HAs molecule given by the atomic ratios (H/C, O/C, C/N, C/H) showed high C/N ratio and low H/C ratio. Correlation between H/C and O/C showed also high stability. Molecular mass and maturity of

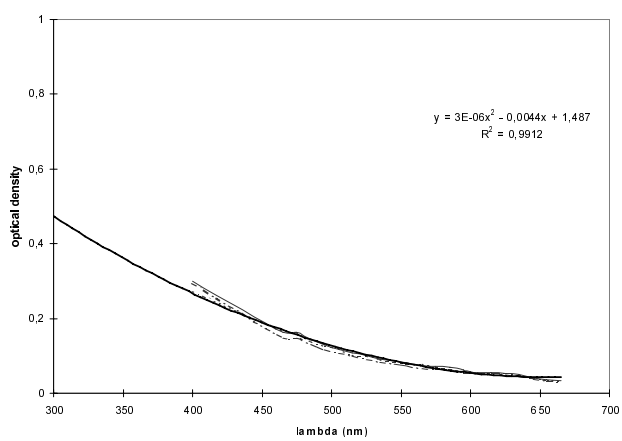

Fig. 1. **UV-VIS spectra of humic acids isolated from Eutric Cambisols**

HAs was high as well as condensation degree and content of aromatic groups. Maturity of HAs on the basic of the delta log K parameter value according to Kumada (1987) performed type A (delta log K up to 0,6). UV-VIS spectra (Fig. 1.) may be an indicator of the extent of humification degree as well. We used optical parameters suggested by Orlov (1985) and Q4/6 is more than 4. According to Kumada (1987) quotient E1/6 varies from 8–10. UV-VIS optical density curve suggested high stability of HAs and middle humification degree. Optical properties are in good agreement with the results of elementary analysis and literature. Linear correlation between elemental composition and optical properties was found (Table II). Position in Van Krevelen diagram indicates that dehydrogenation and demethylation processes are dominating in the HAs molecule and their tendency to mineralisation is not significant.

Table II
Linear correlation between chemical and optical properties of Humic acids isolated from eutric cambisols

	C [%]	E1/6	COOH	H/C
C (%)	1			
E1/6	0.7624	1		
Cooh	–0.8003	–0.7828	1	
H/C	–0.9945	–0.6991	0.7472	1

FTIR spectra (Fig. 2.) indicate bands at 3360–50 cm^{-1} for the O-H various groups, bands at about 2920 cm^{-1} for the aliphatic groups and bands at about 1700–1720 cm^{-1} for the carboxylic groups. The intense band at 1650–1655 cm^{-1} is for the carboxylate and amide (I) groups. Band at about 1100 cm^{-1} is for the SO_3H vibration. Peaks at 1040–1030 cm^{-1} are for the polysacharide chains and 1226–1220 cm^{-1} O-H and C-O vibration of various ether and alcoholic groups.

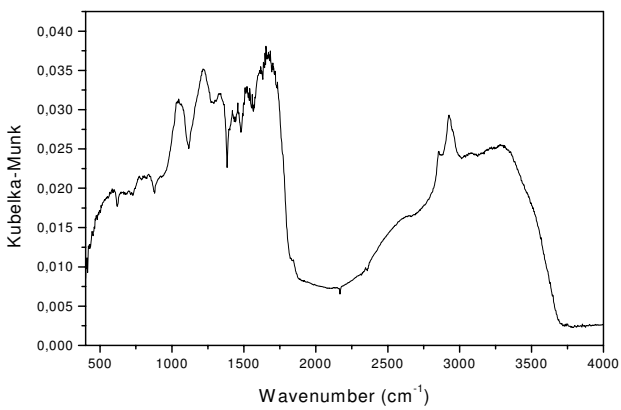

Fig. 2. **FT-IR Spectra of humic acids isolated from Eutric Cambisols**

Conclusions

Humic acids isolated from Eutric Cambisols performed preparation of high aromaticity, condensation degree, stability and not significant tendency to mineralisation. Elemental analysis showed less content of carbon, more hydrogen and oxygen. UV-VIS spectra suggested high stability and middle humification degree. Maturity according to Kumada (1987) performed type B. FTIR spectra indicated the involvement of oxygen (carboxylic), nitrogen (amide) and SO_3H functional groups. Experimental results showed possibilities of evaluation soil organic matter quality and thus quality of soil environment.

REFERENCES

1. Barančíková G., Senesi N., Brunetti G.: Geoderma *78*, 251 (1997).
2. Hayes M. H. B.: *Extraction of Humic Substances from Soil*. In: Aiken, G. R., Wershaw R., L., McKnight D. M., McCarthy P. (Eds.), *Humic Substances in Soil, Sediment and Water*. John Wiley, New York : 329–362 (1985).
3. Kumada K.: *Chemistry of Soil Organic Matter*. Elsevier, Amsterdam 1987.
4. Orlov D. S.: *Chimija počv (Soil Chemistry)*. Izdatelstvo MGU, Moskva 1985.
5. Stevenson F. J.: *Chemistry – Genesis, Composition, Reaction*. John Wiley and Sons, New York 1982.

P31 STUDY OF DISSOCIATION MATTERS IN DIAPHRAGM DISCHARGE IN LIQUIDS

JANA PROCHÁZKOVÁ, ZDENKA STARÁ and FRANTIŠEK KRČMA
Institute of Physical and Applied Chemistry, Faculty of Chemistry, Brno University of Technology, Purkyňova 118, 612 00 Brno, Czech Republic, rozkopalova@fch.vutbr.cz

Introduction

The discharges generated in liquids have been a subject of an intensive research during a few last years. The processes taking place in such discharges are applied in fields of water treatment[1–5], destruction of various organic pollutants dissolved in water[6], surface treatment of polymeric fibres[7] and in specific reactions in the liquid phase. The common discharge configurations are point-to plane[1,2] and coaxial[3], several experiments were done in diaphragm (electrode--less) configuration[4]. During almost all of these experiments, a pulsed high voltage in the range from about 10 to 20 kV was used to create the discharge. The present contribution focuses on the diaphragm discharge created using the non--pulsed DC high voltage, which could be lower than in the case of the pulsed high voltage (only about 2 kV)[5]. Various active species are produced by such discharge (hydroxyl radicals, hydrogen and oxygen radicals, hydrogen peroxide etc.)[2].

Experimental setup

The batch discharge reactor (Fig. 1.) divided into two parts is used in this experiment[8]. The experimental device uses the diaphragm discharge with an applied non-pulsed DC voltage from 1.4 to 2.8 kV. The stainless steel electrodes in the distance of 2 cm from the diaphragm (PET, thickness of 0.25 mm) are used. To protect the experimental medium from the heat caused by the discharge, two cooling boxes are installed in both parts of the reactor. NaCl, $Na_2HPO_4 . 12H_2O$, $KHCO_3$ and $LiNO_3$ electrolytes are dissolved in demineralized water used to obtain the defined conductivity (the optimum is 300–700 μS cm^{-1}) of the solution.

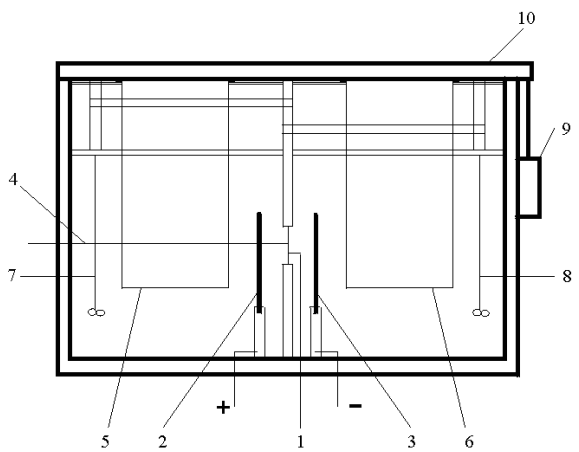

Fig. 1. **A scheme of the discharge reactor: 1 – dielectric diaphragm, 2 – positive electrode (anode), 3 – negative electrode (cathode), 4 – quartz fiber, 5, 6 – cooling boxes, 7, 8 – stirrers, 9 – safety switch, 10 – cap**

During all experiments, the pin-hole (with the initial diameter of 0.4 mm) is altered by the discharge. Its diameter is enlarged by the discharge and the pin-hole becomes slightly irregular in its shape. Due to these effects, the discharge also burns irregularly, and therefore a longer integration time is necessary to use for measuring the emission spectra.

Results and discussion

The emission spectra of the diaphragm discharge were observed during the experiments. The relative OH integral intensity from the range of 306.5–318.0 nm as a quantitative parameter of the diaphragm discharge was calculated for each measurement and plotted as a function of the discharge conditions. The spectroscopic observations were done in selected electrolytes at different initial conductivities (400 and 550 μS cm^{-1}).

The influence of the applied voltage was measured in the solution of $KHCO_3$ (the concentration of 4.0 mmol l^{-1}). The measurements were done at six different voltages. As it can be seen from Fig. 2., the line intensities are near to the noise level at the lower voltage (1.40 and 1.75 kV). At the higher voltage, the intensities of both kalium resonance lines increase proportionally with the increasing applied voltage. On this basis, the tension of 2.80 kV was used in all the following experiments.

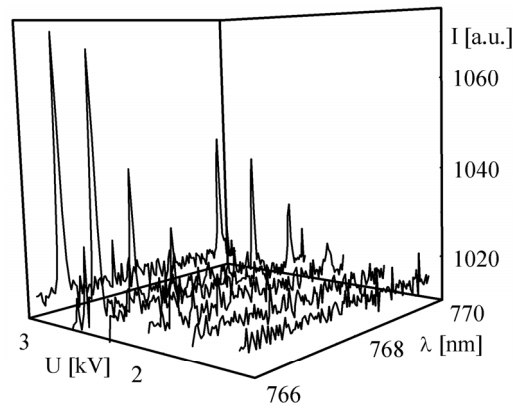

Fig. 2. **Dependence of the potassium resonance lines intensities on the wavelength for the different applied voltages**

The solution conductivity is not constant during the discharge. Water solutions of $LiNO_3$ with the initial conductivity of 400–1100 μS cm^{-1} were used to study this effect. The conductivity increases directly proportional to the initial concentration with a different slope in each part of the reactor (see Fig. 3.). The conductivity increase is caused by the chemical active species (radicals, ions etc.) produced by the discharge in the liquid phase and also by the involved metallic traces (Fe and Cr ions) from the high voltage electrodes[8].

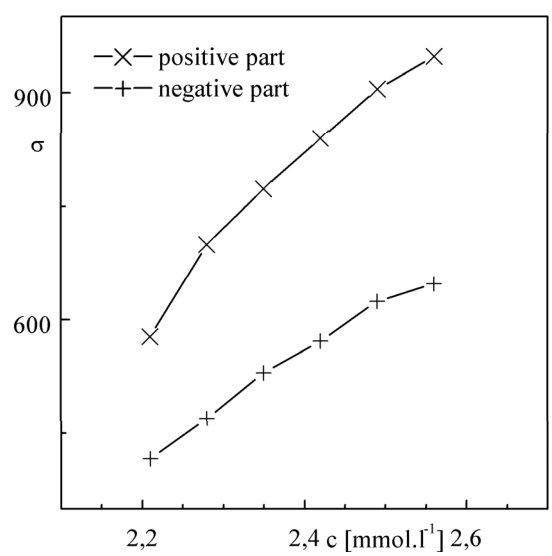

Fig. 3. **Conductivity dependence [μS cm^{-1}] on the $LiNO_3$ concentration after 5 minutes of the discharge in both discharge polarities**

The main part of the experiment was focused on the study of the spectral intensities as a function of concentrations of various salts. The intensities of the hydrogen

lines as well as the integral intensity of the OH radicals are independent of the salt concentration. No significant dependence of their intensities on the salt type was observed.

The resonance line intensities of the alkaline elements (Fig. 4., 5.) are more or less directly proportional to their concentrations in the solution. The direct comparison of different electrolytes containing the same alkaline element is at present impossible due to technical experimental problems and it is planned for the near future.

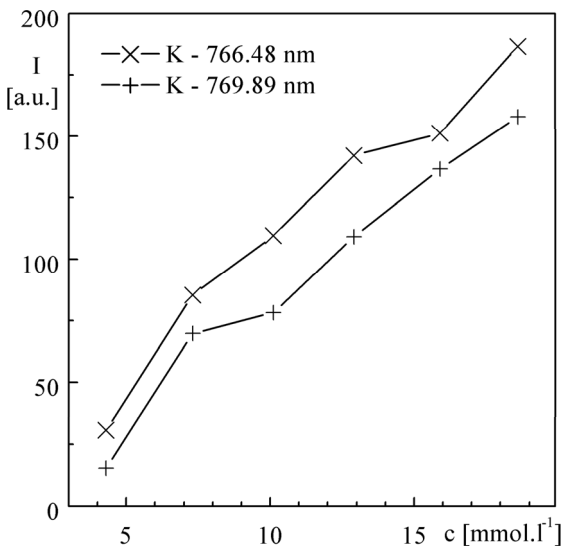

Fig. 4. **Dependence of the K emission intensities (766.48 and 769.89 nm) on the $KHCO_3$ concentration at the applied voltage of 2.8 kV**

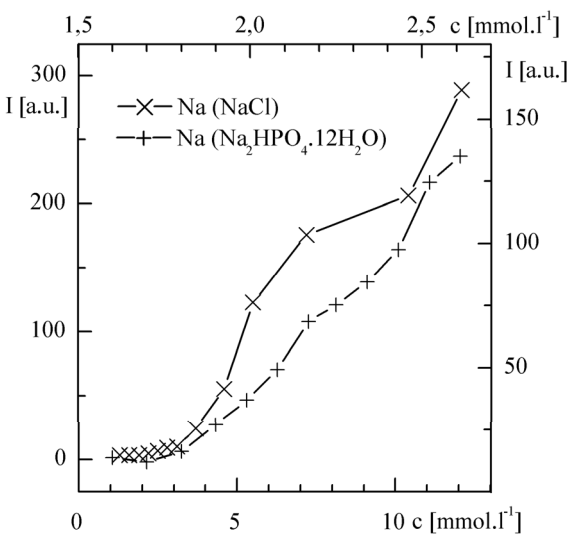

Fig. 5. **Dependence of the Na emission intensities (766.48 and 769.89 nm) on the NaCl and Na_2HPO_4 $12H_2O$ concentration at the applied voltage of 2.8 kV**

Conclusions

This work is focused on optical observations of the DC non-pulsed diaphragm discharge in the liquid phase. The contribution describes the results obtained by the optical emission spectroscopy during the discharge treatment in water solutions of various alkaline metal salts. The dependence of the emission intensity of hydroxyl radicals, atomic H and resonance spectral lines of the used alkaline metals on the salt concentration was studied.

The emission intensities of H and OH are independent of the concentration solutions, while the intensity of alkaline metals resonance lines are dependent more or less linearly on the salt concentration.

These results show that the DC diaphragm discharge can be applied as an alternative source for the atomic emission spectroscopy. A very similar method was recently patented independently of our observations[9,10].

This work was supported by the Grant Agency of the Czech Republic, contract No. 202/03/H162.

REFERENCES

1. Clements J. S., Sato M., Davis R. H.: IEEE Trans. Ind. Appl. IA *23*, 224 (1987).
2. Joshi A. A., Locke B. R., Arce P., Finney W. C.: J. Hazard.Mater. *41*, 6 (1995).
3. Šunka P., Babický V., Člupek M., Lukeš P., Šimek M., Schmidt J., Černák M.: Plasma Source Sci. Tech. *8*, 258 (1999).
4. Kuzhekin I. P.: *Proceedings of 9th International Symposium on High Voltage Engineering*, p. 8073-1, Graz 1995.
5. Krčma F., Stará Z.: Chemical Papers *96*, S82 (2002).
6. Lukeš P.: *Water Treatment by Pulsed Streamer Dodona Discharge, Ph.D. Thesis*, Charles Univerzity, Prague, Czech Republic, 2002.
7. Brablec A., Slavíček P., Sťahel P., Čižmár T., Trunec D., Šimor M., Černák M.: Czechoslovak J. Phys. *52*, D491 (2002).
8. Stará Z.: *The Diaphragm Discharge in Liquids, Thesis*, Brno University of Technology, Brno (2002).
9. Russian patent RU 2, 179, 310 C2.
10. Patent WO 9301486.

P32 NEW CYCLIC SELENIUM OXIDE – TETRASELENIUM DECAOXIDE Se_4O_{10}

LUKÁŠ RICHTERA[a], VOJTĚCH JANČÍK[b], JAN TARABA[c] and JIŘÍ TOUŽÍN[d]
[a]*Institute of Material Chemistry, Faculty of Chemistry, Brno University of Technology, Purkyňova 118, 612 00 Brno, Czech Republic, richtera@fch.vutbr.cz,* [b]*Instituto de Química, UNAM, Circuito Exterior, Ciudad Universitaria, México D. F. 04510, México, vjancik@centrum.cz,* [c,d]*Department of Inorganic Chemistry, Faculty of Science, Masaryk University, Kotlářská 2, 611 37 Brno*

Selenium trioxide reacts with 1,4-dioxane explosively at ambient temperature, but the donor-acceptor compound $SeO_3 \cdot C_4H_8O_2$ can be isolated from the reaction when carried out at low temperature[1–3]. During the formation of this adduct, several other by-products were observed and isolated, among others the cyclic $Se_3O_7 \cdot 2C_4H_8O_2$, containing selenium atoms in oxidation states +IV and +VI, respectively[3]. The conformation of the cyclic Se_3O_7 molecule in $Se_3O_7 \cdot 2C_4H_8O_2$ is different than that of the first reported adduct of triselenium heptaoxide $Se_3O_7 \cdot CH_3NO_2$ (ref.[4]). The two terminal oxygen atoms bonded to Se^{+IV} in $Se_3O_7 \cdot CH_3NO_2$ molecule are located cis to each other, whereas they are trans in the $Se_3O_7 \cdot 2C_4H_8O_2$ molecule.

Recently, other interesting compounds have been isolated and studied by X-ray structure analysis and Raman spectroscopy from a SeO_3/1,4-dioxane system as well as from systems containing additional solvents. For example, two cyclic esters of selenic acid, $C_2H_4O_4Se$ and $C_2H_2O_8Se_2 \cdot C_4H_8O_2$ were obtained and described[5]. All examined compounds are highly sensitive towards moisture.

The extremely high sensitivity of the last observed compound toward moisture and traces of impurities made its separation and identification rather difficult[3]; this white solid decomposes to elementary selenium even during mechanical manipulation. Nevertheless, it was isolated from a reaction carried out in nitromethane and identified by X-ray structural analysis and Raman spectroscopy as $Se_4O_{10} \cdot 2C_4H_8O_2$. The low quality of the crystals only allows us to present the structure of this compound as a ball and stick model (Fig. 1.). Attempts to remove the solvating 1,4-dioxane molecules *in vacuo* resulted in a complete decomposition of the substance. The structure of Se_4O_{10} can be described as a $[Se(O)_2(\mu\text{-}O)Se(O)(\mu\text{-}O)]_2$ eight-member ring and can be easily derived from the above mentioned structure of Se_3O_7 in $Se_3O_7 \cdot 2C_4H_8O_2$ by inserting one SeO_3 unit. The conformation of the eight-membered ring is very close to the preferred boat-chair conformation of cyclooctane[6]. In the layered structure of $Se_4O_{10} \cdot 2C_4H_8O_2$ there are two molecules of 1,4-dioxane coordinated to the equatorial positions of Se^{+IV} ($d_{Se\cdots O}$ = 238.9 and 245.1 pm). The ordinary octahedral environment of the Se^{+IV} atoms is completed by very weak interlayer contacts $Se^{IV}\cdots O = Se^{IV}$ ($d_{Se\cdots O}$ = 344.2 pm). The tetraselenium decaoxide Se_4O_{10} can be considered to be an unstable dimeric form of the much more stable chain polymeric diselenium pentaoxide $(Se_2O_5)_n$ (ref.[7,8]).

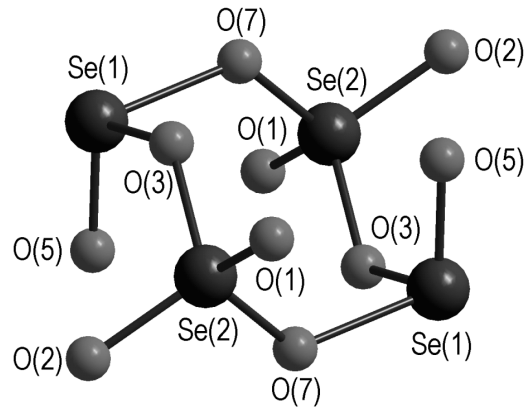

Fig. 1. **The ball and stick presentation of the Se_4O_{10} unit in $Se_4O_{10} \cdot 2C_4H_8O_2$**

Two possible mechanisms for the formation of $Se_4O_{10} \cdot 2C_4H_8O_2$ can be suggested. Whereas the first involves partial reduction of the tetrameric selenium trioxide $(SeO_3)_4$, the second and more probable is based on the presence of sufficient amounts of $Se_3O_7 \cdot 2C_4H_8O_2$ and $SeO_3 \cdot C_4H_8O_2$ in the reaction mixture (Fig. 2.). In this case the $SeO_3 \cdot C_4H_8O_2$ molecule can act as a donor of a monomeric SeO_3 unit and thus its fusion with $Se_3O_7 \cdot 2C_4H_8O_2$ would produce the tetraselenium decaoxide Se_4O_{10}.

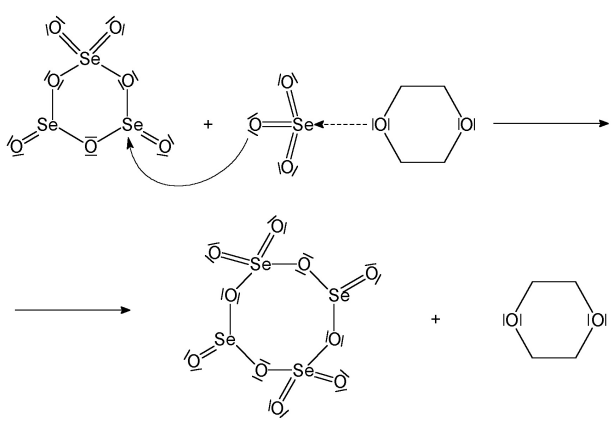

Fig. 2. **The probable mechanism of $Se_4O_{10} \cdot 2C_4H_8O_2$ formation**

REFERENCES

1. Schmidt M., Wilhelm I.: Ber. *97*, 872 (1964).
2. Blanka B., Toužín J.: Collect. Czech. Chem. Commun. *32*, 3284 (1967).
3. Richtera L., Toužín J.: *Pokroky v anorganické chemii – IV. seminář,* Vranov u Brna, 2002, Sborník příspěvků (Příhoda J., Michaličková Z., ed.), p. 56.
4. Toužín J., Kilián P., Žák Z.: Z. Anorg. Allg. Chem. *622*, 1617 (1996).

5. Richtera L., Toužín J.: *53. zjazd chemických spoločností,* Banská Bystrica, 2001, Zborník príspevkov 2 (Tölgyessy J., Kmeťová J., ed.), p. 178.
6. Dunitz J. D., Mugnoli A.: Chem. Commun. 166, 1966.
7. Jerschkewitz H. G.: Angew. Chem. *69*, 562 (1957).
8. Žák Z.: Z. Anorg. Allg. Chem. *81*, 460 (1980).

P33 HUMIDITY SENSORS BASED ON ORGANIC SEMICONDUCTORS

KATEŘINA SEVEROVÁ[a], MARTIN WEITER[a] and STANISLAV NEŠPŮREK[a,b]
[a]*Institute of Physical and Applied Chemistry, Faculty of Chemistry, Brno University of Technology, Purkyňova 118, 612 00, Brno,* [b]*Institute of Macromolecular Chemistry, Academy of Sciences of the Czech Republic, Heyrovský Sq. 2, 162 06 Prague 6, Czech Republic*

Introduction

Humidity sensors are utilized for the measurement of relative humidity in processing control and monitoring of the environment. Organic and especially polymeric materials are investigated and widely used for humidity sensing due to their high sensitivity, quick response, chemical and physical stability and low cost. Materials for the humidity sensors could contain hydrophilic groups to improve water sorption and dissociable segments of the type A^+B^- which, after the dissociation in external electric field, can generate free charge carriers. Thus, electrical conductivity during a humidity exposure increases. The aim of this work is to present a new material for humidity sensors, hydroxyaluminum phthalocyaninesulfonate sodium salt and characterize its electrical answer.

Experimental

Phthalocyanines (Pcs) are thermally and chemically stable organic semiconductors, but usually not soluble. The soluble form, hydroxyaluminum phthalocyaninesulfonate sodium salt [Al(OH)Pc($SO_3Na)_{1–2}$] (Fig.1.) was prepared from hydroxyaluminium phthalocyanine [Al(OH)Pc] dissolved in 10 % fuming sulfuric acid and subsequently heated (85 °C, 6 hours). The reaction mixture was purred into the mixture of water and ice, filtered and washed. The filter cake was dispersed in water and pH adjusted with NaOH to the value

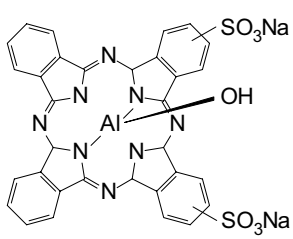

Fig. 1. **The molecular structure of soluble phtalocyanine, [Al(OH)Pc($SO_3Na)_{1–2}$]**

of about 11. Thus, [Al(OH)Pc] was converted into dark blue water soluble sodium salt, which was isolated by evaporation of water by using a water bath. Impedance Analyzer Hewlett Packard 4192A with frequency range 5 Hz–13 MHz was used for measurement of A.C. characteristics. Kinetic responses during the change of RH were measured at constant mode at 100 kHz.

Samples for humidity sensors were prepared by drop casting on ceramic substrates with surface platinum electrode configuration. The distance between the electrodes was 100 μm. The degree of humidity in measuring cell was realized in two ways: (i) Sample was kept in the atmospheres of saturated vapors of inorganic salts (lithium chloride, potassium hydrogen sulphate, etc.), which have defined value of the relative humidity (RH); (ii) The humidity of the atmosphere around the sample was established by mixing dry and wet gases (bubbling through water).

Results and discussion

The studied sensors are based on the increase of electrical conductivity after their exposure to humidity. The process is related to the dissociation of ionic groups chemically attached to the basic π-conjugated skeleton of the molecule:

$$Al(OH)Pc(SO_3Na)^0_{1–2} + \text{humidity} \rightarrow Al(OH)Pc(SO_3^- Na^+).$$

Under the influence of external electric field the ionic groups ($SO_3^- Na^+$) can efficiently dissociate and ionic contribution to the current can be observed. Because the mobility of the ions is relatively low, the ionic contribution is responsible for relatively slow current kinetics. However, the formation of negative SO_3^- groups is responsible for the induction effect; by transfer of movable π-electrons of the Pc skeleton pairs $Pc^+ \ldots SO_3^-$ are formed. This process is very fast and follows immediately after the primary dissociation of $SO_3^- Na^+$. In external electric field the ion-pairs $Pc^+ \ldots SO_3^-$ can dissociate onto free charge carriers Pc^+, holes (positive polarons). They can move relatively fast by charge hopping through Pc molecules: $Pc^+ Pc^0 Pc^0 Pc^0 \rightarrow Pc^0 Pc^+ Pc^0 Pc^0 \rightarrow$ etc. The fast current kinetics is mainly influenced by charge transport of positive polarons.

The charge hopping was tested by the frequency dependence of A. C. conductivity. The sample was kept in air atmosphere with 44 % RH, then the atmosphere was spontaneously changed to 15 % RH. As expected, the conductivity decreased with time (see Fig. 2a) as the number of groups available for the dissociation decreased. The low frequency current decrease was about half-order of magnitude during 70 min. The conductivity increased with frequency as follows from Fig. 2a. It is a feature common to amorphous and disordered materials; conductivity increases approximately linearly with frequency at least in the frequency range $1–10^8$ Hz

$$\sigma_{AC}(\omega) = A\omega^s \qquad (1)$$

where the frequency exponent is usually $s \leq 1$. The total measured conductivity at a given frequency ω is separable into D.C. and A. C. components (if A.C. and D.C. conduction

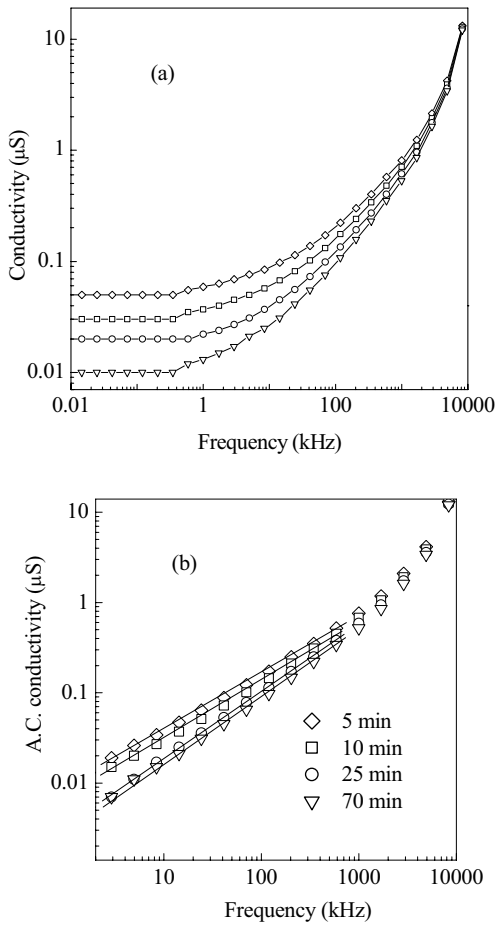

Fig. 2. **Conductivity as a function tivity as a function of frequency [Al(OH)Pc(SO_3Na)$_{1–2}$] at 15 % relative humidity at 22 °C. The curves were measured at time given Fig. 2b after the change of relative humidity from 40 % to 15 %. (a) As measured data, (b) A. C. conductivity calculated as conductivity σ (as measured) minus σ (10 Hz)**

arise from completely separate and different processes or the same basic process is responsible for both types of conductivities, but the states giving rise to the A.C. conductivity are clustered and do not constitute a percolation path throughout the sample)[1]

$$\sigma_{tot}(\omega) = \sigma_{DC} + \sigma_{AC}(\omega). \quad (2)$$

If the same process is responsible for both D.C. and A.C. conduction, σ_{DC} is simply the $\omega \to 0$ limit of $\sigma(\omega)$ and the validity of Eq. 2 is more dubious, but often used by many authors. In Fig. 2a σ_{DC} components can be taken as the values σ (10 Hz). With time, after the change of RH from 40 % to 15 % the density of centres available for the dissociation and σ_{DC} decreases. If $\sigma_{DC} \approx \sigma$ (10Hz) values are taken out from the total conductivities, $\sigma_{tot}(\omega)$, we can get $\sigma_{AC}(\omega)$ which show nearly linear dependences of the type $\log \sigma_{AC}(\omega) \sim s \log \omega$ up to the frequency about 1 MHz, with s being close to 1 (0.9 for the curve measured at after 70 min after the change of RH from 40 % to 15 %, see Fig. 2b and depending slightly on the number of states contributing to the A.C. loss; s decreases with increasing value of σ_{DC}. It is known that in Pcs two processes are important for charge carrier transport: polaron formation due to strong electron-phonon coupling and charge hopping among Pc molecules. The charge carrier transport is realized by hopping through tail states arising from the dispersion of polarization energy (due to the molecular geometrical disorder). The charge transport is in this case influenced by barrier height W separating two sites and having an energy difference Δ. Usually the model assuming that the relaxation variable W is independent of the intersite separation R (and hence the hopping distance is independent of frequency) seems to be too simple. The model of the electron transfer by thermal activation over the barrier between two sites, each having a Coulombic potential well seems to be more appropriate for many real cases. For neighbouring sites at a separation R, the Coulomb wells overlap, resulting in a lowering of the barrier (correlated barrier hopping model).

Note, that the dependence of W on R is the same as one can expect for the overlapping-large-polaron model. In the narrow-band limit ($\Delta << kT$), and assuming that the centres are distributed randomly in space, real part of A.C. conductivity is given approximately by the relation[1]

$$\sigma_{AC}(\omega) = \frac{1}{24}\pi^3 N^2 \varepsilon\varepsilon_0 \omega R_\omega^6 \quad (3)$$

where R_ω is the hopping distance. Thus, σ_{AC} conductivity increases with number N of electronic states, as it follows from Fig. 2b. However, a small decrease of s with increasing N is not very clear yet and needs more discussions. The important experimental fact is that for frequencies higher than 0.8 MHz the σ_{AC} is a superlinear function of frequency, i. e. s increases with ω. This fact can be explained by a non-random distribution of barrier heights.

The kinetics of changes of the conductivity of [Al(OH)Pc(SO_3Na)$_{1–2}$] film during the change of RH (from 15 % to 86 %) at constant measuring frequency 100 kHz is shown in Fig. 3. After the increase of relative humidity A.C. conductivity increases. From the shape of the build-up curve (especially given in semilogarithmic plot) it is clear that at least two physical processes are responsible for the conductivity increase. The conductivity increase during the humidity raise (from 15 % to 86 %) was found to be nearly three orders of magnitude; the full saturation was achieved during about 250 s.

It could be noted that process was much faster if the change of the humidity was realized by flowing gas. After the decrease of RH from 86 % to 15 % to conductivity strongly decreased. The decay can also be characterized by two components (see Fig. 2b); the long time kinetics was the first-order reaction with rate constant $k = 0.017\ s^{-1}$.

Conclusion

Soluble phthalocyanine [Al(OH)Pc(SO_3Na)$_{1–2}$] is suitable material for the preparation of humidity sensors. The change of the conductivity during the step change of the

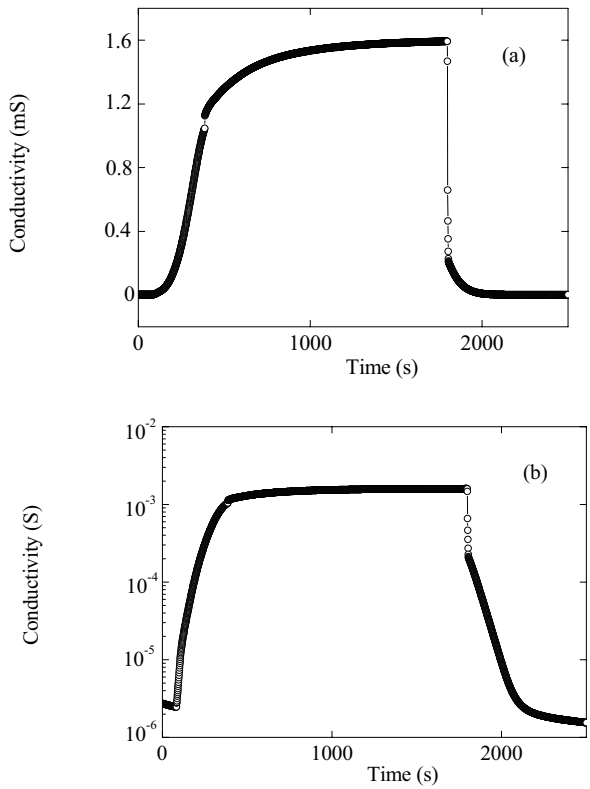

Fig. 3. **Conductivity change of $[Al(OH)Pc(SO_3Na)_{1-2}]$ for step change of relative humidity from 15 % to 86 % at 22 °C at measuring frequency 100 kHz. (a) Linear coordinates, (b) semilogarithmic plot**

relative humidity from 15 % to 86 % was about three orders of magnitude during about 250 s. The build-up and decay kinetics suggest that at least two physical processes are responsible for the conductivity changes. From the frequency dependence of A.C. conductivity follows that charge carrier transport is influenced by charge hopping mechanism over the system of Coulombic potential walls with a non-random distribution of barrier heights.

The financial support by grant FT-TA/036 from the Ministry of Industry and Trade of the Czech Republic is gratefully appreciated.

REFERENCE

1. Elliott S. R.: Adv. Phys. *36*, 135 (1987).

P34 THE EFFECT OF THE LOW TEMPERATURE AIR PLASMA TREATMENT ON THE SURFACE PROPERTIES OF SOME SYNTHETIC POLYMERS

PETR SMOLKA and LUBOMÍR LAPČÍK JR.
The Institute of Physics and Material Engineering, Faculty of Technology, Tomas Bata University in Zlin, Nám. T. G. M. 275, 762 72 Zlín, Czech Republic, smolka@ft.utb.cz,

Introduction

Synthetic polymers belong to a group of materials nowadays widely used in many branches of industry. They offer good processibility, low density and favourable price – value ratio and can substitute conventional materials such as wood and metals. Polymers often have low surface energy resulting in poor adhesion, which can be desirable (non-adherent Teflon®) but in most cases brings problems. Typical examples are glued joints, protective coating application, printing, etc[1,2]. Surface energy can be increased by chemical methods, burning off by a flame or stream of hot air or plasma treatment. Plasma induces chemical and structural changes in the polymer surface layer, bulk properties does not change. Low-molecular components ablation, cross-linking or surface activation occur, according to the plasma type. The main purpose of this work is to study the effect of low-temperature air plasma treatment on the surface properties of polycarbonate (PC) and polystyrene (PS).

Methods and materials

Two polymeric materials were examined: polystyrene KRASTEN (Kaučuk a. s, Kralupy nad Vltavou) and polycarbonate Lexan® 9030 sheet (GE Plastics, Pittsfield). Materials were in a form of sheets with the thickness from 1.0 to 1.5 mm. Samples with dimensions 20 × 20 mm were prepared by cutting. Sample dimensions were measured by a digital micrometer, resulting dimension was an average of four observations. Surface of the sample was cleaned by ethanol and rinsed by distilled water.

Plasma treatment was performed in a vertical cylinder reactor with plane parallel electrodes (quartz reactor chamber, inner diameter 80 mm), in a radio-frequency discharge (13.56 MHz) with power supply 5 to 10 W and working pressure 0.1 to 1.0 torr. Samples were placed on the lower electrode, each side of the sample was treated for 1, 5 and 20 minutes.

Dynamic contact angle measurements were performed on the Tensiometer K12 (Krüss GmbH) at the temperature 20 °C, utilising Wilhelmi plate method. Resulting value was an average of four observations. Redistilled water, ethylene glycol and glycerol were used as testing liquids. Samples modified by plasma were measured directly after removal from the reactor. In order to determine contact angle hysteresis, advanced and receding contact angle values were collected.

Results and discussion

As expected, the values of both advancing and receding contact angles were significantly lower on plasma treated samples compared to referential. The most noticeable changes occurred during first 5 minutes, prolonged plasma treatment can even cause moderate increase of contact angles (Fig. 1.). Special behaviour of glycerol was observed on treated samples, where advancing contact angle declined no lower than to 60 degrees but receding contact angle went to zero after one minute of plasma treatment on both materials, as illustrated by hysteresis of angles (advancing minus receding) in Fig. 2.

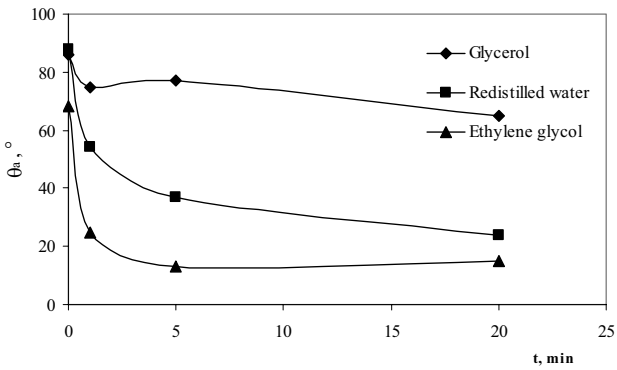

Fig. 1. **Advancing contact angle on polystyrene vs. time of plasma treatment (20 °C)**

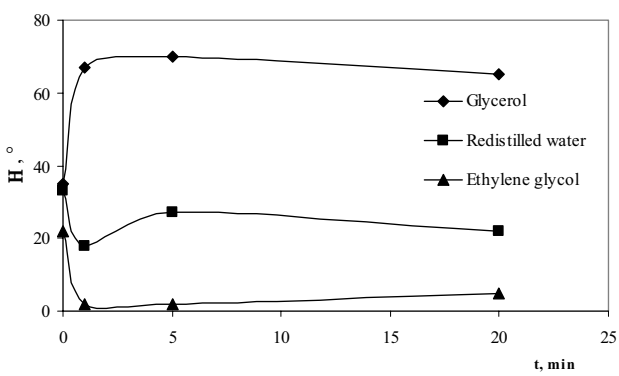

Fig. 2. **Contact angle hysteresis on polycarbonate vs. time of plasma treatment (20 °C)**

Surface energies of the polymers were calculated by harmonic mean method (1) and by Young – Dupre equation (2) in order to compare the results of both methods[3,4]. First method enables determination of disperse and polar components of surface energies while the second allows determination of electron-donor and electron-acceptor parts of the polar component. Calculations were performed in the program Mathematica 4.1. Mean contact angle cosine values (cos θ) were used (3).

$$(1+\cos\theta)\gamma_{L1} = 4\left(\frac{\gamma_{L1}^{d}\cdot\gamma_{S}^{d}}{\gamma_{L1}^{d}+\gamma_{S}^{d}} + \frac{\gamma_{L1}^{AB}\cdot\gamma_{S}^{AB}}{\gamma_{L1}^{AB}+\gamma_{S}^{AB}}\right) \quad (1)$$

$$(1+\cos\theta)\gamma_{L1} = 2\left(\sqrt{\gamma_{S}^{d}\gamma_{L1}^{d}} + \sqrt{\gamma_{S}^{+}\gamma_{L1}^{-}} + \sqrt{\gamma_{S}^{-}\gamma_{L1}^{+}}\right) \quad (2)$$

$$\cos\theta = \frac{\cos\theta_a + \cos\theta_r}{2} \quad (3)$$

These quantities are present in equations: advancing and receding contact angle (θ_a, θ_r, resp.); total, disperse, polar, electron-donor and electron-acceptor liquid surface tension components (γ_L, γ_L^d, γ_L^{AB}, γ_L^- and γ_L^+, resp.); total, disperse, polar, electron-donor and electron-acceptor solid surface energy components (γ_S, γ_S^d, γ_S^{AB}, γ_S^- and γ_S^+, resp.). Results obtained by both methods show significant surface energy increase, particularly the polar component, with the time of plasma treatment (Fig. 3., Fig. 4.).

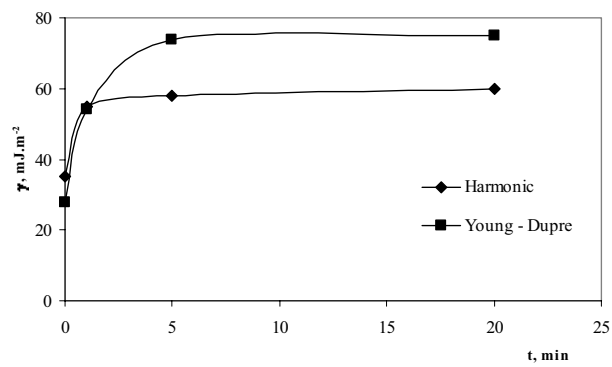

Fig. 3. **Polycarbonate surface energy (γ) determined by harmonic mean method and Young – Dupre equation vs. time of plasma treatment (t)**

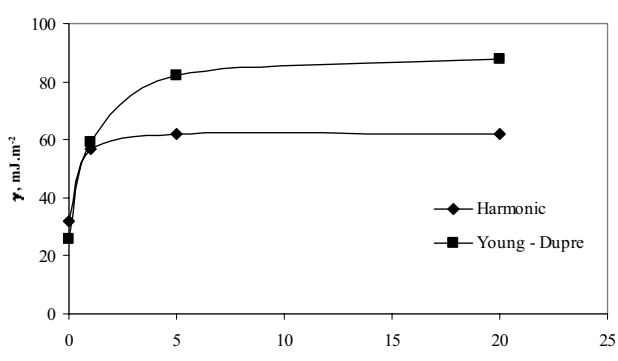

Fig. 4. **Polycarbonate surface energy (γ) determined by harmonic mean method and Young – Dupre equation vs. time of plasma treatment (t)**

The reason for this is that plasma induces incorporation of functional groups containing oxygen into the surface.

Young – Dupre equation provide surface energy values higher than those from the harmonic mean method and favours strongly the polar component (Table I).

The increase in contact angle hysteresis of glycerol on treated surfaces can be possibly attributed to more intensive interaction of polar groups generated by plasma with its –OH groups.

Table I
Polycarbonate surface energy and its components, determined by Young – Dupre equation

Time of plasma treatment [min]	Surface energy [mJ m^{-2}]				
	γ_S^d	γ_S^{AB}	γ_S^+	γ_S^-	γ_S
0	9.70	19.30	5.79	16.09	29.00
1	7.03	45.74	15.03	34.80	52.77
5	0.64	72.38	27.59	47.47	73.02
20	1.08	73.09	23.74	56.25	74.17

This paper is based on Petr Smolka diploma thesis Charakterizace povrchových energií polymerních materiálů opracovaných fyzikálním plazmatem, měření dynamických konstantních úhlů smáčení *(Institute of Physics and Materials Engineering, TBU in Zlín, 2003). Petr Smolka thanks prof. Ing. Lubomír Lapčík, Ph. D. for supervising and help.*

REFERENCES

1. Lapčík L., Raab M.: *Nauka o materiálech II.* TBU in Zlín, Zlín 2000.
2. Langmaier F.: *Adhese a adhesiva.* BUT in Brno, Brno 1999.
3. Wu S., *Polymer interface and adhesion.* Marcel Dekker, New York 1982.
4. van Oss C. J., Chaudhury M. K., Good R. J., Chem. Rev. *88*, 927 (1988).

P35 CYCLODEXTRIN AS A MORPHOLOGY MODIFYING AGENT FOR BISMUTH VANADATE NANO-PARTICLES

PETR SMOLKA[a], TITO TRINDADE[b] and LUBOMÍR LAPČÍK JR.[a]
[a]*The Institute of Physics and Material Engineering, Faculty of Technology, Tomas Bata University in Zlin, Nám. T. G. M 275, 762 72 Zlín, Czech Republic, smolka@ft.utb.cz,* [b]*Department of Chemistry, University of Aveiro, 3810-193 Aveiro, Portugal*

Introduction

Bismuth vanadate ($BiVO_4$) is a non-toxic yellow pigment widely used to substitute potentially harmful cadmium- and lead-containing pigments. It can be prepared by various techniques, which affect the resultant properties of the material (particle shape, size and its distribution and crystalline phase type). Procedures based on precipitation from aqueous solution offer more possibilities to influence these characteristics than solid-state reactions[1]. Modification of the chemical bath deposition process (CBD)[2] was used to prepare solid films of morphologically well-defined particles of $BiVO_4$ at low temperatures (below 100 °C). This method utilises ethylenediaminetetraacetic acid (EDTA), which prevents $BiVO_4$ from spontaneous precipitation. As a chelate agent, EDTA can form very stable metal-EDTA complexes. The main idea in this work is to examine the effect of alpha, beta and gama cyclodextrins (CD) present in the solution. It is well known that CD can form inclusion complexes with various substances. During the formation of the complex, no primary bonds are formed between the host and guest molecule and the stability of the system depends mainly on steric and thermodynamic factors[3].

Methods and materials

Synthesis were performed as follows: first, 2 mmol of EDTA and intended amount of cyclodextrin were dissolved in 15 ml of distilled water and 1,25 mmol of $Bi(NO_3)_3.5H_2O$ was added. This white turbid mixture was stirred at room temperature for 15 minutes. Then 1 mmol of $NaVO_3$ was added and stirring continued for another 7 minutes. After that the pH of the solution was adjusted to 8.5 using 1 and 0.1 M NaOH. Transparent yellow solution formed after heating and stirring in oil bath at 100 °C. Clear liquid was transferred into a glass tube, microscope slide cover (previously rinsed by acetone and destilled water) was placed inside vertically and the tube was sealed by a plastic cap. Deposition was performed in a silicon oil bath at temperatures ranging from 45 to 100 °C during required time. Finally, the substrate with the deposited film was rinsed by destilled water and dried under the air stream.

Morphology and size of the $BiVO_4$ particles were determined by scanning electron microscopy (SEM), analysis of the film chemical composition were performed using infrared (FT-IR), Raman and ultraviolet-visible (UV-Vis) spectroscopies.

Results and discussion

Coating of the glass slip was performed at different temperatures, times of deposition and concentrations of cyclodextrin. Film was formed in all cases, having yellow colour characteristic for $BiVO_4$, but there were significant differences in the film density. Temperature and cyclodextrin concentration seemed to have the main influence on the film formation. Best results were achieved with referential samples at temperatures close to 100 °C. The higher the concentration of cyclodextrin, the thinner the layer of pigment was formed. At concentrations close to 80 mmol dm^{-3} only traces of yellow particles were observed. Without EDTA clear solution did not form and attempts to prepare morphologically well-defined particles were not successful. Spectroscopy analysis confirmed that the film consisted of $BiVO_4$ particles

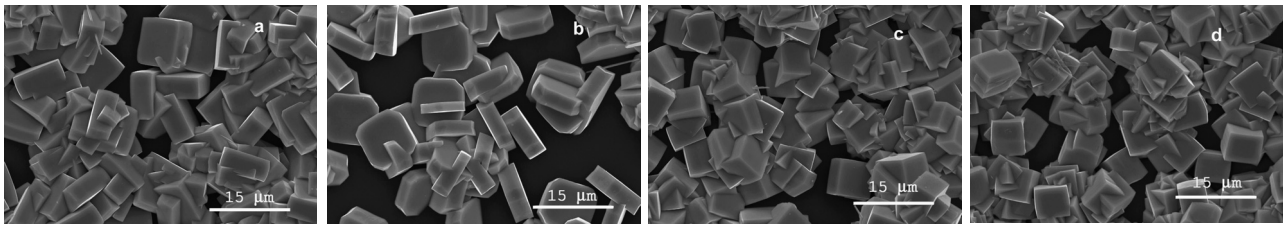

Fig. 1. **SEM images of $BiVO_4$ films taken at 25 kV; a) referential sample R, b) C1 modified by α-CD, c) C2 modified by β-CD and d) C3 modified by γ-CD; 8 hours at 100 °C**

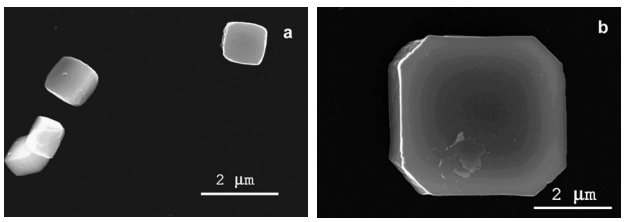

Fig. 2. **SEM images of $BiVO_4$ films taken at 25 kV; a) deposition 20 hours at 45 °C and b) deposition 8 hours at 100 °C**

and no organic compounds were present in it. Cyclodextrin can possibly influence the growth of the crystal, but probably does not incorporate itself into the crystal lattice.

It has been known from previous research[2,4] that crystals prepared by the CBD method had monoclinic structure. Fig. 1. shows details of films prepared with various cyclodextrins at 100 °C during 8 hours. In all samples the film consisted of regular particles distributed uniformly on the substrate. Similarity can be observed between samples R (referential) and C1 (α-CD) where the particles are platelets-like, while crystals in samples C2 (β-CD) and C3 (γ-CD) are cubic and smaller in size. Moreover, chamfered edges can be observed on crystals grown in the presence of α-CD. This feature, however, can not be ascribed only to the influence of cyclodextrin. It has been observed even in referential samples and samples which have grown in the presence of β-CD. Temperature effect is demonstrated in Fig. 2. Both films crystallized from the same solutions (modified by β-CD), but density of the coating deposited at 45 °C in 20 hours is very low and particles are three-times smaller and irregular in shape compared to those synthesised at 100 °C in 8 hours.

Obtained data suggested that cyclodextrin can possibly influence the morphology of $BiVO_4$ particles, its effect was, however, often prevailed by stronger factors such as EDTA concentration and the temperature of reaction mixture.

Petr Smolka thanks EU for the Marie Curie Fellowship contract HPMT-CT-2000-00206-20.

REFERENCES

1. Wood P., Glasser F. P.: Ceramics International *30*, 875 (2004).
2. Neves M. C., Trindade T.: Thin Solid Films *406*, 93 (2002).
3. Valle E. M. M. D.: Process Biochemistry *39*, 1033 (2004).
4. Neves M. C., Lehocký M., Soares R., Lapčík L. Jr., Trindade T.: Dyes and Pigments *59*, 181 (2003).

P36 DEGRADATION OF ORGANIC COMPOUNDS BY THE DIAPHRAGM DISCHARGE

ZDENKA STARÁ and FRANTIŠEK KRČMA
Institute of Physical and Applied Chemistry, Faculty of Chemistry, Brno University of Technology, Purkyňova 118, 612 00 Brno, Czech Republic, stara@fch.vutbr.cz

Introduction

The discharges generated in liquids have a special position among the plasma sources. Various active chemical species such as hydroxyl radicals, hydrogen and oxygen atoms, hydrogen peroxide etc. are produced by this kind of discharge[1]. These active species initiate many further chemical reactions. Therefore the processes taking place in such discharges can be applied in fields of water treatment, surface treatment etc. Especially the destruction of various organic pollutants or organic dyes dissolved in water and specific reactions in the liquid phase are at present the main research fields of discharges in liquids[1–3].

Various configurations of the electrodes were used for the discharge creation in previous works of many authors[1–4]. During almost all of these experiments, a pulsed high voltage in range from about 10 to 20 kV was applied. This work focuses on the diaphragm discharge created using the non-pulsed DC high voltage with the tension of about 2 kV only. The discharge is created in a small pinhole in the dielectric diaphragm which is placed between two planar electrodes. When the DC voltage is used, different plasma channels (so-called streamers) are created in both parts of the reactor (Fig. 1.). These streamers have an inverse polarity and differ in their structure, shape, velocity of propagation and energy of electrons[4].

The degradation process is studied on selected organic dyes and for various discharge conditions (the applied voltage magnitude and polarity, initial conductivity of the solution etc.).

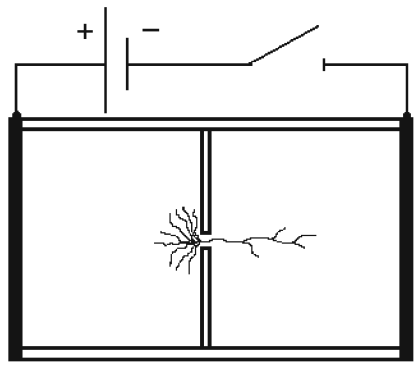

Fig. 1. **A scheme of the diaphragm discharge principle with different plasma channels in the parts of the reactor**

Experimental part

A special batch discharge reactor was used in experiments[5]. It consisted of two chambers divided by a dielectric diaphragm (PET). A small pinhole (initially with the diameter of 0.25 mm) was located in the centre of this diaphragm. Each chamber contained a planar electrode (stainless steel or platinum), a cooling box with a mixture of ice and water, a defined volume of electrolyte (1500 ml) and a mixing system that ensured homogenous conditions. To generate high voltage and to create the discharge, a non-pulsed DC high voltage source (1–3 kV) was applied.

Demineralised water containing electrolyte NaCl, Na_2HPO_4 was used to obtain solution of the defined initial conductivity (the optimum is 300–700 μS cm^{-1}). Various organic dyes dissolved in water with different structure, colour and purpose of use were used in experiments. The initial concentration of the used dyes varied from 1 to 20 mg l^{-1}. As most of the organic dyes were not electrolytes, it was necessary to add extra electrolyte to the solution. The concentration decrease of each dye was determined by photometry at the corresponding maximum absorption wavelength (λ_{max}).

Results and discussion

The first results from the experiments with the dye degradation by the diaphragm discharge were already presented[6]. Fig. 2. shows the relative concentration decrease of the Saturn Red dye during the discharge treatment. The dye concentration decreased almost exponentially in time and the decomposition of the dye was much faster in the negative discharge polarity. While in the positive discharge the relative concentration became about 20 % after 100 minutes of the experiment, in the negative polarity the concentration dropped to 20 % in the first 10 minutes of the discharge. The degradation process was mainly caused by the active species produced in the electric discharge in water[7]. The comparison of both dyes degradation and H_2O_2 generation process as a function of the discharge polarity was presented recently[8].

As the DC non-pulsed high voltage was used to create the discharge, the degradation process could also be influenced by the electrolysis. In this case, the electrochemical oxidation on the anode takes place in the system[9]. Therefore a special experiment focused on the electrolysis was carried out. The same discharge conditions as in previous experiments were established, but the pinhole in the diaphragm was enhanced and the applied voltage was as low as possible to exclude the discharge. The results of this experiments are demonstrate in Fig. 3. It is seen that the degradation process was not avoided, only the dye decomposition was not so significant as in the discharge. The concentration became just about 50 % after the one-hour experiment.

The process of organic dye degradation was investigated as a function of various parameters. One of them was a chemical structure of the used dyes. Four different compounds

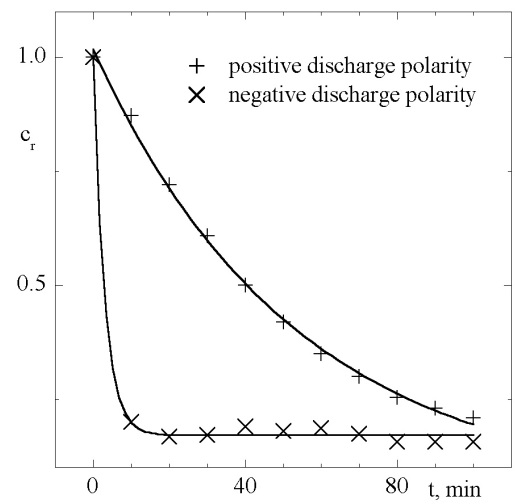

Fig. 2. **Concentration decrease of the Saturn Red dye during the discharge (204 W) – 5 mM NaCl, the initial conductivity of 500 μS cm^{-1}, λ_{max} = 506 nm**

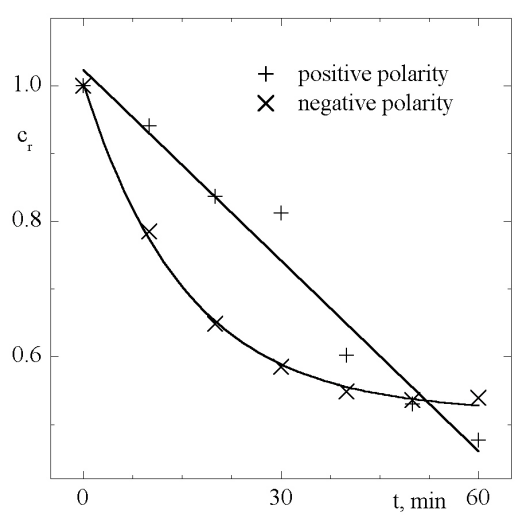

Fig. 3. **Concentration decrease of the Saturn Red dye during the electrolysis (44 W) – 5 mM NaCl, the initial conductivity of 500 μS cm^{-1}, λ_{max} = 506 nm**

dissolved in water were treated by the discharge – their relative concentrations during the discharge treatment are shown in Fig. 4. The experiments show that the solutions of the azo, the diazo-dye and the fluorone had almost similar evaluation in the decolorisation process and the final concentration reached 30–40 % after 100 minutes. The solution of Methylene Blue, which belonged to thiazine compounds, was not decomposed so intensively and the concentration decrease lead to only 80 % in the same time. When the positive discharge was used, the results were almost similar but the dependencies of the dye concentrations on the discharge time were not so fast as in the negative polarity.

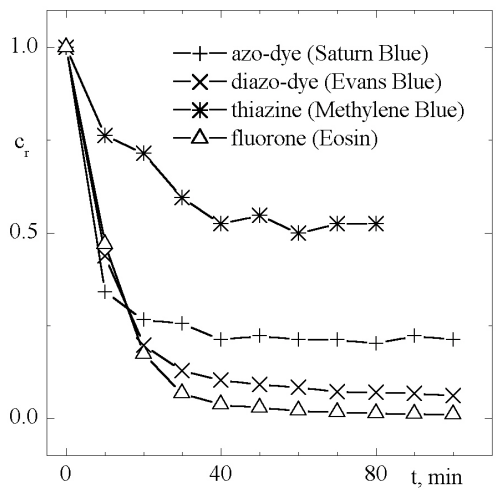

Fig. 4. **Comparison of the concentration decrease for the organic dyes with different chemical structure during the positive discharge (204 W, 5 mM NaCl, the initial solution conductivity of 500 μS cm^{-1}, λ_{max}: Saturn Blue 608 nm, Evans Blue 592 nm, Methylene Blue 576 nm, Eosin 516 nm)**

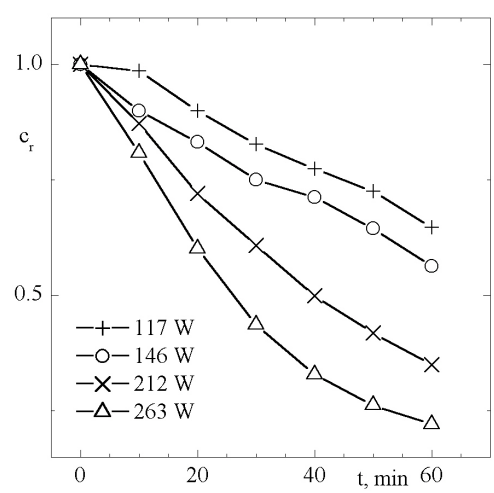

Fig. 5. **Influence of the applied high voltage on the degradation of the organic dye Saturn Red (5 mM NaCl, the initial conductivity of 500 μS cm^{-1}, λ_{max} = 506 nm)**

The influence of the voltage tension on the degradation process was investigated, too. The dependence of the Saturn red concentration on the applied voltage is given in Fig. 5. for the positive discharge polarity. The decomposition was directly proportional to the discharge power. The time evaluations of the dye concentration were very similar in the negative discharge and there was only a slight dependence of the concentration decrease on the voltage tension.

Conclusions

The degradation process of organic dyes dissolved in water was observed during the DC diaphragm discharge. This phenomenon was caused mainly by the active species produced by the discharge in water (radicals, hydrogen peroxide etc.) and it was also enhanced by the electrolysis. The dye decomposition was dependent on the discharge conditions, especially on the applied high voltage. The degradation process was faster with the increasing discharge power and it was more effective in the negative discharge polarity. Various organic dyes with different chemical structure were compared. The destruction efficiency reached up to 80% after 100 minutes of experiments.

This work was supported by the Czech Science Foundation, contract No. 202/03/H162 and by the Grant of the Czech Ministry of Education number 2003/0894.

REFERENCES

1. Šunka P., Babický V., Člupek M., Lukeš P., Šimek M., Schmidt J., Černák M.: Plasma Source Sci. Tech. *8*, 258 (1999).
2. Goheen S. C., Durham D. E., McCulloch M., Heath W. O.: *Proceedings of 2nd International Symposium on Chemical Oxidation*, p. 356, 1992.
3. Pawlat J., Hensel K.: Czechoslovak J. Phys. *54*, C964 (2004).
4. Kuzhekin I. P.: *Proceedings of 9th International Symposium on High Voltage Engineering*, p. 8073-1, Graz 1995.
5. Krčma F., Stará Z.: Chemical Papers *96*, S82 (2002).
6. Krčma F., Stará Z.: *Proceedings of 22nd Symposium on Plasma and Ionised Gases*, p. 601, Bajina Bašta 2004.
7. Stará Z., Krčma F.: Czechoslovak J. Phys. *54*, C1050 (2004).
8. Stará Z., Krčma F.: Acta Phys. Slovaca *55* (2005), submitted.
9. Lukeš P.: *Water Treatment by Pulsed Streamer Corona Discharge,* Ph. D. Thesis, Charles University, Prague, Czech Republic, 2002.

P37 RECOGNITION OF WOOD SPECIES. CLASSIFICATION ACCURACY OF RGB TRISTIMULUS VALUES

ATTILA SZITAS[a], GABRIELA SZEIFFOVA[a], ŠTEFAN VARGA[b], JÚLIUS ANNUS[c] and MARIÁN BABIAK[d]

[a]Department of Chemical Technology of Wood, Pulp and Paper, [b]Department of Mathematics, [c]Department of Chemical Physics, Faculty of Chemical and Food Technology, Slovak University of Technology in Bratislava, Radlinského 9, SK-812 37 Bratislava, Slovak Republic, attila.szitas@stuba.sk, [d]Department of Wood Science, Faculty of Wood Sciences and Technology, Technical University in Zvolen, Masarykova 24, SK- 960 53 Zvolen, Slovak Republic

Introduction

The complex wood processing requires rapid and reliable identification of wood species and nondestructive evaluation (NDE) of qualitative classes of wood raw materials and products. The color information are used for visual sorting of raw materials, sawnwood, fibre and particle boards, paper, decorative paper laminates, flooring and siding materials, furniture and wood-based buildings. Using the color information for machine vision and automation is still limited although the research in this area has been recognized to have the most significant implications for the woodworking industry[1–8]. This may be caused mainly by variability and fuzzy character of wood color[9–13].

The aim of this paper is the quantification of classification accuracy expressed using the parameter of recognition efficiency (RE) of the color RGB tristimulus values at distinguishing broadleaved wood species.

Experimental

The model set of 25 rustical wood lamellas of beech (*Fagus silvatica, L.*); oak (*Quercus robur, L.*); maple (*Acer pseudoplatanus, L.*); ash (*Fraxinus excelsior, L.*); cherry tree (*Cerasus avium, L.*); Measured sample size: $63 \times 345 \times 5$ mm.

The surface was scanned using HP ScanJet 4P color scanner (Hewlett-Packard) with the resolution of 200 dpi. The CIE RGB tristimulus values from the 5 random scan positions were evaluated by means of ScanWood Ekorex SK software at three apertures, 1×1, 10×10 and 100×100 px, respectively. The average RGB tristimulus values, as well as standard deviations were calculated for each scan. Then, multivariate analysis and discriminant analysis were carried out to evaluate classification accuracy, information content and recognition efficiency of the RGB tristimulus values.

Results and discussion

The average RGB tristimulus values, obtained after scanning procedure for each wood lamella sample are depicted at Fig. 1. The here presented 3D projection clearly demonstrates the heterogeneity and complexicity of studied problem.

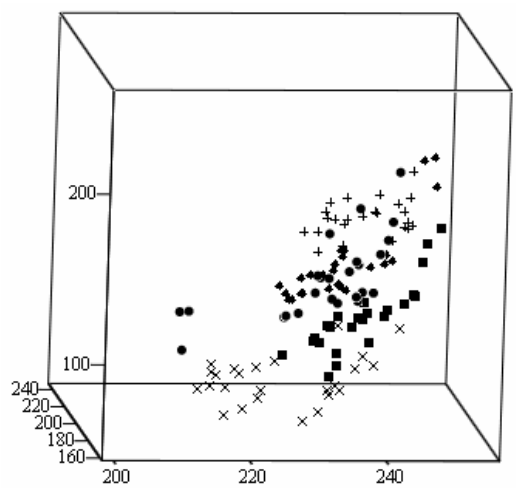

Fig. 1. **3D projection of average RGB tristimulus values, obtained for wood lamellas, made from: oak common(●), beech copper (×), ash common (◆), maple great (+), cherry tree (■)**

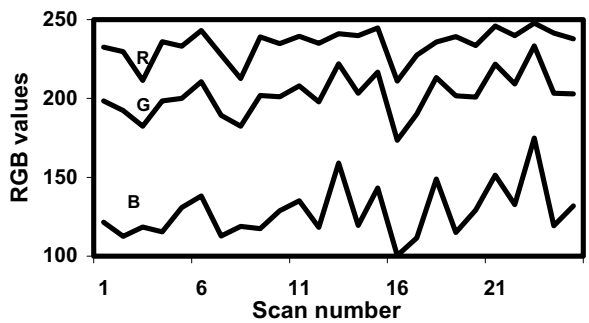

Fig. 3. **The of experimental RGB tristimulus values of beech copper obtained using the aperture of 1×1 px with resolution of 200 dpi (average of 25 individual scan line positions)**

Fig. 2. represents the experimental RGB tristimulus values, obtained using the aperture of 1×1 px with resolution of 200 dpi for 1 scan line position, here for beech. The black line on lamella illustrates the scan line position. Each wood sample undergoes 25 scans (5 for each lamella) from randomly selected positions and the average RGB tristimulus values are then calculated (Fig. 3.). From the mathematical point of view, the homogeneity of multi-dimensional set of RGB values was tested in first step. The tested hypothesis was postulated as follows: „H_0:RGB set is fully homogenous“, but this postulate was soon dismissed (p-value ~ 0). We found out, that each relevant parameter (R, G, B) together with their standard deviations (s_R, s_G, s_B) causes or strongly influences the inhomogeneity of evaluated data set, from which the main causative agent reliable for this phenomenon seemed to be B-values. Using the the discriminant analysis and classification functions ψ_j (Eq. 1), containing the vector of averaged RGB values of each scan ($\vec{y}$) evaluated for each wood sample (j), covariance matrix S_j and the prior

Table I
The recognition efficiency (RE) of the RGB tristimulus values in classifying of wood species, expressed as the percentage of correctly classified scans

Aperture	Number of scans	Number of correctly classified scans					Sum of correctly classified scans	RE
		Beech	Oak	Maple	Ash	Cherry		
1 × 1 px	125	20	25	24	25	25	119	95.2 %
10 × 10 px	125	16	25	22	24	20	107	85.6 %
100 × 100 px	125	19	25	22	24	24	114	91.2 %

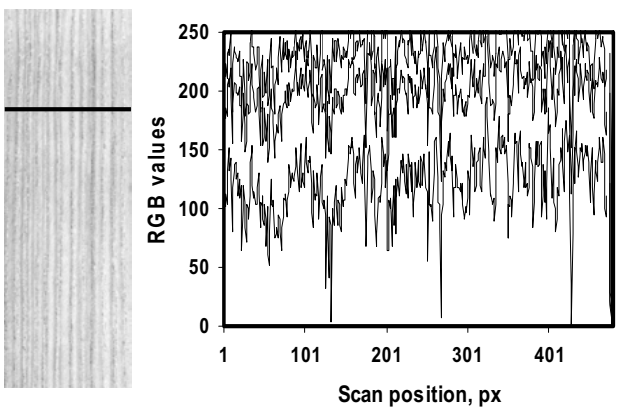

Fig. 2. **The experimental RGB tristimulus values of beech copper obtained using the aperture of 1 × 1 px with resolution of 200 dpi for 1 scan line position**

probability π_j, representing the probability that the specified y value will be assigned to correct "j".

$$\psi_j = -\frac{1}{2}(y-\bar{y}_j)^T S_j^{-1}(y-\bar{y}_j) + \log \pi_j - \frac{1}{2}\log|S_j| \quad (1)$$

According to the values of classification function, the evaluated wood samples were divided into groups, corresponding to the type of wood with the reliability of RE. The obtained recognition efficiency data RE % are summarized in Table 1.

It can be seen that the classification accuracy expressed through number of correctly classified hardwoods using individual scans in the model case of the distinguishing between the 5 hardwoods of beech, oak, maple, ash and cherry tree varies between 107–119 from total 125 scans.

The information value of the RGB tristimulus values at the recognition of the 5 model species is relatively high, varying from 85–95 % percentage of correct decisions, when using only 1 scan for the each decision.

The authors express their thanks to the VEGA agency for financial support of the project No. 1/0061/03.

REFERENCES

1. Kline D. E., Conners R., Araman P. A.: *Proc. Quality Lumber Drying in the Pacific Northwest*. 67–73 2000. USDA/Forest Service.
2. Bond B. H., Kline D. E., Araman P. A.: Wood and Fiber Sci. *34*, 516, (2002).
3. Hatalová B., Pisarčík M., Katuščák S., Paulínyová E.: Proc., The 6th Spectroscopic Conf., Nitra, 1980.
4. Schiessl O., Katuščák S., Werner P., Mlčousek M.: Proc. Lignoautomatika, 82, Intern. Symp., Bratislava, ŠDVÚ, 1982.
5. Katuščák S., Werner P.; Koeditz W., Baurschmidt P.: *Intern. Federation of Automatic Control (IFAC) Symposium on Automatic Measurement and Control in Woodworking Industry*, Pergamon Press, *IFAC*, No. 1, 109–113,1986.
6. Jentner P., Katuščák S., Werner P., Rajkovič E.: CS Pat. 221010 (28. 12. 1982).
7. Katuščák S., Ammann E.: Ital.Pat. No. 1 185 489, 1987.
8. Szeiffová G., Katuščák S., Gorelková T.: *Proc. Intern. Conf. „Technology, Properties, Environment*, Bratislava 2001.
9. Bosonnet J., Bürki P., Culetto K., Witschi M., Einsele A., Katuscak S., Kebs Ch., Kucera L. J. a kol.: *Holz – Farbe – Gestaltung*. SAH Lignum Zürich, 1992.
10. Kucera L. J. und Katuscak S.: *Das Phänomen Holzfarbe*. In: *Holz-Farbe-Gestaltung*, p.43–52, Lignum Verlag Zürich, 1992.
11. Krkoška P, Vizárová K.: Chem. listy *94*, 881 (2000).
12. Katuščák S., Kučera L. J.: Wood Res. *45*, 9 (2000).
13. Katuščák S., Kučera L. J., Varga Š., Vrška M., Čeppan M., Šutý Š., Jablonský M.: Wood Res. *47*, 1 (2002).

P38 THE ELECTRICAL CONDUCTIVITY OF DOPED CERIUM OXIDE

MAGDALÉNA ŠEDOVÁ[a], OLDŘICH ZMEŠKAL[a] and JAROSLAV CIHLÁŘ[b]
[a]*Institute of Physical and Applied Chemistry, Faculty of Chemistry, Brno University of Technology, Purkyňova 118, 612 00 Brno, Czech Republic, xcsedovam@fch.vutbr.cz,*
[b]*Department of Ceramics, Institute of Materials Engineering, Brno University of Technology, Technická 2, 616 69 Brno, Czech Republic*

Introduction

In the present work, the ionic conductivities of cerium oxide doped with yttrium, gadolinium and samarium were studied.

Oxide materials with predominant oxygen ionic conductivity attract great attention for high-temperature electrochemical applications, such as solid oxide fuel cells (SOFCs), oxygen sensors and pumps[1].

Cerium oxide is a well-known fast oxygen ion conductor. It has been frequently studied as a model system for the class of metal oxide electrolytes that exhibit the fluorite crystal structure[2]. Ceria-based solid solutions have been regarded as the most promising electrolytes for intermediate temperature solid oxide fuel cells (SOFC)[3]. The mixed ionic and electronic conduction properties of doped ceria may be desirable in some applications, such as electrode/electrode interfaces[4]. Y^{3+}, Gd^{3+} or Sm^{3+} doped ceramics are potentially the most useful electrolytes for SOFCs since they have the excellent ionic conductivity[5].

In the present work, the ionic conductivities of cerium oxide (doped with yttrium, gadolinium and samarium) were studied as a function of dopant content from 25 °C to 800 °C in air using impedance spectroscopy and I–V measurement.

Experimental part

Sample preparation

Doped cerium oxide powders were prepared by homogeneous co-precipitation, using aqueous solutions of cerium nitrate, mixed with varying amounts of Sm-, Gd-, or Y-nitrate. The obtained doped oxide powders were consolidated into pellets at room temperature and an uniaxial pressure. These specimens were sintered in air for 2 hours at 1500 °C, some of these samples were further annealed in air for 1 h at 800 °C.

Electrical measurements

The samples were measured using impedance spectroscopy (four-point method) in air at temperatures ranging from 20 °C to 800 °C. The four-point method utilizes four electrodes. Two are current carrying electrodes and two are voltage probes[6]. The impedance measurements are performed over the frequency range from 5 Hz to 13 MHz. The applied voltage was 1 V.

It was investigated the influence of the dopant content and of the reaction conditions (surfactant presence, time of milling, ultrasound supply and hydrotermic conditions) on the electrical conductivity of CeO_2.

The I–V characteristics of doped CeO_2 were studied in the temperature range from 25 °C to 800 °C. The I–V measurements were performed by the use a Keithley electrometer.

Results

In the low temperature range doped CeO_2 electrolytes showed the electronic conductivity. On the other hand, at higher temperature the high ionic conductivity was observed. The temperature area where the transition between the electronic and ionic conductivity has been found were at about 250 °C.

All measured doped solid oxides showed an increase in the conductivity in comparison with undoped samples. The conductivity was accordingly increased with increasing the concentration of aliovalent guest cations at the initial stage of doping. However, further doping decreases conductivity after a relatively sharp maximum.

From analysis of the total resistance of combined processes of the bulk and grain boundary, ionic conductivities for ceria doped with the rare earths were calculated[7]. The ionic conductivity in an electrolyte with negligible electronic conduction was determnined by using Ohm s law[8]. In CeO_2-based solid solutions the highest conductivity was supported by the presence of Sm. Doped ceria had σ_{iont} approximately $0.53–1.8 \cdot 10^{-2}$ S cm^{-1} at 600 °C. From the Arrhenius plot it can be calculated the activation energy[9]. The activation energy at 600 °C for doped CeO_2 electrolytes was in the range from 0.75 to 1.00 eV.

It was investigated the influnce of reaction conditions on the electrical conductivity of CeO_2. Triton (surfactant) showed the highest influence on the conductivity increasing, whereas SDS the lowest one. The application of ultrasonic waves showed the highest influence in case of the most intensive support. Specimens with longer milling period exhibited the electronic conductivity under conditions at which samples with shorter milling period showed impurity-controlled ionic conductivity.

Discussion

The results of above experiments showed a different conduction mechanism in the doped sample in comparison with pure one. The addition of rare earth oxide dopants to ceria resulted in structural changes in the crystal lattice and changes in the ionic conductivity. The strong dependence of ionic conductivity on dopant type and concentration has been explained in terms of the lattice distortions introduced by the dopant, with those that produce the least amount of strain causing the smallest variation in the potential energy landscape[10].

In CeO_2-based solid solutions the highest conductivity was supported by presence of Sm. The way of samples preparing showed the influence on the electrical conductivity of CeO_2 as well.

REFERENCES
1. Fonseca F. C., Muccillo R.: Solid State Ionics *166*, 157 (2004).
2. Dokiya M.: Solid State Ionics *152*, 383 (2002).
3. Pena M. A., Fierro J. L. G.: Chem. Rev. *101*, 1981 (2001).
4. Bhalla A. S., Guo R., Roy R.: Mat Res Innovat *4*, 3–26 (2000).
5. Kurzweil P., Fischle H. J.: Journal of Power Sources *127*, 331 (2004).
6. Hsieh G., Mason T. O., Pederson L. R.: Solid State Ionic *91*, 203 (1996).
7. Balazs G. B., Glass R. S.: Solid State Ionics *76*, 155 (1995).
8. Godickemeir M., Gauckler L. J.: J. Elctrochem. Soc *145*, 414 (1998).
9. Mogensen M., Sammes N. M., Tompsett G. A.: Solid State Ionics *129*, 63 (2002).
10. MacDonald J. R.: *Impedance Spectroscopy*. John Wiley & Sons Inc., USA 1987.

P39 POLYMERIZATION OF DISSOLVED HUMIC SUBSTANCES CATALYZED BY IRON AND MANGANESE PORPHYRIN

DANIELA ŠMEJKALOVÁ[a], PELLEGRINO CONTE[b], RICCARDO SPACCINI[b], MILOSLAV PEKAŘ[a] and ALESSANDRO PICCOLO[b]

[a]Institute of Physical and Applied Chemistry, Faculty of Chemistry, Brno University of Technology, Purkyňova 118, 612 00 Brno, Czech Republic, smejkalova@fch.vutbr.cz,
[b]Dipartimento di Scienze del Suolo, della Pianta e dell'Ambiente, Università di Napoli Federico II, via Università 100, 800 55 Portici (Na), Italy, alpiccol@unina.it

Introduction

Even though formation of humic substances (HS) is one of the least understood aspects of humus chemistry, it is recognized that oxidoreductive enzymes, such as polyphenoloxidases produced by microorganisms and plants are directly involved in these processes. The active site of these enzymes is formed by metal porphyrins that are able to catalyze the oxidation of humic constituents – phenolic moieties into free radicals that in turn can be stabilized by spontaneous coupling to each other without additional involvement of the catalyst[1].

Since HS are important contributors to C cycle as major source of CO_2 and C reservoir, it is of paramount importance to increase the stability of these compounds against further biotic and abiotic degradation[2]. Recent insights into humic substances indicated that rather than being high molecular weight polymers, they are associations of heterogeneous molecules stabilized by hydrophobic interactions into only apparently high molecular weights[3]. With this understanding, it could be reasoned to mimic the catalytic coupling of HS phenolic constituents and in this way stabilize humic compounds by increasing the number of intermolecular covalent bonds.

Previous work[4] has shown that synthetic iron porphyrin successfully catalyzed the oxidative polymerization of HS when H_2O_2 was used as singlet oxygen donor. The aim of this work was to verify whether photo-oxidation could substitute the presence of singlet oxygen donor in the biomimetic polymerization of humic material.

Materials and methods

Detailed description of humic material extraction, biomimetic catalysis and High Performance Size Exclusion Chromatography (HPSEC) system used in this work is given elsewhere[4].

Results and discussion

Biomimetic polymerization of lignite humic material, induced by UV light exposure, was followed by HPSEC system coupled with UV and refractive index (RI) detectors. The efficiency of biomimetic catalysts, namely manganese (Mn-pha) and iron porphyrin (Fe-pha) was evaluated by determination of the average molecular weight (*Mwa*) values of control and catalyzed samples.

The addition of metal porphyrin catalyst to the non-exposed humic solutions did not vary the *Mwa* values previously obtained for control humic solution. However, significant changes of molecular weight were detected in the UV light exposed samples. Percentage increase of *Mwa* is shown in Fig. 1. and 2.

According to the UV-detected (280 nm) chromatograms, the irradiated humic material increased *Mwa* by 4 and 11 % after 5.5 h and 14 and 12 % after 13 h of exposure to UV light, in the presence of Mn- and Fe-pha, respectively (Fig. 1.). The time course progression of the UV light induced photo-oxidation was observed when already irradiated samples for 13 h were further collected after 8 and 11 d from the exposition. This time the *Mwa* values reached an increase of 27 and 23 % after 8 d and of 34 % after 11 d since UV exposure (Fig. 1.).

Since UV detector reveals only the molecular absorptivity of chromophore groups at chosen wavelength, the *Mwa* was determined also from chromatograms collected by RI detector that is able to follow the overall mass distribution of humic matter. Evaluation of RI-detected size exclusion chromatograms verified the general increase of *Mwa* values obtained during photo-induced oxidative polymerization of dissolved humic material. In fact, polymerized humic materials increased the *Mwa* values by 9 and 6 % after 5.5 h and 6 % after 13 h of exposure to UV light, in the presence of Mn- and Fe-Pha, respectively, compared to the control HA solution (Fig. 2.). Then a significant increase in molecular dimension was observed for samples analyzed after 8 and 11 d following 13 h irradiation with UV light. In this case, *Mwa* was increased by 24 and 32 % after 8 and 11 d from the UV irradiation in the presence of Mn-pha,

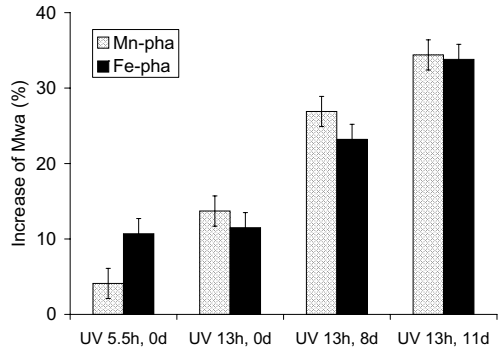

Fig. 1. **Percentage increase of apparent weight-average molecular weight (*Mwa*) of lignite humic solutions added with Mn-pha or Fe-pha catalyst and exposed to UV light for 5.5 or 13 h, right after exposure (0 d), after 8 and 11 d after irradiation end. HPSEC chromatograms were revealed by UV detector**

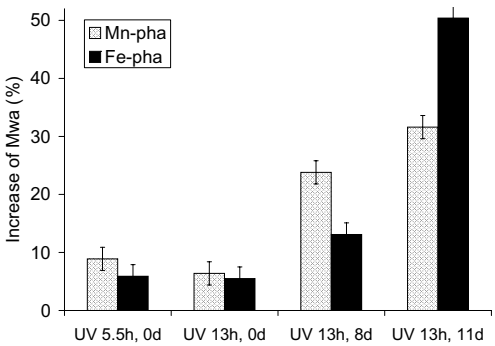

Fig. 2. **Percentage increase of apparent weight-average molecular weight (*Mwa*) of lignite humic solutions added with Mn-pha or Fe-pha catalyst and exposed to UV light for 5.5 or 13 h, right after exposure (0 d), after 8 and 11 d after irradiation end. HPSEC chromatograms were revealed by RI detector**

respectively, whereas the increase of *Mwa* values obtained with the Fe-Pha catalyst was 13 and 50 % after the same time courses (Fig. 2.).

REFERENCES

1. Dec J., Haider K., Bollag, J–M.: Soil Sci. *166*, 660–671 (2001)
2. Clapp C. E., Hayes M. H. B.: Soil Sci. *164*, 777–789 (1999)
3. Piccolo A., Cozzolino A., Conte P., Spaccini R.: Naturwissenschaften, *87*, 391–394 (2000)
4. Piccolo A., Conte P., Tagliatesta P.: Biomacromolecules *6*, 351–358 (2005)

P40 DETERMINATION OF ROTATIONAL MOLECULAR CONSTANTS

HANA SORMOVA[a,b] and JEAN DEMAISON[b]

[a]*Institute of Physical and Applied Chemistry, Faculty of Chemistry, Brno University of Technology, Purkynova 118, 612 00 Brno, Czech Republic, hanka@milansorm.cz*

[b]*Laboratoire de Physique des Lasers, Atomes et Molecules, UMR CNRS 8523, Universite de Lille I, 596 55 Villenevue d'Ascq Cedex, France, Jean.Demaison@univ-lille1.fr*

Introduction

The accuracy of the molecular constants determination is important for prediction of the transition frequency of the observed molecules. If we know the exact molecular constants then it will be easier to measure the spectra of the molecules and also to economize with the time of measurement and the sample.

This article, therefore, describes the methods of determining the rotational molecular constants from the experimental data and of computing their accuracy. This method is part of the program RotSimul[1] which helps to calculate these constants automatically.

The principle of the rotational molecular constants determination

The determination of rotational molecular constants is based on the theoretical calculations of the transition frequencies between the higher and lower energetic states. For example, the formula[2] for the symmetric prolate rotor is as follows:

$$\upsilon = 2B(J+1) - 4D_J(J+1)^3 - 2D_{JK}(J+1)K^2 + \cdots \qquad (1)$$

where υ is the transition frequency, B represents the rotational constant, J and K are the rotational quantum numbers (where $|K| = 0, 1 \ldots J$), D_J and D_{JK} are centrifugal distortion constants – they depend on the bond strength.

The equation (1) is applicable to most measurements, but sometimes it is necessary to use a different higher order correction for centrifugal stretching where H_J, H_{JK}, H_{KJ} are the centrifugal sextic[3]

$$\upsilon = h\{2B(J+1) - 4D_J(J+1)^3 - 2D_{JK}(J+1)K^2 + \\ + H_J(J+1)^3[(J+2)^2 - J^3] + 4H_{JK}(J+1)^3K^2 + \\ + 2H_{KJ}(J+1)K^4\} \qquad (2)$$

If we measure the dependence of the transition frequency υ on the rotational quantum number J, then it is possible to use the multi-linear regression (3) and through this procedure determine the values of rotational molecular constants[4,5].

$$y = b_0 + b_1x_1 + b_2x_2 + b_3x_3 + \ldots \qquad (3)$$

where y represents the transition frequency, x_1, x_2, x_3,… present the terms $(J+1)$, $(J+1)^3$, …and parameters b_1, b_2, b_3,… are the fitting molecular constants. Using the knowledge of

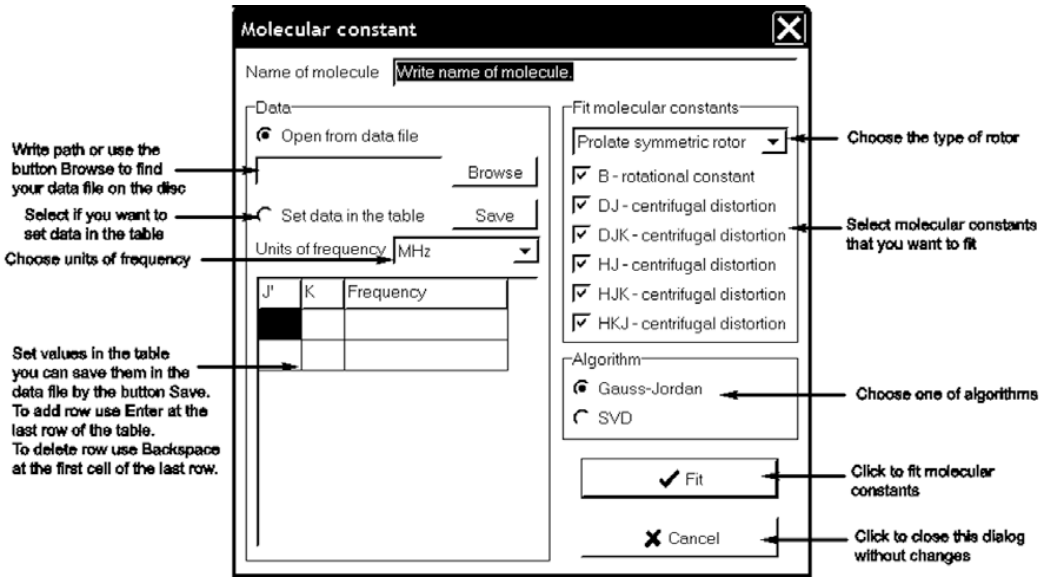

Fig. 1. **The control of rotational molecular constants fitting by the program RotSimul**

statistics it is also possible to calculate the uncertainties of the molecular constants[6].

Results and discussion

The above described principle was analyzed and then the general algorithm was created for the program RotSimul. The possibilities of the molecular constants determination by the created program are shown in Fig. 1. and the results of this procedure are shown in Table I.

Table I
Results of rotational molecular constants determination by the program RotSimul for the $H_3Si^{35}Cl$ molecule. The units of molecular constants in the table are in MHz. Residual error of this fitting is 0.1021 and the coefficient of determination 0.999999

Parameter	Est. value	Std. dev.
B	6673.8238	0.0005
D_I	0.0041253	0.00000025
D_{JK}	0.060577	0.000006
H_J	$-88.29.10^{-11}$	$3.22.10^{-11}$
H_{JK}	$90.06.10^{-9}$	$1.16.10^{-9}$
H_{KJ}	$140.30.10^{-8}$	$1.05.10^{-8}$

Conclusion

The algorithm was created in order to automatically determine rotational molecular constants; the applicability of this algorithm is in the general calculations all of the rotational molecular constants for all of rotor types – linear, spherical, symmetric prolate, symmetric obligate and also asymmetric rotor. This algorithm is a part of the program RotSimul that is a freeware and can be downloaded from the Internet[1].

REFERENCES

1. http://WWW.milansorm.cz/simul, March, 2005.
2. Hollas M. J.: *Modern Spectroscopy*. John Wiley & Sons, Ltd, New York, 2004.
3. Gordy W., Cook R. L.: *Microwave Molecular Spectra*. John Wiley & Sons, Inc., New York, 1976.
4. Edwards A. L.: *Multiple Regression and the Analysis of Variance and Covariance*. W. H. Freeman, San Francisco, CA, 1979.
5. Albritton D. L., Schmeltekopf A. L.: Journal of Molecular Spectroscopy *67*, 132 (1977).
6. Kleinbaum D. G., Kupper L. L.: *Applied Regression Analysis and Other Multivariable Methods*. Duxbury Press, North Scituate, MA, 1978.

P41 STUDY OF THERMAL DIFFUSIVITY IN HEAT-INSULATING MATERIALS

PAVLA ŠTEFKOVÁ and OLDŘICH ZMEŠKAL
Institute of Physical and Applied Chemistry, Faculty of Chemistry, Brno University of Technology, Purkyňova 118, 612 00 Brno, Czech Republic, stefkova@fch.vutbr.cz

Introduction

The building industry is using modern materials that are usually extremely porous to improve the thermal insulation properties. The performance of these materials depends on their thermophysical properties. This paper discusses the heat transport properties in glass wool fibers measured by pulse transient method and deals with the use of new data evaluation method[1]. The method results from generalized relations that were designed for study of physical properties of fractal structures[2]. As it is shown these relations are in a good agreement with the equations used for the description of time responses of temperature for the pulse input of supplied heat[3–5]. Thermal parameters (specific heat, thermal diffusivity and thermal conductivity) calculated are corresponding for both methods.

Theory

The dependence of fractal structures' (characterized by the fractal dimension D in E-dimension space) temperature on the distance from heat source h_T and on the time t was determined[1] using the theory of the space-time fractal field[2]

$$T = \frac{Q}{c_p \rho (4\pi a t)^{(E-D)/2}} \cdot \exp\left(-\frac{h^2}{4at}\right), \qquad (1)$$

where Q is the total heat transferred to the body from the heat source with the thermal conductivity $\lambda = c_p \rho a$. This relation[3–5] is applicable for fractal dimensions D = 0, 1, 2 and topological dimension E = 3, see Fig. 1.

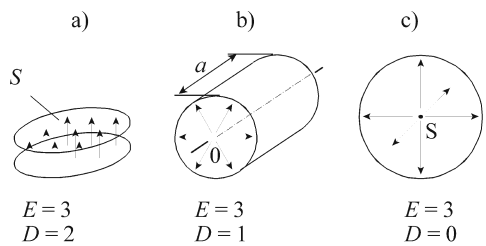

Fig. 1. **Heat flow geometry for a) plane-parallel, b) cylindrical and c) spherical coordinates Euclidean space**

From this equation the thermal diffusivity at the maximal time can be determined

$$a = \frac{h^2}{2t_m f_a} = \frac{h^2}{2(E-D)t_m}, \qquad (2)$$

where f_a is a coefficient that characterizes the deformation of the thermal field[5]. This coefficient is equal to one for the ideal plane source (E = 3, D = 2). The maximum temperature of the response for Dirac thermal pulse is obtained by introducing of the thermal diffusivity (2) in the term (1)

$$T_m = \frac{Q}{c_p \rho} \exp\left(\frac{D-E}{2}\right) \cdot \left(\frac{E-D}{2\pi h^2}\right)^{(E-D)/2}. \qquad (3)$$

It is possible to definite the coefficient f_a (fractal dimension D respectively) for every point of the experimental dependence

$$f_a = E - D = \frac{2\ln(T_m/T)}{\ln(t/t_m) + (t_m/t - 1)},$$

$$f_a = E - D = \frac{2\ln(T_m/T)}{\ln(t/t_m) + (t/t_m - 1)} \quad \text{respectively.} \qquad (4)$$

The relations on the left side are used for the temperature increase; the relations on the right side are used for the temperature decrease. The value of the coefficient f_a could be also affected by the geometry of sample[5] or by the finite pulse width[6], too. When the value f_a is known it is feasible to determine the parameters of the studied thermal system.

Experimental

The Thermophysical Transient Tester 1.02 was used for measuring of the responses to the pulse heat. It was developed at the Institute of Physics, Slovak Academy of Science[6].

Thermal responses from Slovak Academy were used for the data evaluation. The measured sample was round shaped with diameter R = 0.03 m. Its density was ρ = 77.9 kg m^{-3} for its thickness h = 0.0075 mm, the thermal conductivity was λ = 0,0254 W m^{-2} K^{-1}.

Results

The Fig. 2. represents the typical time responses of temperature for the pulse of input power. The coefficient f_a of the fractal heat source for every point of the experimental dependence was calculated using the Eq. 4. The fractal heat source characterizes the distribution of the temperature in the specimen in specific time. From the Fig. 3. it is evident that for very short time there is the value of the fractal dimension $D \approx 2$ and therefore, the plane heat source is formed. The value of the fractal dimension decreases with increasing time value since the heat disperses into the space. From the time $\tau_1 \approx 12$ s (the intersection of tangents of the curves) the fractal dimension is getting settled to the value $D \approx 0.15$. The spatial distribution of the temperature in the sample does not change yet in this area. It is possible to determine the coefficient of the heat source $f_{a0} = 1$ and the diffusivity of the specimen $a \approx 4.679 \cdot 10^{-7}$ m^2 s^{-1} from the extrapolated value of the fractal dimension to the time t = 0 s. This value is identical to value determined by the Institute of Physic, Slovak Academy of Sciences, Bratislava.

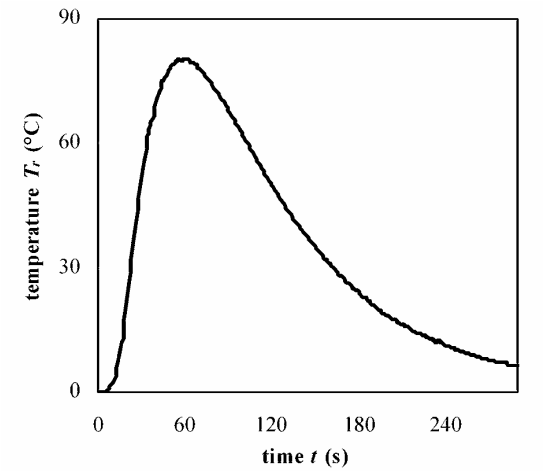

Fig. 2. **Thermal response of the sample measured by the pulse transient method**

From the descending characteristic we can again determine, by using (4) for each point of experimental dependence of measured temperature on time, coefficient f_a, fractal dimension D of the fractal source "*of cold*" presented by specimen surface. From Fig. 3b it is evident that there are not any cold spots over the surface of specimen for time intervals close to the maximum. With rising time the value of fractal dimension of decreasing temperature is smaller again until the value $D \approx 3$. This is a fractal dimension of the specimen volume.

Conclusion

In this article, the results of thermal responses to the pulse of supplied heat evaluations are discussed. To interpret the outcomes, the simplified heat conductivity model is used[1]. The model is based on expectations[3]. Results show the image of heat distribution in the specimen, in various time intervals after the heat supply from the source. These evaluations could be used for more accurate determination of the thermal parameters of studied matters.

REFERENCES

1. Zmeškal O., Buchníček M., Nežádal M., Štefková P., Capoušek R.: *Thermophysics 2003: Thermal Properties of Fractal Structure Materials*, Kočovce, 2003.
2. Zmeškal O., Nežádal M., Buchníček M.: Chaos, Solitons & Fractals 19, 1013 (204).
3. Carslaw H. S., Jaeger J. C.: *Conduction of Heat in Solids.* Clarendon Press London 1959, 496 pp.
4. Krempaský J.: *Measurement of Thermophysical Quantities.* VEDA, Bratislava 1969, 287 pp.
5. Kubičár L.: *Pulse Method of Measuring Basic Thermophysical Parameters.* VEDA, Bratislava and Elsevier Nederland 1990, 344 pp.
6. Boháč V., Kubičár Ľ., Vretenár V.: *TEMPMEKO 2004, 9th International Symposium on Temperature and Thermal Measurements in Industry and Science: Methodology of parameter estimation of pulse transient method and the use of PMMA as standard reference material*, Cavtat – Dubrovnik Croatia, 2004.

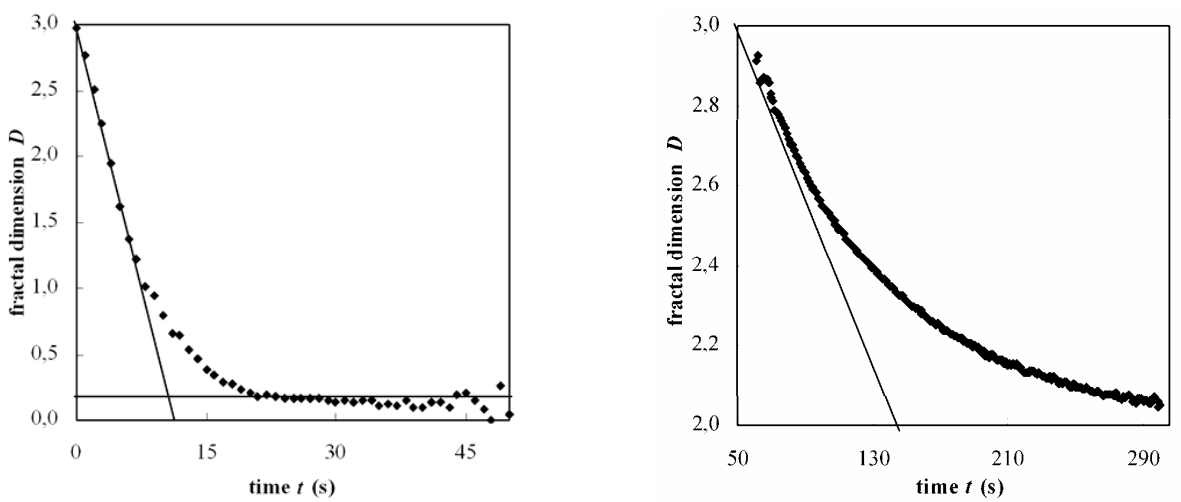

Fig. 3. **Fractal dimension of the heat distribution in the specimen from a) increased and from b) decreased part of characteristics**

P42 THE KINETICS OF POLY(2,6 - DIMETHYLPHENYLENEOXIDE) DISSOLUTION AND SWELLING

PAVEL URBAN[a], ALEŠ MRÁČEK[a], LUBOMÍR LAPČÍK[a, b] and MIROSLAV KUBA[b]
[a]*Department of Physics and Materials Engineering, Faculty of Technology, Tomas Bata University in Zlín, Nad Stráněmi 4511, 760 05 Zlín, Czech Republic, p.urban@centrum.cz,* [b]*Department of Physical and Applied Chemistry, Faculty of Chemistry, Brno University of Technology, Purkyňova 118, 612 00 Brno, Czech Republic*

Introduction

A solid thin polymeric film dissolution in a liquid solvent, at the temperature below the Tg, is characterized by a few kinetic parameters depeAnding on the static or dynamic conditions of the experimental arrangement[1]. The dominant role in the dissolution has been given to the internal diffusion of solvent molecules into the studied macromolecular sample and a proper polymer chains expansion.

The whole process can be divided in two steps: swelling and following real dissolution. The both of the mentioned sub-processes have been studied in the system PFO-benzene, toluene, trichlormethane and o-, p-, metaxylene. It has been found that the values of the integral diffusion coefficients of the solvents in the PFO decrease linearly with increasing molecular weight of the polymer.

For a precise evaluation of numeric features of swelling process has been used specially developed software system[2,3,4]. The application is designed for a direct data mining from camera images to obtain required information. Generally, using of the system is applicable for miscellaneous research activities with similar ideas of data analysis.

Methods of Data Evaluation by Software Application

The observed diffusion process of solvent into polymeric material is recorded in the form of interferograms using appropriate equipment of experimental framework and stored in image files for further analysis.

The interferograms acquired by a digital camera are analysed to evaluate the refractive index distribution along flow coordinate axis and then a distribution of concentration. Consequently, the kinetic and thermodynamic activation parameters are outgoing from knowledge of concentration profile in surface swollen layer of polymer/solvent system by software tool developed in LabVIEW environment. The main idea of the system is to identify the flowline between a polymer and solvent area by recording coordinates, which is followed by computations based on the formulas describing interference in thin or wedge layer. From aquired camera images, the application of functions available in the developed system enables exact determination of refractive indexes and the concentration profile during swelling process of polymers.

The name of the LabVIEW developed system is *SAIA* (*S*ystem for *A*nalysis of *I*nterferogr*a*ms). The SAIA system consists of three integrated modules, support and administrative tools for controlling the whole user-friendly system. The simple scenario for primary getting acquainted with system functions is also available.

Implemented relations:

A. Evaluation of the refractive index ($n(I,i)$) at the corresponding crossing points. The input variables are the number of crossings (k), the tabular value of the refractive index of polymer (n_p) and solvent (n_s).

$$n_{pi} = n_p + i\frac{n_s - n_p}{k}, \qquad (1)$$

where i is the i-th step in evaluation.

B. Evaluation of the concentration ($c(n_i)$) at the corresponding crossing points. The input variables are the previously computed refractive index of polymer in the i-th position (n_{pi}) and coefficients approximated by regression analysis, the initial value of refractive index of solvent (b_0) and effect of unit change to the value of refractive index of solvent/polymer system at crossing point (b_1).

$$n_{pi} = n_p + i\frac{n_s - n_p}{k}, \qquad (2)$$

where i is the i-th step in evaluation.

A recommended sequence of steps in the system application is described in the following flow chart.

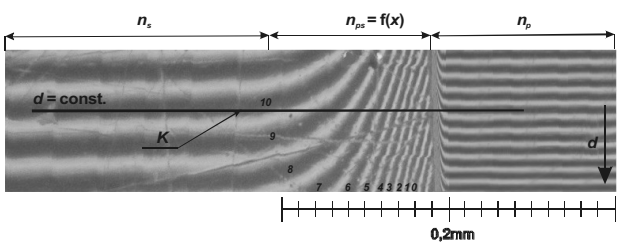

Fig. 1. **Principle of flowline determination**

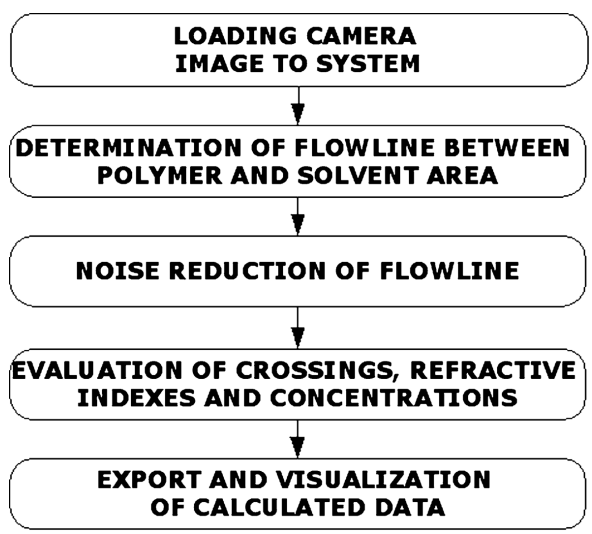

Fig. 2. **Flow chart of recommended operations**

Results and discussion

The activated parametres of swelling, dissolution, internal diffusion and expansion work of PFO under influence of internal pressure, are correlated with the fundamental molecular characteristic of the solvents molecules.

The SAIA system, which was used for data analysis, is designed as a modular system and there is a high flexibility of the enlargement of the functions maintained in the implemented modules. Its main strenght consists in the interconnection of the image analysing and computing batch suites. The new system modules, which could be developed as independent applications, could be simply integrated into the contemporary system. The new intended modules are going to be focused on analysis, mathematical modeling, simulation and statistical description of processes.

The system has been developed with the support of the National Instruments Corporation and DEWETRON-Prague Ltd.

REFERENCES

1. Kellö V., Očadlík J., Polavka J., Lapčík L., Kusý P., Panák J.: Chemické zvesti *33*, 347 (1979).
2. Reitz F. B., Pollack G. H.: Computer Methods and Programms in Biomedicine *70*, 61 (2003).
3. Whitley K. N., Blackwell A. F.: Journal of Visual Languages & Computing, *12*, 435 (2001).
4. Krauss A., Weimar U., Göpel W.: Trends in Analytical Chemistry, *18*, 312 (1999).

P43 PI-CONJUGATED POLYMERS INFLUENCED BY PERMANENT DIPOLE MOMENT FORMATION

MARTIN VALA[a], MARTIN WEITER[a], STANISLAV NEŠPŮREK[a,b] and OLDŘICH ZMEŠKAL[a]
[a]Faculty of Chemistry, Brno University of Technology, Purkynova 118, 612 00 Brno, Czech Republic, xcvala@fch.vutbr.cz, [b]Institute of Macromolecular Chemistry, Heyrovsky Sq. 2, 162 06 Prague 6, Czech Republic

Introduction

PI-conjugated polymers are of a particular interest mainly because they enable to produce cheap, lightweight and large area displays and for their promising applications in solar cells and photodetectors. One of the main advantages of organic semiconductors usually stressed is their wide electronic tunability. In this work, the electronic properties of poly(*p*-phenylenevinylene) derivatives are tuned by reversible light driven permanent dipole moment formation. Dipole moment contributes to the field acting on surrounding molecules and influences polarization energy in its vicinity. The conjugation of π-electrons along a polymer chain (responsible for semiconducting properties) is thus influenced. This feature has been used in the design of special type of optoelectrical switch[1].

Among possible reversible dipole moment forming species, spiro-coumpounds (SP) were used to produce such response[2]. Spiropyran molecules can reversibly change their conformation according to energy absorbed. This results in formation of dipole moment and also in UV-VIS, PL and IR spectra modifications of the whole system. The polymer matrix strongly influences the reaction rate, lifetime of coloured species and the value and distribution of activation energies of the bleaching process.

Experimental

To examine the photophysics of π-conjugated polymeric systems influenced by presence of high dipole moment possessing species, solid solutions of poly[2-methoxy-5-(2'-ethylhexyloxy)-1,4-phenylenevinylene] (MEH-PPV), poly[2methoxy-5-(3',7'-dimethyloctyloxy)-1,4-phenylenevinylene] (MDMO-PPV) and poly[(*p*-phenylenevinylene)-alt-(2-methoxy-5-(2-ethylhexyloxy)-*p*-phenylenevinylene)] poly(MEHPV-alt-PV) as the conjugated matrix with dispersed photochromic 1',3'-dihydro-1',3',3'-trimethyl-6-nitrospiro[2*H*-1-benzopyran-2,2'-(2*H*)-indole] (SP) were prepared by spin-coating method on quartz glass and Si substrates. The thickness of the samples was typically 80–120 nm. To convert the SP into it's highly polar merocyanine (ME) form, a high pressure Hg lamp HBO 200 filtered with 360 ± 20 nm spectral filter was used. The systems were studied using standard absorption, and photoluminescence spectroscopy (PL).

Results and conclusions

It was found, that the rates and activation energies of back reactions (vanishing of the polar centres) depend on the intensity and exposure time of the light used for the photochromic conversion. In the case of MEH-PPV, developing of more than one isomer (possessing different dipole moments) was observed. The rates of their formation and termination significantly differ, which corresponds to diverse interactions between the isomers and the polymeric matrix.

Study of degradation processes by absorption and PL spectroscopy shows blue shift of the maximums. In energetically disordered systems this means good migration of excitons and bleaching of energetically lower lying sites. The presence of polar centres (produced by photochromic conversion) led to a further quenching of PPV photoluminescence and in the case of high concentration of SP (30 % wt.) in a poly(MEHPV-alt-PV), radiative energy transfer was observed (Fig. 1.). According to our previous work[2], we contribute this to a reduction of charge transfer in favour of energy transfer, which is demonstrated in a drop of polymers' photoconductivity. The most stable and simultaneously showing the best on/off contrast ratio turned out to be the system based on the poly(MEHPV-alt-PV) polymer.

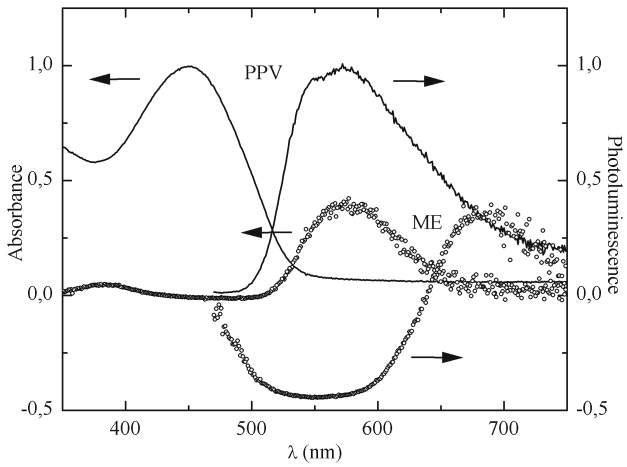

Fig. 1. **Normalised absorbance and luminescence spectra (full lines) of poly(MEHPV-alt-PV) with dispersed spiropyran and their relative changes (scattered) after 1 minute illumination at 360 nm. A new absorbance maximum (coming from merocyanine) followed by a drop of the polymer luminescence was observed. Furthermore, excitation at 450 nm (polymer absorption) led to a noticeable luminescence at 660 nm (coming from merocyanine). The energy absorbed by poly(MEHPV-alt-PV) was hence transferred to merocyanine and radiative decay was observed**

This work was supported by the grant 3446/2005/G1 from the Development Fund of Universities and by the project No. 203/03/133 from the Czech Science Foundation.

REFERENCES

1. Nešpůrek S., Sworakowski J., Combellas C., Wang G., Weiter M.: Appl. Surf. Sci. *234*, 395 (2004).
2. Weiter M., Vala M., Nešpůrek S., Sworakowski J., Salyk O., Zmeškal O.: *4th International Symposium on Photochromism, Artcachonu, France, 2004,* Book of Abstracts (Desvergne J. P., Pozzo J. L., ed.), Bordeaux: Univ. Bordeaux, (2004), pp. 42.

P44 UV/VIS SPECTROSCOPY OF MODELS OF COMPLEXATION OF HUMIC ACIDS

DANA VÁLKOVÁ, MARTINA KLUČÁKOVÁ and MILOSLAV PEKAŘ
Institute of Physical and Applied Chemistry, Brno University of Technology, Purkyňova 118, 612 00 Brno, Czech Republic, Valkova-d@fch.vutbr.cz

Introduction

Humic acids and humin represent the major part of soil organic matter, which is known to play a key role in the environment by increasing or maintaining soil fertility and stability. Humic acids are not chemical individuals, but mixture of various compounds[1]. Their chemical structure remains largely unknown, as a consequence of the complexity and heterogeneity of these "macromolecular" compounds. The basic structure is aromatic rings of the di- or ri-hydroxyl-phenol type bridged by –O–, $–CH_2–$, –NH–, –N=, –S–, and other groups containing all free OH groups and carboxylic groups and quinone groups (C = O)[2]. Presence of a wide range of functional groups on molecules of humic acids makes them very reactive and influential in soil and natural water chemistry. Out of these functional groups, the carboxylic and phenolic ones are most abundant and most influential in regards to metal complexation[3]. Therefore model compounds containing at least one of these functional groups have been chosen to model interactions of humic acids with metal ions. We can find both aromatic and aliphatic compounds among the models which have been chosen. As metal component, copper was used for experiments due to stability of its complexes with humic acids.

Material and methods

Ethanol, tert-butyl alcohol, phenol, benzoic acid, acetic acid, pyrocatechol, resorcinol, hydroquinone, salicylic acid, oxalic acid, tartaric acid and EDTA were chosen to model possible binding sits in humic acids. Model compounds were prepared in water solutions. As a source of cupric ions 0.5 M solution of $CuCl_2$ were utilized. UV/VIS spectrometry was used to characterize the system in equilibrium and to follow course of complexation. The time development of absorbance at maximum wave-length was measured after mixing solution of a model compound with solution of cupric ions. The UV/VIS spectra both of the model and the complex of model with cupric ion were measured after establishment of the equilibrium.

Results and discussion

The maximums of absorbance in spectrums of acetic acid, oxalic acid, tartaric acid and EDTA are situated at the beginning of measured range. It is possible that the maximums of absorbance are situated at lower wave-length, because they are aliphatic compounds forming colourless solutions. In some cases e. g. in aromatics compounds the absorbance higher then 2.5 were found. In system of phenol with cupric ions we can see shift of the maximum characteristic for phenol to higher wave-length and its increase of absorbance. In cases of pyrocatechol and resorcinol shifts of theirs maximums to lower wave-length and decreases of the absorbance were founded. The maximum of absorbance of the salicylic acid after complexation increases, on the other side in case of hydroquinone the maximum of its absorbance decreases. In some cases we detected shifts of maximum characteristic for cupric ions to lower wave-length. We can find new zone of absorbance in cases of both pyrocatechol and hydroquinone. Maximums characteristic for acetic acid, oxalic acid, tartaric acid and EDTA were coincided with absorbance of cupric ions. (See Table I)

Table I
UV/VIS characterisation of models and their Cu-complexes

Model compound	Maximum of the model	Shift of maximum of the model	Model	Complex	Shift of maximum of Cu	New zone
	λ_{max}/A_{max}	λ_{max}/A_{max}	A810	A810	λ_{max}/A_{max}	λ_{max}/A_{max}
Ethanol	none		0.0003	0.3055	810/0.3055	none
Tert-butyl alcohol	none		0.0006	0.1474	810/0.14735	none
Phenol	250/>2.5	265/>2.5	0.0015	0.3044	810/0.3044	none
Benzoic acid	270/1.5878	270/>2.5	0.0000	0.3101	810/0.3101	none
Acetic acid	200/0.1350	–	0.0004	0.3122	807/0.3125	none
Pyrocatechol	275/2.2485	272/>2.5	0.0000	0.2274	788/0.2313	441/0.0790
Resorcinol	273/1.8306	268/>2.5	0.0006	0.3032	810/0.3032	none
Hydroquinone	289/>2.5	280/1.4903	0.0009	0.2373	804/0.2382	326/0.4118
Salicylic acid	297/>2.5	296/>2.5	0.0001	0.3061	810/0.3061	none
Oxalic acid	200/1.7060	–	0.0000	0.1549	810/0.1549	none
Tartaric acid	200/0.2689	–	0.0000	0.3097	810/0.3097	none
EDTA	200/0.4126	–	0.0004	0.3188	797/0.3196	none

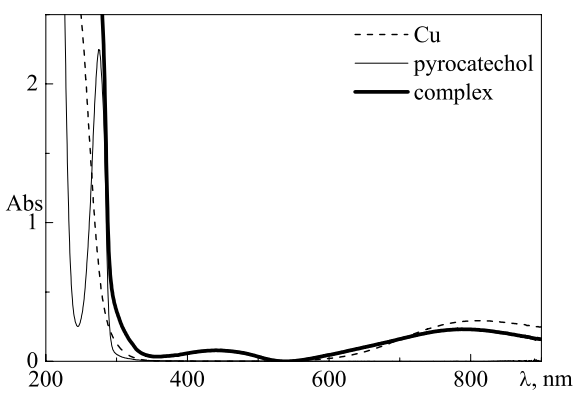

Fig. 1. **UV/VIS spectra of all the pyrocatechol, the Cu-complex of pyrocatechol and cupric ion**

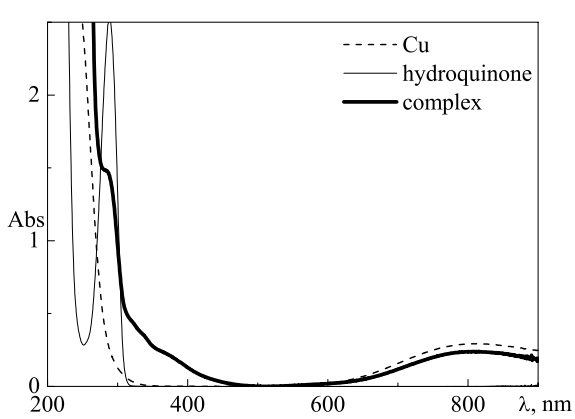

Fig. 2. **UV/VIS spectra of all the hydroquinone, the Cu-complex of hydroquinone and cupric ion**

Dependence of absorbance of the maximum of new zone on time was measured. We detected increase of absorbance on time in both cases. There is not detectable decrease of absorbance at 810 nm. Growth of absorbance at wave-length of the maximum of the new zone is steeper in the case of pyrocatechol.

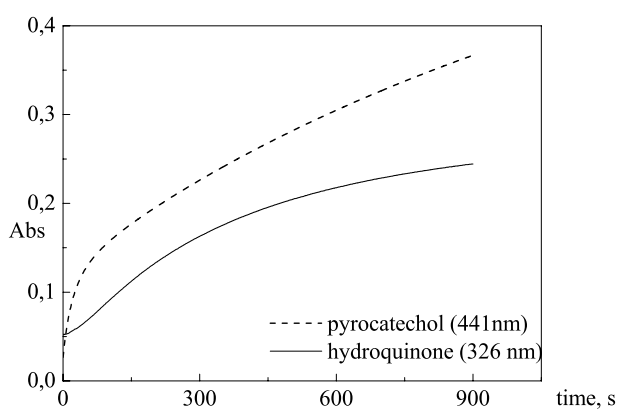

Fig. 3. **Dependence of absorbance on the time after mixing pyrocatechol resp. hydroquinone with cupric ions**

Conclusion

Genesis of new zone of absorbance in cases of both pyrocatechol and hydroquinone is visual noticeable so we can visibly follow course of complexation in these cases. Colour of the solutions was changing from blue to green in the case of pyrocatechol and from blue to powder-blue in case of hydroquinone. Decrease of the maximum of the absorbance of hydroquinone may be indicative of bonding of hydroquinone with cupric ion.

This work was supported by Grant Agency of Czech Republic – Project No. 104/02/D036.

REFERENCES

1. Stevenson F. J.: *Humus Chemistry: Genesis, Composition, Reactions*. J. Wiley, New York, 1994.
2. Lubal P., Široký D., Fetsch D., Havel J.: Talanta *47*, 401 (1998).
3. Klučáková M., Pelikán P., Lapčík L., Lapčíková B., Kučerík J., Kaláb M.: J. Polym. Mater. *17*, 350 (2000).

P45 REMOVING OF PAINTFILMS AND THEORY OF COATINGS DISSOLUTION

LUCIE WOLFOVÁ

Institute of Physical and Applied Chemistry, Brno University of Technology, Purkyňova 118, 612 00 Brno, Czech Republic, wolfova@fch.vutbr.cz

Summary

The purpose of this article is to present partial results of experimental work, whose principal objective are the studies of plastic materials surficial finishing resistance towards selected organic solvents. Our attention is concerned mainly on the coating resistance testing of systems based on nitrocellulose, epoxide, acrylate and polyurethane. We study the effects of organic solvents derived from pyrrolidone, glycols, acetates, glykolacetates,glycolethers, glycolesters atc and projected mixed solvent agents. These substances should provide a well-performing option to the harmful substances (such as dichlormethane) used so far without the negative effect on the environment.

The subject of our study is mainly the impact of types and chemical structure of the given solvents on the degradation of said coating types. Especially, the study is focused on the impact of physical and chemical properties and chemical structures of given solvents and paintfilms on their chemical degradation. Mainly it is concerned to the determination and study of solubility parameters of the solvents and their mixtures and of the paintfilms and to the projection of new solvents mixtures with well-performing option for the coating and graffiti removing, too.

The projected agents must have finely tuned properties, so that they are capable of selective removing of unwanted paints, leaving the substrate material or coating unaffected and/or even renovated.

We expect the use of the obtained results of the executed study in the industrial practice. Of special interest is removing of paintfilms and for the cleaning and refreshing non-porous materials overpainted with graffiti.

Theroretical Background of the Problem

The term "chemical resistance of coatings" means the ability to retain visual apperance and original qualities upon the exposure to organic solvents. It could be defined as physical and chemical interactions between film-forming components of the paint and chemical surroundings, which leads to changes in paint qualities.

It is evident, that the dissolution and solubility of paint film depend on a lot of attributes, such as:

- paint film morphology, porosity, pigmentation and type of used pigments,
- character, structure and properties of polymer macromolecules,
- physical and chemical properties of the solvents,
- type of individual interaction, penetration of chemical solvent in the polymer,
- coating permittivity, intermolecular interactions, which relate other thermodynamical characteristic such as the change of Gibb's energy, and especially parameters of solubility of concerned components.

From the therodynamic point of view, degree of solvent affinity to polymert is given by the Gibb's energy change, which is determined by the interaction between solvent molecules and macromolecular chain elements. Then, the solubility is mainly determined by the enthalpy value $\Delta H_{\text{mix.}}$, which therethrough relates a change of internal energy during evaporation $\Delta H_{\text{ev.}}$ This value related to unit volume $\Delta H_{\text{ev}}/V$ is the density of cohesive energy $\Delta\varepsilon$. A root of this formula is mentioned the *solubility parameter* δ.

The solubility parameter of the solvents could be calculated from general equation:

$$\delta = \sqrt{\frac{\text{interal evaporative heat} \times \text{density}}{\text{relative molecular mass}}} = \sqrt{\frac{L - RT}{V}}$$

where L is work executed during isothermal volume growth by constant pressure.

However, the solubility parameters of polymers couldn't be determined by this way. Instead, often they are determined according to the behaviour of polymers in interaction with solvents with known value of δ. For example by the coefficients of swelling:

$$Q_1 = Q_{\max} \cdot \exp\left[-KV_1 \cdot (\delta_1 - \delta_2)^2\right]$$

Or by viscometric measurements according to equation:

$$[\eta] = [\eta]_{\max} \cdot \exp\left[-KV_1 \cdot (\delta_1 - \delta_2)^2\right]$$

Then, these solubility parameters can be determined for example from the internal pressure or polymer structure.

The smaller is the difference δ of solvent and polymer, the better is dissolution. The polymers are mostly soluble in that solvents, which their $< \delta >$ correspond to middle interval of polymer solubility approximately to two units.

The Experimental Part

Table I

The result of testing of alkyd coating system – made from basic synthetic paint and enamel synthetic paint – resistance towards selected types of organic solvents

Solubility parameters δ of tested solvents [10^{-3} $J^{1/2}$ $m^{-3/2}$]			
Weak hydrogenous bond		Medium hydrogenous bond	
Cyclohexane	16.77	Ethyl methyl ketone	19.01
Heptane	15.19	Acetone	20.16
Benzene	23.39	Cyclohexanone	18.92
Toluene	18.73	Ethylene glycol	21.49
Xylene	18.22	N,N dimethyl formamide	24.82
Dichlormethane	18.36	dimethyl sulfoxide	24.60
Strong hydrogenous bond			
isopropyl alcohol	23.25	Alkyd coating	19.22

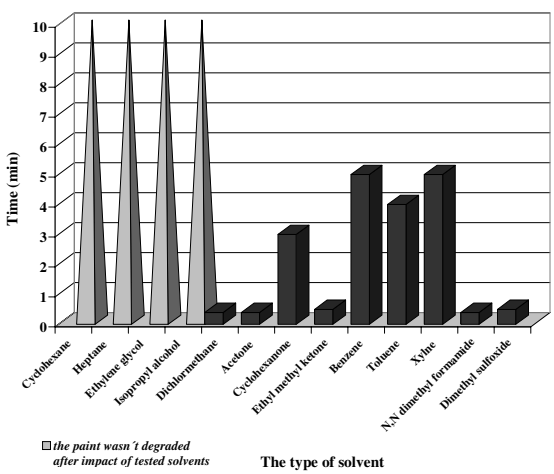

Fif. 1 **Dependence of type of solvents on duration of infuence needed to coating degradation**

Conclusions

Obtained results of testing of selected solvents mainly correspond to theory of coating solubility based on the solubility parameters, with the exception of three solvents – ethylene glycol, N,N dimethyl formamide, dimethyl sulfoxide. It could be accounted for some factores – for example such as impact of types and chemical structure of the given solvents on the degradation of said coating types, type of individual interaction and penetration of chemical solvent in the polymer etc.

REFERENCES

1. Mandík L., Kašpar F.: The selection of solvents for film-forming substances, Pardubice 1972.
2. Mleziva J., Šňupárek J.: Polymers – processing, structure, attributes and application, Prague 2000.
3. Pouchlý J.: Physical chemistry of macromolecular and colloid systems, Prague 2001

P46 PHOTOCATALYTIC REMOVAL OF METAL IONS ON TiO_2 CATALYST

JIŘÍ ZITA, PETRA MOŽÍŠKOVÁ, MARKÉTA PETEROVÁ and MICHAL VESELÝ
Brno University of Technology, Faculty of Chemistry, Institute of Physical and Applied Chemistry, Purkyňova 118, 612 00 Brno, Czech Republic, zita@fch.vutbr.cz

Introduction

Photodegradation using semi-conductors has proved to be a promising technology for pollution remediation. Catalysts developed by the sol–gel method and the addition of rare earth oxides have received much attention. The effect of coating substrates and the system parameters such as temperature, UV intensity, relative humidity and residence time have been investigated.

Titanium dioxide is a non-toxic material. TiO_2 thin films exhibit high stability in aqueous solutions, no photocorrosion under band gap illumination and exceptional surface properties. TiO_2 thin films are already widely used in dye-sensitized solar cells, and lithium insertion batteries. Titanium dioxide appears to be one of the most important photocatalytic materials in the area of environmental purification and especially in heterogeneous photocatalysis, an attractive low temperature, low cost, non-energy consuming technique, where a catalyst is capable of entirely decomposing organic pollutants in both the liquid and gaseous phase by using solar light illumination. The material in the form of powder suspensions has extensively been used for water treatment involving a large number of organic substrates[1].

Photoremoval of metals

We used an immersion well photoreactor for a reaction on TiO_2 powder (Degussa Aeroxide 25) as a catalyst.

When the powder catalyst was tested, its concentration was 0.4 g dm^{-3}.

In the case of immobilized catalyst, the thin TiO_2 film was prepared by sol–gel method from titan-tetrabutoxide. For reaction on immobilized TiO_2 catalyst we used multi--tube flow reactor and desk reactor[2].

Silver ions Ag^+

Reaction solution was made from $AgNO_3$, starting concentration of Ag^+ was set to 200 mg dm^{-3}. All reactions with silver ions proceeded in 0.005 M ethanol solution.

Cupric ions Cu^{2+}

Reaction solution was made from $CuSO_4$, starting concentration of Cu^{2+} was set to 50 mg dm^{-3}. All reactions with cupric ions proceeded with two different electron donors. Thiosulphate of 0.005 M concentration was used in first case, ethanol of 0.05 M concentration together with acetate buffer set to pH 4 in the second.

Mercuric ions Hg^{2+}

Reaction solution was made from $HgCl_2$, starting concentration of Hg^{2+} was set to 100 mg dm^{-3}. All reactions with mercuric ions proceeded in 0.005 M ethanol solution.

Results and diskusion

Every chosen metal ion was tested in presence of ethanol, because the photocatalytic reduction with ethanol added as electron donor will always take place. And that is why ethanol is good for comparison of the first order reaction rates of the process. In Fig. 1. we can se the behavior of the metal ions reduction in presence of ethanol and in Fig. 2. we can compare its rate constants. It is clear, that the fastest rate constant has mercuric ion.

For cupric ions the reaction rate in presence of ethanol was not so fast, and the whole process was not so easy as with other metal ions. The reduction always stopped, when the pH

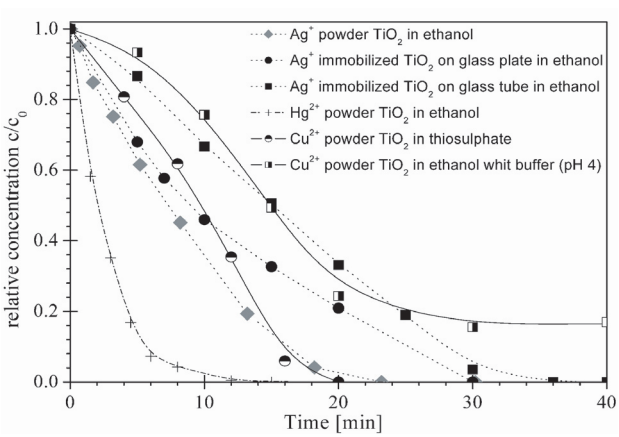

Fig. 1. **Behavior of photocatalytic metal ions reduction on immobilized(glass tube and plate) and powder TiO_2 (0.4 g dm^{-3}) catalyst in ethanol (0.05 M) and thiosulphate (0.005 M) solution**

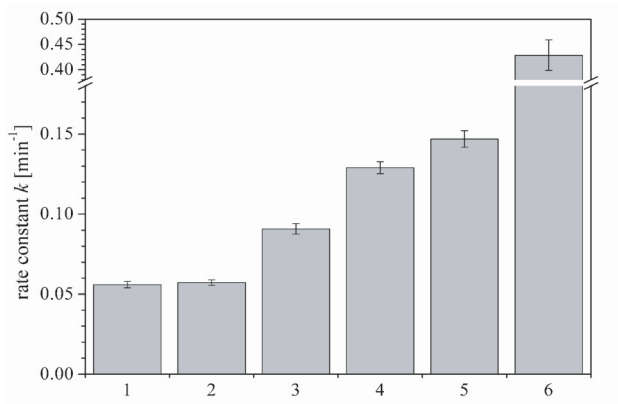

Fig. 2. **First order rate constants of photocatalytic metal ions removal: 1–Cu^{2+} on powder TiO_2 (0.4 g dm^{-3}) in ethanol (0.05 M) and acetate buffer solution (pH 4), 2–Ag^+ on immobilized TiO_2 in multi-tube reactor in ethanol solution (0.05 M), 3– Ag^+ on immobilized TiO_2 in desk reactor in ethanol solution (0.05 M), 4– Cu^{2+} on powder TiO_2 (0.4 g dm^{-3})in thiosulphate solution**

of the reaction solution has reached value of 3. That is why we have added the buffer solution, and than the reaction ran with higher rate constant and the final concentration was lower. We have tested also different electron donor for cupric ions reduction. We have found, that thiosulphate will be a good one. We have tested many concentrations of thiosulphate, bat the highest rate constant was in the case of 0.005 M, when it is comparable with silver ions reduction.

We have also tested immobilized layers of TiO_2 for silver ions reduction. The reaction rate constants in two different photochemical reactors were approximately the same. On the comparison with powder catalyst they were much slower, but immobilization of the catalyst brings so many advantages, that in the future catalyst only in immobilized form will be used.

Consultions

We have found out that reactions on powder catalyst are faster than on immobilized one, because of the high surface area of TiO_2 powder. However, powder catalyst has many disadvantages, such as centrifugation or filtration of powder from reaction media, necessity of catalyst regeneration which means high energy consumption. On the other hand it is impossible to use powder catalyst for greater amounts of metal ions, because it blocks the access of radiance to the photoactive sites on catalyst by reducing metal. After the whole particle is being coated by metal, it becomes inactive and the reaction rate decreases. One side of the immobilized catalyst layer is always exposed to the light and the decrease of reaction rate was not observed (depending on the adjustments of the reactor).

REFERENCES

1. Arabatzis I. M., Antonaraki S., Stergiopoulos T.: J. of Photochem. and Photobiol. A: Chem. *149*, 237 (2002).

2. Veselý M., Zita J., Možíšková P.: *The diference between siver photreduction on powder and immobilized TiO_2*, SPEA3, 3rd European Meeting on Solar chemistry and Photocatalysis: Enviromental applications, Book of Abstracts, Barcelona, p. 303–304, 2004.

P47 SOME TECHNIQUES FOR FT-IR SPECTROSCOPY OF HUMIC ACIDS

PAVLA ŽBÁNKOVÁ and MARTINA KLUČÁKOVÁ
Institute of Physical and Applied Chemistry, Brno University of Technology, Purkyňova 118, 612 00 Brno, Czech Republic, zbankova@vch.vutbr.cz

Introduction

Humic substances are the main components of soil organic matter. They occur not only in soil, but also in peat, coal, natural water, sediments, lignins and other natural deposits. They have a widespread distribution in all terrestrial and aquatic environments[1]. Humic substances represent a heterogeneous mixture of compounds, which do not have a uniform structural formula, but can be divided into three groups: humic acid, fulvic acid a humin.

Infrared spectroscopy has been widely used for characterization of humic substances and can provide valuable information on the structural and functional properties of natural organic matter molecules[2]. The application of FT-IR spectroscopy on solid organic phase provides information about the nature, reactivity and structural arrangement of oxygen/containing functional groups, the occurrence of protein and carbohydrates constituents, the relative proportions of aromatic versus aliphatic moieties, and a deeper insight of all overall evolution of the organic materials with depth long the profile[3]. A major problem in the application of IR spectroscopy for analysis of humic substances is interference caused by absorbed moisture, which produces bands in the 3300 to 3000 and 1720 to 1500 cm^{-1} region. Interference is particularly serious when pressed discs of alkali halides are used[4].

Experimental part

Humic acids were extracted from South-Moravia lignite according to following procedure. 100 grams of lignite were mixed with 2 litres of 0.5 M NaOH and 0.1 M $Na_4P_2O_7$ solution and shaken 24 hours under N_2 atmosphere. After centrifugation the supernatant was treated with 20% HCl up to pH = 1. Then humic solution was extensively purified by three cycles of dissolution in 1 M NaOH and subsequently precipitated in 20% HCl. After precipitation solution was shaken for 36 hours with HCl – HF solution to remove residual ashes. It was dialyzed (dialysis tubes, 3000 Mw cut – off) against distilled water until chloride – fluoride free and finally dried 72 hours with 25 °C.

Infrared spectra of extracted humic acids and leonardite humic acids standard (IHSS) were measured by two various techniques (Nicolet Impact 400). Traditional KBr pellets (1 mg of sample, 100 mg of KBr) and thin layer on the silicon plate were used. Sample of humic acid was always dissolved in DMSO, deposited on the silicon plate and dried with infrared lamp. The whole process was repeated several times to achieve optimal humic acid layer for measurement.

Result and discussions

FT-IR spectra of the humic acids from lignite are relatively un-complex. Absorption bands of aromatic, aliphatic and carboxylic groups were mainly observed.

The major spectra bands were assigned as follow: 3400 cm^{-1} (OH stretch of the bound water), 3000–2800 cm^{-1} (aliphatic C-H stretching), 1725–1600 cm^{-1} (C=O groups), 1620–1600 cm^{-1} (C=C aromatic stretching), 1510 cm^{-1} (aromatic skeletal vibrations), 1450–1410 cm^{-1} (CH deformation of CH_3 and CH_2, C=C aromatic ring stretching), 1370 cm^{-1} (O-H deformation and C-O stretching of phenolic OH groups, COO^- asymmetric stretching), 1260–1230 cm^{-1} (C-O stretching of ethers and COOH), 1010 cm^{-1} (O-H stretching in polysaccharides, aromatics), 900–650 cm^{-1} (out-of-plane deformation), 840 cm^{-1} (C-H vibration of aromatic rings)[1,2,3,4].

Both spectra, lignite humic acid and IHSS humic acid, are similar in the position of main bands. The differences could be observed only in relative intensity of some specific absorption bands. Generally, the spectra measured with silicon plate are more intensive and differentiated than spectra recorded with KBr pellets. The main differences in the intensity are visible in the area from 2000 to 800 cm^{-1}.

Fig. 1 shows FT-IR spectra of humic acid extracted from lignite. The largest differences in the spectra are in the region from 1200 to 800 cm^{-1}, the region which contains mainly information about oxygen compound.

Fig. 2. shows the FT-IR spectra of IHSS humic acid. In spectra acquired with silicon plate measurement is missing broad band from 3500 to 3200 cm^{-1}. This band is due to the OH stretching motions of the bound water and to some OH groups present in the humic acids, partly also assignment to the NH groups.

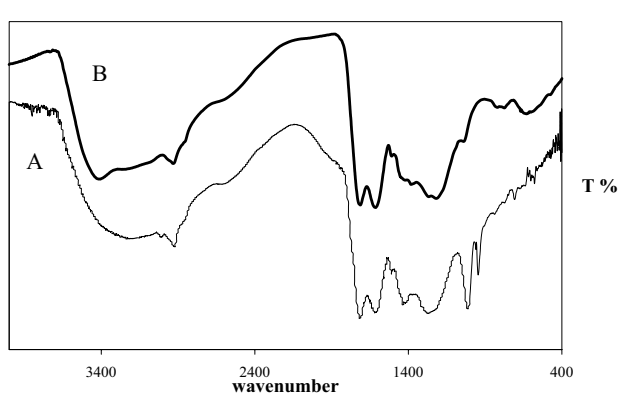

Fig. 1. **FT-IR spectra of humic acid; A – spectra run on silicon plate, B – spectra run like KBr pellet**

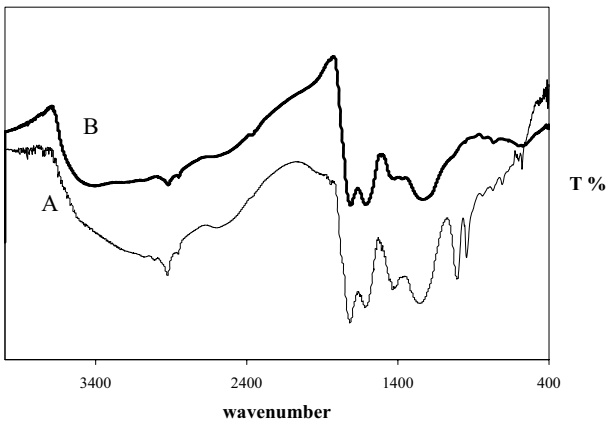

Fig. 2. **FT-IR spectra of IHSS humic acid; A – spectra run on silicon plate, B – spectra run like KBr pellet**

A major problem in the application of IR spectroscopy for analysis of humic substances is interference caused by absorbed moisture, which produces bands in the 3300 to 3000 and 1720 to 1500 cm^{-1} region. Interference is particularly serious when pressed discs of KBr are used. It was observed that spectra measured using silicon plate are more suitable for comparison of various humic samples because they are more detailed than those measured in KBr pellets. The spectra do not show any significant structural differences between using KBr pellets and Si plate.

This work was supported by the Ministry of Education, Youth and Sport of the Czech Republic, project no. 3400/ 2005.

REFERENCES

1. Ribeiro, J. S., Ok, S. S., Garrigues, S, de la Guardia, M.: Spectroscopy letters *34* (2), 179 (2001).
2. Chen, J., Gu, B., LeBoeuf, E. J., Pan, H., Dai, S.: Chemosphere *48*, 59 (2002).
3. Cocozza, C., D'Orazio, V., Miano, T. M., Shotyk, W.: Organic Geochemistry *34*, 49 (2003).
4. Stevenson, F. J.: *Humus chemistry: Genesis, Composition, Reactions,* second ed. Wiley & Sons, New York 1994.